Differences in Epigenetic, Transcriptional and Protein Adaptations to Exercise in Skeletal Muscle of Responders and Low-Responders in Insulin Sensitivity

Dissertation

der Mathematisch-Naturwissenschaftlichen Fakultät

der Eberhard Karls Universität Tübingen

zur Erlangung des Grades eines

Doktors der Naturwissenschaften

(Dr. rer. nat.)

vorgelegt von

Thomas Goj

aus Spaichingen

Tübingen

2023

Gedruckt mit Genehmigung der Mathematisch-Naturwissenschaftlichen Fakultät der Eberhard Karls Universität Tübingen.

Tag der mündlichen Qualifikation:	21.02.2024
Dekan:	Prof. Dr. Thilo Stehle
1. Berichterstatter:	Prof. Dr. Hubert Preißl
2. Berichterstatterin:	Prof. Dr. Cora Weigert

Contents

Abbreviation

AKR1C1	aldo keto-reductase 1
AKR1C2	aldo keto-reductase 2
AKR1C3	aldo keto-reductase 3
AKT	AKT Serine/Threonine Kinase
AMPK	protein kinase AMP-activated catalytic subunit
AU	arbitrary units
AUC	area under the curve
BH	Benjamini-Hochberg
BMI	body mass index
BMIQ	beta-mixture quantile normalization
BP	biological process
bp	base pair
BSA	bovine serum albumin
CC	cellular component
CHRNA1	cholinergic receptor nicotinic α 1 subunit
COX7A2	cytochrome c oxidase subunit 7A2
CpG site	methylation site
CRP	C-reactive protein
CSF1	colony stimulating factor 1
CSF1R	colony stimulating factor 1 receptor
CST5	cystatin D
CXCL1	C-X-C motif chemokine ligand 1
CXCL5	C-X-C motif chemokine ligand 5
CXCL10	C-X-C motif chemokine ligand 10
DABG	detection above background
ECM	extracellular matrix
ELISA	enzyme-linked immunosorbent assay
ERK1/2	mitogen-activated protein kinase 1/2
FC	fold change
FDR	false-discovery rate
GDM	gestational diabetes mellitus
GLUT4	insulin-responsive glucose transporter type 4
GO	gene ontology
HbA_{1C}	hemoglobin A1C
HDHD5	haloacid dehalogenase-like hydrolase domain-containing 5
hMT	human myotube
IAT	individual anaerobic threshold
IGF	insulin-like growth factor
IL6	interleukin 6
IL34	interleukin 34
INSR	insulin receptor
IQR	interquartile range
IRS	insulin receptor substrate
ISI_{Mats}	insulin sensitivity according to DeFronzo and Matsuda
KEGG	Kyoto encyclopedia of genes and genomes
LC	liquid chromatography
LRE	low-responder
MCP1	monocyte chemoattractant protein-1

MF	molecular function
MS	mass spectrometry
mTOR	mammalian/mechanistic target of rapamycin kinase
mtTFA	mitochondrial transcription factor A
NK cells	natural killer cells
NPX	normalized protein expression
NRE1	non-response to exercise study 1
NRE2	non-response to exercise study 2
NRF	nuclear receptor factor
OCR	oxygen consumption rate
OGTT	oral glucose tolerance test
OSM	oncostatin M
OXPHOS	oxidative phosphorylation
PBS	phosphate buffered saline
PCA	principal component analysis
PEA	proximity extension assay
PERM1	PPARGC1 and ESRR induced regulator 1
PGC1α	see PPARGC1A
PPARGC1A	peroxisome proliferative activated receptor gamma coactivator 1 α
PPME1	protein phosphatase methylesterase 1
pRXTOP	Retro-X™ Tet-One™ puro
qPCR	quantitative polymerase chain reaction
REAC	Reactome
RES	responder
RNA-Seq	RNA sequencing
SCAT	subcutaneous adipose tissue
SDC1	syndecan 1
SDS	sodium dodecyl sulfate
SOP	standard operating procedure
ST1A1	sulfotransferase family 1A member 1
SVD	singular value decomposition
T1DM	type 1 diabetes mellitus
T2DM	type 2 diabetes mellitus
TAC	transcriptome Analysis Console
TCA cycle	tricarboxylic acid cycle
TFA	trifluoroacetic acid
TGFA	transforming growth factor α
TGFB	transforming growth factor β
TNF	tumor necrosis factor
TNFSF14	tumor necrosis factor superfamily member 14
VAT	visceral adipose tissue
VO_2peak	peak oxygen consumption

List of Figures

List of Tables

Abstract

Type 2 diabetes mellitus (T2DM) is one of the most challenging diseases of our current century due to its high prevalence and economic burden. It is, therefore, of high interest to reduce the prevalence by improving prevention therapies. Regular physical activity has a high potential to prevent or delay the onset of T2DM. However, it is known that people respond very differently to exercise, even when the relative exercise intensity is comparable. Participants of exercise interventions who improve their insulin sensitivity or other metabolic parameters are called responders (RES), and participants not improving or worsening are called low-responders (LRE). Although multiple tissue and molecular adaptations to exercise have been elucidated, which can lead to the improvement of insulin sensitivity and thus prevention of T2DM, the driving forces for the distinction between RES and LRE are unclear.

We, therefore, performed proteomics, transcriptomics, and epigenomics analyses of human skeletal muscle biopsies of RES and LRE in insulin sensitivity (assessed using a standard oral glucose tolerance test) and analyzed serum cytokine abundance after acute exercise and prolonged endurance training. The study was conducted in subjects with a high risk for T2DM due to overweight or obesity who performed a supervised 8-week training intervention consisting of 30 min bike and 30 min treadmill training at 70 % VO_2peak. Muscle biopsies and blood samples for the multi-omics analyses were collected before and after the intervention in the resting state and after acute exercise.

In the first approach, the transcriptome and epigenome datasets were analyzed separately and in combination to select transcripts with robust differential regulation in RES and LRE on transcript and DNA methylation levels. Among them are IL34 and AKR1C3 and its two family members, AKR1C1 and AKR1C2, which showed a negative correlation to the change in insulin sensitivity. The different regulation of AKR1C3 was also found on protein level. The candidates were further analyzed in cell culture experiments by treating human myotubes with soluble IL34 or inducible overexpression of the AKR1C-proteins in the mouse muscle cell line C2C12. The cells were analyzed for insulin-induced AKT phosphorylation and mitochondrial respiration. Neither IL34 nor AKR1C3 altered the analyzed parameters in insulin signaling or respiration. Additional experiments revealed that while human myotubes expressed and released IL34, they did not respond to IL34 by activation of receptor-mediated signaling, which suggests that myofibers are not the target of IL34 within skeletal muscle tissue. AKR1C3 was previously described as an insulin-regulated transcript in other tissues, which might explain the upregulation in skeletal muscle of LRE but not RES.

The proteome analysis revealed that over all subjects several mitochondrial proteins were increased after training, many of those correlated with an increased mitochondrial respiration measured in isolated muscle fibers. The increased abundance of PERM1 after training was paralleled by transcriptional upregulation of *PERM1* and altered methylation pattern on 4 methylation sites (CpG sites) over all subjects. The increase in PERM1 correlated not only with increased respiration but also with the increase in insulin sensitivity. The increase in PPME1 showed a positive correlation with the change in insulin sensitivity after the training, but also the abundance of PPME1 in the resting biopsies was positively correlated with the pre- and post-intervention insulin sensitivity. The potential function of PERM1 and PPME1 as regulators of insulin sensitivity in skeletal muscle needs to be validated. The fold change of other proteins increased after training did not correlate with the change in insulin sensitivity.

As a last approach, changes in serum cytokine concentrations were studied using a proximity extension assay (PEA) and a panel of 92 inflammatory cytokines. This analysis revealed multiple cytokines highly increased in serum after an acute exercise bout that have not been studied in the context of exercise yet. We correlated the acute changes of the cytokines with the clinical parameters and found significant correlations with pre-intervention parameters of obesity that diminished after the training intervention. In contrast, the training intervention did not change resting cytokine levels.

In summary, this thesis shows the potential of multi-omics analysis in studying the differential training response of individuals and gives insight into potential molecular mechanisms influencing the impact of regular exercise on insulin sensitivity. Furthermore, the obtained datasets provide a comprehensive pattern of exercise-induced molecular adaptations in skeletal muscle and can be utilized for selecting additional candidates, potentially explaining the different responses of RES and LRE to finally improve diabetes prevention by customizing the training sessions more individually.

Zusammenfassung

Der Typ-2-Diabetes mellitus (T2DM) ist aufgrund seiner hohen Prävalenz und volkswirtschaftlichen Belastung eine der herausforderndsten Krankheiten unseres Jahrhunderts. Es ist daher von großem Interesse, die Prävalenz von T2DM durch verbesserte Präventionstherapien zu verringern. Regelmäßige körperliche Aktivität hat ein hohes Potenzial, das Auftreten von T2DM zu verhindern oder zu verzögern. Es ist jedoch bekannt, dass Menschen sehr unterschiedlich auf körperliche Aktivität reagieren, selbst wenn die relative Trainingsintensität vergleichbar ist. Teilnehmer an Bewegungsinterventionen, die ihre Insulinsensitivität oder andere Stoffwechselparameter verbessern, werden als Responder (RES) bezeichnet, Teilnehmer, die sich nicht verbessern oder verschlechtern, als Low-Responder (LRE). Obwohl viele Trainingsanpassungen im Muskelgewebe und auf molekularer Ebene bekannt sind welche zur Verbesserung der Insulinsensitivität und damit zur Prävention von T2DM führen können, sind die molekularen Mechanismen für die Unterscheidung zwischen RES und LRE unklar.

Wir haben daher Proteomik-, Transkriptomik- und Epigenomik-Analysen menschlicher Skelettmuskelbiopsien von RES und LRE in Bezug auf die Insulinsensitivität (bestimmt mit einem Standard oralen Glukosetoleranztest) durchgeführt, sowie die Konzentration von Zytokinen im Serum nach akuter Belastung und längerem Ausdauertraining analysiert. Die Studie, bestehend aus 30 Minuten Fahrrad- und 30 Minuten Laufbandtraining bei 80 % peak oxygen consumption (VO_2peak), wurde an Probanden, welche aufgrund von Übergewicht oder Adipositas ein hohes Risiko für T2DM haben, durchgeführt. Muskelbiopsien und Blutproben wurden für die Multi-Omics-Analysen vor und nach der Intervention im Ruhezustand und nach akuter Belastung entnommen.

Im ersten Ansatz wurden die Transkriptom- und Epigenom-Datensätze separat und in Kombination analysiert, um Transkripte mit einer robusten differenziellen Regulation in RES und LRE auf Transkript- und DNA-Methylierungsebene zu finden. IL34 und AKR1C3 sowie AKR1C1 und AKR1C2 zeigten eine negative Korrelation mit der Veränderung der Insulinsensitivität. Die unterschiedliche Regulierung von AKR1C3 wurde auch auf Proteinebene festgestellt. Die ausgewählten Kandidaten wurden in Zellkulturexperimenten weiter analysiert, indem humane Myotuben mit IL34 behandelt oder die AKR1C-Proteine in der Mausmuskelzelllinie C2C12 überexprimiert wurden. Die Zellen wurden in Bezug auf die Insulin-induzierte AKT-Phosphorylierung und die mitochondriale Atmung untersucht. Weder IL34 noch AKR1C3 veränderten jedoch die analysierten Parameter des Insulin Signalwegs oder der Atmung. Zusätzliche Experimente ergaben, dass menschliche Myotuben zwar IL34 exprimierten und freisetzten, aber nicht mit einer Aktivierung der rezeptorvermittelten Signalübertragung auf IL34 reagierten, was darauf hindeutet, dass Muskelfasern nicht das Ziel von IL34 im Skelettmuskelgewebe sind. AKR1C3 wurde zuvor als insulinreguliertes Transkript in anderen Geweben beschrieben, was die Hochregulierung im Skelettmuskel von LRE, aber nicht von RES erklären könnte.

Die Proteomanalyse ergab, dass bei Betrachtung aller Probanden viele mitochondriale Proteine nach dem Training erhöht waren, von denen viele mit der in isolierten Muskelfasern gemessenen erhöhten mitochondrialen Atmung korrelierten. Die erhöhte Abundanz des Proteins PERM1 nach dem Training ging einher mit einer transkriptionellen Hochregulierung von PERM1 und einem veränderten Methylierungsmuster an 4 Methylierungsstellen (CpG-Stellen). Der Anstieg von PERM1 korrelierte nicht nur mit der erhöhten Atmung, sondern auch mit dem Anstieg der Insulinsensitivität. Der Anstieg des Proteins PPME1 zeigte eine positive Korrelation mit der Veränderung der Insulinsensitivität nach dem Training, aber auch in den Ruhebiopsien korrelierte PPME1 positiv mit der vor und nach der Intervention gemessenen Insulinsensitivität. Die potenzielle Funktion von PERM1 und PPME1 als Regulatoren der Insulinsensitivität im Skelettmuskel muss jedoch noch validiert wer-

den. Die Veränderung anderer Proteine, die nach dem Training zunahmen, korrelierte nicht mit der Veränderung der Insulinsensitivität.

Als letzter Ansatz wurden die Veränderungen der Konzentration von Serumzytokinen mit einem Proximity-Extension-Assay untersucht. Diese Analyse von 92 Zytokinen, die mit Entzündungsprozessen assoziiert sind, ergab, dass viele Zytokine im Serum nach einer akuten Trainingseinheit stark erhöht sind, von denen einige bisher noch nicht im Zusammenhang mit Sport untersucht wurden. Wir korrelierten die akuten Veränderungen der Zytokine mit klinischen Parametern und fanden signifikante Korrelationen mit den Parametern der Fettleibigkeit vor der Intervention, wobei die Zusammenhänge nach der Trainingsintervention nicht mehr sichtbar waren. Im Gegensatz zur akuten Regulation waren die Zytokinkonzentrationen im Ruhezustand nach der Trainingsintervention nicht verändert.

Zusammenfassend zeigt diese Arbeit das Potenzial von Multi-Omics-Analysen bei der Untersuchung der unterschiedlichen Trainingsreaktionen von Personen und gibt Einblicke in potenzielle molekulare Mechanismen, welche die Auswirkungen von regelmäßigem Training auf die Insulinsensitivität beeinflussen. Darüber hinaus liefern die gewonnenen Datensätze ein umfassendes Muster der trainingsinduzierten molekularen Anpassungen in der Skelettmuskulatur und können für die Auswahl weiterer Kandidaten genutzt werden, die möglicherweise die individuellen Unterschiede in der Anpassung auch anderer Parameter wie der muskulären mitochondriellen Atmung und der Ausdauerleistung erklären können. Insgesamt könnte dies die Möglichkeit eröffnen die Diabetesprävention durch eine individuellere Gestaltung der Trainingseinheiten zu verbessern.

1 Introduction

1.1 Type 2 diabetes and prediabetes

The human body strictly regulates the blood glucose levels. For this, the interplay of multiple hormones is necessary, including insulin and glucagon, thyroxin, adrenaline, somatropin, glucocorticoids, and incretins [1–3]. When this regulation fails, it comes to hyperglycemia or hypoglycemia for increased or decreased blood glucose levels, respectively. The chronic dysregulation of glucose metabolism is a major driver of the development of diabetes mellitus. The term is a combination of the two Greek words "mellitus", which means "sweet or pleasant tasting like honey", and "diabetes", which means "to pass through" [4, 5].

Diabetes mellitus is among the most challenging diseases in the current century [6]. In 1980, the world health organization (WHO) estimated that about 108 million people would be diagnosed patients with diabetes. This number increased by about four times in 2014 [7]. The International Diabetes Federation (IDF) estimates that by 2045 about 783 million people will have diabetes, with a prevalence of 9.9 % of all adults between 20 – 79 years [8]. This leads to a great burden on the healthcare system. In the study from Bommer et al., it was estimated that the global cost of diabetes was around 1.31 billion US$ only for adults between 20 and 79 years in 2015 [9]. With increases in the number of patients, the costs will rise as well. Cheap and high-caloric industrial food, longer life expectancy, and lack of physical activity lead to increased obesity in the world population [10, 11]. Although not all obese individuals develop diabetes [12], a high correlation is seen [13, 14].

Diabetes can be classified into four types. Type 1 diabetes mellitus (T1DM) is an autoimmune disease [15], in which antibodies recognize proteins of pancreatic beta-cells as foreign and induce cell death [16]. The result is the sudden loss of beta-cells and the inability to produce insulin [17], which is why lifelong insulin therapy is essential [18]. This form of diabetes often manifests in childhood [19, 20]. Type 2 diabetes mellitus (T2DM), on the other hand, has a gradual onset and develops mostly in adults. This form is often related to disruption of the insulin signaling cascade for various reasons, leading to insulin resistance and beta-cell exhaustion. Gestational diabetes mellitus (GDM), the third type of diabetes, typically develops during the second or third trimester of pregnancy and is a major risk factor for developing T2DM in later life [21]. The last type of diabetes is not clearly determined as one singular type but can be divided into further rare forms of diabetes. This type originates, for example, when the pancreas is affected (e.g., pancreatitis or cystic fibrosis) or is induced by drugs and chemicals (e.g., treatment of HIV/AIDS, after organ transplantation, or use of glucocorticoid) [22].

Table 1: Criteria for diagnosis of diabetes and prediabetes. These criteria were defined by the American Diabetes Association [23]. For the diagnosis, at least one criterion is sufficient.

Patient Category	**HbA_{1C}**	**Fasting plasma glucose**	**Oral glucose tolerance test, plasma glucose after 120 min**
Normal	<5.7 %	<100 mg/dL	<140 mg/dL
Prediabetes	5.7 % – 6.4 %	100 mg/dL – 125 mg/dL	140 mg/dL – 199 mg/dL
Diabetes	>6.4 %	>125 mg/dL	>199 mg/dL

With about 90 % of all cases, T2DM is the most common form of diabetes [24]. Although T2DM was for a long time the type of diabetes with onset in adults around 40 years, our current lifestyle leads to a strong increase of diagnosed cases in juveniles and children. It has not a sudden onset but rather a slow progression, which can be classified as a prediabetic state [25]. The criteria for the distinction between healthy, prediabetes, and diabetes are listed in Table 1. For the detection, either the hemoglobin A1C (HbA_{1C}) is used, the fasting plasma glucose levels, or the plasma glucose level after 120 min when an oral glucose tolerance test (OGTT) is performed. Diabetes can result in negative consequences like diabetic microangiopathy (retinopathy), diabetic macroangiopathy (in brain vessels or splenic vessels) [26], diabetic polyneuropathy, or cardiac autonomic neuropathy, and therefore increased risk for cardiovascular mortality. About 30 % – 50 % of patients with T2DM suffer from diabetic nephropathy with micro- or macroalbuminuria [27]. With the epidemic proportions of diabetes, it is of great interest for our society to improve the treatment and therapy and prevent the onset of T2DM. The main goal in treating (pre)diabetes is to normalize blood glucose levels and prevent late complications. This can be achieved by increasing whole-body insulin sensitivity to improve glucose tolerance. Therefore, the first step is a lifestyle change by increasing daily physical activity and changing nutrition to healthier food to reduce obesity. It was shown in multiple studies, like the DPP and DPS studies, that physical exercise delays the occurrence of T2DM (see more in section 1.2). For many patients, weight loss and increased fitness would be sufficient to prevent or delay the onset of T2DM. Skeletal muscle plays a major role in the prevention of T2DM since it is responsible for about 80 % – 90 % of the insulin-dependent glucose uptake [28, 29], although it contributes with only about 40 % to total body weight [30]. Furthermore, the skeletal muscle is highly used during exercise, and shows pronounced adaptation to both acute [31] and long-term training [32]. During exercise, glucose uptake in skeletal muscle can increase up to 50-fold, an effect that is not hampered in people with T2DM [33, 34]. Additionally, during exercise, the muscle releases metabolites and cytokines, also called myometabokines [35, 36], that are mediators for inter-organ crosstalk [37–39]. In conclusion, skeletal muscle plays a central role in diabetes prevention and treatment by exercise. Therefore, this thesis focuses on the skeletal muscle, while the contributions of other organs and cell types in the beneficial effects of exercise are not ignored.

1.2 Exercise as a cornerstone in the prevention of (pre)diabetes

In the past, multiple studies demonstrated the benefits of exercise for diseases such as hyperlipidemia, hypertension, heart diseases, stroke, cardiovascular diseases, and T2DM [22, 40–46]. For the treatment of T2DM, physical activity and diet changes are the first actions to be considered [47, 48]. Many studies, like the DPP (Diabetes Prevention Program), demonstrated significant benefits of exercise in preventing and delaying the onset of T2DM [49]. The study comprised 3,234 participants assigned into three groups: one lifestyle intervention group, one metformin-treated group, and one placebo control group. Participants recruited in the DPP study showed a 58 % reduced risk of developing T2DM compared to the control group, while the risk was reduced by 31 % in the metformin group. This outcome was seen not only for individuals from various racial and ethnic backgrounds but also for both sexes. Notably, a substantial 71 % decreased risk of T2DM was seen in participants of at least 60 years or above. The 10-year results of the Diabetes Prevention Program Outcomes Study (DPPOS) showed that both the lifestyle intervention and metformin treatment also improved the risk of developing cardiovascular diseases [50]. In the second follow-up after 15 years, the onset of T2DM was delayed by 27 % and 18 % in the lifestyle intervention and metformin groups, respectively [51]. In the placebo control group, 62 % developed diabetes, whereas only 56 % of the metformin group and 55 % of the lifestyle intervention group were diagnosed with T2DM.

The Finnish Diabetes Prevention Study (DPS) showed similar results [52]. The study comprised 522 participants assigned into one control and one intervention group. After one year of follow-up,

the results showed an overall weight loss of 0.8 kg in the control group, while the intervention group decreased their body weight by 4.2 kg. After two years of follow-up, the control group maintained a weight loss of 0.8 kg, while the intervention group lost 3.5 kg across all subjects. More interestingly were the cumulative incidences of newly diagnosed T2DM, which were around 23 % in the control group and only 11 % in the intervention group after four years. Therefore, it was concluded that lifestyle interventions prevent the onset of T2DM in high-risk subjects [52].

In addition to these studies, there are also lifestyle intervention studies with longer follow-up, such as the Da Qing study with 30-year results [53]. Briefly summarized, the original study comprised 577 participants assigned into three intervention groups with diet, exercise, and diet with exercise and one control group. The participants were between 25 and 74 years old and had impaired glucose tolerance. For the long-term follow-up, all three intervention groups were combined since no significant difference in diabetes incidences was found between the groups. The follow-up showed a delay in the onset of T2DM of about 3.96 years in the intervention group compared to the control. Additionally, fewer events and deaths of cardiovascular diseases, less incidence of microangiopathy, and increased life expectancy with lower mortality were found in the intervention group compared to the control [53].

However, there are hundreds of studies analyzing the effect of training on various outcomes of the human body. Therefore, several meta-analyses were carried out to combine the individual results and improve the validity. For example, one meta-analysis combined 7 studies with 266 participants in total who performed at least an 8-week training intervention of patients with T2DM. The study observed significant improvement in the peak oxygen consumption (VO_2peak) [54]. In another meta-analysis composed of 14 studies (12 endurance and 2 resistance exercise) of at least 8 weeks and 251 subjects, the HbA_{1C} was seen to be highly improved without a significant improvement on the body weight [55]. This improvement was confirmed by another meta-analysis consisting of 7 aerobic training intervention studies with 220 subjects [56].

In summary, all the studies and meta-analyses shown here indicate that regular physical activity has a positive effect on the body and improves T2DM.

1.3 Adaptations in skeletal muscle involved in the improvement of glucose tolerance and insulin sensitivity

1.3.1 Tissue adaptations

It has been known for a long time that continuous physical exercise improves physical performance [57–59]. This is based on cellular and molecular regulatory mechanisms leading to physiological adaptation. One of the key factors in these processes is the modification of molecular pathways, both intracellular and extracellular, which can lead to changes in gene and protein expressions, ultimately resulting in cellular and tissue phenotypic alterations [32]. This is triggered by signals such as metabolic disturbance, sarcoplasmic calcium release, changes in the balance of acids and bases, changed redox state, increased hormones, catecholamine signaling, or increased body temperature [60]. Computational approaches have identified approximately 300 proteins secreted from skeletal muscle, which are involved in cell signal transduction pathways [61]. Moreover, a study focusing on a 6-week endurance exercise demonstrated that it influenced the expression of 800 genes in human skeletal muscles, with around 100 genes significantly altered comparing subjects with the highest and lowest response in improving aerobic capacity [62]. Furthermore, different physiological adaptations occur depending on the type of exercise and training stimulus. Resistance exercise leads to an increase in muscle mass and muscle fiber diameter [63]. This is mediated by an increased abundance of myofibrillar and mitochondrial proteins [64]. On the other hand, endurance training leads to

improved cardiorespiratory fitness that can be determined by increased maximal oxygen uptake and muscle oxidative capacity. This is driven by increased mitochondrial biogenesis and vascularization, while changes in muscle mass are less pronounced [65]. Changes in the protein abundance are seen for mitochondrial proteins but not in the overall myofibrillar protein synthesis [64]. The improvement of mitochondrial respiration and mitochondrial content improves energy restoration from fatty acid and carbohydrate oxidation [66], and endurance capacity [67, 68]. Increased vascularization improves the blood flow capacity and, therefore, maximal oxygen consumption, supplying the muscle optimally with oxygen [69, 70].

All these physiological adaptations improve substrate oxidation and storage in skeletal muscle and increase the proportion of skeletal muscle on whole-body metabolic homeostasis, which drives the improvement in glucose tolerance and insulin sensitivity after prolonged exercise training [71–77].

1.3.2 Molecular adaptations

Skeletal muscle glucose uptake is mediated by translocation of GLUT4 to the plasma membrane [33], which is not only induced by insulin but also upregulated by endurance training [78] and resistance exercise [79]. Multiple pathways are involved in the exercise-induced glucose uptake. Muscle contraction triggers the influx of Ca^{2+}, which activates the calmodulin calcineurin/NFAT signal transduction [80, 81] and induces GLUT4 translocation [82]. Another mechanism is via the AMPK pathway, which additionally increases fatty acid oxidation [83] and, therefore, contributes to restoring the energy balance in skeletal muscle [84, 85]. The AMPK pathway regulates further pathways important for muscle adaptation, such as regulating PGC1α. Activation of the transcriptional coactivator PGC1α [86] leads, together with the nuclear respiratory factors (NRF1 and 2), to the expression of mitochondrial transcription factor A (mtTFA) and, therefore, mitochondrial biogenesis [87]. It has been shown that the knockout of PGC1α leads to impaired training adaptations and dysregulation of lipid or glucose metabolism genes [88]. AMPK-regulated pathways are, therefore, essential in regulating the adaptive response to exercise.

Other molecular adaptations include activating the mammalian/mechanistic target of rapamycin kinase (mTOR), which plays an important role in muscle hypertrophy and muscle mass increase [89]. Increased muscle mass is associated with improved glucose uptake and insulin sensitivity [90, 91]. The activation of mTOR is initialized by the binding of insulin-like growth factor 1 (IGF1) to its receptor, triggering a signaling cascade [92] and leading to AKT activation. AKT is involved in multiple downstream pathways, such as protein synthesis [92–95], proliferation [96–98], or glucose metabolism [99–101]. Furthermore, mTOR plays important roles in lipid metabolism [102, 103] and mitochondrial biogenesis [104, 105].

Endogenous factors and various extracellular messengers also play a role in molecular adaptation to exercise. This includes reactive oxygen or nitrogen species and messengers such as norepinephrine, epinephrine, growth hormone, cytokines, or cortisol [106, 107]. However, these will not be further evaluated in this thesis.

1.4 Not all benefit in the same way – responder (RES) versus low-responder (LRE)

Although the results of the mentioned studies in section 1.2 seem very promising in treating T2DM, some publications are stating otherwise. Increased insulin sensitivity, which is a desired outcome in the prevention of T2DM, was not observed in all participants of prolonged exercise intervention studies (examples are listed in Table 2). Individuals who do not have beneficial effects or worsen their current state are called non-responders or low-responders (LRE), whereas individuals responding well are called responders (RES).

In Table 2, between 7 and 63 % of all participants are clustered in the LRE group [108–118]. The response was here defined by improved parameters reflecting glucose homeostasis, such as the improvement in plasma fasting insulin or glucose, HbA_{1C}, 2 h glucose, or triglycerides. It is worth noting that multiple studies report a similar effect that approximately 15 % – 20 % of individuals participating in training intervention studies fail to improve their glucose homeostasis and insulin sensitivity or increase muscle mitochondria density [119, 120]. However, it is important to mention that participants who were classified as LRE in glucose homeostasis often benefit other parameters like exercise performance or physical fitness.

Table 2: Exercise intervention studies with percentage of LRE. The table shows different clinical trials of lifestyle intervention studies which determined the number of participants without beneficial or adverse effects. These participants were called low-responder (LRE). The table is a modified version from Böhm et al. [121]. [1]: Low-response means no improvement in the declared endpoint if it was not stated otherwise. [2]: Participants showed adverse effects. AUC: area under the curve, OGTT: oral glucose tolerance test

Intervention program	Duration [weeks]	Number of subjects	Subject condition	Endpoint	LRE[1] [%]	Source
endurance training program	20	693	healthy	plasma fasting insulin	8	Bouchard [108]
moderate-intensity exercise of 160 min per week and decreased daily caloric intake (−500 kcal)	52	104	abdominal obesity, dyslipidemic	fasting glucose and 2 h glucose after OGTT	63	Borel [109]
endurance training of 3 times per week at 55 % – 75 % VO_2peak	20	596	healthy	insulin sensitivity by intravenous glucose tolerance test	42	Boulé [110]
endurance training of 3 times per week at 50 % – 70 % VO_2peak	26	110	healthy	fasting plasma insulin or OGTT-AUC	25 or 20	Hagberg [111]

Continued on next page

Table 2 – continued from previous page

Intervention program	**Duration** [**weeks**]	**Number of subjects**	**Subject condition**	**Endpoint**	**LRE**[1] [**%**]	**Source**
aerobic exercise with low-moderate, low-vigorous or high-vigorous	24	288	overweight, dyslipidemic	plasma fasting insulin	6	Kraus [112]
unsupervised nordic walking of 5 h per week	20	14	prediabetic	2 h glucose after OGTT	36	Osler [113]
endurance training with 4/8/12 kcal/kg per week	24	362	healthy, overweight or obese women, with high-normal blood pressure and post-menopausal	plasma fasting insulin	10	Morss [114], Church [115]
aerobic training or resistance training, or a combination of both	36	42	diabetic	decrease in HbA_{1C}, and % of body fat, and BMI, and increase in skeletal muscle mitochondrial DNA	21	Stephens [116]
supervised aerobic exercise at 60 % – 80 % VO_2peak	16	85	healthy	plasma fasting insulin	14	Thompson [117]
education program promoting physical health with and without the use of personalized pedometers	52	58	prediabetic	fasting glucose, 2 h glucose of OGTT, triglycerides, and HDL-cholesterol	60[2]	Yates [118]

For the definition of response, several factors need to be considered that influence the outcome of exercise intervention studies. Adherence to training sessions and comparable exercise intensity and quantity must be controlled, as well as diet and physical activity during the intervention [122]. Despite that, other factors can influence the response, such as insulin sensitivity at baseline, duration,

and exercise modalities. It is important to note that certain types of exercise may not be appropriate for everyone based on their limitations, such as being overweight [123, 124]. Generally speaking, although the adaptations to endurance or resistance training differ, both effectively reduce the risk of developing T2D [125]. Resistance exercise results in muscle hypertrophy, whereas endurance training increases cardiorespiratory function and mitochondrial biogenesis [125]. Recent research suggests, therefore, that combining endurance and resistance training yields superior effects on insulin sensitivity and glucose homeostasis compared to either type of training alone [126, 127].
One potential factor influencing the differential response is age. Multiple studies report impaired muscle hypertrophy in older individuals after resistance training [128–130]. However, the effectiveness depends on the duration of training, intensity, but also diet. [32, 131]. Studies have shown that high-intensity aerobic training diminishes the age-related effect [132]. Furthermore, chronically trained older subjects showed high exercise efficiencies, mitochondrial content, and function [133]. Another factor that potentially impacts the differential training response is sex, although its influence is debatable. Whereas one study showed a sex-dependent effect on the abundance of proteins related to muscle metabolism [134], recent studies do not show a sex-specific effect after acute exercise and short-term training intervention [135, 136]. Besides these factors, genetic variations like single nucleotide polymorphism can play a role in the differentiation between RES and LRE. The study from Pesta et al. showed that single nucleotide polymorphism in the mitochondrial gene *NDUFB6* leads to an impaired insulin sensitivity by modulating mitochondrial function [137]. This could hold true for multiple more genes as well. Furthermore, epigenetic modification can result in differential responses to aerobic training. It was shown that the epigenomic profile in skeletal muscle cells is highly different between the RES and LRE groups [138]. Another factor that is not mentioned very often is the gut microbiome, which was shown to have a significant effect by altering the capacity of short-chain amino acids and short-chain fatty acids biosynthesis [139]. The positive correlation between cardiorespiratory fitness and insulin sensitivity was demonstrated in many studies [140, 141]. Some studies also showed a positive correlation between improvements in cardiorespiratory fitness through physical exercise and increased insulin sensitivity [142] and glucose homeostasis [143], but this does not hold true for every subject.

To conclude, the variability in the individual improvement in glucose control as a response to exercise interventions is huge and cannot be fully explained by the above mentioned factors. Nevertheless, it is of utmost importance to understand the parameters driving effective prevention and treatment of T2DM by exercise.

1.5 Training intervention studies NRE1 and NRE2

Further research is needed to uncover the specific factors that explain the differences observed between RES and LRE individuals. Therefore, our group performed two studies at the university hospital of Tübingen, which were called non-response to exercise studies, NRE1 and NRE2, to explore this phenomenon [144, 145]. Both studies recruited subjects with at least one high-risk factor to develop T2DM. The criteria for high risk were defined as a body mass index (BMI) of at least 27 or higher, a first-degree family member with diagnosed T2DM, or women with previously diagnosed GDM. Furthermore, all participants were untrained, meaning less than 120 min physical exercise per week. They performed a supervised 8-week endurance training without other lifestyle changes. For more detailed information about the participants or the 8-week training intervention, see section 3.10. The clinical and anthropometric data of the participants in NRE1 and NRE2 are shown in Table S1 and Table S2.

Table 3: Anthropometric data of ISI response groups from the NRE2 study. The participants were split into the responder (RES) and low-responder (LRE) groups. RES showed an increase in the insulin sensitivity according to DeFronzo and Matsuda (ISI_{Mats}) of at least 1.15-fold, whereas the LRE did not exceed the threshold. The numbers are shown as mean ± SD. Numbers in brackets show the range from minimum to maximum. The p-values were calculated using a paired Student's t-test or Wilcoxon signed rank test for non-normal distributed parameters.

Parameter	**Pre-8-week**		**Post-8-week**		**Fold change post/pre**		**P-value comparing fold change post/pre of RES and LRE**
Group	RES	LRE	RES	LRE	RES	LRE	-
Sex	8f, 6m	8f, 3m	-	-	-	-	-
Age [years]	29.0 ± 6.68	30.8 ± 9.71	-	-	-	-	-
Height [cm]	171 ± 9.51	169 ± 9.85	-	-	-	-	-
Body mass [kg]	91.0 ± 15.4	92.3 ± 16.6	89.7 ± 15.6	91.9 ± 16.8	0.98 ± 0.02	1.00 ± 0.03	>0.1
BMI [kg/m^2]	31.0 ± 3.34	32.1 ± 4.96	30.5 ± 3.48	32.0 ± 5.08	0.98 ± 0.02	1.00 ± 0.03	>0.1
Waist-to-hip ratio	0.90 ± 0.07	0.88 ± 0.04	0.89 ± 0.06	0.88 ± 0.05	0.99 ± 0.02	1.00 ± 0.02	**0.045**
Total AT tissue volume [L]	38.5 ± 8.19	41.6 ± 13.4	37.3 ± 8.62	41.2 ± 13.0	0.96 ± 0.03	0.99 ± 0.04	0.099
Subcutaneous AT [L]	14.6 ± 4.21	15.8 ± 6.59	13.7 ± 4.07	15.7 ± 6.89	0.93 ± 0.06	0.99 ± 0.06	**0.026**
Visceral AT [L]	3.69 ± 1.71	3.07 ± 1.34	3.48 ± 1.68	3.00 ± 1.18	0.93 ± 0.11	1.01 ± 0.14	>0.1
IAT_{ergo}/BM [W/kg]	1.12 ± 0.19	1.08 ± 0.23	1.35 ± 0.25	1.30 ± 0.25	1.21 ± 0.14	1.20 ± 0.09	>0.1
VO_2peak_{ergo}/BM [mL/(kg × min)]	25.4 ± 2.79	24.3 ± 5.02	26.7 ± 3.72	27.3 ± 5.48	1.06 ± 0.12	1.13 ± 0.15	>0.1
Glucose fasting [mmol/L]	5.09 ± 0.38	5.14 ± 0.38	5.08 ± 0.39	4.95 ± 0.32	1.00 ± 0.05	0.97 ± 0.06	>0.1
Glucose $OGTT_{120\ min}$ [mmol/L]	5.96 ± 1.24	5.32 ± 1.04	5.37 ± 0.86	5.70 ± 2.08	0.93 ± 0.18	1.10 ± 0.45	>0.1
Insulin fasting [pmol/L]	120 ± 36.5	85.7 ± 40.1	95.6 ± 36.3	106 ± 36.2	0.81 ± 0.21	1.32 ± 0.29	**0.001**

Continued on next page

Table 3 – continued from previous page

Parameter	Pre-8-week		Post-8-week		Fold change post/pre		P-value comparing fold change post/pre of RES and LRE
Insulin $OGTT_{120\ min}$ [pmol/L]	666 ± 437	392 ± 285	444 ± 309	474 ± 375	0.67 ± 0.27	1.29 ± 1.02	**0.004**
ISI_{Mats} [AU]	6.88 ± 2.97	11.0 ± 5.87	9.42 ± 4.27	8.97 ± 4.68	1.36 ± 0.22	0.83 ± 0.14	**<0.001**
HbA_{1C} [mmol/mol Hb]	34.2 ± 2.88	34.4 ± 2.01	32.9 ± 2.91	34.4 ± 1.61	0.96 ± 0.06	1.00 ± 0.03	0.065
HbA_{1C} [%]	5.28 ± 0.26	5.29 ± 0.18	5.16 ± 0.27	5.29 ± 0.15	0.98 ± 0.04	1.00 ± 0.02	0.067
Leukocytes [1/µL]	6874 ± 1349	7067 ± 1528	6460 ± 1233	6505 ± 1506	0.95 ± 0.15	0.94 ± 0.19	>0.1
CRP [mg/dL]	0.44 ± 0.76	0.54 ± 0.54	0.30 ± 0.33	0.43 ± 0.43	1.15 ± 0.77	1.52 ± 1.75	>0.1

Most data obtained in the thesis were based on analyses of skeletal muscle biopsies collected in NRE2. In this study, and highly comparable to the outcome of NRE1, all participants improved their cardiorespiratory fitness, which was shown as significantly improved (p-value < 0.05) individual anaerobic threshold (IAT) and VO_2peak (Table S1, S2). Although the study focused on the training intervention and not dietary changes, a slight but significant reduction in body mass and BMI could be seen. Additionally, a significant decrease (p-value < 0.05) was seen for the total, subcutaneous, and visceral adipose tissue. Looking at the insulin sensitivity, solely the insulin level 120 min after the OGTT improved significantly across all subjects. In contrast, solely a trend for improvement or no change was seen for the other parameters. Lastly, we did not observe changes in the inflammation determined by CRP and the number of leukocytes, although a trend to a decreased number is visible.

The main focus of both studies was determining the exercise-induced molecular mechanisms leading to the distinction of RES and LRE subjects. In the NRE1 study, it was found that the change in insulin sensitivity determined by OGTT and Matsuda index correlate with changes in the expression of genes involved in mitochondrial respiration and the activation of upstream regulators, such as PGC1α and AMPKα2 [144]. Furthermore, reduced regulation of mitochondrial genes and upstream regulators in the LRE group was associated with the activation of TGFβ. Cell culture experiments demonstrated that treating primary human myotubes with TGFβ1 significantly reduces mitochondrial genes like *TFAM*, *PRKAA2*, or *PGC1*α. This effect could be reversed by treating the cells additionally with the TGFβ1 inhibitor SB434542 [144]. Follow-up experiments showed that TGFβ1 significantly increased the expression of miR143 and miR145 transcripts. After performing a downstream target analysis for these micro RNAs, the insulin receptor (INSR) and the insulin receptor substrate 1 (IRS1) were determined as potential targets. The INSR and IRS1 transcript and protein were significantly downregulated after treatment of primary human myotubes with TGFβ1 and negatively correlated with miR143 and miR145 transcript levels in skeletal muscle biopsies [146]. Although these results seem to be promising in elucidating the mechanism of being a LRE, it must be mentioned that TGFβ1

is a master regulator of multiple processes in the cell, such as apoptosis and proliferation [147–149], differentiation [150], and extracellular matrix synthesis [151–153]. It is, therefore, not an optimal target for the potential conversion of LRE into RES.

First data analysis of the NRE2 study showed that the change in insulin sensitivity was negatively correlated with the change in subcutaneous adipose tissue (SCAT) [145], which is also evident from the data divided in RES and LRE (Table 3). The fold change in SCAT and in the waist-to-hip ratio after the intervention was different comparing RES and LRE. The only other parameters showing a different regulation are the insulin concentrations, which explains the different change in insulin sensitivity (Table 3). The change of mitochondrial respiration in skeletal muscle, assessed by high-resolution respirometry, in isolated myofibers was not correlated with the change in insulin sensitivity, while across all participants, the mitochondrial respiration was significantly increased post-intervention [145].

In conclusion, while first insights into the molecular mechanism of LRE in glucose control exist, a more global approach is needed to provide a comprehensive picture and to discover additional molecular drivers of the desired response or low-response in insulin sensitivity after training. By understanding these mechanisms more deeply, we can better adjust exercise interventions and optimize their effectiveness for individuals.

2 Aim of the study

Previous studies have shown that people at risk of developing type 2 diabetes mellitus (T2DM) benefit differently from structured and regularly performed exercise in parameters of insulin sensitivity and glucose control. Differences in the molecular response and long-term adaptation in skeletal muscle of responder (RES) and low-responder (LRE) can help to understand the effectiveness and limitations of exercise to prevent T2DM. Considering the multiple molecular pathways in skeletal muscle that can be activated by exercise and their interplay to modulate whole-body metabolism and exercise performance, this thesis aimed to describe the response of skeletal muscle of RES and LRE on different levels. To do so, we apply a multi-omics approach to skeletal muscle biopsies collected before and after an intervention (8-week endurance training intervention, 3 weekly sessions for 60 min at 80 % VO_2peak) performed at the University Hospital in Tübingen. Additionally, the acute changes after one single bout of endurance exercise (30 min ergometer exercise at 80 % VO_2peak) were studied.

In detail, whole genome transcriptome analysis, DNA methylation analysis, and proteomics analysis were performed, and the datasets were analyzed separately and in combination. The results provide comprehensive datasets of acute exercise and training-induced alterations in skeletal muscle transcripts, DNA methylation, and proteins. The data were also analyzed to find differences between RES and LRE either by separation into the groups or by correlation analysis of changes in transcripts and proteins with glucose metabolism parameters and mitochondrial respiration. The latter approach was performed to elucidate the mechanisms of increased mitochondrial respiration found after the 8-week training. Genes or proteins were selected for further analysis when their response in RES and LRE differed in more than one dataset, and they have not been described as regulators of insulin sensitivity. These candidates were then further analyzed in skeletal muscle cell culture on their effect on insulin response and mitochondrial respiration.

Moreover, a panel of 92 cytokines in serum samples and their response to acute exercise and long-term training was investigated using proximity extension assay (PEA). The results were also analyzed to find differences between RES and LRE by correlation analysis of changes in cytokines with glucose metabolism parameters. Furthermore, we studied whether clinical and anthropometric data can predict the observed response.

The overall goal is to discover novel exercise-induced genes and proteins expressed in the skeletal muscle, which can explain the distinction of subjects into RES and LRE. They could have the potential to become a novel target in the treatment of T2DM in patients who do not benefit from physical activity alone.

3 Materials and methods

3.1 Materials

3.1.1 Antibodies

Table 4: Primary Antibodies

Antibody	Dilution	Supplier	Catalog Nr.
AKT	1:500	BD Transduction laboratories, Erembodegem, Belgium	610860
CSF-1R/M-CSF-R	1:1,000	Cell Signaling Technology, Frankfurt, Germany	3152
FLAG M2	1:1,000	Sigma-Aldrich, St. Louis, MO, USA	F1804
GAPDH	1:20,000	Abcam, Cambridge, UK	ab8245
ERK1/2	1:1,000	Cell Signaling Technology, Frankfurt, Germany	9102
phospho AKT (Ser-473)	1:1,000	Cell Signaling Technology, Frankfurt, Germany	9271
phospho CSF-1R/M-CSF-R (Tyr723)	1:1,000	Cell Signaling Technology, Frankfurt, Germany	3155
phospho ERK1/2 (Thr202/Tyr204)	1:1,000	Cell Signaling Technology, Frankfurt, Germany	9101

Table 5: Secondary Antibodies

Antibody	Dilution	Supplier	Catalog Nr.
IRDye Infrared Dye donkey anti-mouse 680LT	1:20000	Licor, Lincoln, NE, USA	926-68022
IRDye Infrared Dye donkey anti-rabbit 800CW	1:10000	Licor, Lincoln, NE, USA	925-32213
IRDye Infrared Dye goat anti-mouse 680RD	1:20000	Licor, Lincoln, NE, USA	925-68070
IRDye Infrared Dye goat anti-rabbit 800CW	1:10000	Licor, Lincoln, NE, USA	926-32211

3.1.2 Buffers

Table 6: Buffers

Buffer	Ingredients
Lysis buffer (RIPA, pH 7.6) (stored at 4 °C)	25 mM TRIS pH 7.6 150 mM NaCl 0.1 % (w/v) SDS 0.5 % (w/v) NaDOC 1 % (v/v) Triton-X-100
Lysis buffer was supplemented with 1x cOmplete protease inhibitor (see Table 9) and 1x phosphatase inhibitor buffer (see below) shortly before use.	
10x Phosphatase buffer (stored at −20 °C)	10 mM Sodium fluoride 5 mM Sodium pyrophosphate 10 mM Sodium orthovanadate 10 mM β-Glycerophosphate
5x Laemmli sample buffer (pH 6.8) (stored at −20 °C)	60 mM TRIS-HCl 12.5 % (v/v) Glycerol 1 % (w/v) SDS 5 % (v/v) β-Mercaptoethanol 0.1 % (w/v) Bromphenolblue
Stacking gel buffer (pH 6.8) (stored at RT)	0.5 M TRIS 2 % (w/v) SDS
Separation gel buffer (pH 8.8) (stored at RT)	1.5 M TRIS 2 % (w/v) SDS
10x Electrophoresis buffer (stored at RT)	250 mM TRIS 1.92 M Glycine 1 % (w/v) SDS
10x Blotting buffer (stored at RT)	480 mM TRIS 390 mM Glycine 0.4 % (w/v) SDS
1x Blotting buffer (stored at RT)	10 % (v/v) 10x Blotting buffer 20 % (v/v) Methanol 70 % (v/v) H_2O
10x NET-G (blocking buffer) (stored at 4 °C)	2.5 % (w/v) Gelatine 1.5 M NaCl 50 mM EDTA 500 mM TRIS 0.5 % (v/v) Triton-X-100
To obtain 1x NET-G for blocking, 10x NET-G was diluted 1:10 using ultra-pure water and pH adjusted to 7.4 using 37 % (w/v) HCl.	

Continued on next page

Table 6 – continued from previous page

Buffer	Ingredients
10x TBS (pH 7.6) (stored at RT)	250 mM TRIS 1.5 M NaCl
To obtain 1x TBS-T, 10x TBS was diluted was diluted 1:10 using ultra-pure water and 0.1 % (v/v) Tween-20 was added.	
50x TAE buffer (pH 8) (stored at RT)	1.25 M TRIS 625 mM Acetic acid 50 mM EDTA
To obtain 1x TAE, 50x TAE buffer was diluted was diluted 1:50 using ultra-pure water.	
1x TE buffer (pH 7.6)	10 mM TRIS (pH 7.4) 1 mM EDTA (pH 8)
2x HEBS (pH = 7.10)	2 g/l Glucose 10 g/L HEPES 0.74 g/L KCl 16 g/L NaCl 0.22 g/L Na_2HPO_4
MIR05 buffer (pH 7.1)	0.5 mM EGTA 20 mM HEPES 3 mM $MgCl_2(H_2O)_6$ 60 mM K-lactobionate 20 mM Taurine 20 mM KH_2PO_4 110 mM Sucrose 1 g/L BSA

3.1.3 Cell culture media

Table 7: Cell culture media

Medium	Ingredients
C2C12 Growth Medium	DMEM, high glucose 10 % (v/v) FBS superior 1 % (v/v) Penicillin-Streptomycin 1 % (v/v) Glutamine
C2C12 Fusion Medium	DMEM, high glucose 2 % (v/v) FBS superior 1 % (v/v) Pen-Strep 1 % (v/v) Glutamine
C2C12 Fasting Medium	DMEM, high glucose 1 % (v/v) Pen-Strep 1 % (v/v) Glutamine

Continued on next page

Table 7 – continued from previous page

Medium	Ingredients
C2C12 Freezing Medium	DMEM, high glucose 20 % (v/v) FBS superior 10 % (v/v) DMSO
hMT Growth Medium	38 % (v/v) MEM Alpha Medium 38 % (v/v) Ham's F-12 Nut mix 20 % (v/v) FBS superior 1 % (v/v) Glutamine 1 % (v/v) Pen-Strep 1 % (v/v) Chicken Extract 0.2 % (v/v) Amphotericin B
The chicken extract was reconstituted in 11 mL of a 1:1 mixture of MEM alpha and Ham's F12, centrifuged for 10 min at 2,300 rpm and only the supernatant was used.	
hMT Fusion Medium	MEM Alpha Medium 1 % (v/v) Glutamine 1 % (v/v) Pen-Strep 0.2 % (v/v) Amphotericin B 50 µM Palmitate 50 µM Oleate 100 µM Carnitine
The fatty acids were dissolved in ethanol and coupled to BSA in PBS by shaking the mixture at 37 °C overnight. Carnitine was dissolved and ultra-pure water and sterile filtered (0.22 mm PES filter). The fusion medium was freshly prepared each time and used right away.	
hMT Fasting Medium	MEM Alpha Medium 1 % (v/v) Glutamine 1 % (v/v) Pen-Strep 0.2 % (v/v) Amphotericin B
hMT Freezing Medium	80 % (v/v) FBS superior 20 % (v/v) DMSO
THP-1 Growth Medium	RPMI-1640 5 % (v/v) FBS superior 1 % (v/v) Pen-Strep
THP-1 Freezing Medium	RPMI-1640 10 % (v/v) FBS superior 10 % (v/v) DMSO
Seahorse Assay Medium	Seahorse XF DMEM 10 mM Seahorse XF Glucose 2 mM Seahorse XF Glutamine 1 mM Seahorse XF Pyruvate

3.1.4 Cell lines and competent bacteria

Table 8: Cell lines

Cell	Supplier
Murine myoblasts C2C12 (CRL-1772)	ATCC, Manassas, VA, USA
Primary human skeletal muscle cells (hMT)	cultured from muscle biopsies
Platinum E Retroviral Packaging Cell (RV-101)	Cell Biolabs Inc., San Diego, CA, USA
PBMC (Peripheral Blood Mononuclear Cell)	isolated from whole blood of volunteers
THP-1	friendly gift from Sabrina Ehnert, BGA, Tübingen

3.1.5 Chemicals, enzymes and inhibitors

Table 9: Chemicals, enzymes and inhibitors

Item	Supplier	Catalog Nr.
β-Glycerolphosphate	Sigma-Aldrich, St. Louis, MO, USA	35675
β-Mercaptoethanol	Sigma-Aldrich, St. Louis, MO, USA	M3148
Acetic Acid	Merck KGaA, Darmstadt, Germany	100063
Acetonitrile	Sigma-Aldrich, St. Louis, MO, USA	271004
ADP	Merck KGaA, Darmstadt, Germany	117105-1GM
Agarose, peqGOLD Universal	Peqlab, Erlangen, Germany	35-1020
Ammonium persulfate	Sigma-Aldrich, St. Louis, MO, USA	A3678
Amphotericin B solution	Sigma-Aldrich, St. Louis, MO, USA	A2942
Ampicillin	Sigma-Aldrich, St. Louis, MO, USA	A5354
Antimycin A	Sigma-Aldrich, St. Louis, MO, USA	A8674
BamHI	New England BioLabs, Beverly MA, USA	R0136L
BioWhittaker Pen-Strep	Lonza Group, Basel, Schweiz	DE17-602E
Bromphenolblue	Sigma-Aldrich, St. Louis, MO, USA	B6131
BSA	Sigma-Aldrich, St. Louis, MO, USA	A6003
BSA (in DPBS)	Sigma-Aldrich, St. Louis, MO, USA	A1595
BstZ17I-HF	New England BioLabs, Beverly MA, USA	R3594L
Chicken Extract	Life Science Production, Sandy, UK	MDL-004E-UK
Chloracetamide	Sigma-Aldrich, St. Louis, MO, USA	C0267
Chloroacetamide	Sigma-Aldrich, St. Louis, MO, USA	C0267
CloneAmp HiFi PCR Premix	Takara Bio Inc., Kusatsu, Japan	639298
cOmplete Protease Inhibitor Cocktail	Roche, Basel, Swiss	11697498001

Continued on next page

Table 9 – continued from previous page

Item	Supplier	Catalog Nr.
Cytochrome c	Sigma-Aldrich, St. Louis, MO, USA	C7752
Digitonin	Sigma-Aldrich, St. Louis, MO, USA	D5628
DMEM, high glucose	Thermo Fisher Scientific, Waltham, MA, USA	41965
DMSO	Carl Roth GmbH & Co. KG	A994.1
Doxycycline	Sigma-Aldrich, St. Louis, MO, USA	D3447
Dulbecco's PBS	Thermo Fisher Scientific, Waltham, MA, USA	14190
EcoRI-HF	New England BioLabs, Beverly MA, USA	R3101L
EDTA	Sigma-Aldrich, St. Louis, MO, USA	E1644
EGTA	Carl Roth GmbH & Co. KG	E0396
Ethanol, absolute p. A.	Applichem GmbH, Darmstadt, Germany	A1613
Ethanol, denatured	SAV Liquid Production GmbH, Flintsbach am Inn, Germany	ETO-5000-99-1
FBS Superior	Sigma-Aldrich, St. Louis, MO, USA	S0615
FCCP	Sigma-Aldrich, St. Louis, MO, USA	C2920
Gelatine	Merck KGaA, Darmstadt, Germany	104070
Gibco Geltrex	Thermo Fisher Scientific, Waltham, MA, USA	A1413301
Glutamate	Sigma-Aldrich, St. Louis, MO, USA	G1626
Glycerol	Merck KGaA, Darmstadt, Germany	8187091000
Glycine	Carl Roth GmbH & Co. KG	3790.3
Ham F-12 Nut mix	Thermo Fisher Scientific, Waltham, MA, USA	21765
HEPES	Carl Roth GmbH & Co. KG	6763.1
Insulin	Sigma-Aldrich, St. Louis, MO, USA	I5500
Insulin dissolved in HEPES	Roche, Basel, Swiss	11376497001
Insulin-like Growth Factor 1 human	Sigma-Aldrich, St. Louis, MO, USA	I3769
Interleukin 34 human	BioLegend, San Diego, CA, USA	I5500
Interleukin 34 human	R&D Systems, Minneapolis, MN, USA	5265-IL-010
Isopropanol	VWR, Darmstadt, Germany	20842.330
K-lactobionate	Sigma-Aldrich, St. Louis, MO, USA	153516
LB Broth	Sigma-Aldrich, St. Louis, MO, USA	L3022
LB Broth with agar	Sigma-Aldrich, St. Louis, MO, USA	L2897
L-Carnitine hydrochloride	Sigma-Aldrich, St. Louis, MO, USA	C0283
LysC	Wako, Osaka, Japan	121-05063

Continued on next page

Table 9 – continued from previous page

Item	Supplier	Catalog Nr.
Magnesium chloride hexahydrate	Sigma-Aldrich, St. Louis, MO, USA	M2670
Malic acid	Sigma-Aldrich, St. Louis, MO, USA	M1000
MEM Alpha Medium	Thermo Fisher Scientific, Waltham, MA, USA	22561
Methanol	VWR, Darmstadt, Germany	20847
Monopotassium phosphate	Merck KGaA, Darmstadt, Germany	104873
NaeI	New England BioLabs, Beverly MA, USA	R0190L
Octanoylcarnitine	Tocris Bioscience, Bristol, UK	0605
Oleic Acid	Sigma-Aldrich, St. Louis, MO, USA	O1008
Palmitate	Sigma-Aldrich, St. Louis, MO, USA	P0500
Polybrene Transfection Reagent	Merck KGaA, Darmstadt, Germany	TR-1003-G
Ponceau S solution	Sigma-Aldrich, St. Louis, MO, USA	P7170
Puromycin-Dihydrochlorid	Thermo Fisher Scientific, Waltham, MA, USA	A1113803
Rotenone	Sigma-Aldrich, St. Louis, MO, USA	R8875
Rotiphorese Gel 30 (37.5:1)	Carl Roth GmbH & Co. KG	3029.2
RPMI-1640	Sigma-Aldrich, St. Louis, MO, USA	R0883
Saponin	Sigma-Aldrich, St. Louis, MO, USA	S4522
Seahorse XF Calibrant	Agilent Technologies, Santa Clare, CA, USA	100840-000
Seahorse XF DMEM Medium, pH 7.4	Agilent Technologies, Santa Clare, CA, USA	103575-100
Seahorse XF Glucose Solution	Agilent Technologies, Santa Clare, CA, USA	103577-100
Seahorse XF Glutamine Solution	Agilent Technologies, Santa Clare, CA, USA	103579-100
Seahorse XF Pyruvate Solution	Agilent Technologies, Santa Clare, CA, USA	103578-100
Seahorse XFe24 Extracellular Flux Assay Kit	Agilent Technologies, Santa Clare, CA, USA	102340-100
SOC Outgrowth Medium	New England BioLabs, Beverly MA, USA	B9020
Sodium chloride	Merck KGaA, Darmstadt, Germany	106404
Sodium deoxycholate	Sigma-Aldrich, St. Louis, MO, USA	D6750
Sodium Dodecyl Sulfate	Bio-Rad Laboratories, Inc, Herculaes, CA, USA	1610302
Sodium fluoride	Sigma-Aldrich, St. Louis, MO, USA	S1504
Sodium orthovanadate	Applichem GmbH, Darmstadt, Germany	A2196
Sodium pyrophosphate decahydrate	Honeywell, Charlotte, NC, USA	71516

Continued on next page

Table 9 – continued from previous page

Item	Supplier	Catalog Nr.
Sodium pyruvate	Sigma-Aldrich, St. Louis, MO, USA	P2256
Succinate	Sigma-Aldrich, St. Louis, MO, USA	S2378
Sucrose	Merck KGaA, Darmstadt, Germany	107687
SYBR Safe DNA Gel Stain	Thermo Fisher Scientific, Waltham, MA, USA	S33102
Taurine	Sigma-Aldrich, St. Louis, MO, USA	T0625
TEMED	Carl Roth GmbH & Co. KG	2367.1
Trifluoroacetic acid	Honeywell, Charlotte, NC, USA	91699
TRIS	Sigma-Aldrich, St. Louis, MO, USA	T1503
Tris(2-carboxymethyl)phosphine	Thermo Fisher Scientific, Waltham, MA, USA	77720
TRIS-HCl	Sigma-Aldrich, St. Louis, MO, USA	T3253
Triton-X-100	Sigma-Aldrich, St. Louis, MO, USA	X100
Trypsin	Promega, Madison, WI, USA	VA9000
Trypsin (for cell culture)	Sigma-Aldrich, St. Louis, MO, USA	T1426
Tween20	Sigma-Aldrich, St. Louis, MO, USA	P9416

3.1.6 Consumables

Table 10: Consumables

Item	Supplier	Catalog Nr.
Ampliseal sealer, clear, for qPCR	Greiner Bio-One GmbH, Frickenhausen, Germany	676040
Bergström needle	Pelomi Medical, Albertslund, Denmark	
Cell culture flask T-75	Sarstedt AG & Co.KG, Nümbrecht, Germany	83.3911.002
Cell scraper	Corning B.V. Life Sciences, Amsterdam, Netherland, Amsterdam, The	3010
Combitips Adv.Biopur 5 mL	OMNILAB -Laborzentrum GmbH & Co KG	5431822
Combitips advanced 2,5 mL	OMNILAB -Laborzentrum GmbH & Co KG	5431803
Corning Cell Strainer 70 µm	Thermo Fisher Scientific, Waltham, MA, USA	10788201
Gel blotting sheets, Whatman	VWR, Darmstadt, Germany	10426994
Immobilon-P membrane, PVDF, 0.45 µm	Merck KGaA, Darmstadt, Germany	IPVH00010
Microplate PS F-Form	Greiner Bio-One GmbH, Frickenhausen, Germany	655101

Continued on next page

Table 10 – continued from previous page

Item	Supplier	Catalog Nr.
Nitrocellulose blotting membranes, 0.45 µm	VWR, Darmstadt, Germany	10600007
Nunc Cryogenic tubes 2ml	Thermo Fisher Scientific, Waltham, MA, USA	368632
PAXgene tubes	Qiagen, Hilden, Germany	762165
PCR SingeCap 8er-SoftStrips 0.2 mL	Biozym Scientific GmbH, Oldendorf, Germany	710980
Pipette Tips GP LTS 20 µL F 960A/10	Mettler Toledo, Columbus, OH, USA	30389274
Reloads Ep. 2 µL – 200 µL	OMNILAB -Laborzentrum GmbH & Co KG	5445685
Ritips 1.25 mL	Ritter GmbH (part of Aventor), Schwabmünchen, Germany	40002 – 0001
Safe-Lock Tubes 1.5 mL	Eppendorf, Hamburg, Germany	0030 120.086
Safe-Lock Tubes 2.0 mL	Eppendorf, Hamburg, Germany	0030 120.094
Sapphire Microplate, 96 Well	Greiner Bio-One GmbH, Frickenhausen, Germany	669285
Scepter Cell Counter Sensors	Merck KGaA, Darmstadt, Germany	PHCC360250
Seahorse XF24 cell culture microplates	Agilent Technologies, Santa Clare, CA, USA	100777-004
Serological Pipets 10 mL	Corning B.V. Life Sciences, Amsterdam, Netherland	4101
Serological Pipets 50 mL	Corning B.V. Life Sciences, Amsterdam, Netherland	4501
Serological Pipets 5 mL	Corning B.V. Life Sciences, Amsterdam, Netherland	4051
serum collecting tubes	Sarstedt AG & Co.KG, Nümbrecht, Germany	03.1397
Silverseal sealer, Aluminium	Greiner Bio-One GmbH, Frickenhausen, Germany	676090
STAGE tips SDB-RPS, polystyrenedivinylbenzene-reversed phase	CDS Analytical, Oxford, PA, USA	98-0604-0226-4
Syringe 2ml	B. Braun SE, Melsungen, Germany	4606027V
Syringe filters, PES, 0.45 µm	VWR, Darmstadt, Germany	514-0509
TipOne Filter Tip, graduated, 0.1 µL – 10 µL	STARLAB GmbH, Hamburg, Germany	S1121-3810-C
TipOne Filter Tip, graduated, 10 µL	STARLAB GmbH, Hamburg, Germany	S1123-1810-C
TipOne Filter Tip, graduated, 100 µL	STARLAB GmbH, Hamburg, Germany	S1123-1840-C

Continued on next page

Table 10 – continued from previous page

Item	Supplier	Catalog Nr.
TipOne Filter Tip, graduated, 1.000 µL	STARLAB GmbH, Hamburg, Germany	S1126-7810-C
Tissue Culture Dish 10 cm	TPP, Trasadingen, Switzerland	93150
Tissue Culture Dish 15 cm	TPP, Trasadingen, Switzerland	93100
Tissue culture testplate 12-well	TPP, Trasadingen, Switzerland	92012
Tissue culture testplate 24-well	TPP, Trasadingen, Switzerland	92024
Tissue culture testplate 48-well	TPP, Trasadingen, Switzerland	92048
Tissue culture testplate 6-well	TPP, Trasadingen, Switzerland	92006
Tissue culture testplate 96-well	TPP, Trasadingen, Switzerland	92096
Tube 15 ml, CELLSTAR, conical bottom	Greiner Bio-One GmbH, Frickenhausen, Germany	188271-N
Tube 50 ml, CELLSTAR, conical bottom	Greiner Bio-One GmbH, Frickenhausen, Germany	210261
Tube 50 ml, Falcon, conical bottom	OMNILAB -Laborzentrum GmbH & Co KG	FALC352070

3.1.7 Kits

Table 11: Kits

Kit	Supplier
ELISA kit IL34 (D3400)	R&D Systems, Minneapolis, MN, USA
ELISA kit IL6 (HS600C)	R&D Systems, Minneapolis, MN, USA
ELISA kit VEGFA (DVE00)	R&D Systems, Minneapolis, MN, USA
In-Fusion HD Cloning Kit	Takara Bio Inc., Kusatsu, Japan
MinElute PCR purification kit	Qiagen, Hilden, Germany
miRNease kit	Qiagen, Hilden, Germany
PAXgene Blood RNA kit	Qiagen, Hilden, Germany
Pierce BCA protein assay kit	Thermo Fisher Scientific, Waltham, MA, USA
Plasmid Maxi Kit	Qiagen, Hilden, Germany
QIA quick PCR purification	Qiagen, Hilden, Germany
QIAprep Spin Miniprep Kit	Qiagen, Hilden, Germany
QIAquick Gel Extraction Kit	Qiagen, Hilden, Germany

Continued on next page

Table 11 – continued from previous page

Kit	Supplier
QuantiFast SYBR Green PCR kit	Qiagen, Hilden, Germany
RNeasy Mini Kit	Qiagen, Hilden, Germany
Transcriptor First Strand cDNA Synthesis Kit	Roche, Mannheim, Germany
WT PLUS Reagent Kit	Thermo Fisher Scientific, Waltham, MA, USA

3.1.8 Laboratory equipment

Table 12: Laboratory equipment

Device	Supplier
ADVIA 1650 clinical chemical analyzer	Siemens Healthcare Diagnostics, Fernwald, Germany
ADVIA centaur immunoassay system	Siemens Healthcare Diagnostics, Fernwald, Germany
Agarose gel chamber midi	Harnischmacher Labortechnik, Kassel, Germany
Agilent 2100 Bioanalyzer	Agilent, Santa Clara, CA ,USA
Biofuge pico mikrolitercentrifuge	Heraeus, Hanau, Germany
C18 trap column	Thermo Fisher Scientific, Schwerte, Germany
Centrifuges 5427 R, 5415 R, 5804 R, 5417 R	Eppendorf, Hamburg, Germany
Corning CoolCell containers	Thermo Fisher Scientific
Dionex Ultimate 3000 RSLC	Thermo Fisher Scientific, Schwerte, Germany
GeneChip Scanner 3000 7G	Thermo Fisher Scientific, Schwerte, Germany
Gradient maker	Hoefer, Holliston, MA, USA
Heating block Thermostat Plus	Eppendorf, Hamburg, Germany
Hera Safe hood (KS 12)	Thermo Fisher Scientific
iMark Microplate Absorbance Reader	Bio-Rad Laboratories, Inc, Herculaes, CA, USA
Incubator Binder C150	BINDER GmbH, Tuttlingen, Germany
Incubator Binder CB210	BINDER GmbH, Tuttlingen, Germany
Incubator Function Line	Heraeus, Hanau, Germany
Laboratory balance ALJ160-4NM	Kern & Sohn, Balingen-Frommern, Germany
Laboratory balance BL1500	Sartorius, Göttingen, Germany
Laboratory balance RC210-D	Sartorius, Göttingen, Germany
Lightcycler 480 system	Roche, Mannheim, Germany
Magnetic stirrer MH15	Roth, Karlsruhe, Germany
Microscope Axiovert 25	Zeiss, Oberkochen, Germany

Continued on next page

Table 12 – continued from previous page

Device	Supplier
Milli-Q Gradient A10	Merk Millipore, Burlington, MA, USA
Nanodrop 2000	Thermo Fisher Scientific, Schwerte, Germany
nanoEase MZ HSS T3 Column	Waters, Milford, MA, USA
Neubauer chamber	Paul Marienfeld, Lauda-Königshofen, Germany
Odyssey infrared scanner	Licor, Lincoln, NE, USA
Oroboros Oxygraph 2k	Oroboros Instruments GmbH, Innsbruck, Austria
PerfectBlue Doppel-Gelsystem Twin ExW S	VWR, Darmstadt, Germany
Power supply Consort E 802	Consort nv, Turnhout, Belgium
Power supply E42/1	Behringwerke AG, Mahrburg, Germany
Precellys 24 homogenizer	Bertin, Montigny-le-Bretonneux, France
Probe Sonicator EppiShear	ActiveMotif, Carlsbad, CA, USA
Q-Exactive HF-X mass spectrometer	Thermo Fisher Scientific, Schwerte, Germany
Rainin EDP3-plus multichannel pipette	Mettler Toledo, Columbus, OH, USA
Scepter 2.0 handheld automated cell counter	Merck KGaA, Darmstadt, Germany
Seahorse XFe24 Analyzer	Agilent, Santa Clara, CA ,USA
semi-dry blotting chamber	Hölzel, Wörth, Germany
Shaker incubator TH 30	Edmund Bühler, Hechingen, Germany
SpeedVac	Concentrator plus, Eppendorf, Hamburg, Germany
Table centrifuge HSA 18340	Biozym Scientific GmbH, Oldendorf, Germany
Table shaker ST5 348/1	Assistent Hecht Glaswarenfabrik GmbH & Co KG
Thermocycler Mastercycler 5333	Eppendorf, Hamburg, Germany
Thermomixer Comfort 5355	Eppendorf, Hamburg, Germany
TissueLyser II	Qiagen, Hilden, Germany
Vortex Genie 2	Scientific industries, USA
Water Bath GFL 1003	Lauda-GFL, Burgwedel, Germany
Water Bath MP-7A Typ & Julabo MP-5 Circulator	Julabo GmbH, Seelbach, Germany

3.1.9 Molecular markers

Table 13: Molecular markers

Marker	Supplier	Catalog Nr.
Chameleon Duo pre-stained protein ladder	Licor, Lincoln, NE, U.S.A.	928-60000
Quickload 1 kb DNA ladder	New England BioLabs, Beverly MA, USA	N0468L
Quickload 100 bp DNA ladder	New England BioLabs, Beverly MA, USA	N0467L

3.1.10 Primers for qPCR

Table 14: Primers for qPCR

Gene	Supplier	Catalog Nr.
CXCL1 (human)	Qiagen, Hilden, Germany	QT02559186
CXCL5 (human)	Qiagen, Hilden, Germany	QT00095431
IL6 (human)	Qiagen, Hilden, Germany	QT00083720
IL34 (human)	Qiagen, Hilden, Germany	QT00063119
OSM (human)	Qiagen, Hilden, Germany	QT00209286
TBP (human)	Qiagen, Hilden, Germany	QT00000721
TGFA (human)	Qiagen, Hilden, Germany	QT00033887
TNF (human)	Qiagen, Hilden, Germany	QT01079561
TNFSF14 (human)	Qiagen, Hilden, Germany	QT01011682

3.1.11 Software, databases and additions

Table 15: Software

Software	Supplier
DatLab v7.4.0.4	OROBOROS INSTRUMENTS, Innsbruck, Austria
Excel 2019	Microsoft, Redmond, WA, USA
Image Studio Lite v5.2	Licor, Lincoln, NE, USA
JabRef v5.5	JabRef e.V., Sindelfingen, Germany
Lightcycler 480 software v1.5.0.39	Roche, Mannheim, Germany
OLINK NPX Manager v3.1.0.393	Olink Holding, Uppsala, Sweden
Photoshop CS6	Adobe Inc., Mountain View, CA, USA
Proteome discoverer v2.4.1.15	Thermo Fisher Scientific, Schwerte, Germany

Continued on next page

Table 15 – continued from previous page

Software	Supplier
R v4.2.1	R Core Team (Ross Ihaka, Robert Gentleman)
Rstudio v2022.02.3+492	Posit PBC (Joseph J. Allaire)
Seahorse Wave v2.6.3.5	Agilent Technologies, Santa Clara, CA , USA
Serial Cloner v2.6.1	Serial Basics (Frank Perez)
Transcriptome Analysis Console v4.0.0.25	Thermo Fisher Scientific, Schwerte, Germany

Table 16: Databases

Database	Notes	Source
GeneCards	online v5.16.0 Build 1012	`https://www.genecards.org/`
gProfiler	published Nov 02 2022 (Ensemble v107)	`https://biit.cs.ut.ee/gprofiler/gost`
HGNC	downloaded on 24.11.2022	`https://www.genenames.org/`
Human protein atlas	version 21.1 (Ensemble v103.38)	`https://www.proteinatlas.org/`
MitoCarta	version 3.0	`https://www.broadinstitute.org/mitocarta/mitocarta30-inventory-mammalian-mitochondrial-proteins-and-pathways`
MitoEvidence (IMPI)	version 2021Q4pre	`https://www.mrc-mbu.cam.ac.uk/research-resources-and-facilities/impi`
SwissProt human database	release February 2020	`https://www.uniprot.org/help/downloads`
Uniprot	downloaded on 02.02.2022	`https://www.uniprot.org/`

Table 17: R packages

R package	Version	R package	Version
base	4.2.1	magrittr	2.0.3
Biobase	2.56.0	manipulateWidget	0.11.1
BiocGenerics	0.42.0	markdown	1.1
BiocParallel	1.30.3	MASS	7.3.58.1
biomaRt	2.52.0	Matrix	1.5.1
Biostrings	2.64.1	MatrixGenerics	1.8.1

Continued on next page

Table 17 – continued from previous page

R package	Version	R package	Version
bumphunter	1.38.0	matrixStats	0.62.0
Cairo	1.6.0	meffil	1.3.1
ChAMP	2.24.0	methods	4.2.1
ChAMPdata	2.28.0	mgcv	1.8.40
cluster	2.1.4	minfi	1.42.0
colorRamps	2.3.1	multcomp	1.4.20
ComplexHeatmap	2.12.1	mvtnorm	1.1.3
datasets	4.2.1	nlme	3.1.159
DESeq2	1.36.0	openxlsx	4.2.5
DMRcate	2.10.0	parallel	4.2.1
DNAcopy	1.70.0	plotly	4.10.0
doSNOW	1.0.20	plyr	1.8.7
dplyr	1.0.10	preprocessCore	1.58.0
DT	0.25	purrr	0.3.4
fastICA	1.2.3	quadprog	1.5.8
forcats	0.5.2	qvalue	2.28.0
foreach	1.5.2	readr	2.1.3
futile.logger	1.4.3	reshape2	1.4.4
gdsfmt	1.34.1	rlang	1.0.6
genefilter	1.78.0	RPMM	1.25
GenomeInfoDb	1.32.4	RSpectra	0.16.1
GenomicRanges	1.48.0	rstudioapi	0.14
ggplot2	3.3.6	S4Vectors	0.34.0
ggrepel	0.9.1	sandwich	3.0.2
ggsignif	0.6.3	SmartSVA	0.1.3
gprofiler2	0.2.1	snow	0.4.4
graphics	4.2.1	statmod	1.4.37
grDevices	4.2.1	stats	4.2.1
grid	4.2.1	stats4	4.2.1
gridExtra	2.3	stringr	1.4.1
htmlwidgets	1.5.4	SummarizedExperiment	1.26.1
httr	1.4.4	survival	3.4.0
Illumina450ProbeVariants.db	1.32.0	sva	3.44.0
IlluminaHumanMethylationEPICmanifest	0.3.0	svDialogs	1.1.0
illuminaio	0.38.0	tcltk	4.2.1

Continued on next page

Table 17 – continued from previous page

R package	Version	R package	Version
IRanges	2.30.1	tcltk2	1.2.11
isva	1.9	TH.data	1.1.1
iterators	1.0.14	tibble	3.1.8
JADE	2.0.3	tidyr	1.2.1
knitr	1.40	tidyverse	1.3.2
limma	3.52.4	utils	4.2.1
lme4	1.1.30	VennDiagram	1.7.3
lmtest	0.9.40	XVector	0.36.0
locfit	1.5.9.6	zoo	1.8.11

References to the R packages used are written separated in the reference section on page 114.

3.2 Cultivation of cells

3.2.1 C2C12 cell culture and insulin treatment

C2C12 mouse skeletal muscle cells were seeded in a density of 1.0x10^5 cells per well in a 6-well plate with 2 mL C2C12 growth medium. After reaching 80 % – 90 % confluency, the medium was changed to C2C12 fusion medium. The medium was changed regularly every 2 – 3 days. On day 5 of differentiation, the mouse myotubes were treated with either 100 ng/mL doxycycline diluted in growth medium or DMSO in the same dilution in growth medium. After 48 h of treatment, the myotubes were used for further experiments. For treatment with insulin, the cells were fasted by adding 2 mL C2C12 fasting medium per well for at least 3 h. Afterwards, 10 nM insulin was added for 10 min. All treatments were performed at standard incubation parameters. The cells were incubated at 37 °C and 5 % CO_2.

3.2.2 Human skeletal muscle cell culture and IL34 treatment

Human myoblasts were seeded in a density of 1.0x10^4 per well in a 6-well plate with 2 mL hMTs growth medium. After reaching 80 % – 90 % confluency, the medium was changed to hMTs fusion medium. The medium was changed regularly every 2 – 3 days. After 10 days of differentiation, the human myotubes were used for further experiments. For the treatment with IL34, the cells were fasted in hMTs fasting medium for 3 h. Afterwards, 100 µL of 100 nM was added for 1 min or 5 min. The treatment was immediately stopped by washing with PBS and lysis with 100 µL RIPA buffer containing inhibitors (see Table 6). For the negative control, 100 µL PBS was used, and for the positive control, 100 µL of 0.1 µM TPA and 1 µg/mL LPS. All treatments were performed at standard incubation parameters. The cells were incubated at 37 °C and 5 % CO_2.

3.2.3 THP-1 cell culture and IL34 treatment

THP-1 cells were cultured in T25 cell culture flasks and grown until confluency. For IL34 experiments, 1.5x10^6 cells were place in 1.5 mL safe-lock tubes and centrifuged for 5 min at 500g. The supernatant was discarded, and the remaining cells were treated with 100 µL of 100 nM IL34 for 1 min or 5 min. For the negative control, 100 µL PBS was used, and for the positive control, 100 µL of 0.1 µM TPA containing 1 µg/mL LPS. The treatment was immediately stopped using 1 mL ice-cold PBS. The cells were pelleted by centrifugation for 5 min at 500g. The supernatant was discarded, and 100 µL RIPA buffer containing inhibitors (see Table 6) was added for lysis. All treatments were performed at standard incubation parameters. The cells were incubated at 37 °C and 5 % CO_2.

3.3 Seahorse measurement

C2C12 mouse muscle cells were seeded in a density of 3.0x10^3 cells per well in a Seahorse XFe24 cell culture microplate with 500 µL C2C12 growth medium. The cells were cultured and treated as written in section 3.2.1. After 48h treatment, the cells were washed 3x with PBS, and 500 µL Seahorse assay medium was added. Mitochondrial respiration was measured before substrate injection and after injection with a final concentration of 1 mM oligomycin, 2 mM FCCP, and 5 mM rotenone with 5 µM antimycin A. For each injection, 3 cycles of 3 min mix, 2 min waiting, and 3 min measurement were considered. Experiments were performed with five wells per treatment. The measurements were performed using the Seahorse XFe24. After the measurement, the cells were lysed in 25 µL RIPA buffer containing inhibitors (see Table 6), and the protein amount was measured using Pierce BCA protein assay kit. The oxygen consumption rate (OCR) per well was normalized to the protein amount. The key parameters were calculated per well as written in the standard operating procedure (SOP), and the mean value per treatment are shown. The analysis was performed using the Seahorse Wave software.

3.4 Plasmid construction

Plasmids containing the gene of interest were generated by GenScript (https://www.genscript.com/). The coding sequence of the gene of interest was synthesized and cloned into the empty vector Retro-X™ Tet-One™ puro (pRXTOP). A 3x flag-tag was added to the N-terminal site of all sequences for simplified detection by antibodies. The plasmids were amplified using high competent *E. Coli* transformed by heat shock of 45 s at 42 °C and 5 ng plasmid. The bacteria were cultured in 2 mL LB medium overnight at 37 °C. The plasmids were purified using the QIAprep Spin Miniprep Kit according to the SOP and verified by enzymatic digestion using appropriate restriction enzymes and sequencing. Verified plasmids were amplified using the glycerol stock of the transformed high competent bacteria in 100 mL LB medium overnight at 37 °C. The plasmids were purified using the Plasmid Maxi Kit according to SOP and stored at −20 °C. The bacteria glycerol stocks were stored at −80 °C.

3.5 C2C12 stable cell line generation

Platinum E cells were seeded in a density of 5.0x10^5 cells per well in a 6-well plate with 2 mL C2C12 growth medium. After 24 h, the cells were transfected using the calcium phosphate method. Briefly, 5 µg plasmid was mixed with 10 µL 2.5 M $CaCl_2$ in a total volume of 100 µL 0.1x TE buffer. The mixture was added dropwise into 100 µL of 2x HEBS buffer and instantly added to the cells. After 24 h, the medium was exchanged with fresh growth medium. On the same day, C2C12 cells were seeded in a density of 3.0x10^4 cells per well in a 6-well plate with 2 mL C2C12 growth medium. After 24 h, the 2 mL supernatant of the Platinum E cells was collected and filtered through a 0.45 mM PES filter. From the filtered supernatant containing the virus, 1 mL was mixed with 2 mL growth medium, and polybrene was added to a final concentration of 2 µg/mL. The medium of the C2C12 cells was replaced with the virus-polybrene mixture. The cells were centrifuged for 60 min at 1,200g and room temperature. Afterwards, the cells were placed in the incubator. After 24 h, the C2C12 were enzymatically detached using trypsin-EDTA for 8 min in the incubator. The detached cells were transferred onto a 15 cm cell culture dish, and 2.5 µg/mL puromycin was added. After 8 days of selection and regular change of selection medium (growth medium + puromycin), the cells were enzymatically detached as previously stated, counted using the cell scepter, and frozen in a density of 5.0x10^5 cells per cryo vials at −80 °C. After cooling, the vials were stored for long-term storage in liquid nitrogen. The cells were incubated at 37 °C and 5 % CO_2 if not otherwise stated.

3.6 Immunoblotting

For immunoblotting experiments, the cells were cultured as written in section 3.2.1 and section 3.2.2. The cells were lysed in RIPA buffer containing inhibitors (see Table 6) and frozen overnight at −80 °C. The lysed cells were transferred into a 1.5 mL tube and centrifuged for 15 min at >20,000g and 4 °C. The supernatant was collected, and the protein amount was determined using Pierce BCA protein assay kit. All measurements were performed in duplicates. At least 15 µg protein was diluted in a total volume of 30 µL ultra-pure water containing 1x Laemmli sample buffer. The protein mixture was heated for 5 min at 95 °C and centrifuged for 1 min. The samples were loaded onto a 10 % (v/v) SDS polyacrylamide gel and run for 1.5 h at 150 V. The stacking gel was removed, and the proteins in the separation gel were blotted onto a methanol-activated PVDF membrane by semi-dry blotting at 86 mA per gel for 3 h. The protein blotting was confirmed by incubating the membrane in Ponceau S solution for 1 min. The membrane was blocked in NET-G buffer for 3x 10 min at room temperature. The primary antibody was diluted in NET-G buffer and incubated overnight at 4 °C or for 3 h at room temperature. The secondary antibody was diluted in NET-G buffer and incubated for 1 h – 2 h at room temperature. All washing steps between antibody incubations were performed in TBS-T buffer for 3x 10 min at room temperature.

3.7 Quantitative polymerase chain reaction (qPCR)

3.7.1 RNA extraction

RNA was extracted from cultured cells using the RNeasy Mini kit according to the SOP. In short, cultured cells were washed once with PBS and lysed with 350 µL RLT-buffer supplemented with 1 % (v/v)-β-mercaptoethanol per well of a 6-well plate. The plates were frozen at −80 °C. The lysed cells were applied onto the QIAshredder spin column and centrifuged for 1 min. One volume (350 µL) of 70 % (v/v) ethanol was added, transferred to the RNeasy spin column, and centrifuged. The spin column was once washed by adding 350 µL RW1 buffer. Subsequently, DNase treatment was performed by adding 80 µL DNase I incubation mix (10 µL DNase I (1,500 Kunitz units) in RNAse-free water with 70 µL RDD buffer) to the spin column for 15 min. Afterwards, the columns were washed once by adding 350 µL RW1 buffer and once by adding 500 µL RPE buffer. The column was centrifuged once more to remove any residual liquid. RNA was eluted in RNAse-free water by centrifugation. All centrifugation steps were performed at >10,000 rpm. Quality control and concentration were measured using the Nanodrop 2000.

3.7.2 Reverse transcription

Reverse transcription from RNA to cDNA was performed using the Transcriptor First Strand cDNA Synthesis Kit from Roche according to the SOP. In short, 500 ng RNA was diluted in 10 µL RNAse-free water and denatured for 10 min at 65 °C. Next, 10 µL of reverse transcription mastermix consisting of 2 µL random hexamers (600 µM), 1 µL anchored-oligo$(dT)_{18}$ primers (50 µM), 4 µL 5x buffer, 0.5 µL RNAse inhibitor (40 U/µL) and 0.5 µL reverse transcriptase (20 U/µL) was added. The mixture was heated for 10 min at 25 °C, 30 min at 55 °C, and 5 min at 85 °C. Subsequently, 80 µL PCR-grade water was added and stored at −80 °C.

3.7.3 Real-time quantification in Lightcycler 480

The real-time quantification was performed using the Lightcycler 480 according to the SOP. In short, 5 µL of previously extracted RNA was mixed with 15 µL mastermix consisting of 10 µL 2x QuantiFast, 2 µL of 10 µM primer mix, and 3 µL water in Sapphire 96-well microplates. The RNA was denatured for 5 min at 95 °C. Subsequently, 40 cycles of denaturing, annealing, and elongation were conducted by heating 10 s at 95 °C and 30 s at 62 °C. Next, RNA was denatured completely by heating 10 s at 95 °C, 5 s at 62 °C, and continuous heating up to 98 °C. Lastly, the RNA was cooled down to 4 °C. The expressed RNA was quantified using a standard curve ranging from 5 pg/µL to 0.5 ag/µL. According to the SOP, the standard was prepared from isolated RNA of cultured cells and purified using the MinElute PCR purification kit from Qiagen. The standard samples were measured at the Nanodrop 2000, diluted to 5 ng/µL, and stored in aliquots at −20 °C. The expression was quantified using the Lightcycler 480 software and determining the crossing points of the standard and samples.

3.8 ELISA measurement of IL34

The ELISA measurement was performed with the help of Nadine Sanabria Valdés using the human interleukin 34 (IL34) Quantikine ELISA Kit from R&D Systems according to the SOP. Briefly, 100 µL assay diluent was added to each well of a 96-well plate. Afterwards, 50 µL of undiluted sample or standard control was added and incubated at room temperature for 2 h. The solution was aspirated, wells were washed four times, and 200 µL of conjugate was added to the well. The plates were sealed, and the conjugate was incubated at room temperature for 2 h. Conjugate was aspirated and washed four times. Subsequently, 200 µL substrate solution was added and incubated light-protected at room temperature for 30 min. Afterwards, 50 µL stop solution was added. Lastly, the plate was measured at 450 nm wavelength within 30 min.

3.9 RNA isolation of whole blood

The isolation and measurement were performed by Alke Guirguis from our group. Whole blood samples were collected in a fasting state in PAXgene tubes. RNA was isolated from whole blood samples using the PAXgene Blood RNA kit (Qiagen) according to the SOP. Briefly, samples were incubated for 2 h at room temperature and afterwards centrifuged for 10 min at 4,000 rpm. The supernatant was removed and the pellet was washed with 4 mL RNase-free water, and centrifuged for 10 min at 4,000 rpm. Next, 350 µL BM1 buffer was added to dissolve the pellet. Afterwards, 300 µL BM2 buffer and 40 µL proteinase K were added and incubated for 10 min at 55 °C. The mixture was transferred onto spin columns that were centrifuged for 3 min at maximum speed. The supernatant was removed, and the pellet was washed with 700 µL isopropanol and centrifuged in the spin column for 1 min at 17,000g. Next, 350 µL BM3 buffer was added and centrifuged. Next, 80 µL DNase mixture (10 µL DNase I (1,500 Kunitz units) in RNAse-free water with 70 µL RDD buffer) was added onto the spin column and incubated for 15 min at room temperature. The spin column was washed once with 350 µL BM3 buffer and twice with 500 µL BM4 buffer with 2 min centrifugation at 17,000g. Afterwards, the supernatant was removed, and the column was centrifuged for 1 min at 17,000g to remove any residual liquid. The RNA was eluted in 40 µL BR5 buffer by centrifugation for 1 min at 17,000g. RNA was reverse transcribed to cDNA as mentioned in section 3.7.2 with the minor change of using 1 µg RNA.

3.10 Training intervention study (NRE1 and NRE2)

The exercise training intervention study used here was conducted at the Institute for Diabetes Research and Metabolic Diseases (IDM) of Helmholtz Munich at the University of Tübingen and registered as NCT03151590 at Clinicaltrials.gov. None of the following parts described in section 3.10 and section 3.11 were performed by myself. The clinical and mitochondrial respiration data were first published by Hoffmann et al. [145]. The following information on study participants and design is given to describe the biological sample material (plasma, serum, skeletal muscle biopsies), which are the basis of my thesis. The training study with all six time points is schematically shown in Figure 1. Time points in this thesis are written uniformly as T0 – T5. When time points are compared by a fold change or difference it is written as TxTy, where x and y are one of the six time points. For fold changes TxTy $= \frac{Tx}{Ty}$, and differences (Δ) TxTy $=$ Tx $-$ Ty. Additionally, the NRE1 training intervention study was used in parts of the thesis in a combined analysis with the NRE2 study. This distinct study, performed with a different set of subjects, was published by Böhm et al. [144]. The main difference in the NRE1 study compared to the NRE2 study is that biological samples were solely collected at the resting time points (T0 and T5 in Figure 1).

3.10.1 Study participants

For the training intervention, only healthy subjects were recruited. All were sedentary, which was defined as less than 120 min physical activity per week. Subjects had a high risk for T2DM, which was defined by having at least one of the following factors: BMI greater than 27 $\frac{kg}{m^2}$, family history of at least first degree of T2DM, or former GDM. In total, 26 volunteers fitted these criteria, of which one was excluded due to a newly diagnosed autoimmunity thyroiditis. Therefore, 25 subjects were included in the final analysis. The anthropometric data are summarized in Table S1. Participants with significant medical conditions were excluded after a thorough assessment, including medical history, medication review, physical examination, routine laboratory tests, and electrocardiogram analysis. Written consent was obtained from all participants enrolled in the training intervention study. The study protocol was approved by the ethics committee of the University of Tübingen and conducted in accordance with the principles outlined in the Declaration of Helsinki.

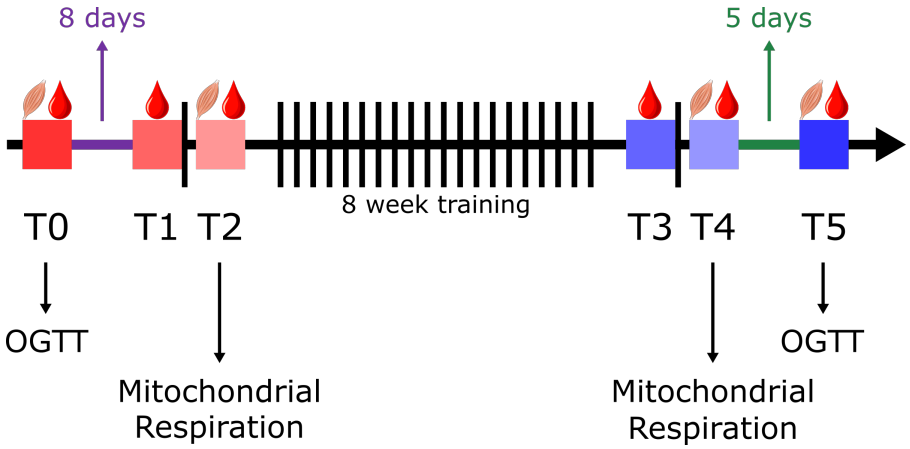

Figure 1: Schematic representation of the NRE2 training study. Representation of the NRE2 study with all six time points. Pre-intervention time points are marked in red, while post-intervention time points are marked in blue. Vertical lines represent one training bout. Muscle images are placed at time points where muscle biopsies were obtained 1 h after exercise or OGTT, while blood drops represent blood sample collection 5 min after exercise or in a fasted state. Time points T0 and T5 represent resting time points before and after the 8-week training intervention. Time points T1 and T3 represent resting time points before the first and last training bout. Time points T2 and T4 represent acute time points right after the first and last training bout. OGTT = oral glucose tolerance test.

3.10.2 Study design

Participants performed an aerobic, supervised 8-week endurance training intervention. Training intensity was individually set to 80 % of the VO_2peak, which was determined before the intervention and kept for each subject throughout the training intervention. All participants performed an OGTT 8 days before and 5 days after the training intervention program. The OGTT was conducted after overnight fasting by giving the participants 75 g glucose in solution. Blood samples were collected at the time points 0 min, 30 min, 60 min, 90 min, and 120 min after the glucose intake. Additionally, blood samples were collected before the glucose intake for routine clinical parameters. Muscle biopsies from the *vastus lateralis* were taken at the resting time points before and after the training intervention, 60 min after the OGTT, and 60 min after the first and last exercise bout of the training intervention. The participants had a standardized breakfast consisting of 1 bun, 20 g butter, 1 slice of cheese, 150 g apple puree, and water *ad libitum* 45 min before the first and last exercise bout.

3.10.3 Routine analysis and anthropometry

The clinical routine parameters were measured using the ADVIA 1650 clinical chemical analyzer and ADVIA centaur immunoassay system. The muscle and body fat mass and distribution were measured by magnetic resonance imaging. The insulin sensitivity index was estimated by using the formula and method developed by Matsuda and DeFronzo (ISI_{Mats}) [154] and measured at the resting time points T0 and T0 (Figure 1). In short, the insulin concentrations (Ins) and glucose concentrations (Glc) are used with the following formula:

$$\frac{10,000}{Ins_{0min} * Glc_{0min} * Ins_{mean} * Glc_{mean}}$$

$$\text{with} \quad Ins_{mean} = \frac{Ins_{0min} * Ins_{30min} * Ins_{60min} * Ins_{90min} * Ins_{120min}}{5}$$

$$\text{and} \quad Glc_{mean} = \frac{Glc_{0min} * Glc_{30min} * Glc_{60min} * Glc_{90min} * Glc_{120min}}{5}$$

3.10.4 Performance measurement and exercise intervention

Each subject performed every exercise bout at an individual training intensity. Before and after the training intervention, cardiopulmonary exercise testing on the bike was conducted to determine the individual aerobic threshold and VO_2peak. Additionally, the heart rate was traced. The heart rate fitted to 80 % VO_2peak was set as the target heart rate to control the exercise intensity individually. Of 25 participants, 21 completed 20 training session, whereas the remaining 4 completed either 18, 19, 21, or 24 training sessions. Each exercise consisted of running 30 min on the treadmill and cycling 30 min on the bike.

3.11 Skeletal muscle biopsies

3.11.1 Biopsy collection

Muscle biopsies were taken from the *vastus lateralis* of each subject. The biopsies were collected by cutting the skin, fat tissue, fascia, and muscle epimysium using a sterile scalpel under local anesthesia. A piece of the muscle was collected using the Bergström needle. The remaining wound was treated *lege artis* together with a compression bandage for at least 12 h.

3.11.2 High-resolution respirometry measurement

Results of the high-resolution respirometry were already published by Hoffmann et al. [145]. The respiration measurement was performed with muscle biopsies from the time points T2 and T4 (Figure 1). In short, single fibers were picked under binoculars in a drop of MIR05 on ice. The fibers were treated with saponin (50 µg/mL in MIR05 buffer) for 30 min at 4 °C and slow shaking. Subsequently, three washing steps with MIR05 were conducted for 10 min at 4 °C. Afterwards, 2 mg permeabilized and washed fibers were placed in one chamber of Oroboros Oxygraph 2k in a total volume of 2 ml MIR05. During the measurement, the temperature was kept constant at 37 °C and oxygen concentration between 100 µM and 180 µM. The following substrates were added in this order to the chamber: 1.28 µM malate, 0.5 µM octanoylcarnitine, 2.5 mM ADP, 5 mM sodium pyruvate, 2.5 mM succinate, 10 µM cytochrome c, 125 nM stepwise titration of FCCP, 1.25 µM rotenone, 5 µM antimycin A. The non-mitochondrial respiration was subtracted from each measurement, and the oxygen consumption rates were normalized to the wet tissue weight. The maximal coupled respiration used in my thesis corresponds to the oxygen consumption rate after adding succinate.

3.12 Proteomics

3.12.1 Sample preparation

The sample preparation and measurement were done at the Helmholtz center Munich in the metabolomics and proteomics core facility (Dr. Stefanie Hauck) and performed by Dr. Christine von Törne. Frozen muscle biopsies were supplemented with 200 µL of pre-cooled sodium deoxycholate lysis buffer (4 % (w/v) sodium deoxycholate, 100 mM TRIS-HCl pH 8.5). Samples were homogenized by shaking twice for 20 s with 5,500 cycles per minute and 5 s break in between using 1.4 mm ceramic beads in the Precellys 24 homogenizer. Homogenized samples were heated for 5 min at 95 °C and rapidly frozen with dry ice. Afterwards, samples were sonicated at an intensity of 80 with 1 s pulse and 5 s off for 5 intervals using the Probe Sonicator EppiShear. Protein concentration was determined using Pierce BCA protein assay kit, and 800 µg per sample were used. Protein samples were reduced and alkylated simultaneously using 20 mM chloroacetamide and 5 mM tris(2-carboxymethyl)phosphine, while heating for 10 min at 45 °C. Afterwards, proteins were digested overnight with a protein-to-enzyme ratio of 1:100 for both LysC and trypsin using a ThermoMixer with a shaking rate of 2,000 rpm at 37 °C. For whole proteome samples, 40 µg peptide solution was cleaned-up by loading onto three-layer styrenedivinylbenzene-reversed phase sulfonated STAGE tips.

STAGE tips were previously activated by washing with 100 % acetonitrile, 30 % (v/v) methanol in 1 % (w/v) trifluoroacetic acid (TFA), and 0.2 % (w/v) TFA. The following adjustments were performed to the protocol described by Kulak et al. [155]: Washing with 100 µL TFA dissolved in ethyl acetate followed by 100 µL 1 % (w/v) TFA dissolved in isopropanol and 150 µL 0.2 % (w/v) TFA. The samples were eluted with 5 % (w/v) NH_4OH dissolved in 80 % (v/v) acetonitrile and fully dried using the SpeedVac for 40 min at 45 °C. Final samples were stored at −20 °C.

3.12.2 Measurement

Proteins were measured using a liquid chromatography (LC) separation and performing a tandem mass spectrometry (MS/MS) proteomics approach. LC-MS/MS analysis was performed in data-dependent acquisition mode. MS analysis was performed using a Q-Exactive HF-X mass spectrometer, which was online coupled to an Ultimate 3000 RSLC. Tryptic digested samples were automatically loaded onto a C18 trap column (300 µM inner diameter × 5 mm, Acclaim PepMap100 C18, 5 µM, 100 Å) using a flow rate of 30 µL/min. Additional separation was performed by using a C18 reversed phase analytic column nanoEase MZ HSS T3 Column (100 Å, 1 µM, 75 µM x 250 mm) using a flow rate of 250 nl/min. A 95 min non-linear acetonitrile gradient ranging from 3 % (v/v) – 40 % (v/v) in 0.1 % (v/v) formic acid was used. MS spectrums were captured in high-resolution at 60,000 full width at half maximum. The mass range was set to 300 – 1,500 m/z. The automatic gain control target was set to 3×10^6 and a maximum injection time of 30 ms. For further fragmentation, the 15 most abundant peptide ions from the first MS scan were selected if they were doubly charged in combination with a dynamic exclusion time of 30 s. The following MS/MS spectrum was captured at a resolution of 15,000. The automatic gain control target was set to 1×10^5 and a maximum injection time of 50 ms. Spectra were captured in profile mode, and the normalized collision energy was set to 28.

3.12.3 Data processing

The data processing, transforming spectra into protein identifications, and quantification were performed in cooperation with Dr. Christine von Törne. The data filtering, statistical analysis, and all subsequent work were carried out by myself. Data processing was performed with the proteome discoverer software for the identification of proteins and peptides using the integrated database search algorithm Sequest HT against the SwissProt human database. The criteria were defined as only fully tryptic specificity, a maximum of 2 missing tryptic cleavages, and a 10 ppm and 0.02 Da tolerance for precursor mass and fragment mass, respectively. The static modification was carbamidomethylation of cysteine, whereas the dynamic modifications comprised oxidation of methionine, deamidation of glutamine and asparagine, and a combination of methionine loss with acetylation of the protein N-terminus. The Percolator algorithm validation was applied, and only the top hit of a matched peptide with the peptide spectrum was used. The false-discovery rate (FDR) and posterior error probability were set to <0.01. Protein abundance was calculated by adding up all single abundances of admissible peptides using the highest maximal intensity values. Data was normalized to the total protein amount to correct for sample loading errors. Only proteins with at least 90 % quantified data for at least one experimental group were used for analysis to ensure reproducibility. Afterwards, principal component analysis (PCA) was used to detect outliers, resulting in the exclusion of one sample at the post-acute time point (T4). This sample was 9x above the median absolute deviation due to a high number of missing values (>15 %). Missing values in the remaining samples ($\approx$ 2,600 values, 1.4 %) were imputed using a downshift of 1.5 from the mean and a width of 0.5 from the SD. Differences in the protein amount between time points were calculated using (paired) limma analysis. The correlations were calculated using the Pearson correlation to determine the correlation direction and unadjusted p-values. In the case of p-value adjustment, a linear model was calculated. MitoCarta 3.0 was used for the annotation to mitochondria. Enrichment analyses were performed

using gProfiler. For the heatmaps, the data was sorted using Euclidean distance complete linkage clustering. The proteomics data was $\log_2$-transformed. For time point comparisons, the fold change was calculated.

3.13 Transcriptomics

3.13.1 Sample preparation

The frozen muscle biopsy was homogenized in buffer RLT using the TissueLyser II (Qiagen, Hilden, Germany). Afterwards, the RNA was extracted and purified using the miRNeasy fibrous tissue Kit (Qiagen, Hilden, Germany). The purified RNA was verified for high-quality using the Agilent 2100 Bioanalyzer, and only RNA with an integrity number of at least 7 or higher was used.

3.13.2 Measurement

Amplification and measurement were done by Dr. Martin Irmler (Institute of Experimental Genetics, Helmholtz Zentrum München). Amplified cDNA was hybridized on Human Clariom S arrays (Thermo Fisher Scientific). Staining and scanning (GeneChip Scanner 3000 7G) was done according to manufacturer's instructions.

3.13.3 Data processing

Data processing was done in cooperation with Dr. Martin Irmler. The statistical analysis and subsequent work were carried out by myself. Quality control was performed with the Transcriptome Analysis Console (TAC; version 4.0.0.25; Thermo Fisher Scientific), which was also used for gene annotation (Clariom_S_Human.r1.na36.hg38.a1.transcript.csv) and to obtain SST-RMA data. Statistical analysis of the data was performed in RStudio (v4.2.1). Differential gene expression was calculated by a (paired) gene-wise limma t-test. Background correction and reduction were applied using the detection above background (DABG). Genes with DABG p-value < 0.05 in at least 50 % or more in at least one of the treatment groups for each comparison were used for the analysis. The transcriptomics data was $\log_2$-transformed. For time point comparisons, the fold change was calculated.

3.14 Epigenomics

3.14.1 Sample preparation

The genomic DNA isolation was done in cooperation with the German institute of Human Nutrition (DIfE, Potsdam) in the group of Prof. Dr. Annette Schürmann and performed by Dr. Meriem Ouni and Leona Kovac. From the frozen muscle biopsies, genomic DNA was extracted using Invisorb Genomic DNA Kit II (STRATEC Molecular GmbH, Berlin, Germany). Isolated genomic DNA samples were sent to Eurofins Genomics GmbH (Ebersberg, Germany) for further processing.

3.14.2 Measurement

The measurement was performed by Eurofins Genomics GmbH. Hybridization was performed on Infinium MethylationEPIC BeadChip (Illumina, San Diego, CA) GEO:GPL21145. The MethylationEPIC 850K BeadChip covers over 935,000 methylation sites (CpG sites) located in the gene body, promotor site, enhancer region, and CpG-islets.

3.14.3 Data processing

The data processing was performed in cooperation with Markus Jähnert at the DIfE. The statistical analysis and subsequent work were carried out by myself. Measured data was processed using RStudio (v4.2.1). From the data, 3 sex and 2 age outliers were excluded, and only full data sets

per participant were included. Furthermore, the data was filtered for bad probes, non-CpG sites, gonosomal chromosomes, CpG sites near single nucleotide polymorphism, and multihits. Quality control was done using sample clustering and density plots. Beta-mixture quantile normalization (BMIQ) was applied for intra-sample normalization and singular value decomposition (SVD) to distinguish between biological and technical variations. By applying ComBat batch correction using an empirical Bayes framework, the data was corrected for age. Limma analyses were performed for statistical analysis. Additionally, the data was merged with the transcriptome data. For this, the position of the transcript on the chromosome was extended for 2,000 base pairs on both sites, and CpG sites inside the transcript position were annotated. The epigenomics data was $\log_2$-transformed. For time point comparisons, the difference was calculated.

3.15 Proximity extension assay (PEA)

3.15.1 Sample preparation

Blood samples were collected from all participants in a fasted state. For serum collection, the blood samples were collected in serum collecting tubes (No. 03.1397, Sarstedt) and incubated for 30 min on ice. Subsequently, the tubes were centrifuged for 10 min at 2,000 g and 4 °C. The samples were aliquoted and frozen at −80 °C.

3.15.2 Measurement

The measurement was performed in cooperation with the Olink Platform of the Core Facility Metabolomics and Proteomics at Helmholtz Munich. Collected serum samples were measured using the OLINK Target 96 Inflammation panel. The panel contains 92 pro- and anti-inflammatory cytokines and chemokines, as well as growth factors and factors involved in acute inflammation, angiogenesis, endothelial activation, immune response, and fibrosis. Additionally, the two cytokines, IL6 and VEGFA, were measured using an ELISA kit (R&D Systems; VEGFA catalog No. DVE00, Antibody Registry: AB_2800364; IL6 catalog No. HS600C, Antibody Registry: AB_2893335). Extracted RNA from whole blood samples was measured by qPCR using the LightCycler 480 according to section 3.7.3 and primers listed in Table 14.

3.15.3 Data processing

The data processing was done by Dr. Miriam Hoene from our group. The statistical analysis and subsequent work were carried out by myself. Measured OLINK data were analyzed with the OLINK NPX Manager (v3.1.0.393). The values are on a $\log_2$ scale and normalized using three inter-plate controls. The data are displayed as normalized protein expression (NPX) in arbitrary numbers. The data was filtered, and only proteins that contained at least 80 % values above the limit of detection in at least on time point were used resulting in 69 proteins. The NPX data showed a high correlation with $\log_2$-transformed protein concentration measured by ELISA for both IL6 ($r = 0.86$, p-value < 0.001) and VEGF ($r = 0.93$, p-value < 0.001). The qPCR data from the cDNA purified from whole blood samples were analyzed using the Lightcycler 480 software and crossing points, as mentioned in section 3.7.3. Using a PCA, two outliers were detected and removed from the analysis.

4 Results

4.1 Novel candidates potentially explaining the individual response in insulin sensitivity based on transcriptomics and epigenetic analyses

4.1.1 Transcriptomics analysis (NRE2)

As the first approach in finding novel exercise-responsive molecular targets, we analyzed the skeletal muscle transcriptome. Transcriptomic data from the muscle biopsies of all participants were measured as described in section 3.13. The dataset comprised 97 samples, with each 21,449 measured transcripts. Three samples were excluded due to bad probe material. First, we conducted an analysis of the differential regulation of these transcripts. In the context of acute response, comparing the time points T2 and T0, we identified 1,820 transcripts that were significantly regulated (adjusted p-value < 0.05) (Figure 2). To evaluate the training effect, we compared the time points T5 and

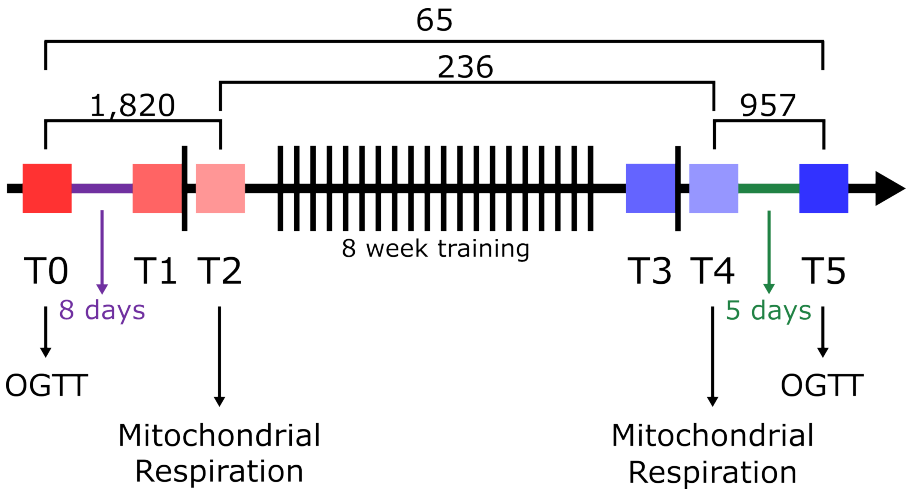

Figure 2: Exercise-induced differential expression of transcripts. A schematic representation of the differentially expressed transcripts in skeletal muscle biopsies during the training intervention. The numbers represent the transcripts that are significantly up- or downregulated (adjusted p-value < 0.05) comparing the indicated time points. The p-values were adjusted using the Benjamini-Hochberg method to correct for multiple testing. At T1 and T3, no muscle biopsies were collected. N = 25, or 23 for T4, or 24 for T5. OGTT: oral glucose tolerance test.

T0 and found 65 transcripts that exhibited significant regulation (adjusted p-value < 0.05). To evaluate the effect of the 8-week training intervention on the acute response, we further compared the two acute time points T4 and T2 resulting in 236 transcripts that were significantly regulated (adjusted p-value < 0.05) (Figure 2). For these comparisons (T2T0, T4T2, and T5T0), the top 50 significantly regulated (adjusted p-value < 0.05) transcripts by fold change are shown in a heatmap (Figure 3). All four time points are plotted to visualize their expression once for the compared time points and additionally their regulation at the other time points. For the comparison of T2T0, the top upregulated transcripts are the nuclear receptors *NR4A3* and *NR4A1*, followed by the thiamine transporter *SLC19A2* and *TRIM63*. Notably, in the list of top upregulated transcripts *PPARGC1A*, also known as PGC1α, and the two inhibitors of differentiation *ID1* and *ID2* are found. The most downregulated transcripts include *MYOG* and *MSTN*. The top 50 transcripts were also elevated at T4 to a lesser extent (Figure 3A). When comparing T4T2, the most upregulated transcripts belong to the extracellular matrix (ECM), such as *MXRA5* or collagens (*COL3A1*, *COL4A1*), suggesting less upregulation at the acute time point after the training period. Notably, in the list of top downregulated transcripts *NR4A3*, *NR4A1*, and *TRIM63* are found. It is worth mentioning that while the upregulation is less pronounced, the downregulation is clearly visible (Figure 3B). For the comparison of T5T0, multiple transcripts associated with the extracellular matrix (ECM) such as

BGN, *ASPN*, *IGFBP7*, or *TIMP1* were elevated (Figure 3C). Overall, the acute time points T2 and T4 showed more pronounced changes compared to T5.

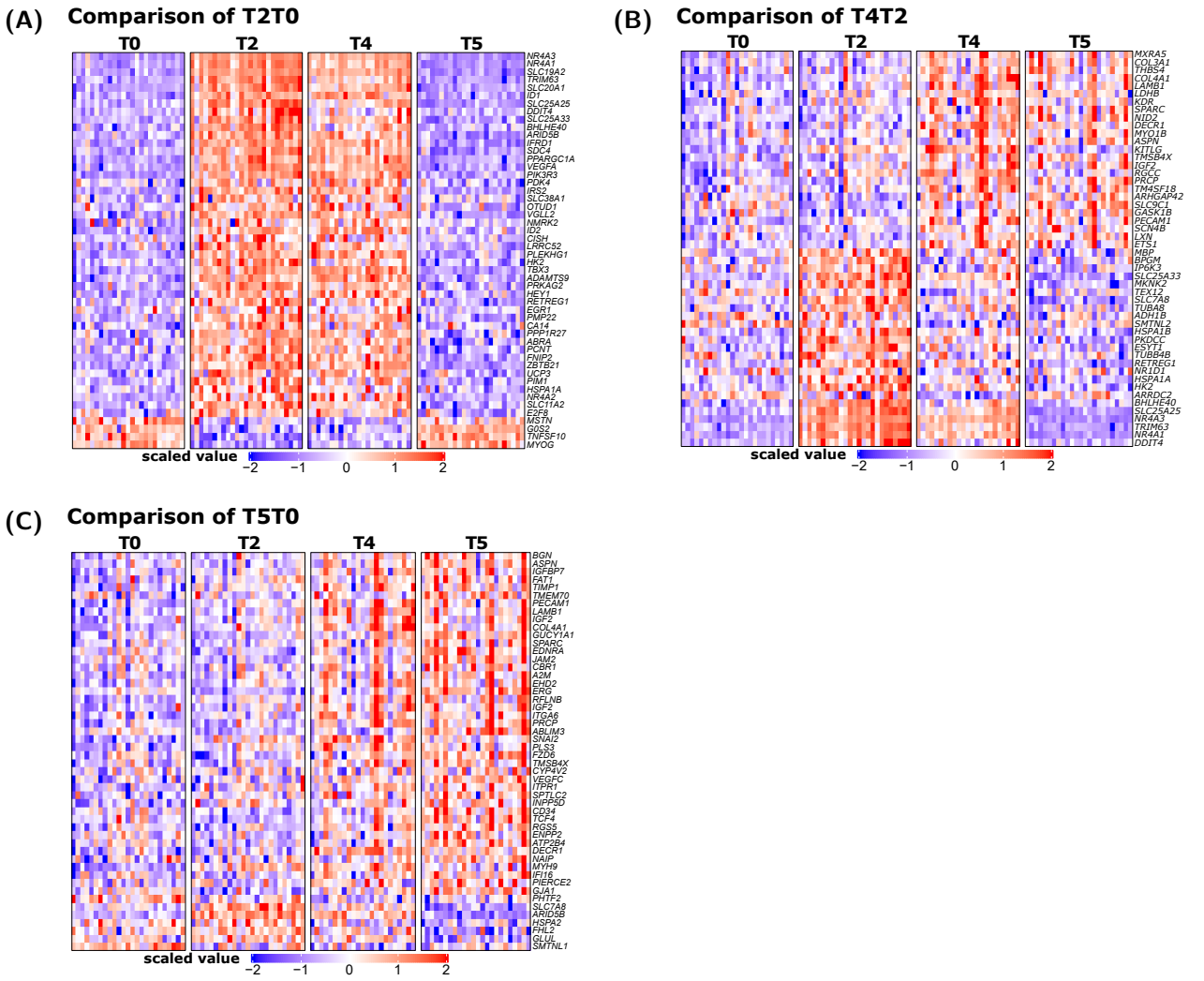

Figure 3: Heatmaps of the top 50 significantly regulated transcripts by fold change. Heatmaps showing the most up- and downregulated transcripts by fold change (adjusted p-value < 0.05) for the comparisons (A) T2T0, (B) T4T2, and (C) T5T0. The values are shown for each individual and all four time points. Values were scaled (by centering the data using the mean and dividing by the standard deviation) for comparison between transcripts, and the heatmaps were sorted using Euclidean distance complete linkage clustering for the rows. Blue means decreased expression, while red means increased expression at the time point. N = 25, or 23 for T4, or 24 for T5.

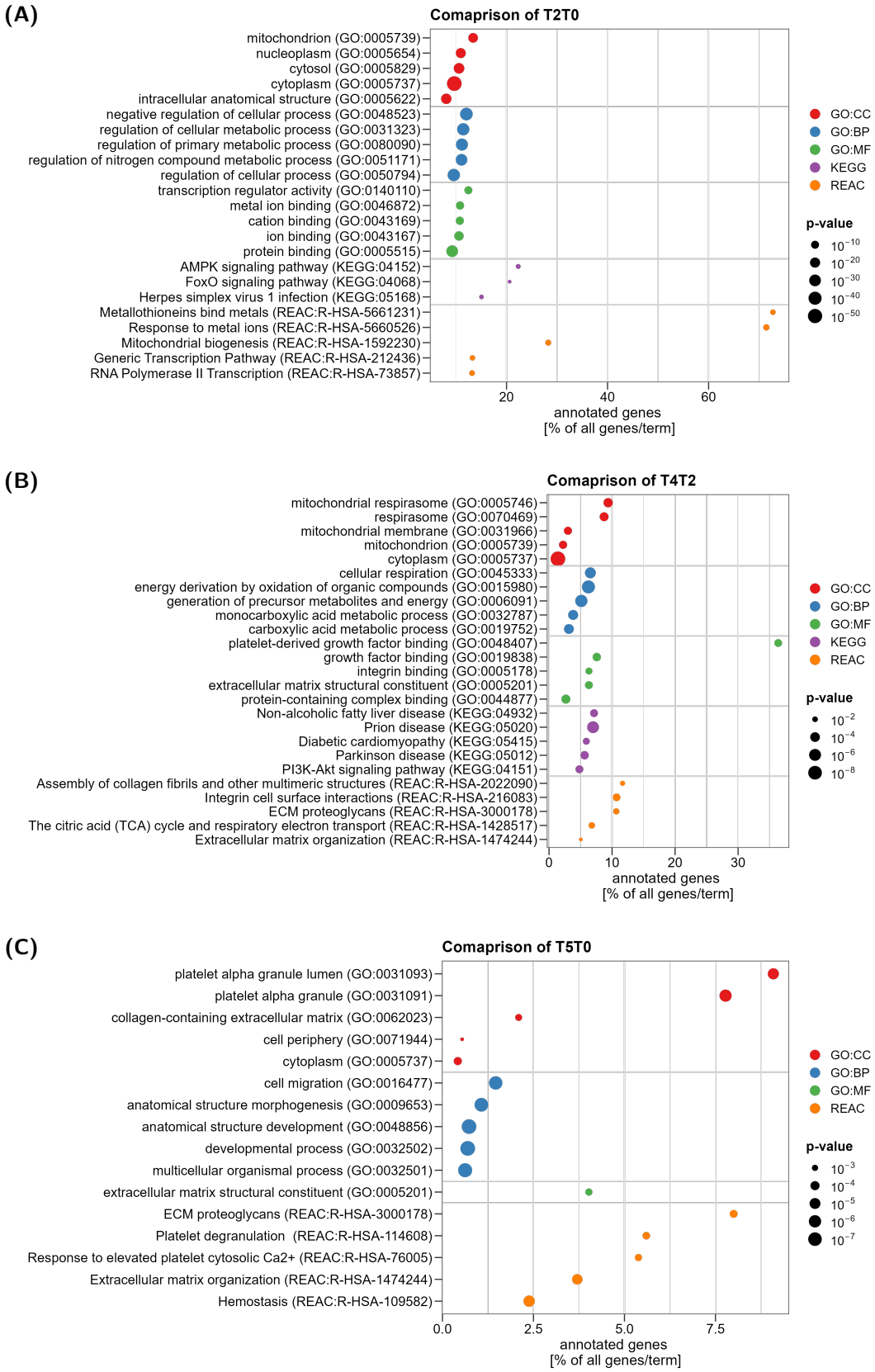

Figure 4: Gene enrichment analysis of significantly regulated transcripts by training. The significantly regulated (adjusted p-value < 0.05) transcripts when comparing (A) T2T0, (B) T4T2, and (C) T5T0 were analyzed for gene enrichment using gProfiler. On the x-axis, the percentage amount of significantly regulated transcript per total transcript in the term is shown. The top five terms by percentage are shown if a significance level of p-value < 0.05 was reached. The point size represents the significance level of enrichment. Point colors show the different categories of pathways. BP: biological process; CC: cellular component; GO: gene ontology; KEGG: Kyoto encyclopedia of genes and genomes; MF: molecular function; REAC: Reactome.

For all comparisons between the time points, we performed gene enrichment analysis focusing on gene ontology (GO) pathways, including biological process (BP), cellular component (CC) and molecular function (MF), as well as Reactome (REAC) and Kyoto encyclopedia of genes and genomes (KEGG) pathways. The results are visualized in Figure 4. The gene enrichment analysis revealed that the most significantly regulated pathways were associated with mitochondrion and mitochondrial biogenesis immediately after the acute training T2T0 (Figure 4A). Interestingly, when comparing the two acute time points T4T2 (Figure 4B), most terms were still related to the mitochondrion, focusing on the mitochondrial respiration process, such as the respirasome or tricarboxylic acid cycle (TCA cycle). Furthermore, some terms indicated the reorganization of the ECM. Following the 8-week training intervention, comparing T5T0 (Figure 4C), the dominant terms primarily pertained to the ECM and structural development. Subsequently, we investigated which transcripts might influence the training response in insulin sensitivity. As shown in Table S1, insulin sensitivity did not exhibit a significant change across all subjects (Figure 5A). However, upon examining individual changes, we identified two distinct groups. The RES group demonstrated an improvement in their insulin sensitivity of at least 1.15-fold increase after the 8-week training intervention, whereas the LRE group did not improve. Some individuals in the latter group showed worsened insulin sensitivity after the training intervention. The distribution of the two groups is visualized in the boxplot in Figure 5B.

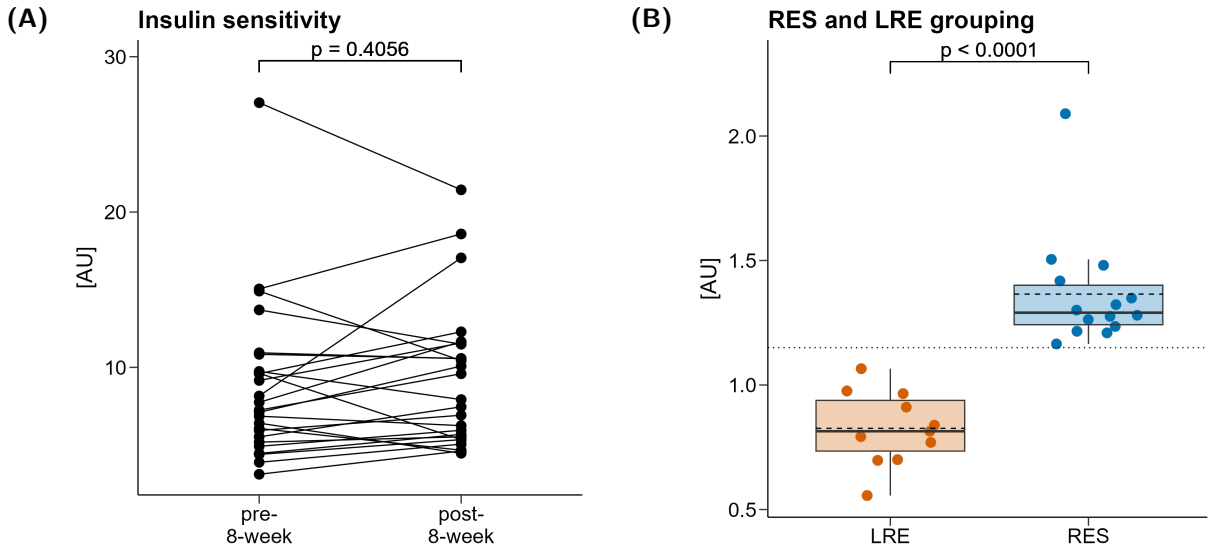

Figure 5: Insulin sensitivity after 8-week training intervention. (A) The insulin sensitivity according to DeFronzo and Matsuda (ISI_{Mats}) is shown for all individuals. The pre-values show the insulin sensitivity before the 8-week training intervention, while the post-value show the sensitivity after. The two values corresponding to the same individual are connected with a line. The p-value was calculated using a paired Student's t-test. (B) The fold change of post vs. pre was calculated for each subject. The subjects were grouped into the responder (RES) group, which increased their ISI_{Mats} at least 1.15 times (blue), and the low-responder (LRE), which failed to increase their ISI_{Mats} (orange). The p-value was calculated using an unpaired Student's t-test. The dotted line represents the 1.15-fold change line. The dashed line represents the mean value, while the solid black line represents the median. The boxes represent the interquartile range (IQR) from the first to the third quartiles. The whiskers extend the box to the lowest and highest value at most 1.5 $\times$ IQR. N = 25 (LRE = 11, RES = 14) AU: arbitrary units.

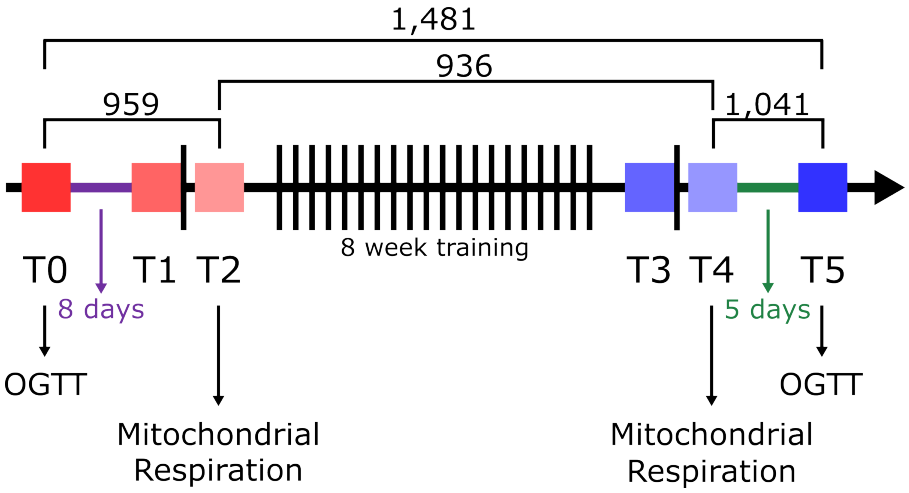

Figure 6: Differential transcriptional regulation in ISI_{Mats} response groups. A schematic representation of the differentially regulated transcripts at the indicated time points comparing responder (RES) and low-responder (LRE) groups. The numbers represent the transcripts with significantly higher or lower fold change (p-value < 0.05) in either group. N = 25, or 23 for T4, or 24 for T5. OGTT: oral glucose tolerance test.

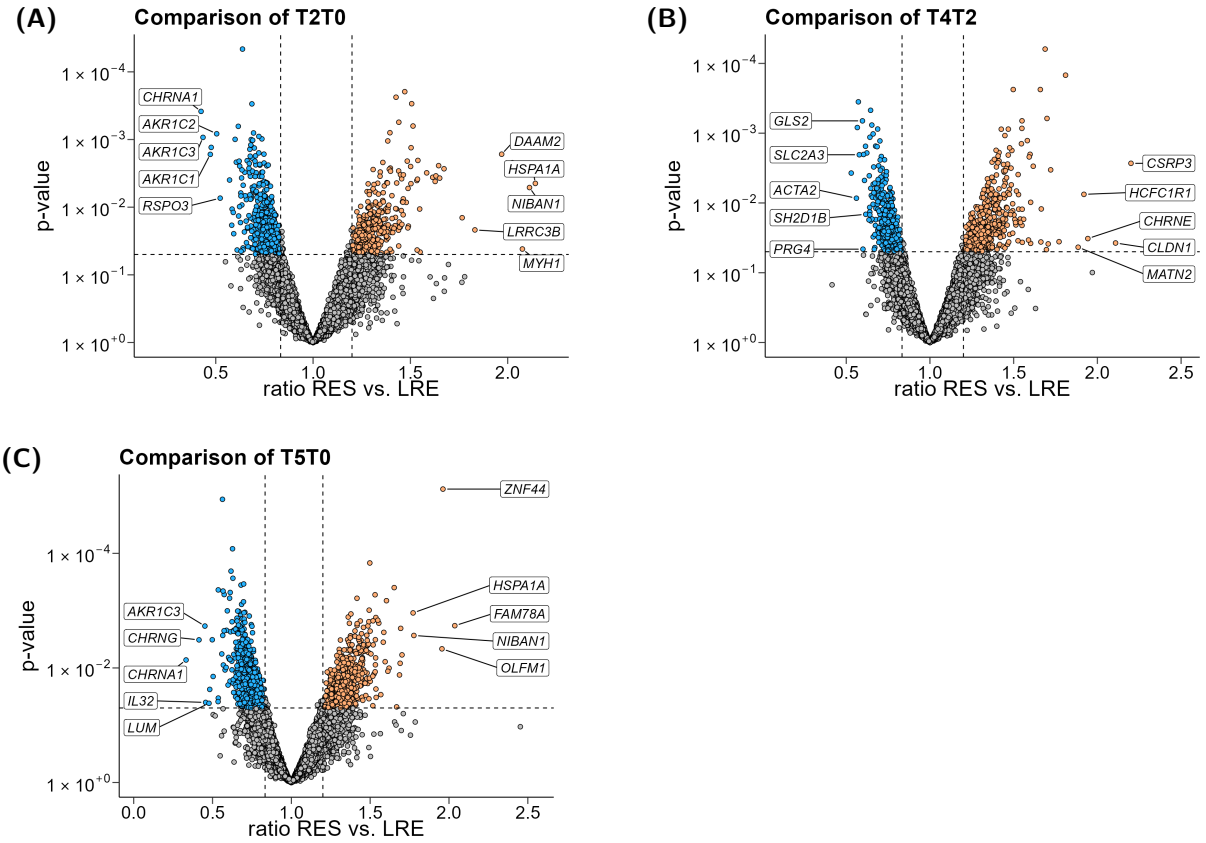

Figure 7: Volcano plot of transcripts differentially expressed between ISI_{Mats} response groups. The significantly (p-value < 0.05) and differentially regulated genes between the responder (RES) and low-responder (LRE) are shown in a volcano plot. The data are shown for the comparisons (A) T2T0, (B) T4T2, and (C) T5T0. On the x-axis, the ratio between RES and LRE is shown, and the p-value is on the y-axis. The ratio and p-value were calculated using limma-analysis. The top five genes (excluding micro RNAs) increased in the RES group are annotated. The horizontal line represents the significance level of p-value < 0.05. The vertical lines represent an increased expression of at least 1.2-fold in the RES (right side) or at least 1.2-fold in the LRE (left side). Blue points show transcripts significantly increased in the LRE group with a fold change of at least 1.2, while orange represents significantly regulated transcripts in the RES group with a fold change of at least 1.2. N = 25, or 23 for T4T2, or 24 for T5T0.

For each subject, the fold change for the comparisons T2T0, T4T2, and T5T0 was calculated, and the dataset was split by the defined response groups. Upon comparing the groups, we observed significant differential regulation of transcripts (Figure 6). Specifically, we identified 959 transcripts with significant differential regulation (p-value < 0.05) for the comparison of T2T0, of which the top five transcripts with a higher fold change in the RES group were *DAAM2*, *HSPA1A*, *LRRC3B*, *MYH1*, and *NIBAN1* (Figure 7A). The top five transcripts with a lower fold change in the RES group were *AKR1C1*, *AKR1C2*, *AKR1C3*, *CHRNA1*, and *RSPO3*. By comparing T4T2, 936 significantly regulated transcripts were found. The top five transcripts showing a higher fold change in RES were *CHRNE*, *CLDN1*, *CSRP3*, *HCFC1R1*, and *MATN2*, and the top five transcripts with a lower fold change were *ACTA2*, *GLS2*, *PRG4*, *SH2D1B*, and *SLC2A3* (Figure 7B). When comparing T5T0, 1,481 transcripts were significantly differentially regulated, with *FAM78A*, *HSPA1A*, *NIBAN1*, *OLFM1*, and *ZNF44* being the transcripts showing a higher fold change in the RES group, whereas *AKR1C3*, *CHRNA1*, *CHRNG*, *IL32*, and *LUM* were the top five transcripts showing lower fold change (Figure 7C). However, none of the transcripts remained significant after applying the Benjamini-Hochberg correction for multiple testing.

We selected a few transcripts out of the top regulated between the RES and LRE groups, which might be interesting. Boxplots demonstrate the individual fold changes of the respective transcripts in RES and LRE. Three members of the AKR1C family (*AKR1C1*, *AKR1C2*, and *AKR1C3*) exhibited no change or a slight increase in the LRE group and a decrease in the RES group after acute exercise (T2T0) (Figure 8A – C). For *CHRNA1*, we saw a similar pattern with no change in the LRE group and a strong decrease in the RES at T2T0 (Figure 8D). The transcript *HSPA1A* showed an increase in both groups comparing T2T0, however, this increase was more pronounced in the RES group (Figure 8E). *MATN2* showed a slight decrease in the LRE group and an increase in the RES group (Figure 8G) comparing T4T2, and the transcript *SLC2A3* was slightly increased in the LRE and decreased in the RES (Figure 8H). After training intervention (T5T0), *AKR1C3*, *CHRNA1*, and *HSPA1A* showed a similar differential regulation in RES and LRE groups after acute exercise. *AKR1C3* and *CHRNA1* were unchanged in the RES group and increased in the LRE group (Figure 8I – J). *HSPA1A* showed a slight increase in the RES group and a decrease in the LRE (Figure 8K).

Our next approach was to correlate the change of each transcript with the individual change in insulin sensitivity. Here, we used only the change of transcripts comparing T5T0 to correlate it with the change in ISI_{Mats} since the insulin sensitivity was measured at the time points T5 and T0 (section 3.10.3). This analysis yielded 1,244 transcripts (640 negative, 604 positive) significantly (p-value < 0.05) correlated (Figure 9A). We performed gene enrichment analysis using gene ontology biological process (GO:BP), gene ontology cellular component (GO:CC), gene ontology molecular function (GO:MF), REAC, and KEGG. Our analysis revealed that transcripts correlated with changes in insulin sensitivity, whether positively or negatively, were primarily associated with transcriptional regulation, including the ribosomes and translation initiation. In addition, when looking at selected transcripts in Table 18, we saw a significant negative correlation with the change in expression and change in ISI_{Mats} for the transcripts *AKR1C1*, *AKR1C2*, *AKR1C3*, *CHRNA1*, *IL32*, and *MATN2*. Solely for *HSPNA1A* a significant positive correlation was seen. *CSRP3* and *SLC2A3* showed no significant correlation with the change in ISI_{Mats}.

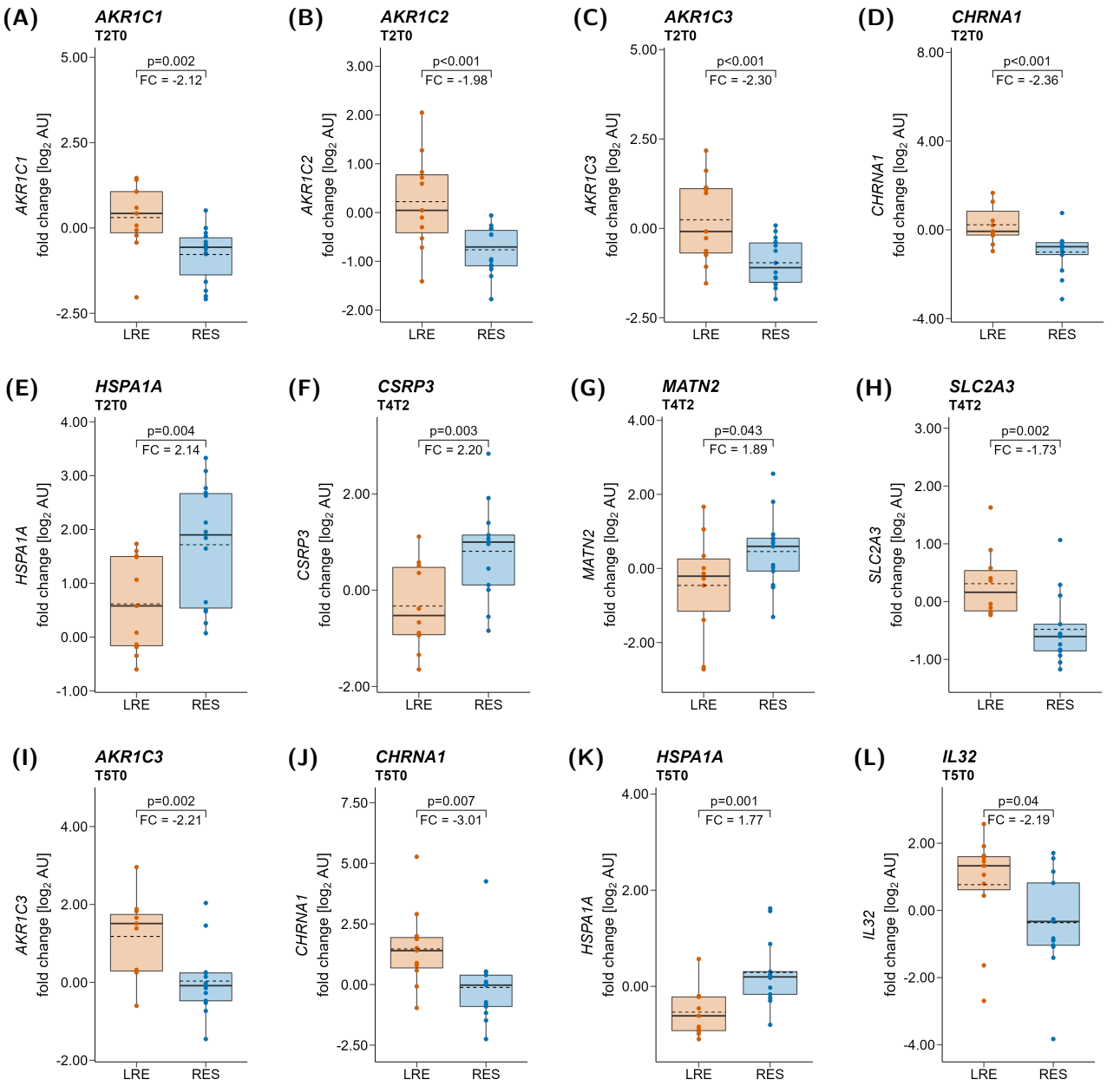

Figure 8: Differential transcriptional regulation of top selected transcripts between ISI_{Mats} response groups. The boxplots show the differential transcriptional regulation of the transcripts *AKR1C1*, *AKR1C2*, *aldo keto-reductase 3 (AKR1C3)*, *CHRNA1*, *CSRP3*, *HSPA1A*, *IL32*, *MATN2*, and *SLC2A3* between the responder (RES) and low-responder (LRE) groups. The plots (A – E) show the regulation at T2T0, (F – H) at T4T0, and (I – L) at T5T0. The solid black line represents the median of the data, while the dashed black line represents the mean. The boxes represent the interquartile range (IQR) from the first to the third quartiles. The whiskers extend the box to the lowest or largest value no further than 1.5 × IQR. The p-values and fold changes were calculated using limma-analysis. N = 25 for T2T0 (LRE = 11, RES = 14), or 23 for T4T2 (LRE = 10, RES = 13), or 24 for T5T0 (LRE = 11, RES = 13). AU: arbitrary units.

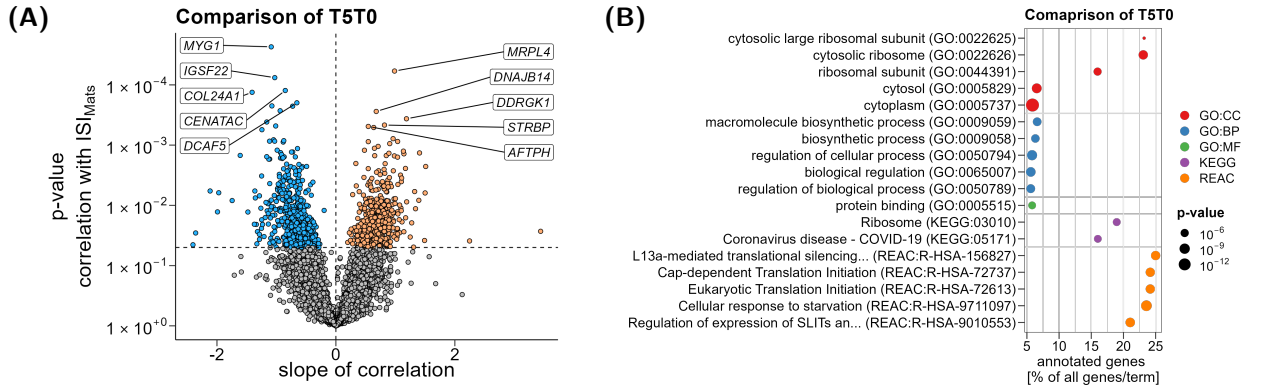

Figure 9: Volcano plot and gene enrichment analysis of transcripts correlating with ISI_{Mats}. (A) Volcano plots showing the correlation of the change of all transcripts with the change in insulin sensitivity according to DeFronzo and Matsuda (ISI_{Mats}) comparing T5T0. On the x-axis, the slope of the correlation is plotted, and the unadjusted p-value of the correlation is on the y-axis. The top five significantly and positively correlated transcripts are annotated. The horizontal line represents the significance level of p-value < 0.05. The vertical lines represent the zero line of correlation. Blue points show transcripts significantly negatively correlated, while orange represents significantly positively correlated transcripts. (B) The significantly correlated (p-value < 0.05) changes in transcripts with the change in ISI_{Mats} were analyzed for gene enrichment using gProfiler. On the x-axis, the percentage amount of significantly regulated transcript per total transcript in the term is shown. The top five terms by percentage are shown if a significance level of p-value < 0.05 was reached. The point size represents the significance level of enrichment. Point colors show the different categories of pathways. N = 24. BP: biological process; CC: cellular component; GO: gene ontology; KEGG: Kyoto encyclopedia of genes and genomes; MF: molecular function; REAC: Reactome.

Table 18: Correlation change of selected transcripts with the change in ISI_{Mats}. The table shows the selected transcripts which exhibited the greatest fold change between the RES and LRE group and the correlation of the change at T5T0 with the change in ISI_{Mats}.

Gene name	p-value	Pearson R
AKR1C1	0.0083	−0.5257
AKR1C2	0.0129	−0.4998
AKR1C3	0.0062	−0.5424
CHRNA1	0.0451	−0.4126
CSRP3	0.5261	0.1316
HSPA1A	0.0059	0.5449
IL32	0.0287	−0.4465
MATN2	0.0058	−0.5461
SLC2A3	0.8545	0.0395

4.1.2 Epigenomics analysis (NRE2)

In addition to transcriptional analysis, we also conducted epigenetic analysis. Some participants had to be excluded from the analysis due to specific criteria such as age. It is already known that epigenetic patterns are age-dependent, which in turn can serve as a predictor of biological age [156]. Two participants in our study had a significantly higher age compared to the mean age of 31 years of the overall participant group, with one participant being 46 years old and the other participant being 59 years old. We decided to exclude these subjects to reduce the age-specific effect seen in the epigenetic pattern. Furthermore, three samples were removed due to the highly significant influence of the parameter "sex" determined by singular value decomposition (SVD) analysis. Lastly, only full datasets comprising all four analyzed time points were included. Therefore, the epigenomics analysis consists of 18 out of 25 participants while maintaining the male-to-female ratio (11 female, 7 male). The epigenomics dataset comprised 847,460 methylation sites (CpG sites), of which 591,393 CpG sites could be annotated to genes using the USCS genome browser, resulting in 22,955 unique genes. The annotated CpG sites could be further classified based on their location in the promoter or gene body regions. This classification revealed 309,496 CpG sites in the gene body and 281,897 CpG sites in the promoter sequence (Figure 10).

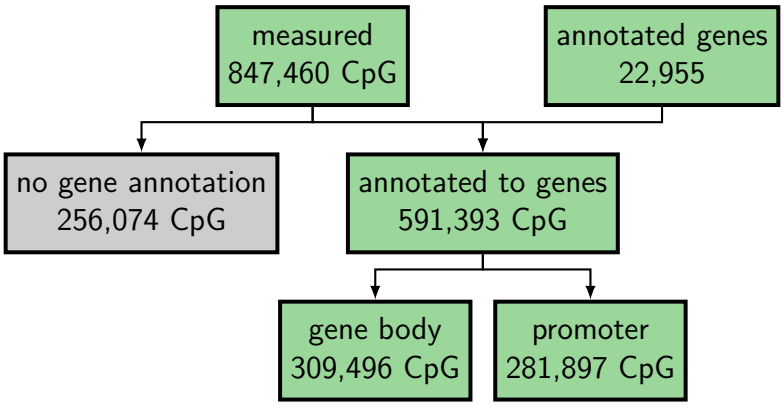

Figure 10: Scheme of measured and annotated CpG site. A schematic representation showing the amount of detected methylation sites (CpG sites) using the MethylationEPIC 850K BeadChip. The CpG sites were annotated to genes using the UCSC genome browser and further discriminated in the gene body and promoter sequence. N = 18.

Similarly to the transcriptomics analysis, we compared the acute effect T2T0, the training effect T5T0, and the two acute time points T4T2 regarding differential methylation. The results are presented in Figure 11. The amount of significantly differentially regulated (p-value < 0.05) CpG sites ranged from 38,700 CpG sites when comparing T2T0 to 105,000 CpG sites when comparing T5T0. The comparison of T4T2 exhibited 92,788 significantly regulated CpG sites. While 33 % of the CpG sites could not be annotated to a specific gene according to the UCSC genome browser, 67 % were annotated with a particular gene. The highest number of significantly regulated CpG sites were found for the comparison T5T0, with 105,182 CpG sites, of which 46,257 CpG sites were hypomethylated (mean: -2.30 ± 1.08 %) and 58,925 were hypermethylated (mean: 2.81 ± 1.22 %). This is followed by the comparison of T4T2 with 92,788 CpG sites, of which 55,248 CpG sites were hypomethylated (mean: -2.05 ± 0.97 %), and 37,539 CpG sites were hypermethylated (mean: -2.56 ± 1.22 %). In these comparisons, 69,355 and 62,067 CpG sites could be annotated to 16,300 and 16,194 genes, respectively. The comparison T2T0 showed 38,712 regulated CpG sites with 19,012 hypomethylated CpG sites (mean: -2.03 ± 1.11 %) and 19,700 hypermethylated CpG sites (mean: 1.81 ± 0.98 %). Of all CpG sites from the comparison at T2T0, 25,841 CpG sites were annotated to 11,924 genes. The annotated CpG sites could be further categorized based on their location in the gene body or promoter sequence. Notably, more CpG sites were annotated to the gene body for all comparisons.

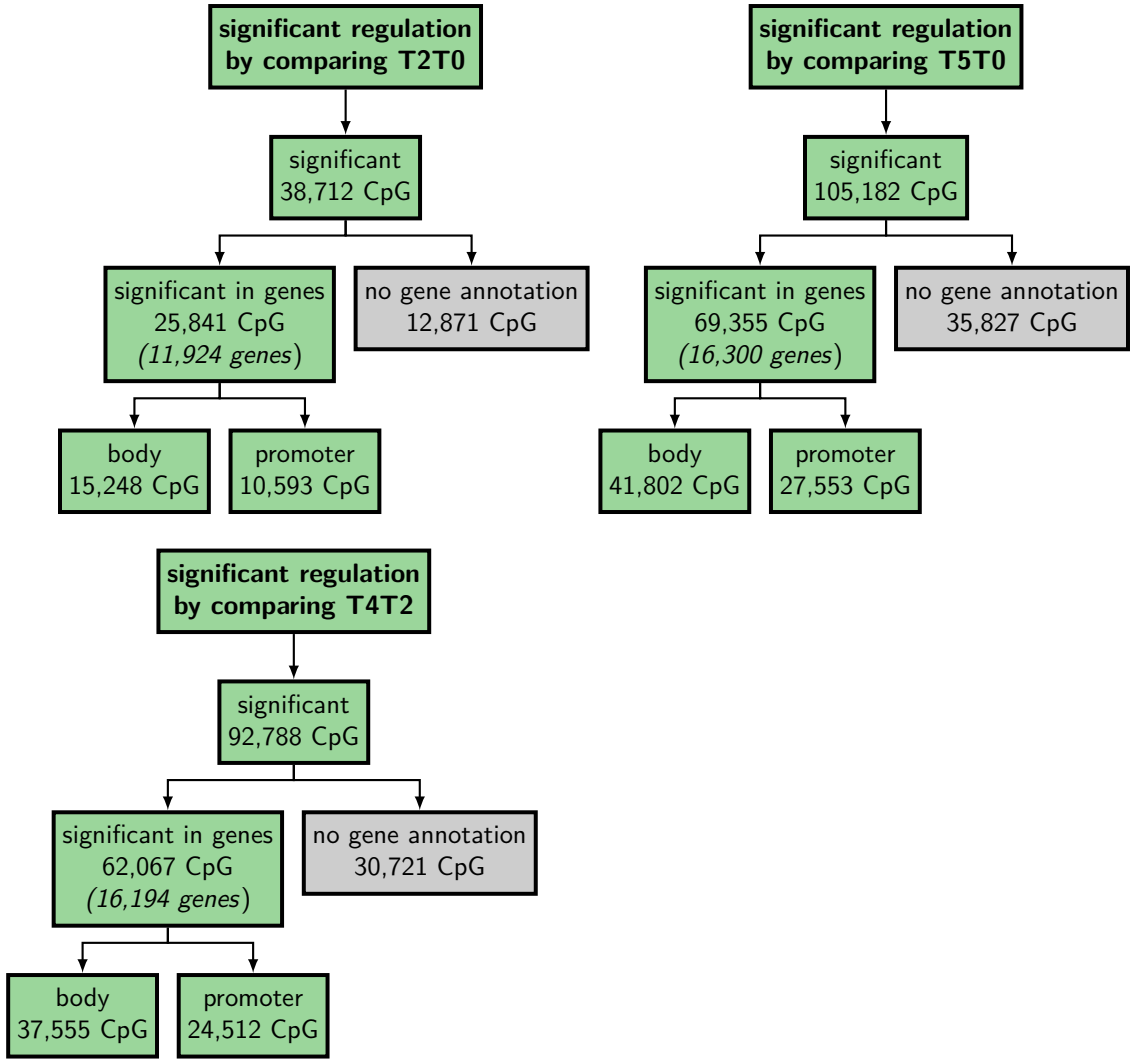

Figure 11: Counts of differential regulated CpG sites. The figure shows the number of significantly regulated CpG sites at the different time point comparisons T2T0, T5T0, and T4T2. Below are the counts of CpG sites found inside a gene according to the UCSC genome browser and the further discrimination in the gene body and promoter N = 18.

Subsequently, the epigenomics data was split into the RES and LRE groups for each time point comparison, as already performed for the transcriptomics dataset. Notably, we observed the most significant differences between the groups comparing T2T0, with 50,372 CpG sites with 37,185 hypomethylated CpG sites (mean: $-4.58 \pm 2.21\,\%$) and 13,187 hypermethylated CpG sites (mean: $4.08 \pm 2.03\,\%$). Comparing T5T0, 48,865 CpG sites were significantly regulated with 17,543 hypomethylated CpG sites (mean: $-3.69 \pm 2.30\,\%$) and 31,322 hypermethylated CpG sites (mean: $4.03 \pm 1.91\,\%$). Lastly, by comparing T4T2, 48,329 CpG sites exhibited significant regulation of which 9,452 CpG sites were hypomethylated (mean: $-3.55 \pm 2.29\,\%$), and 38,877 were hypermethylated (mean: $-3.82 \pm 1.92\,\%$). Consistent with previous findings, approximately two-thirds of the CpG sites could be annotated to a specific gene across all comparisons. Overall, approximately 13,000 to 13,700 genes were found to be regulated in at least one CpG site. Interestingly, more CpG sites were localized in the gene body compared to the promoter sequence, a trend observed across all comparisons (Figure 12).

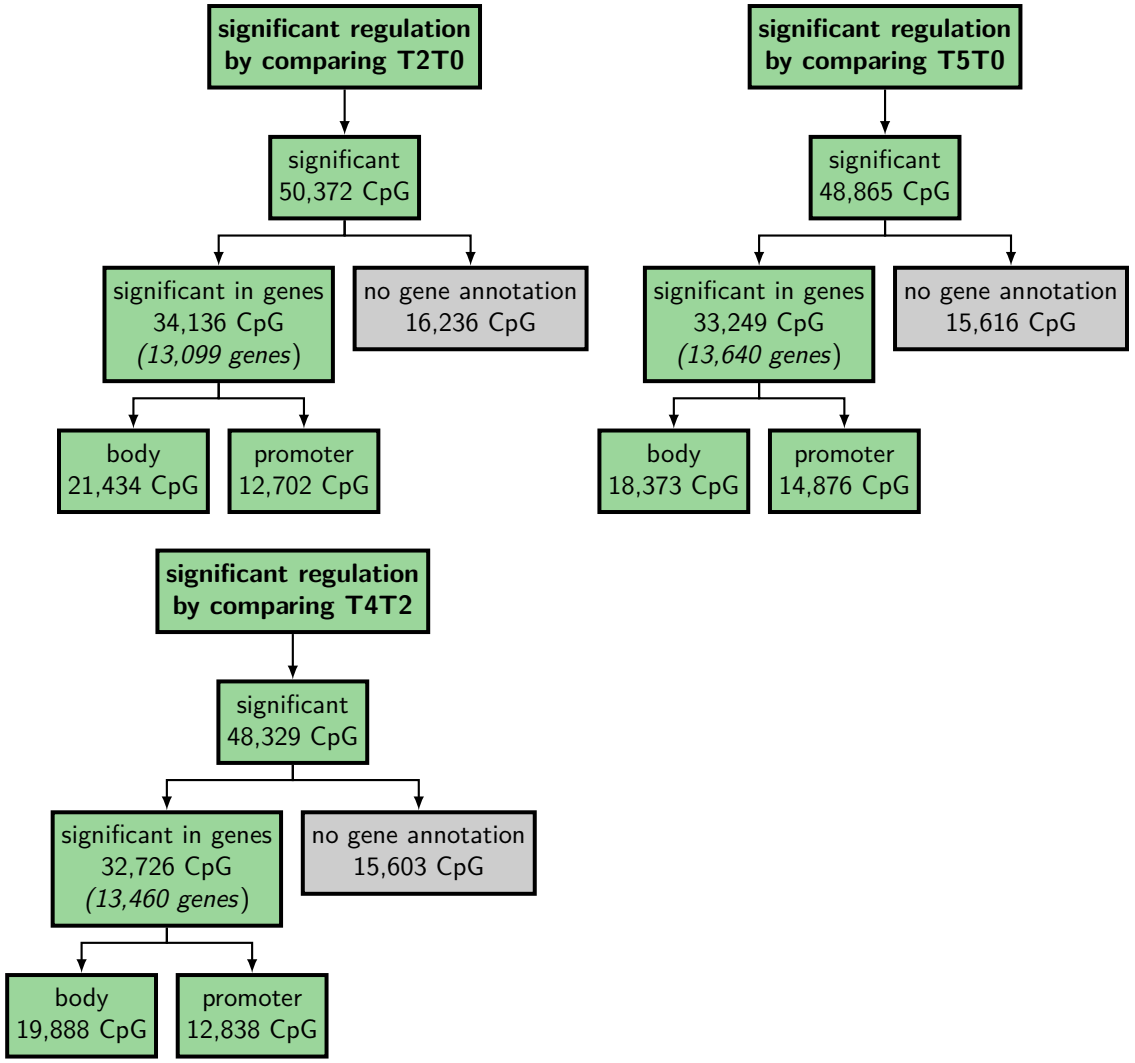

Figure 12: Differential methylation regulation on CpG sites comparing RES and LRE groups according to ISI_{Mats}. The figure shows the number of significantly regulated CpG sites at the different time point comparisons T2T0, T5T0, and T4T0 between the responders (RES) and low-responders (LRE). Below are the counts of CpG sites found inside a gene according to the UCSC genome browser and the further discrimination in the gene body and promoter. N = 18.

4.1.3 Overlapping analysis of transcriptomics with epigenomics

The epigenomics dataset was matched with the transcriptomics data for the integrated analysis of both datasets. To achieve this, the gene positions on the chromosome were extended by 2,000 base pairs (bp) at both ends. Subsequently, the CpG sites located between the newly created start and stop sites on the same chromosome were matched to the corresponding transcripts. This process yielded 20,344 unique genes, encompassing a total of 712,939 CpG sites, with 622,156 being unique to a single transcript. Afterwards, we investigated which of the significantly regulated (p-value < 0.05) transcripts also contained significantly regulated (p-value < 0.05) CpG sites. The comparison of T2T0 exhibited the highest number of significantly regulated transcripts, with 1,998 transcripts containing at least one of the 4,754 significantly regulated CpG sites. By comparing T4T2, 1,730 transcripts were regulated, encompassing a total of 8,317 regulated CpG sites. The most significant regulation of CpG sites was observed comparing T5T0, with 10,208 CpG sites identified in 1,730 transcripts (Figure 13). Additionally, the direction of regulation was considered.

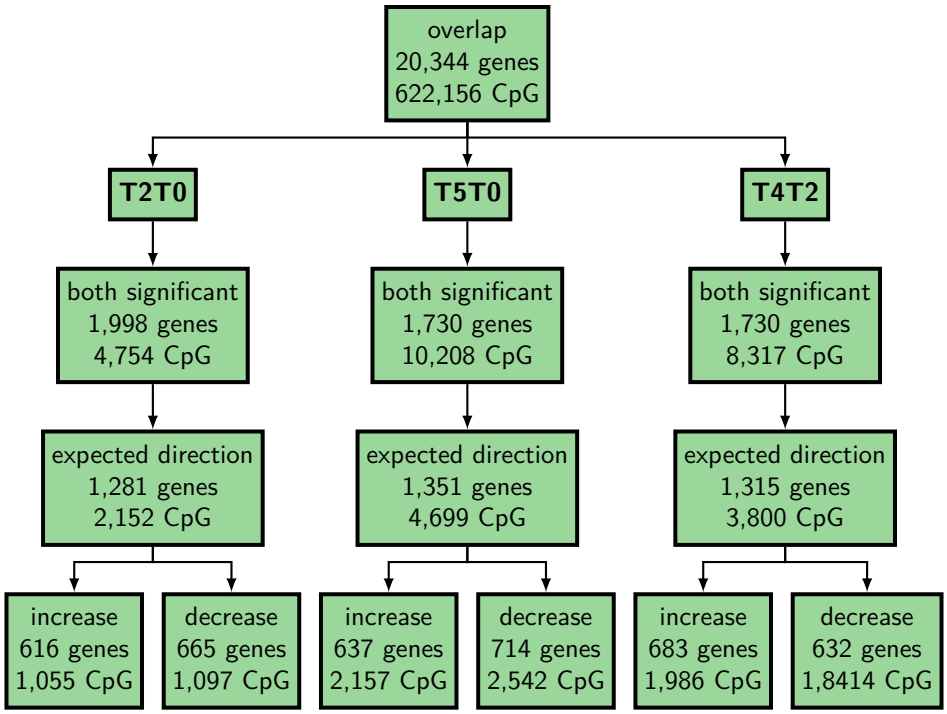

Figure 13: Counts of overlapping transcriptomics and epigenomics per time point comparison. The tree diagrams show the number of unique regulated CpG sites overlapping with regulated genes in the transcriptomics data for the time point comparisons T2T0, T5T0, and T4T2. Below are the numbers of significantly regulated (p-value < 0.05) transcripts that contain at least one significantly regulated (p-value < 0.05) CpG site. Afterwards are the counts of genes that contain at least one CpG site in the expected direction, and both are significantly regulated. The last boxes show the number of transcripts with regulated CpG sites that were increased or decreased. N = 18.

The correct or expected direction criteria are schematically shown in Figure 14. The expected relationship is that lower methylation in the promoter region corresponds to activated transcriptional expression, while higher methylation corresponds to reduced expression. Conversely, higher methylation in the gene body correlates to increased transcription, while reduced methylation is associated with lower transcription. By applying these criteria to the regulated transcripts with at least one regulated CpG site, we identified 1,281 significantly regulated transcripts containing at least one of the 2,152 significantly regulated CpG sites in the expected direction when comparing T2T0. The most regulated transcripts and CpG sites were found, with 1,351 transcripts and 4,699 CpG sites when comparing T5T0. Comparison at T4T2 showed 1,315 regulated transcripts and 3,800 regulated CpG sites. Notably, we observed no clear preference for increased or decreased transcriptional expression. A comparison between T2T0 and T5T0 revealed a slight increase in upregulated transcripts and a

higher number of CpG sites. On the other hand, the comparison between T4T2 showed a slight increase in downregulated transcripts and a higher number of CpG sites (Figure 13).

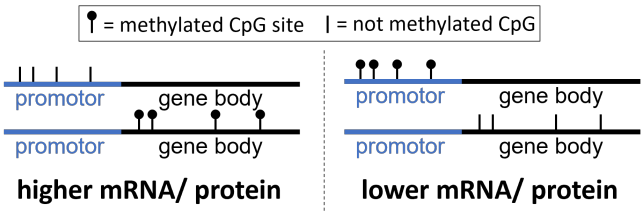

Figure 14: Expected direction of transcriptional expression and methylation. The figure shows the expected direction of transcriptional expression and methylation of CpG site sits. When the methylation (shown with) in the gene body increases, a higher mRNA and protein amount is expected. On the other hand, higher methylation in the promoter leads to a decreased expression. Demethylation in the promoter (shown with |) also leads to increased expression, while decreased methylation in the gene body results in lower expression.

Similarly, the same analysis was performed for the split analysis. For each subject, the fold change for the comparisons T2T0, T4T2, and T5T2 was calculated, and the datasets were split into the response groups (Figure 5B). This was performed for the epigenomics dataset and transcriptomics dataset. Following the split, the datasets were again merged, as written before, using the CpG site position in the gene with elongated start and stop sites. Additionally, the criteria for the expected direction were applied. The results showed 514 transcripts with 1,051 CpG sites, which are significantly regulated between both groups and in the expected direction when comparing T2T0. One-fourth of the transcripts were increased in the LRE group, which comprised furthermore one-fourth of the CpG sites in the expected direction. The other 75 % of the transcripts were increased

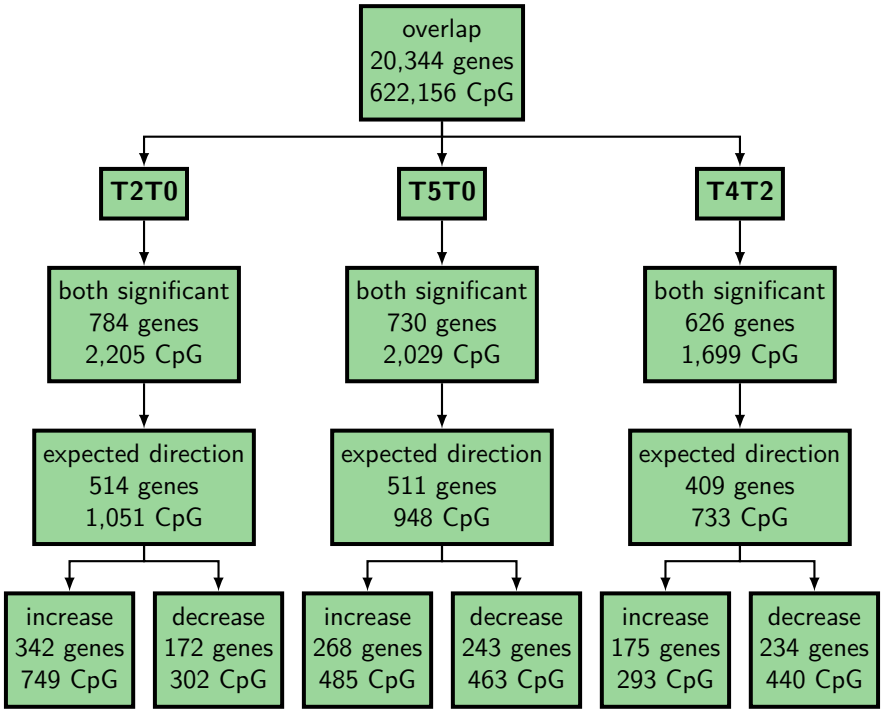

Figure 15: Counts of overlapping transcriptomics and epigenomics per time point comparison and ISI_{Mats} response groups. The figure shows the number of unique CpG sites overlapping with genes in the transcriptomics per time point comparison and divided into response groups. Below are the numbers of significantly regulated (p-value < 0.05) transcripts between the RES and LRE that contain at least one significantly regulated (p-value < 0.05) CpG site between the response groups. Next are the counts of genes that contain at least one CpG site in the expected direction, and both are significantly regulated between the two groups. The last boxes show the number of transcripts with CpG sites that increased or decreased in the RES. N = 18.

in the RES group. The second most differences were found with 511 transcripts comprising 947 CpG sites comparing T5T0. Notably, no clear preference between the groups could be detected in upregulation and downregulation. Approximately half of the transcripts were higher in the LRE group, while slightly more were increased in the RES group, a similar effect is seen with the CpG sites. For the comparison T4T2, 409 transcripts with 733 CpG sites were significantly regulated and in the expected direction. The LRE group contained about two-thirds of the transcripts and CpG sites higher expressed than the RES group, which contained one-third of the transcripts and CpG sites (Figure 15).

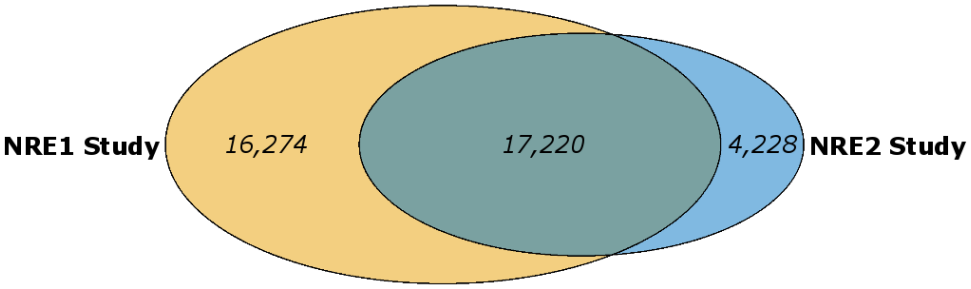

Figure 16: Overlap of transcriptomics data from NRE1 and NRE2 study. The VennDiagram shows the number of transcripts measured in the NRE1 and NRE2 studies. The number in the middle shows the number of transcripts after combining the datasets of both studies.

In order to increase the statistical power of the analysis, the transcriptomics dataset from the NRE2 study was merged with the transcriptomics data from the NRE1 study. These two studies are highly comparable, with the distinction that the NRE1 study solely included the time points T0 and T5. This merging resulted in a dataset comprising 41 individuals for analysis. Unfortunately, the two studies were measured with different microarray platforms. The NRE1 study used the Affymetrix Human Transcriptome Array 2.0, which consists of 33,494 transcripts, while the NRE2 study employed the Thermo Fisher Scientific Human Clariom S arrays containing 21,448. The data from both studies were combined using the unique public gene ID associated with each transcript, resulting in a unified dataset comprising 17,220 transcripts (illustrated in Figure 16). Utilizing the combined transcriptomics dataset, the differential regulation of each transcript was correlated to the changes in ISI_{Mats}. Among all transcripts, 1,132 transcripts exhibited a significant regulation (p-value < 0.05) in relation to the altered ISI_{Mats}.

All transcripts significantly correlating with the ISI_{Mats} were overlapped with all transcripts significantly regulated between the response groups and containing at least one CpG site significantly regulated as well in the expected direction for the comparison T5T0 from the NRE2 study. To reduce the dataset for selecting potential genes of interest, different p-value thresholds were applied. When using a p-value < 0.05 for both datasets, 124 transcripts were left. Reducing the p-value threshold of the correlation analysis to 0.01, 37 transcripts remained, while reducing the p-value of the split epigenomics dataset to 0.01, 13 transcripts remained. When the p-value < 0.01 was used for both datasets, 7 transcripts remained. These transcripts are AKR1C3 with 1 CpG site, IL34 with 4 CpG sites, P3H2 with 7 CpG sites, PLP1 with 1 CpG site, SPECC1 with 8 CpG sites, SPI1 with 3 CpG sites and TNFSF14 with 1 CpG site. Subsequently, the two transcripts, AKR1C3 and IL34, were selected for laboratory experiments to study their function in the context of insulin sensitivity. IL34 was chosen since it is a secreted protein, allowing treatment of cells with recombinant human IL34. AKR1C3 was selected since also its superfamily members AKR1C1 and AKR1C2 were found to be significantly correlated with the ISI_{Mats} on the transcriptional level and were among the significantly regulated transcripts between the RES and LRE group at T2T0 (Figure 7A). Furthermore,

the effect on insulin sensitivity, physical activity, or mitochondrial respiration is unknown for both chosen proteins.

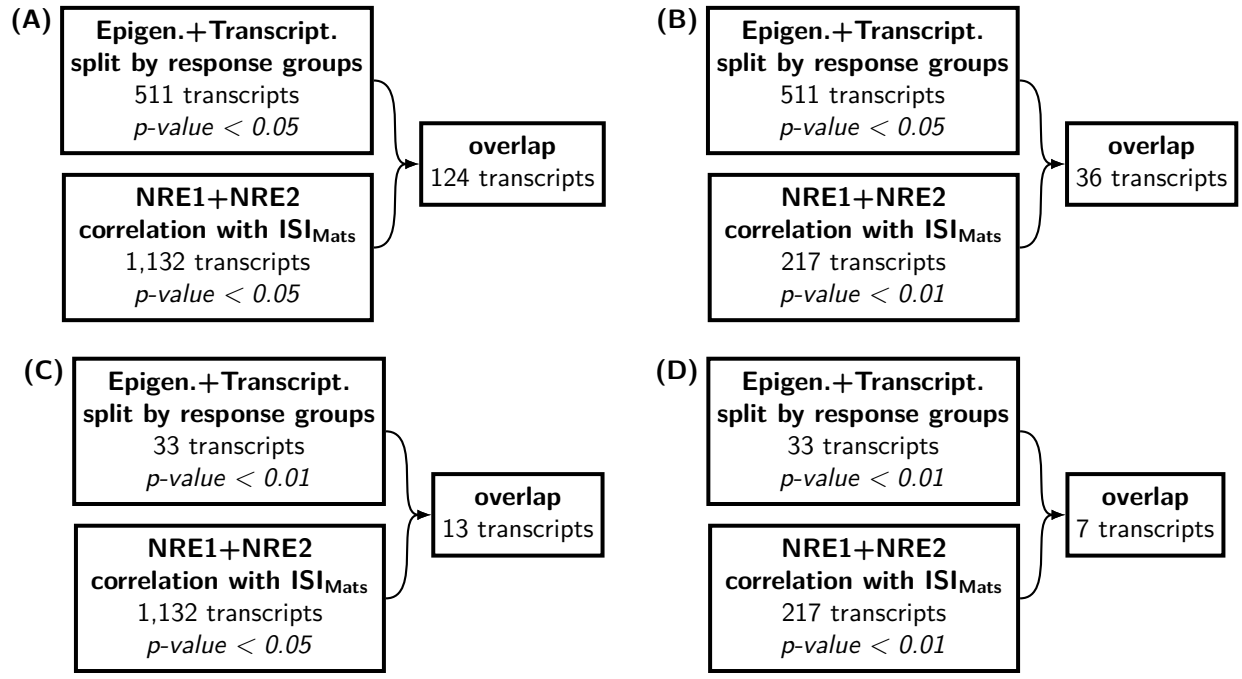

Figure 17: Overlapping of ISI_{Mats} correlated transcripts with epigenomics data for T5T0. The figure shows the overlapping transcripts, which correlate significantly with the ISI_{Mats} using the merged transcripts from NRE1 and NRE2, with genes significantly regulated between the response groups and containing at least one significant CpG site in the expected direction when comparing T5T0. The four plots differ in the significance level of the two datasets. (A) Both dataset p-values < 0.05, (B) correlation analysis p-value < 0.01 and split epigenomics dataset p-value < 0.05, (C) correlation analysis p-value < 0.05 and split epigenomics dataset p-value < 0.01, (D) both dataset p-values < 0.01.

4.1.3.1 Interleukin 34 (IL34)

Through our combined analysis of epigenomics and transcriptomics data, we identified IL34 as a gene of potential interest for further studies. In both the NRE1 and NRE2 study, as well as in the merged dataset, IL34 exhibited significantly higher expression in the LRE group compared to the RES post-intervention (Figure 18A – C). Intriguingly, its receptor, CSF1R, demonstrated a similar pattern in both studies and was significantly higher in LRE compared to RES (Figure 18D, E). Furthermore, two CpG sites were found to be significantly regulated and exhibiting the expected direction of expression post-intervention. These CpG sites, located in the promoter sequence of IL34, were hypomethylated in the LRE group while remaining unchanged or slightly hypermethylated in RES (data not shown).

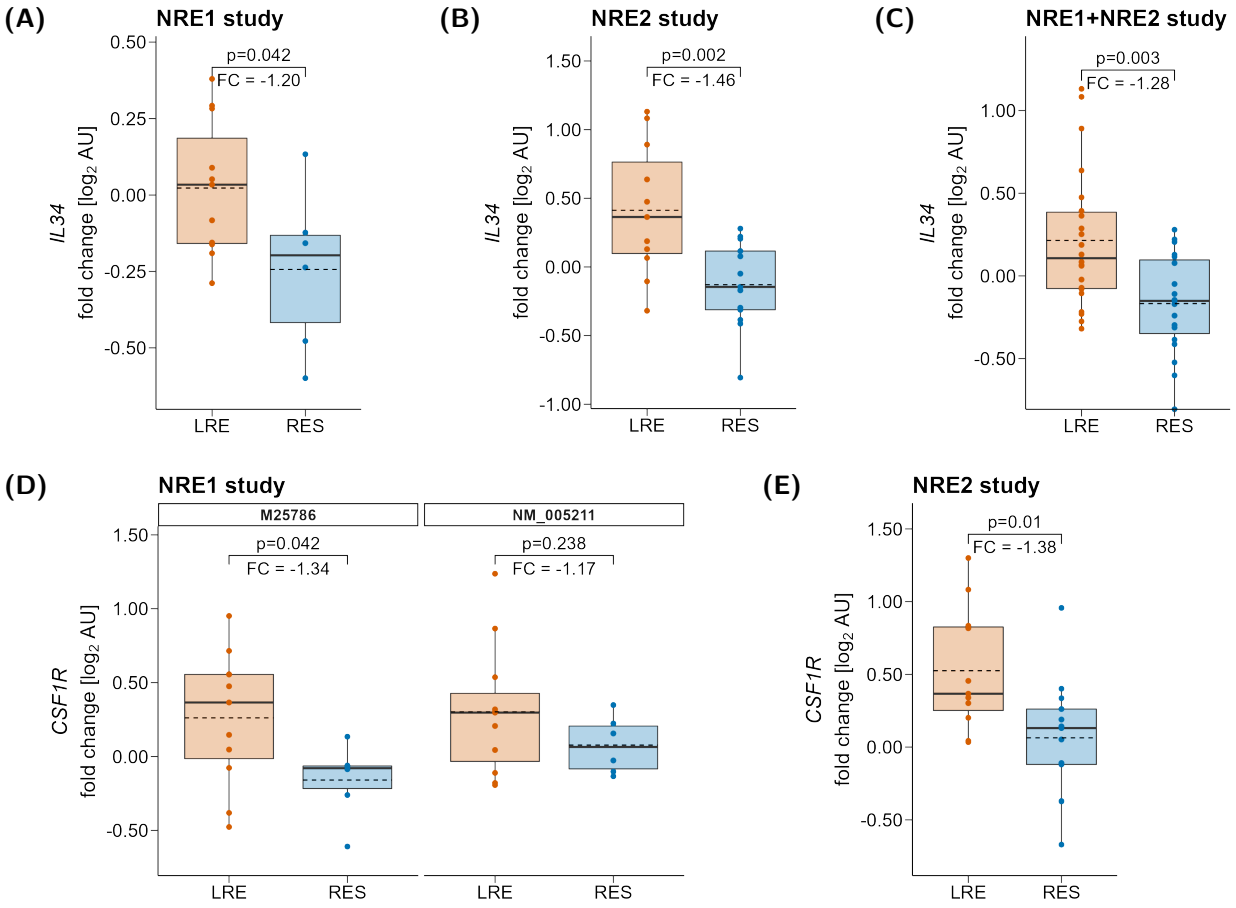

Figure 18: Transcriptomics data of IL34 and its receptor CSF1R expression between ISI_{Mats} response groups. The boxplots show the differential transcriptional expression of interleukin 34 (IL34) and its receptor colony stimulating factor 1 receptor (CSF1R) between the responder (RES) and low-responder (LRE) groups after the training intervention (T5T0). It is shown for (A, D) NRE1 study, (B, E) NRE2 study, and (C) merged dataset of NRE1 with NRE2 study. The solid black line represents the median of the data, while the dashed black line represents the mean. The boxes represent the interquartile range (IQR) from the first to the third quartiles. The whiskers extend the box to the lowest or largest value no further than 1.5 × IQR. The p-values and fold changes were calculated using limma-analysis. The CSF1R was measured in the NRE1 study under two different public IDs (M25786 and NM_005211), which neither matched the public ID (NM_001288705) measured in the NRE2 study. Values were log_2-transformed. N = 17 for NRE1 (LRE = 11, RES = 6), or 24 for NRE2 (LRE = 11, RES = 13) or 41 for NRE1+NRE2 (LRE = 22, RES = 19). AU: arbitrary units.

Given that IL34 expression was measurable in the transcriptomics dataset of human skeletal muscle biopsies, we further investigated whether the human myotubes express and secrete IL34. To explore this, we cultured human myoblasts and induced their differentiation into hMTs for six days. During the differentiation process, cells were harvested at various time points, and the amount of IL34 transcript was quantified using qPCR. The results indicated that the cells rapidly expressed IL34, with the highest levels observed two days after initiation the differentiation process and, subsequently, gradually decreased in the following days (Figure 19A). The supernatant was collected from all cells to measure the secreted amount of IL34 protein by ELISA. The results demonstrated an increase in the secreted protein during differentiation, reaching its maximum three days after the induction of differentiation, followed by a subsequent decrease (Figure 19B). This temporal pattern of protein secretion aligned with the transcriptional pattern.

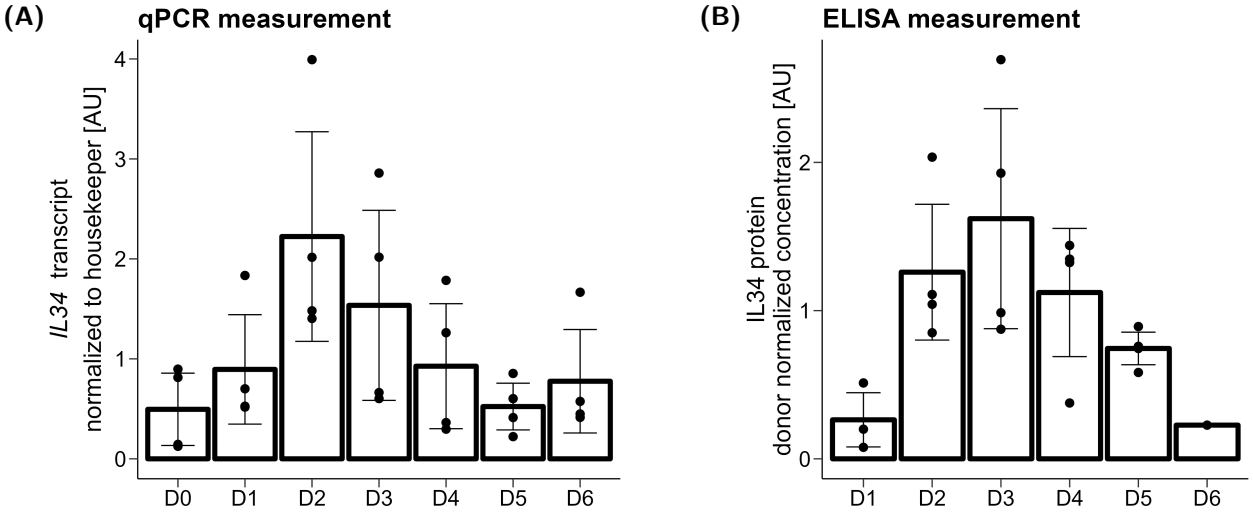

Figure 19: Transcriptional expression of IL34 in hMTs and its secretion. The figures show (A) the expression of interleukin 34 (IL34) transcript measured by quantitative polymerase chain reaction (qPCR) and (B) the secreted IL34 protein in the supernatant measured using enzyme-linked immunosorbent assay (ELISA) during cell differentiation. The cells were differentiated for 6 days (abbreviated with D0 – D6), and differentiation was initialized at D0. The differentiation medium was changed every 24 h. The qPCR data were normalized to the housekeeper gene *RPS28* and normalized by the mean expression per donor. The IL34 protein amount was calculated by standard curve and normalized by the mean amount per donor. Data are shown with ± SD. N = 4. AU: arbitrary units.

As a next step, we studied whether human myotubes respond to IL34 treatment. First, we tested the activity of the recombinant IL34 protein by using the human monocyte cell line THP-1, which is known to respond to stimulation with IL34 by increased phosphorylation of ERK1/2 [157]. The cells were cultured as described in section 3.2.3 and treated with 100 ng/mL IL34 for 1 min and 5 min. The treatment was immediately stopped by adding ice-cold PBS. The results showed that IL34 induced ERK phosphorylation after 1 min, whereas the signal was diminished after 5 min. Different recombinant IL34 proteins induced similar signal intensities (Figure 20).

To investigate the effect of IL34 on human myotubes, isolated human myoblasts were cultured and differentiated following the procedure outlined in section 3.2.2. The experiment was conducted in three biological replicates, each measured in two technical replicates. Cells were treated with 100 ng/mL IL34 for 1 min and 5 min. The results revealed that IL34 induced the phosphorylation of ERK, neither after 1 min nor after 5 min of treatment. Additionally, the phosphorylation of AKT was observed since the signaling cascade of CSF1R leads to increased pAKT for up to 10 min after treatment with IL34 in human monocytes [157]. An increased AKT phosphorylation could not be detected after treatment with IL34, which matched the results of ERK phosphorylation (Figure 21).

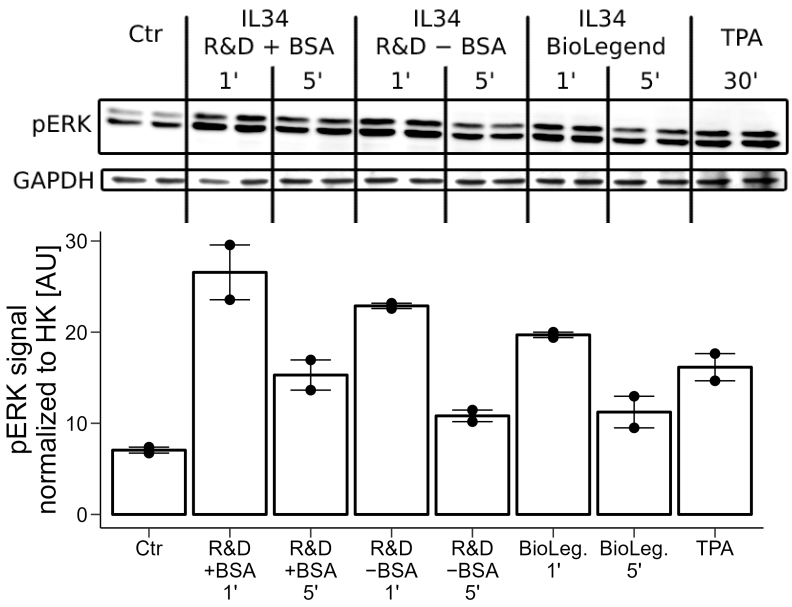

Figure 20: Treatment of THP-1 cells with IL34. THP-1 cells were treated with 100 ng/mL interleukin 34 (IL34) from different suppliers (R&D Systems or BioLegend) for 1 min or 5 min. The control cells were treated with PBS containing 0.1 % BSA for 5 min. For positive control, 0.1 µM TPA together with 1 µg/mL LPS were used and treated for 30 min. The treatments were performed at 37 °C and 5 % CO_2. The signal intensity of phosphorylated ERK was evaluated and normalized to the housekeeping gene *GAPDH*. Data are shown as mean ± SD. N = 2 (biological replicates). AU: arbitrary units.

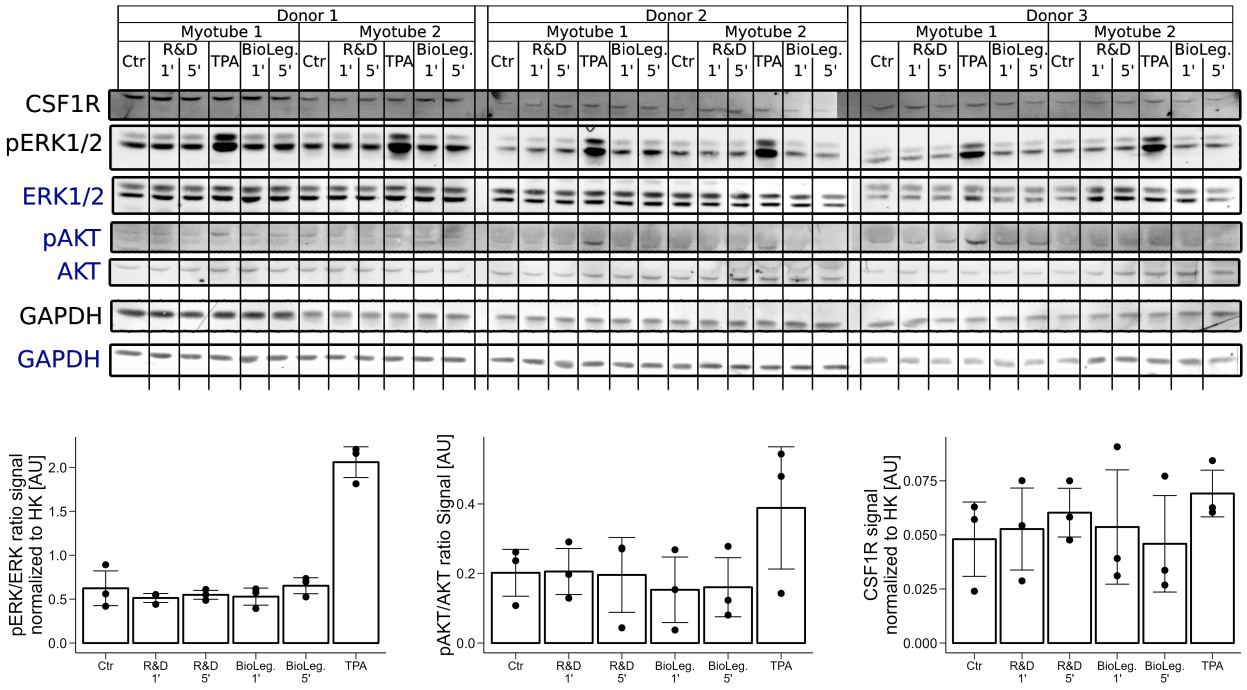

Figure 21: Treatment of human myotubes with IL34. Human myoblasts were differentiated for 10 days into human myotubes. Afterwards, cells were treated with 100 ng/mL interleukin 34 (IL34) from different suppliers (R&D Systems or BioLegend) for 1 min or 5 min. The control cells were treated with PBS containing 0.1 % BSA for 5 min. For positive control, 0.1 µM TPA with 1 µg/mL LPS was used and treated for 30 min. The treatments were performed at 37 °C and 5 % CO_2. Proteins were loaded onto two separated membranes, and the detected proteins per membrane were marked with different colors (black and blue). The CSF1R and pERK/ERK ratio were normalized to the membrane-specific housekeeper GAPDH. Data are shown as mean ± SD. N = 3. AU: arbitrary units.

Furthermore, no detectable phosphorylation of the CSF1R receptor was observed, which is the major receptor identified to be responsible for transducing IL34 action [157, 158]. The signal intensity of the receptor remained unaltered (Figure 21).

In an attempt to understand the lack of ERK pathway activation following IL34 treatment in differentiated cells, human myoblasts were treated with IL34 prior to differentiation. However, increased ERK phosphorylation was still undetectable (data not shown). This prompted us to question whether the receptor CSF1R is expressed in sufficient quantities. We examined RNA sequencing (RNA-Seq) data from the differentiated human myotubes to address this. After normalization to transcripts per million, it became apparent that the expression level of CSF1R was relatively low, while the expression of SDC1, which was also reported to be involved in IL34 signal transduction [159], was slightly higher (Figure 22). Notably, human myotubes showed pronounced expression of CSF1 compared to IL34. As an outlook, co-cultivation experiments with immune cells such as macrophages or monocytes known to react to IL34 and interact with the skeletal muscle could be performed. IL34 might then trigger the release of other cytokines from the immune cells, which in return influence the function of skeletal muscle.

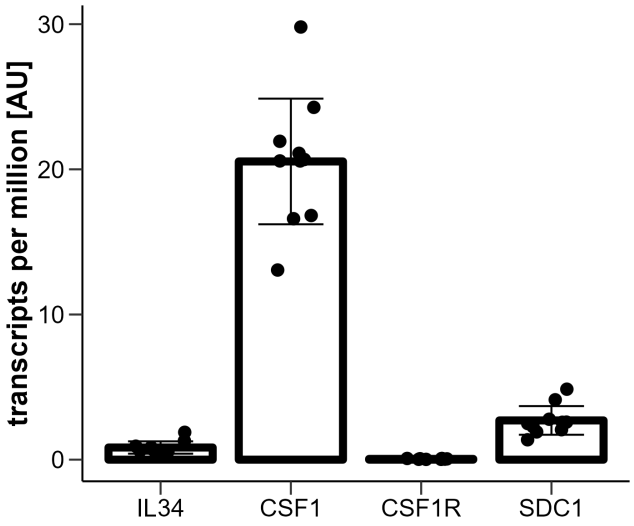

Figure 22: Transcriptional expression of IL34, CSF1R, and their receptor in human myotubes. The human myotubes (hMTs) were analyzed by RNA sequencing (RNA-Seq). The expression of interleukin 34 (IL34) and colony stimulating factor 1 (CSF1), together with their receptors colony stimulating factor 1 receptor (CSF1R) and syndecan 1 (SDC1), are shown as bar plots. The data are shown as transcripts per million with mean $\pm$ SD. N $= 10$. AU: arbitrary units.

4.1.3.2 Aldo keto-reductase 3 (AKR1C3)

The AKR1C3 was discovered as the second gene of interest due to its significant correlation with the change in ISI_{Mats} in both studies, separated and merged. Furthermore, it also exhibited significant differences in expression and methylation levels between RES and LRE following the 8-week training

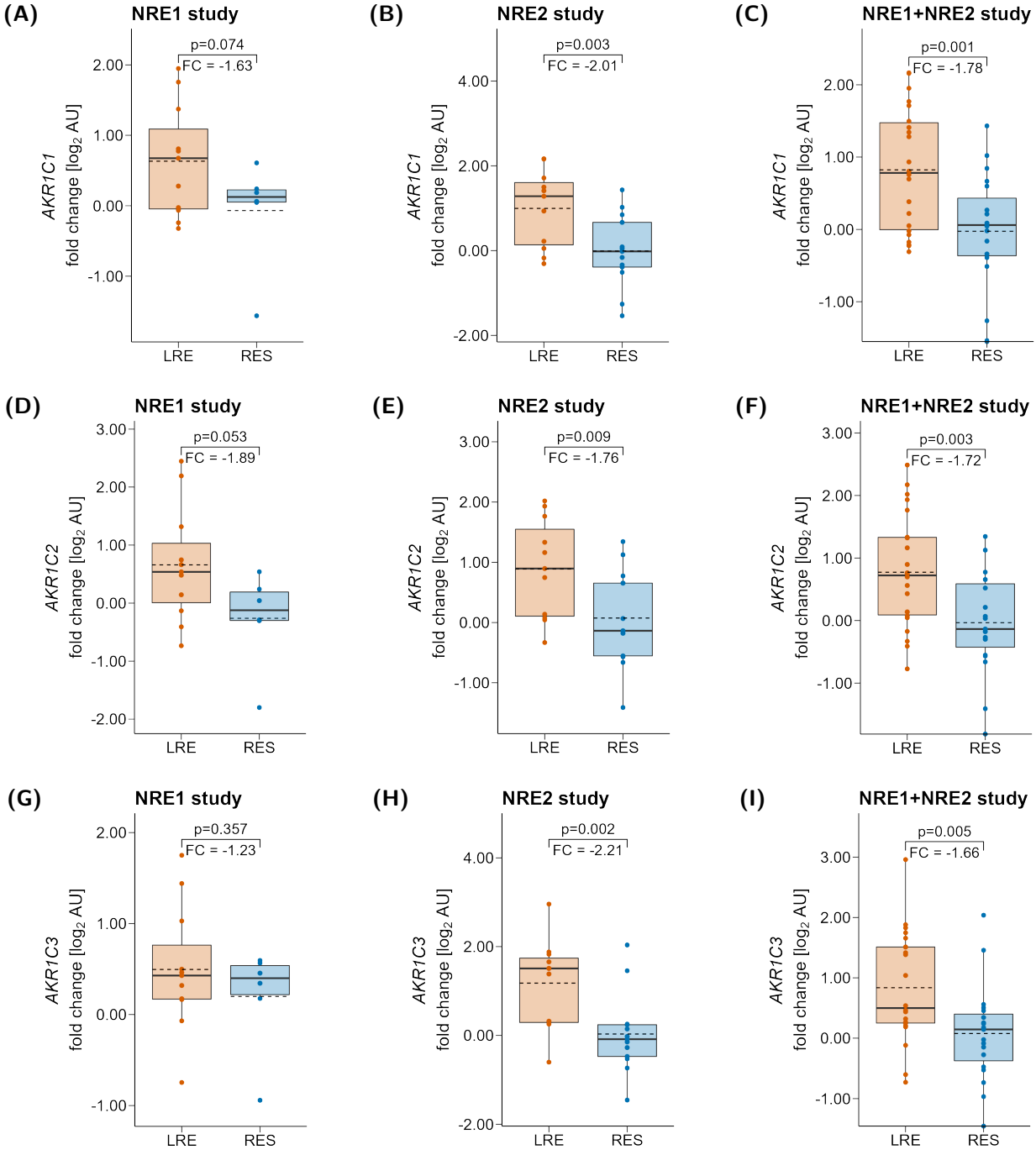

Figure 23: Transcriptomics data of AKR1C family expression between ISI_{Mats} response groups. The boxplots show the differential transcriptional expression of *AKR1C1*, *AKR1C2*, and *AKR1C3* between the responder (RES) and low-responder (LRE) groups after the training intervention (T5T0), respectively. It is shown for (A, D, G) NRE1 study, (B, E, H) NRE2 study, and (C, F, I) merged dataset of NRE1 with NRE2 study. The solid black line represents the median of the data, while the dashed black line represents the mean. The boxes represent the interquartile range (IQR) from the first to the third quartiles. The whiskers extend the box to the lowest or largest value no further than 1.5 × IQR. The p-values and fold changes were calculated using limma-analysis. Data in (H) were already shown in Figure 8I. N = 17 for NRE1 (LRE = 11, RES = 6), or 24 for NRE2 (LRE = 11, RES = 13), or 41 for NRE1+NRE2 (LRE = 22, RES = 19). AU: arbitrary units.

intervention. In addition to AKR1C3, skeletal muscles also express the two other family members, AKR1C1 and AKR1C2. Interestingly, all three family members exhibited a similar expression pattern with higher expression in the LRE group compared to the RES group after the training intervention (Figure 37A). In addition, AKR1C3 was detected in the proteomics analysis (section 4.2) and the data support a significant negative correlation with the change in ISI_{Mats} (Figure 37B). To investigate their function, we cloned the transcripts into an inducible overexpression vector and stably transducted them into the C2C12 mouse muscle cell line. The overexpression was induced by 100 ng/mL doxycycline treatment for 48 h (Figure 24). The stable cell lines did not exhibit any noticeable growth, differentiation, or phenotype behavior (data not shown).

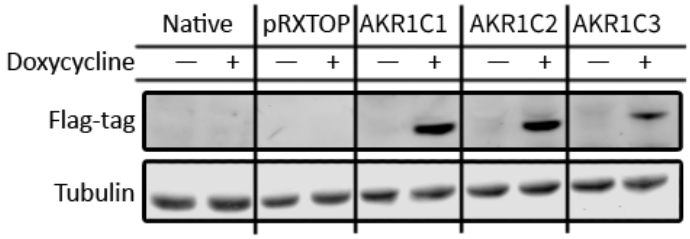

Figure 24: Overexpression of AKR1C1, AKR1C2, and AKR1C3 in C2C12 cell lines. Western blot showing the overexpression of AKR1C1, AKR1C2, and AKR1C3, respectively, in the mouse muscle C2C12 cell line before and after treatment with 100 ng/mL doxycycline for 48 h Native (non-transducted) C2C12 cells as well as cells containing the empty vector (pRXTOP) were used as controls. The aldo-keto reductases (AKRs) were detected by the added N-terminal 3x flag-tag. Tubulin was used as a loading control.

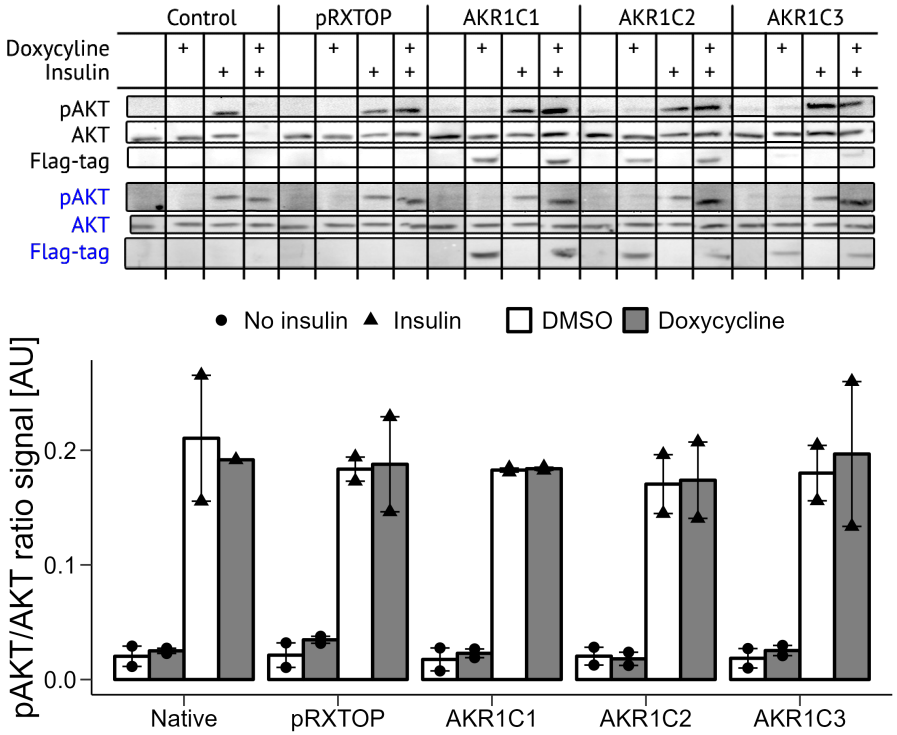

Figure 25: Insulin treatment of C2C12 overexpressing AKR1C1, AKR1C2, or AKR1C3. Mouse muscle C2C12 cells were differentiated into myotubes for 5 days. Afterwards, 100 ng/mL doxycycline was added for 48 h. The cells were starved for 3 h and treated with 10 nM insulin for 10 min. Proteins detected on one membrane are shown with the same label color. The western blot was manually reordered to fit the diagram for simplified comparison. The AKRs were detected by the added N-terminal 3x flag-tag. Native (non-transducted) C2C12 cells and cells containing the empty vector (pRXTOP) were used as controls. Data are shown with ± SD. N = 2 (One data point of control with insulin and doxycycline was removed due to no detection of AKT).

Next, we examined the effect of insulin on cells overexpressing one of the AKR family members. In order to do this, we differentiated the myoblasts into myotubes for five days, as described in section 3.2.1. Subsequently, 100 ng/mL doxycycline was added for 48 h. Following the treatment, the cells were fasted for 3 h in a serum-free medium and treated with 10 nM insulin for 10 min at 37 °C. We utilized the increased phosphorylation of serine 473 of AKT as a read-out. Native cells and cells with stable integration of the empty vector (pRXTOP) were used as controls. Despite detecting the overexpression for each of the three family members, no alterations in the insulin effect on AKT phosphorylation were observed (Figure 25). The basal phosphorylation of AKT was similar among all stable cell lines and comparable to the controls. Following insulin treatment, AKT phosphorylation was increased. However, no differences were observed between the stable cell lines with the empty vector and those overexpressing AKR1C1, AKR1C2, or AKR1C3 (Figure 25).

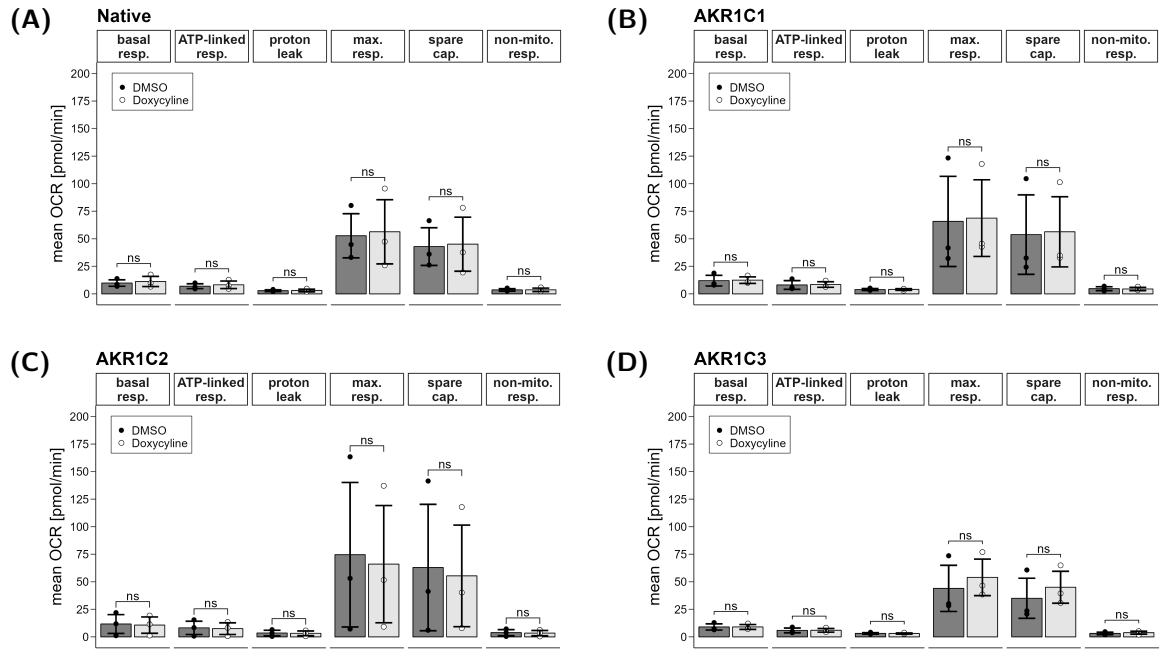

Figure 26: Mitochondrial respiration of C2C12 cells overexpressing AKR1C1, AKR1C2, or AKR1C3. Mouse muscle C2C12 cells were differentiated for 5 days and afterwards treated with 100 ng/mL doxycycline for 48 h. Afterwards, the cells were measured using the Seahorse XF analyzer. The cells were treated with 10 µM oligomycin, 20 µM FCCP, 5 µM rotenone with 5 µM antimycin A. The key parameters were calculated according to the SOP from the manufacturer and normalized to protein amount. The p-values were calculated using an unpaired two-sided Student's t-test. Native cells were used as control, and DMSO was used as treatment control. Data are shown as mean ± SD. Cap.: capacity; max.: maximum uncoupled; mito.: mitochondrial; OCR: oxygen consumption rate; resp.: respiration. N = 3.

We also asked the question of whether the overexpression of the AKRs alters mitochondrial respiration. Therefore, the cells were fused to myotubes, treated as before with doxycycline for 48 h, and respiration was measured using the Seahorse XF analyzer. The measurement was performed as written in section 3.3. The key parameters of the analysis were calculated according to the standard protocol. Each parameter was statistically analyzed using an unpaired Student's t-test with control (DMSO) versus doxycycline treatment. To exclude any potential effect of the doxycycline treatment, native cells were measured with and without treatment. However, we observed no changes in any parameter following doxycycline treatment (Figure 26A). Additionally, neither of the stable cell lines exhibited a significant difference in mitochondrial respiration after the overexpression of AKR1C1, AKR1C2, or AKR1C3 (Figure 26B – D), respectively. Thus, their overexpression alone does not seem to have a strong influence neither on the insulin signaling, nor mitochondrial respiration. Since these proteins convert testosterone [160, 161] and prostaglandins [162], further experiments with overexpression and the addition of their substrates could be performed.

4.2 Changes in the skeletal muscle proteome after the 8-week training and the relation to improvement in mitochondrial respiration and insulin sensitivity

After the selection of potential interesting candidates from the transcriptomics and epigenomics analyses alone, we focused then on the proteome for additional candidates. In our proteomics approach, we used liquid chromatography (LC) to separate the peptide mixture with subsequent tandem mass spectrometry (MS/MS). The proteomics dataset consisted of detected 2,431 proteins. The dataset was filtered for proteins with a top-scoring hit with false-discovery rate (FDR) <0.01 and a posterior error probability of <0.01. Furthermore, solely proteins containing at least 90 % measured values in at least one of the four time points were considered. This resulted in a final amount of 1,857 proteins included in the statistical analysis. Furthermore, one sample was removed due to bad probe material, and one sample was removed due to a high number of missing values, resulting in being an outlier detected by principal component analysis (PCA). The final dataset included, therefore, 98 out of 100 samples. The first analysis focused on examining differential protein abundance

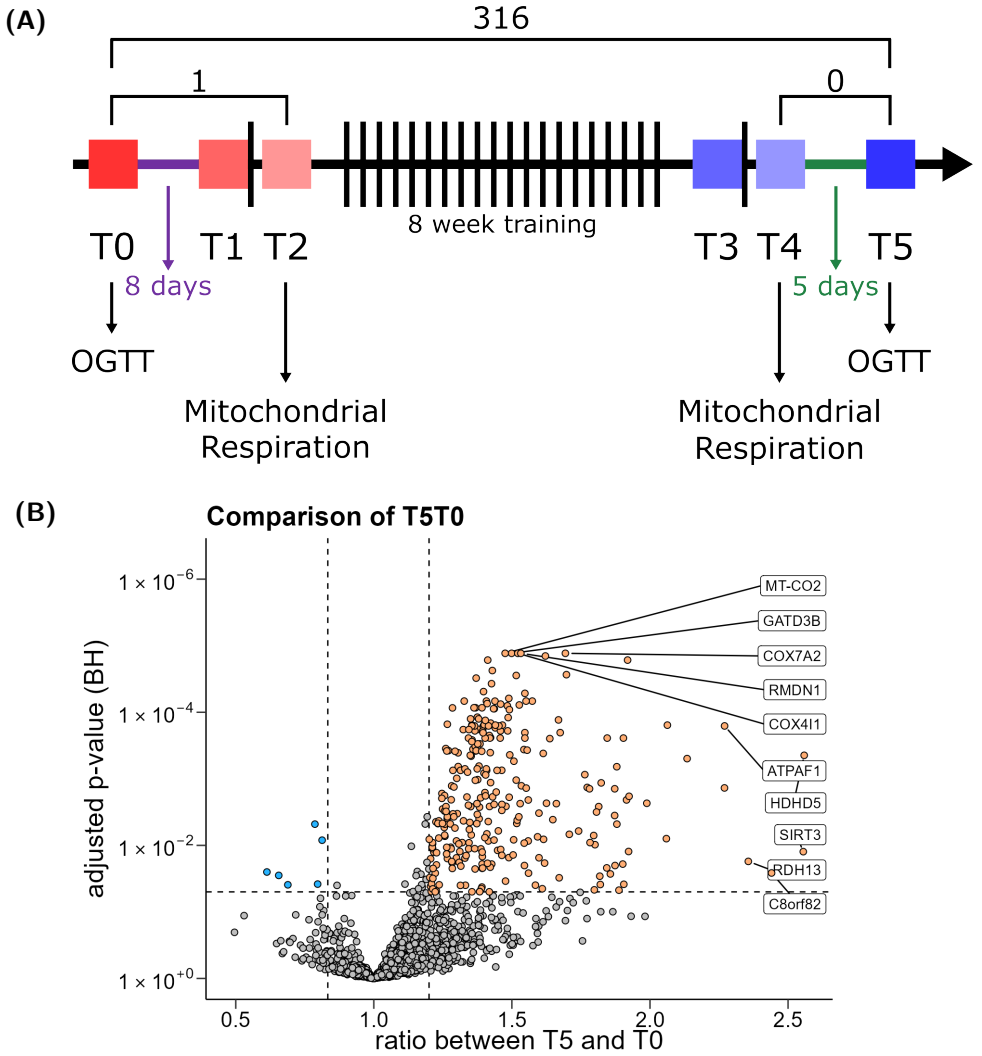

Figure 27: Exercise-induced differences in protein abundance in skeletal muscle biopsies. (A) A schematic representation of the training intervention study. The numbers show the significantly regulated proteins between the time points (adjusted p-value < 0.05). (B) The volcano plot shows the differential protein change for the comparison of T5T0. Proteins with a significant regulation (adjusted p-value < 0.05) and a fold change of at least ± 1.2 were colored in blue for downregulation and orange for upregulation. The five most significant proteins and the five most upregulated proteins were annotated. N = 25, or 23 for T4. OGTT: oral glucose tolerance test.

between the different time points. The results are summarized in Figure 27A. The acute response before the training intervention (T2T0) exhibited only one protein that was significantly altered (adjusted p-value < 0.05), and no proteins were significantly altered as an acute response after the training intervention (T4T5). When comparing the two resting time points T5T0 to study the effect of the 8-week training period, 316 proteins exhibited significantly changed abundance (adjusted p-value < 0.05), with 97.6 % (309 out of 316) of them being upregulated. By applying a fold change cutoff of at least 1.2 (corresponding to a minimum 20 % up- or downregulation), 299 proteins remained, of which 293 were upregulated and 6 were downregulated (Figure 27B). The most significantly regulated protein was COX7A2 (cytochrome c oxidase subunit 7A2) with an adjusted p-value $= 1.3\text{x}10^{-5}$ and 1.69-fold increase, while the most upregulated protein was HDHD5

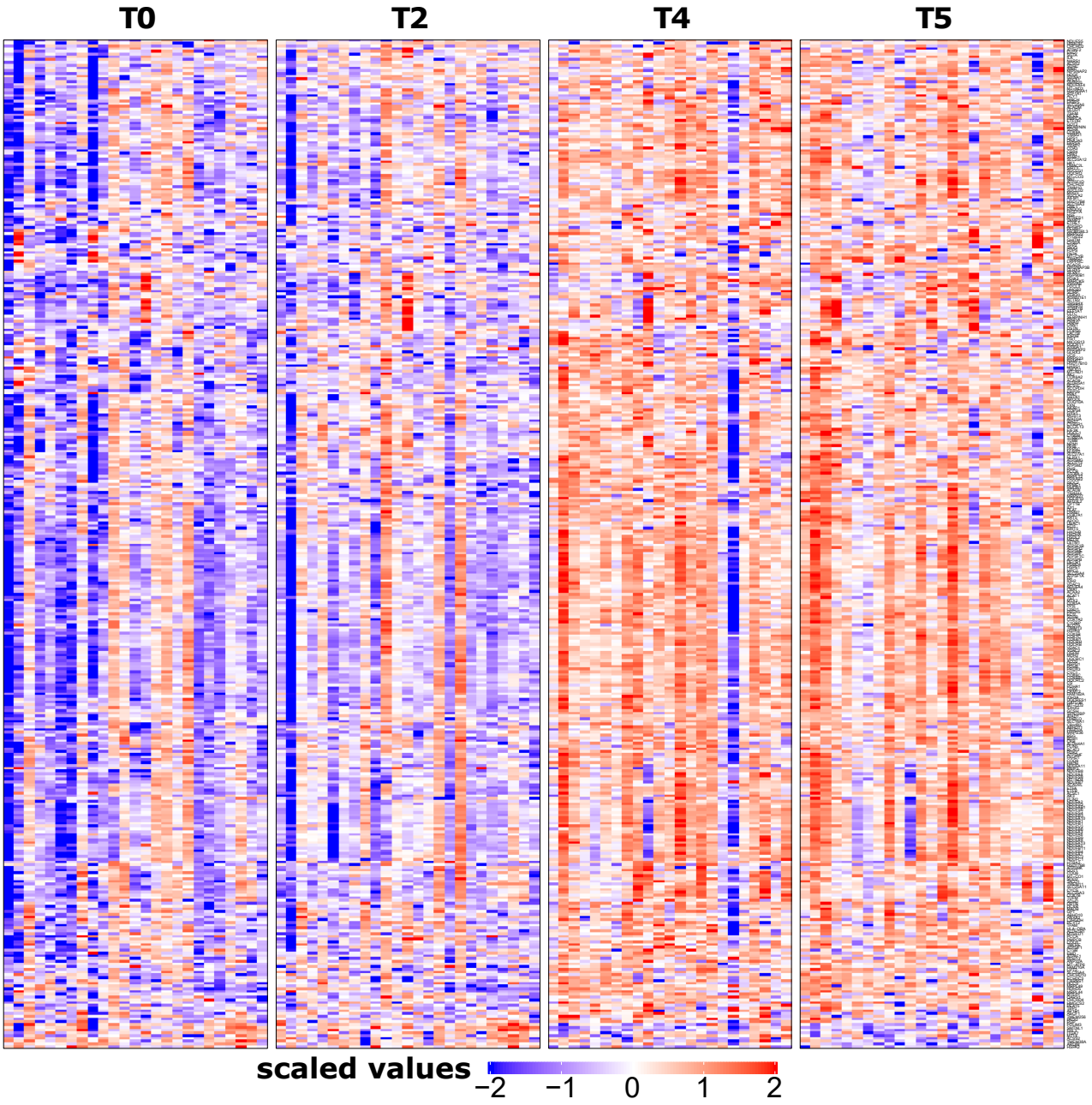

Figure 28: Heatmap with scaled protein change at each time point. The heatmap shows the protein abundance for each subject and time point. The measured values were scaled for comparison between different proteins. Blue represents a low abundance at the indicated time point, while red represents a high abundance. Only significantly regulated (adjusted p-value < 0.05) proteins for the comparison T5T0 or T4T0 are shown. The rows were sorted using the Euclidean distance complete linkage clustering. N = 25, or 23 for T4.

(haloacid dehalogenase-like hydrolase domain-containing 5) with 2.56-fold increase. Furthermore, when comparing the last exercise time point T4 with the first resting time point T0, 301 proteins exhibited a significantly altered abundance (adjusted p-value < 0.05), of which 251 showed the same direction of change compared with T5T0. To visualize this, a heatmap was created, showing the scaled measured values per subject for all proteins that were significantly altered at either the training comparison T5T0 or the comparison T4T0 (Figure 28). The heatmap demonstrates that the protein levels are elevated after the 8-week training intervention at time point T4 and remained elevated after five days of no training at time point T5.

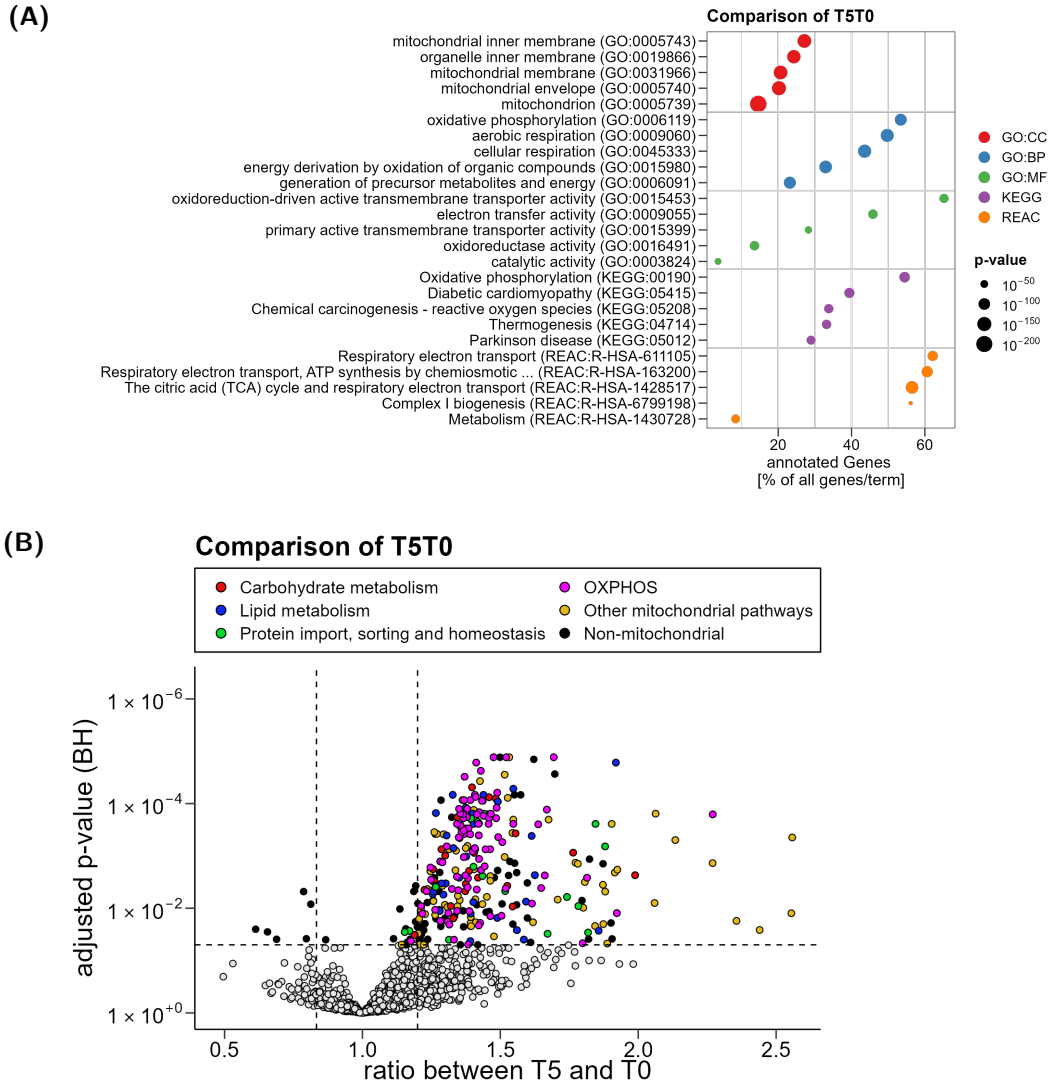

Figure 29: Enrichment of mitochondrial proteins after the training intervention. (A) The 316 significantly altered (adjusted p-value < 0.05) proteins after the training intervention were analyzed for enrichment. For the data source, the GO cellular component (CC, red), biological process (biological process, blue) and molecular function (MF, green), and the biological pathways of Reactome (REAC, purple) and Kyoto encyclopedia of genes and genomes (KEGG, orange) were used. (B) The differential protein change is plotted as a volcano plot. Significantly altered proteins are colored according to their mitochondrial pathway or shown in black for non-mitochondrial proteins according to MitoCarta 3.0. Non-significantly changed proteins are marked as empty circles. The p-values for plotting were adjusted for multiple testing using to Benjamini-Hochberg (BH).

Subsequently, an enrichment analysis was performed on the 316 significantly changed proteins after the training intervention. The data was analyzed using GO:BP, GO:CC, GO:MF, REAC, and KEGG (Figure 29A). The results exhibited multiple mitochondria-associated pathways such as the TCA cycle, oxidative phosphorylation (OXPHOS), or respiratory electron transport. Consequently, utilizing the MitoCarta 3.0 database, the 316 proteins were annotated to their respective mitochondrial pathway, if available (Figure 29B). One can observe that none of the downregulated proteins is annotated to mitochondria. However, most significantly upregulated proteins (76 %, 240 out of 316) are associated with mitochondria or mitochondrial pathways. For a more comprehensive analysis and

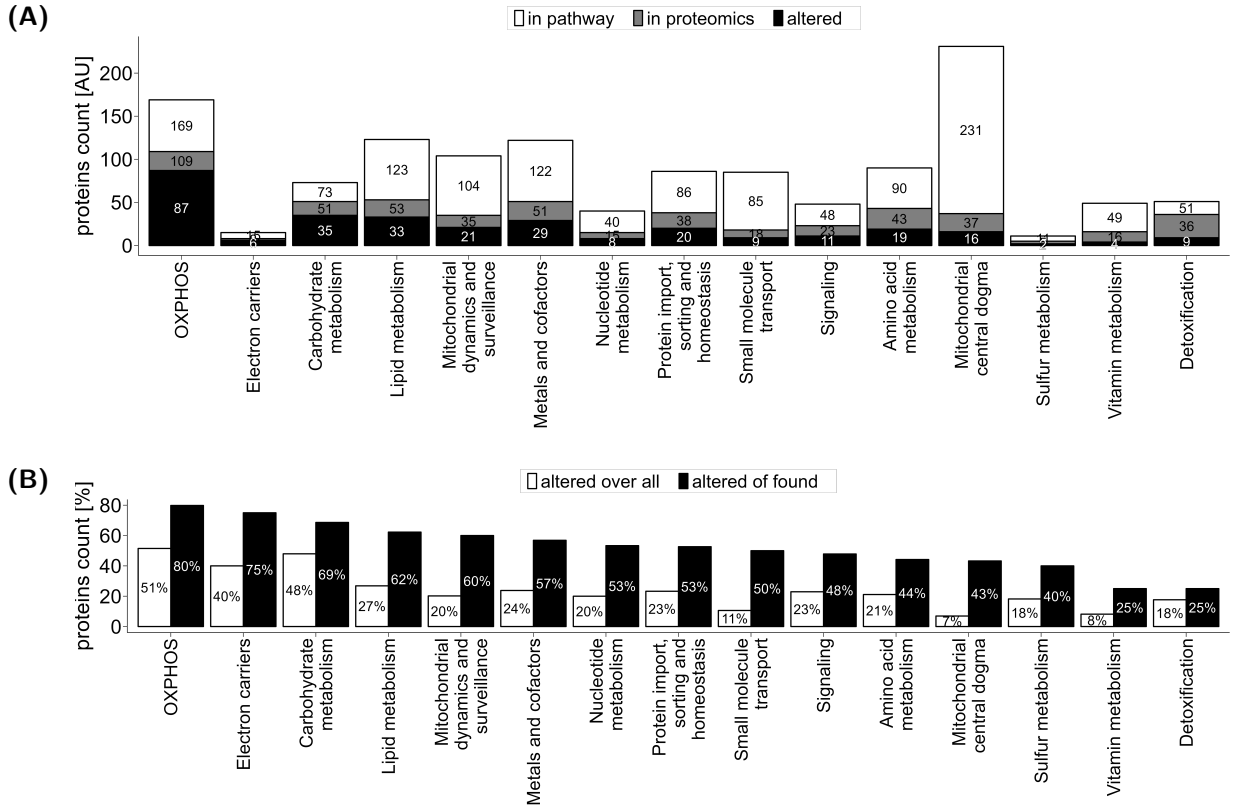

Figure 30: Proteins with changed abundance altered training and mitochondrial. (A) The bar plot shows the main mitochondrial pathways in MitoCarta. The white bar represents the number of all proteins annotated to the pathway (according to MitoCarta 3.0), the gray bar shows the number of these proteins found in our proteomics dataset, and the black bar represents the number of altered proteins per pathway. (B) The bar plot shows the percentage of altered proteins belonging to the pathway by the white bar, and the black bar shows the percentage of altered proteins over all detected proteins in the pathway. The alteration was defined as significantly changed (adjusted p-value < 0.05) at T5T0.

visualization of the pathways found in the database, bar plots were generated (Figure 30A). They display the number of proteins belonging to the specific pathways according to the MitoCarta 3.0 database, the number of proteins found in the proteomics dataset, and the number of significantly regulated proteins (T5T0) of the dataset per pathway. Furthermore, Figure 30B shows the percentage of regulated proteins out of all proteins in the pathway or out of all detected proteins in this pathway. The pathways with the highest percentage are OXPHOS with 80 %, electron carriers with 75 %, and carbohydrate metabolism with 69 %. To enhance understanding, a schematic representation of the OXPHOS pathway, one of the key energy metabolism pathways in mitochondria, was created (Figure 31A). All identified proteins, as well as significantly changed proteins, were marked and assigned to their respective complexes within the pathway. Proteins with significantly increased (adjusted p-value < 0.05) abundance were found in all complexes. Similarly, a graphic was created for the TCA cycle (Figure 31B).

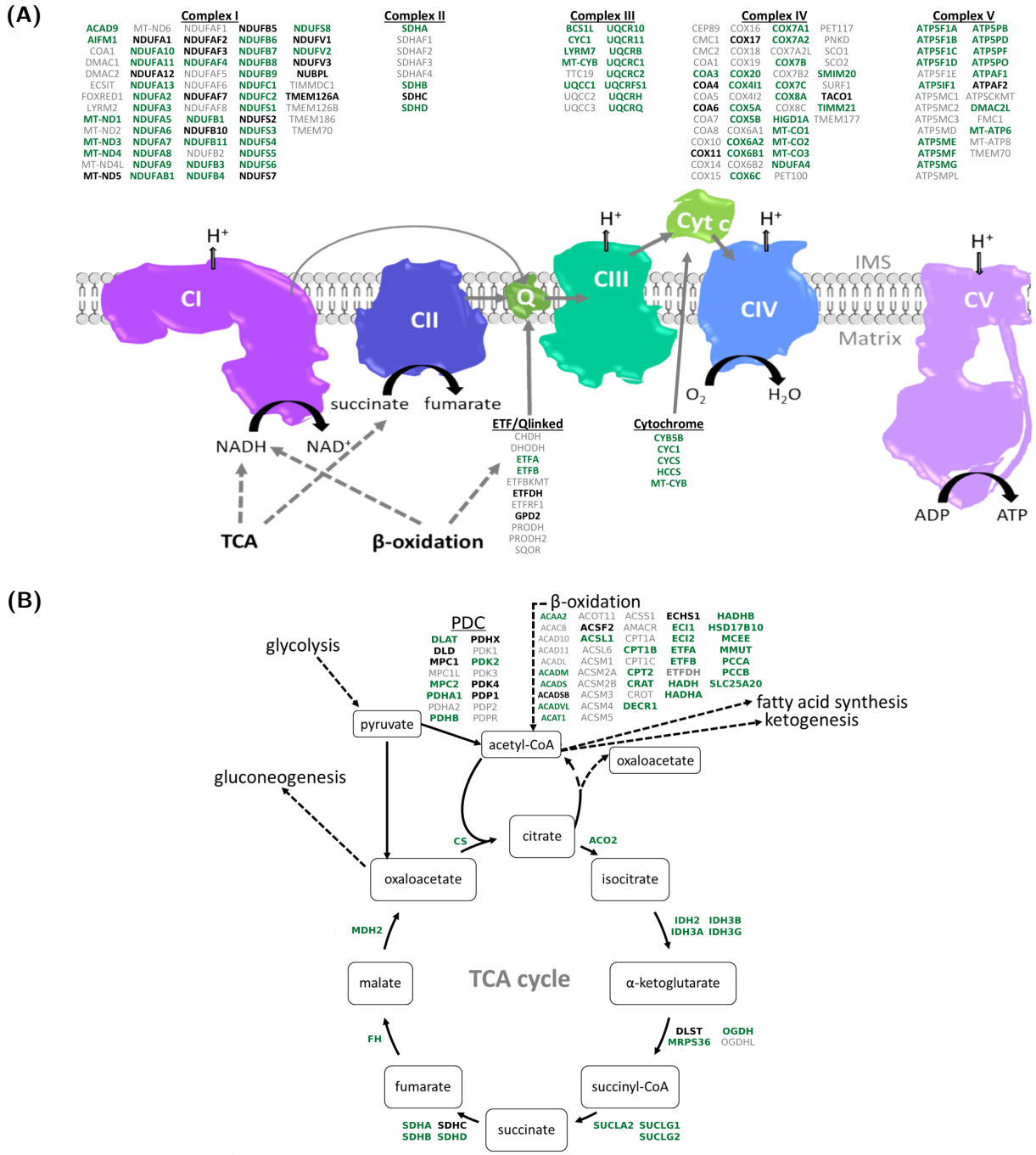

Figure 31: Schematic representation of OXPHOS and TCA cycle. The schemes show the mitochondrial pathways (A) oxidative phosphorylation (OXPHOS) and (B) tricarboxylic acid cycle (TCA cycle). The proteins belonging to the individual complexes and pathways were added. In gray are proteins belonging to the complex or pathway (according to MitoCarta 3.0) but not measured in the data. In black are found proteins in the dataset, and in green found and significantly altered (adjusted p-value < 0.05) proteins when comparing T5T0.

The upregulation of mitochondrial proteins raised the question of whether this is correlated to the increase in mitochondrial respiration in isolated muscle fibers. Mitochondrial respiration was analyzed in muscle fibers obtained from muscle biopsies at the time points T2 and T4 by high-resolution respirometry. As published in Hoffmann et al. [145], mitochondrial respiration significantly increased (p-value < 0.05) across all subjects (Figure 32A). Subsequently, the changes in the protein abundance of the 316 training-regulated proteins between these time points were correlated with the increase in mitochondrial respiration. The results are depicted as a volcano plot (Figure 32B), and the

proteins were colored according to mitochondrial pathways using MitoCarta 3.0. Out of all proteins, 127 proteins (40 %, 125 positive, and 2 negative) exhibited significant correlation (p-value < 0.05). It is worth noting that only 9 positively correlated proteins were not assigned to a mitochondrial pathway according to the MitoCarta 3.0 database, namely BRAWNIN, CD93, CYB5R1, GATD3B, GOT1, GPT, PERM1, PSMD4, and SCCPDH.

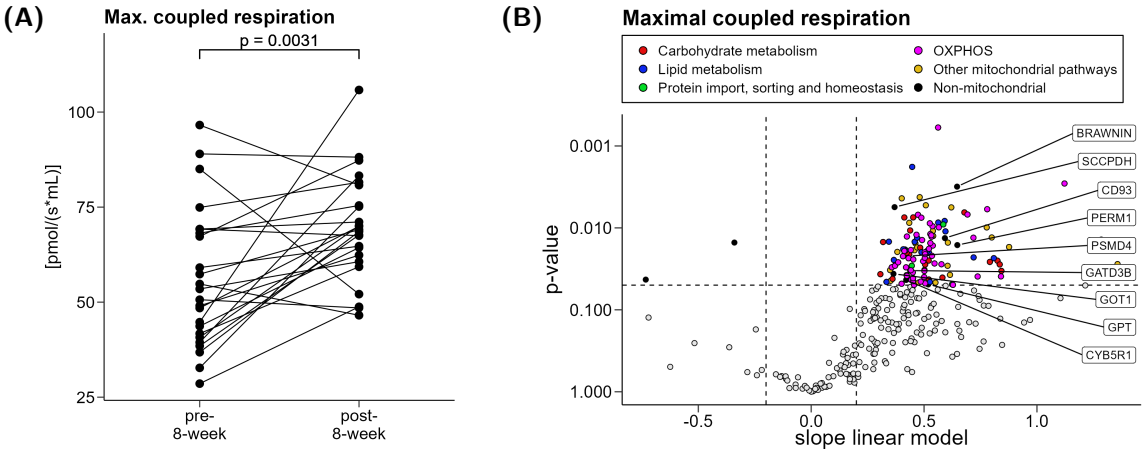

Figure 32: Mitochondrial respiration correlation with altered protein amount. (A) The mitochondrial respiration was measured at the time points T2 and T4 and the maximum coupled respiration is shown for each individual before and after the training intervention. The corresponding points belonging to one subject are connected with lines. The Significance level was calculated using a paired Student's t-test. (B) The differential protein amount for the comparison T4T2 was correlated with the change in the maximum coupled respiration. Only the 316 significantly altered (adjusted p-value < 0.05) proteins when comparing T5T0 are plotted. Mitochondrial and significantly (p-value < 0.05) correlated proteins were colored depending on their belonging pathways. Non-mitochondrial (according to MitoCarta 3.0) and significantly regulated proteins are shown in black, and positively correlated are additionally annotated. Non-significantly correlated proteins are shown as empty circles.

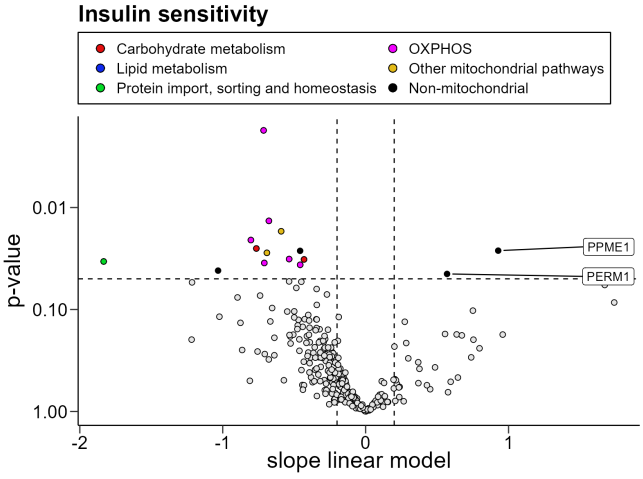

Figure 33: ISI_{Mats} correlation with altered protein amount. The differential protein change when comparing T5T0 was correlated with the change in insulin sensitivity according to DeFronzo and Matsuda (ISI_{Mats}). Only the 316 significantly altered (adjusted p-value < 0.05) proteins when comparing T5T0 are plotted. Mitochondrial and significantly (p-value < 0.05) correlated proteins were colored depending on their belonging pathways. Non-mitochondrial (according to MitoCarta 3.0) and significantly regulated proteins are shown in black, and positively correlated are additionally annotated. Non-significantly correlated proteins are shown as empty circles.

Next, we aimed to identify proteins regulated by the training intervention that correlated with the change in ISI_{Mats}. The correlation results are presented in the volcano plot (Figure 33), and the proteins were colored according to mitochondrial pathways using MitoCarta 3.0., showing the

316 proteins regulated by training (T5T0). Solely 15 proteins (5 %, 2 positive, and 13 negative) correlated significantly (p-value < 0.05) with an increase in ISI_{Mats}. The two positively correlated proteins were PPME1 and PERM1.

4.2.1 Protein phosphatase methylesterase 1 (PPME1)

After the 8-week training intervention study, the expression of protein phosphatase methylesterase 1 (PPME1) over all subjects was significantly increased at T4 and remained at a high level following five days of no training at T5 (Figure 35A). Furthermore, the change in PPME1 protein exhibited a significant positive correlation (p-value = 0.0343, r = 0.4247) with the increase in ISI_{Mats} post-intervention (Figure 34B). Additionally, a significant positive correlation of both resting levels (T0 and T5) of ISI_{Mats} with the resting protein expression of PPME1 (p-value = 0.0348, r = 0.4237 for T0, p-value = 0.0279, r = 0.4396 for T5) was observed (Figure 34C, D), respectively. The residuals of the correlation analysis were considered as normal distributed based on the Shapiro-Wilk test, which was the case for all correlations.

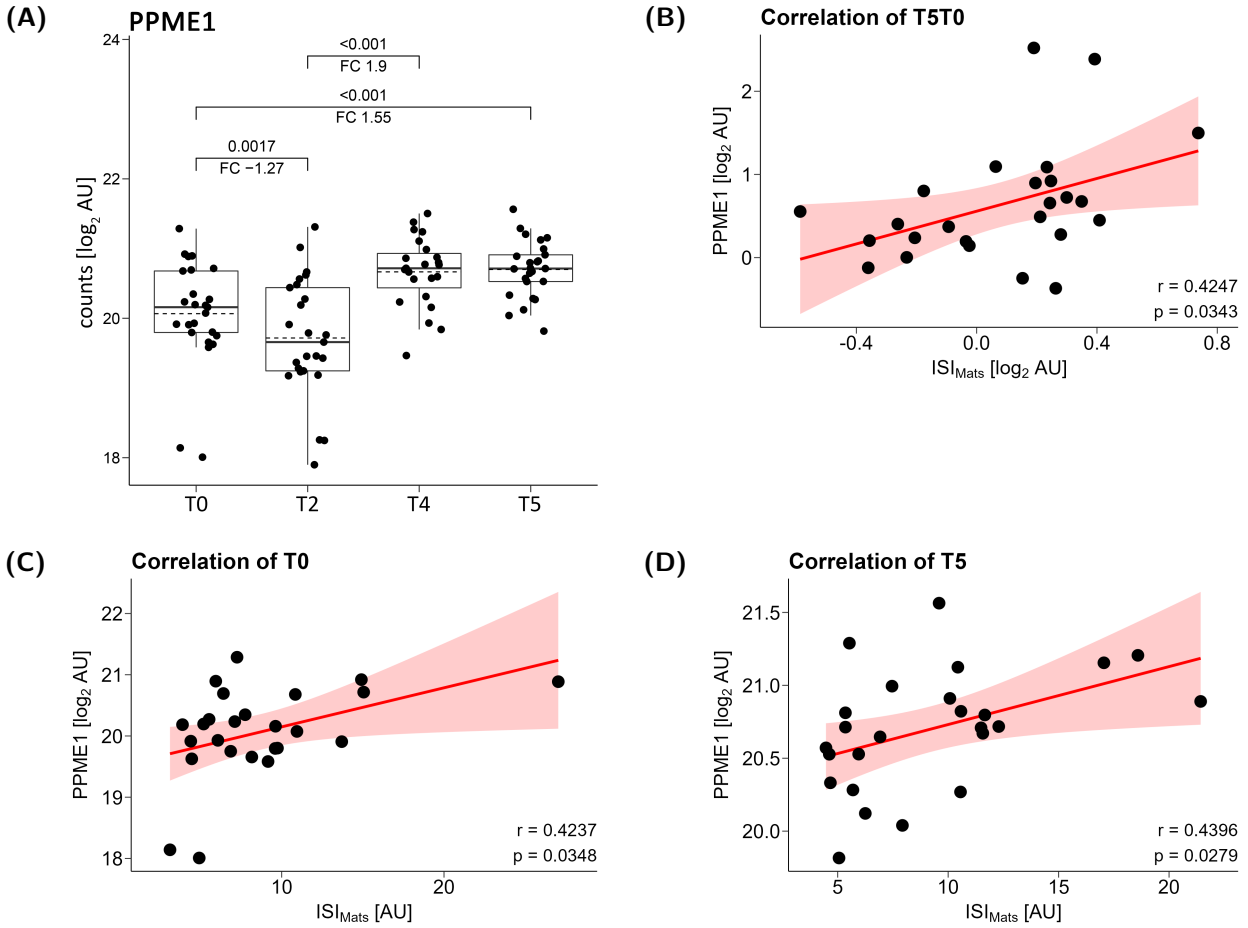

Figure 34: Expression of protein phosphatase methylesterase 1 (PPME1) and correlation with ISI_{Mats} (A) Boxplot of the protein expression of PPME1 for the four time points The box represents the interquartile range (IQR, 25th to 75th percentile). The solid black line represents the median of the data, while the dashed black line represents the mean. The whiskers extend the box to the lowest or largest value no further than 1.5 × IQR. The p-values and fold changes were calculated using limma-analysis. The correlation of the fold change in abundance of PPME1 with the fold change ISI_{Mats} is shown for the comparison of (B) T5T0, whereas (C) shows the correlation of the abundance of the protein with the ISI_{Mats} at baseline T0, and (D) at post-intervention T5. The red line represents the regression line. The shaded red area around the regression line represents the 95 % confidence interval. The p- and r-values were calculated using a Pearson correlation. Residuals of the correlation analyses were tested for normally distribution (p-value > 0.05) using the Shapiro-Wilk normality test. All residuals were found to be normal distributed. N = 25, or 23 for T4.

4.2.2 PPARGC1 and ESRR induced regulator 1 (PERM1)

The second potential interesting protein based on the proteome data is PPARGC1 and ESRR induced regulator 1 (PERM1). PERM1 protein exhibited a significant increase following the 8-week training intervention when comparing both resting time points T5T0 over all subjects (Figure 35A). Additionally, a significant positive correlation was observed with the change in ISI_{Mats} (p-value = 0.0464, r = 0.4020, Figure 35B) as well as with the increase of maximal coupled mitochondrial respiration (p-value = 0.0162, r = 0.4954, Figure 35C). Thus, both proteins, PPME1 and PERM1, are considered as interesting candidates for future functional studies.

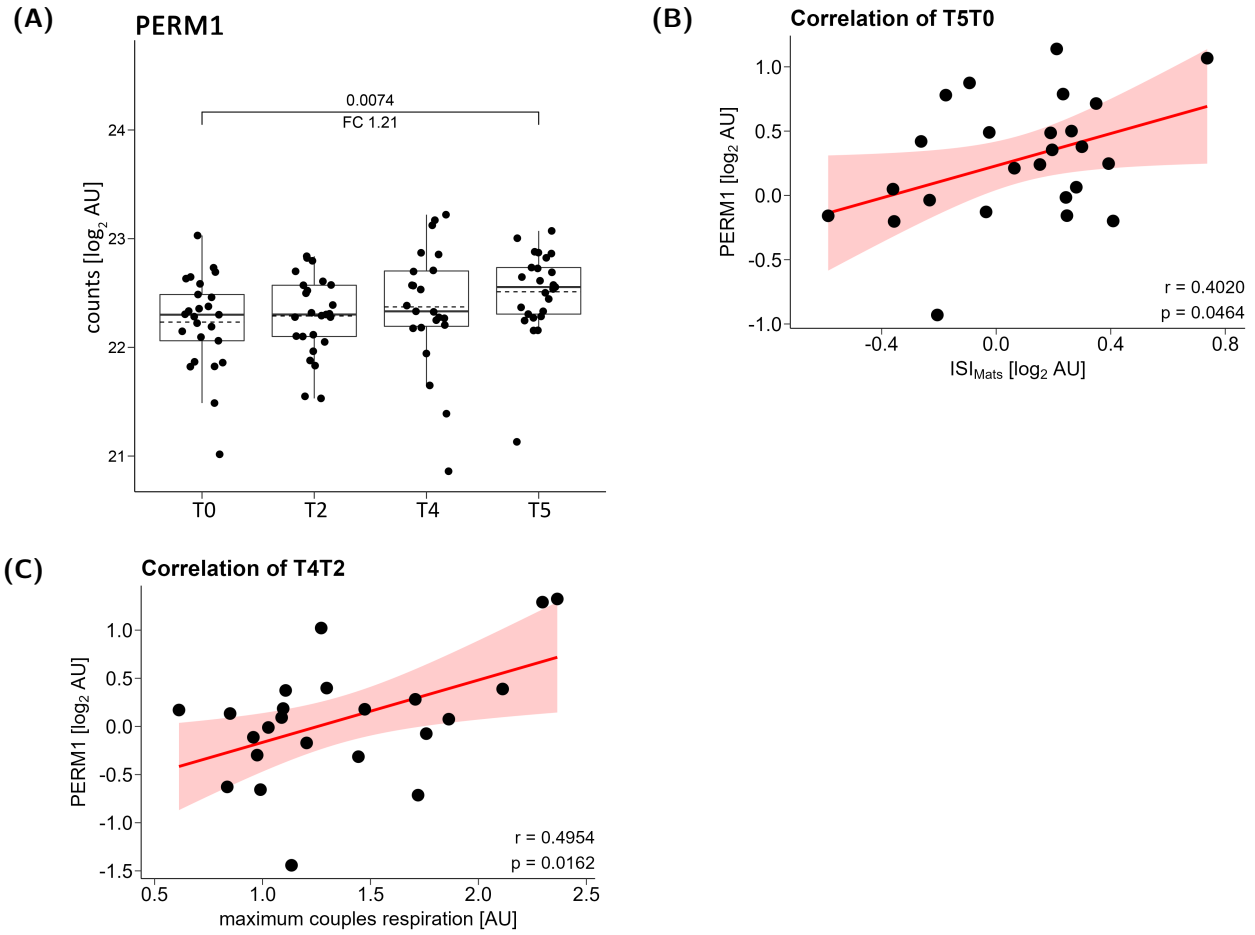

Figure 35: Expression of PPARGC1 and ESRR induced regulator 1 (PERM1) and correlation with ISI_{Mats} and respiration (A) Boxplot of the protein expression of PERM1 for the four time points The box represents the interquartile range (IQR, 25th to 75th percentile). The solid black line represents the median of the data, while the dashed black line represents the mean. The whiskers extend the box to the lowest or largest value no further than 1.5 × IQR. The p-values and fold changes were calculated using limma-analysis. The correlation of the expression of PERM1 with ISI_{Mats} for the comparison T5T0 (B) and the correlation with maximal coupled respiration (C) is shown. The red line represents the regression line. The shaded red area around the regression line represents the 95 % confidence interval. The p- and r-values were calculated using a Pearson correlation. Residuals of the correlation analysis were tested for normal distribution using the Shapiro-Wilk normality test and a threshold of p-value < 0.05. N = 25, or 23 for T4.

4.2.3 Combined analysis of proteomics, transcriptomics, and epigenomics datasets

As a last step of our multi-omics analysis, we performed combined analyses of the proteomics, epigenomics, and transcriptomics datasets. Firstly, we compared the regulation of the 316 differentially altered proteins after training (T5T0) with the regulation of their corresponding transcripts. The fold changes comparing T2T0, T4T0, and T5T0 were calculated for each subject. This was done for the proteomics data as well as transcriptomics data and plotted side-by-side (Figure 36). For 299 out of the 316 altered proteins, a corresponding transcript was found. The heatmap analysis revealed a notable pattern where many proteins that were upregulated at T5T0 had corresponding transcripts that showed an initial increase at T2T0 and T4T0 but were declined at T5T0. The data demonstrate the different kinetics of exercise-induced alterations in the abundance of muscular transcripts and proteins. Afterwards, we merged all three datasets and used the protein name and

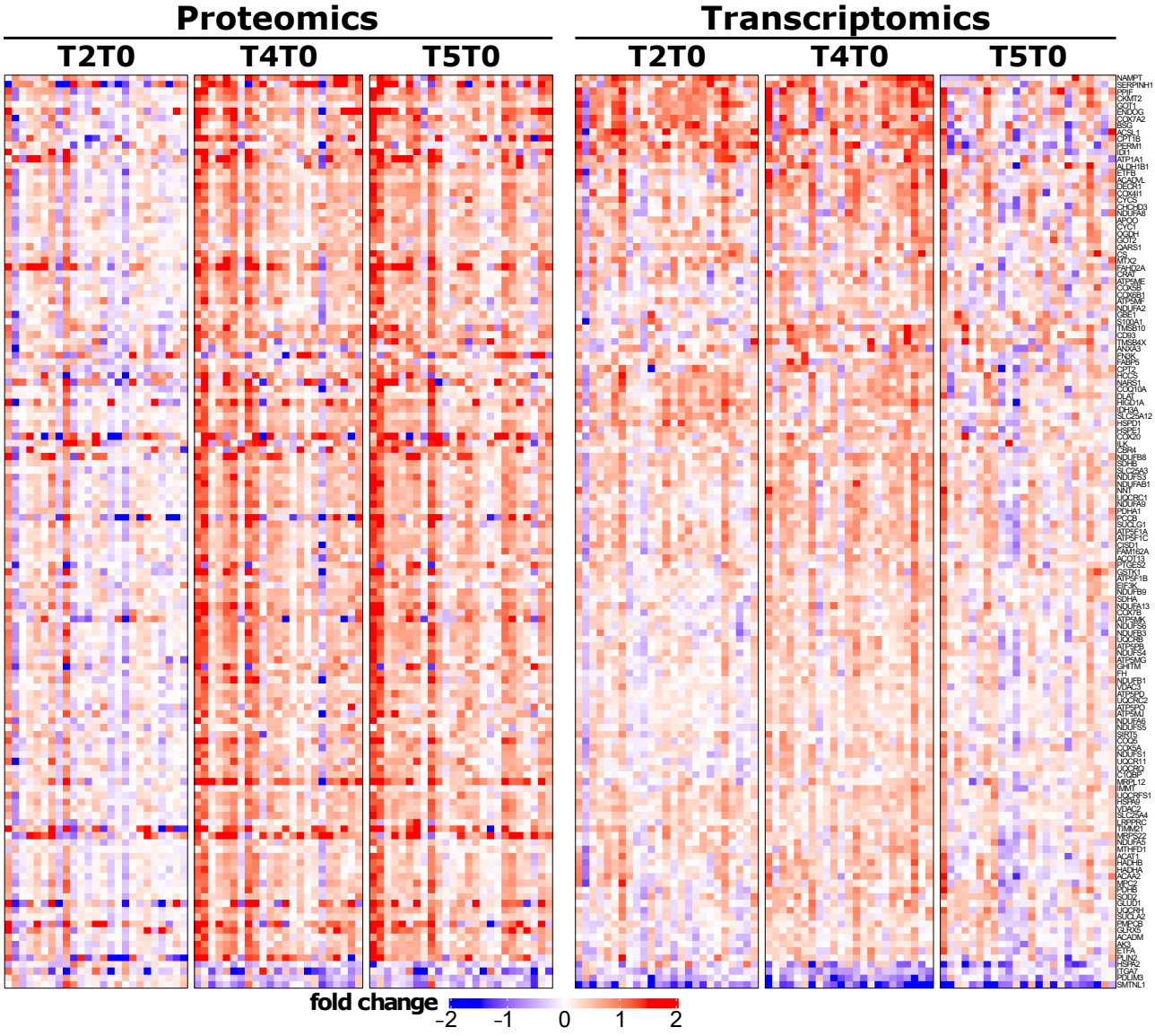

Figure 36: Comparison of proteomics and transcriptomics data at various time points. For each subject, the individual fold change in protein and transcript abundance was calculated for various time point comparisons. The comparisons T2T0, T4T0, and T5T0 are shown side-by-side. The three left heatmaps belong to proteomics data, while the three right heatmaps to transcriptomics data. Only the 299 out of 316 significantly altered (adjusted p-value < 0.05) with a corresponding transcript are shown. The abundance was scaled for comparison between different proteins. Red represents increased abundance compared to the resting level, while blue represents decreased abundance. The rows were sorted using the Euclidean distance complete linkage clustering. N = 25, or 23 for T4T0, or 24 for T5T0 (only transcriptomics).

gene symbol of the transcriptomics-epigenomics dataset from section 4.1. The protein names and gene symbols were revised to the currently used names using the HGNC atlas. After additionally including the epigenomics dataset, 298 altered proteins with a corresponding transcript and at least one CpG site remained.

Due to the high turnover and stability of mRNA, only a few transcripts (65 transcripts) were significantly regulated (adjusted p-value < 0.05) at the training comparison T5T0 in the transcriptomics data. Due to the sequential time resolved nature of RNA and Protein, T4T0 was used as the training comparison for the transcriptomics-epigenomics dataset, whereas T5T0 was used for the proteomics data. For this analysis, we used an unadjusted p-value for the epigenomics dataset and an adjusted p-value for the proteomics as well as transcriptomics datasets. This resulted in 68 significantly changed (adjusted p-value < 0.05) proteins at T5T0, which have a corresponding transcript significantly regulated (adjusted p-value < 0.05) at T4T0 and containing at least one significantly regulated (p-value < 0.05) CpG sites at T4T0. By including the correct or expected direction, as shown in Figure 14, 48 proteins and corresponding transcripts containing at least one regulated CpG site remained. These proteins are listed in Table 19 with the amount of significantly regulated CpG sites. Interestingly, the results displayed once more PERM1 as a potential protein of interest with 9 regulated CpG sites. However, when considering the response groups RES and LRE, neither PERM1 nor PPME1 showed a differential transcriptional regulation at any time, although some CpG sites were differentially regulated.

Table 19: Significantly regulated proteins with corresponding transcript and CpG sites. The table lists all proteins significantly regulated for the comparison T5T0, with a corresponding significantly regulated transcript and at least one significantly regulated CpG site comparing T4T0. The numbers in brackets show the amount of significantly regulated CpG sites. Proteins marked with a star (*) are non-mitochondrial, according to the MitoCarta 3.0 database. For the significance, an adjusted p-value was used for the protein and transcript expression, and an unadjusted p-value for the epigenetic data. The significance level was set to <0.05.

ACADM (2 CpG)	CHCHD3 (5 CpG)	HCCS (3 CpG)	NNT (2 CpG)
ACADVL (1 CpG)	COQ10A (3 CpG)	HIGD1A (2 CpG)	PDHA1 (2 CpG)
ACAT1 (4 CpG)	COX20 (3 CpG)	ILK (1 CpG)*	PDLIM3 (1 CpG)*
ANXA3 (1 CpG)*	COX4I1 (1 CpG)	IMMT (1 CpG)	PERM1 (4 CpG)*
ATP1A1 (3 CpG)*	CPT1B (1 CpG)	ITGA7 (6 CpG)*	SDHA (1 CpG)
ATP5F1A (1 CpG)	CPT2 (1 CpG)	LRPPRC (1 CpG)	SERPINH1 (2 CpG)*
ATP5F1B (2 CpG)	DLAT (1 CpG)	MRPS22 (2 CpG)	SLC25A3 (1 CpG)
ATP5F1C (2 CpG)	ETFA (2 CpG)	NARS1 (1 CpG)*	SLC25A4 (2 CpG)
ATP5MG (1 CpG)	ETFB (2 CpG)	NDUFA9 (1 CpG)	SMTNL1 (6 CpG)*
ATP5PD (1 CpG)	GOT1 (5 CpG)*	NDUFAB1 (2 CpG)	SUCLG1 (2 CpG)
BSG (3 CpG)*	HADHA (1 CpG)	NDUFB8 (1 CpG)	TMSB4X (2 CpG)*
CD93 (4 CpG)*	HADHB (3 CpG)	NDUFS1 (1 CpG)	UQCRC1 (3 CpG)

Of the 7 transcripts, *AKR1C3*, *IL34*, *P3H2*, *PLP1*, *SPECC1*, *SPI1*, and *TNFSF14*, which were considered as candidates with a distinct regulation in RES and LRE based on the epigenetic data and the transcriptional data as shown in section 4.1.3, only AKR1C3 was detected by our proteomics analysis. AKR1C3 protein abundance was not changed by training over all subjects, but it was differently regulated in RES and LRE, with an increase in LRE and almost no regulation in RES after the 8-week training intervention (Figure 23H and I, Figure 37A). This is also reflected by a negative correlation of the change in insulin sensitivity and the change in protein abundance (Figure 37B).

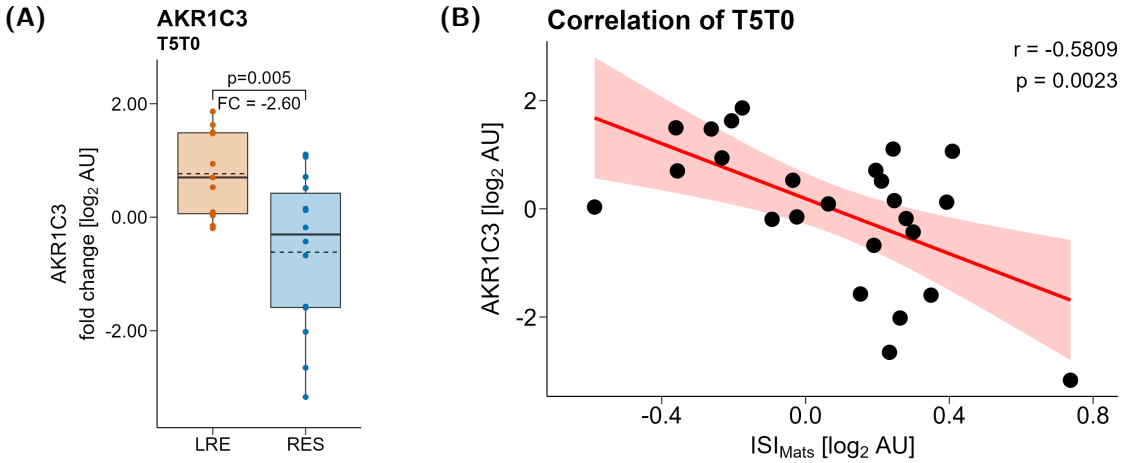

Figure 37: Proteomics data of AKR1C3 and its correlation with ISI_{Mats}. The change in the protein abundance of AKR1C3 (A) in the response groups and (B) the correlation with the change in insulin sensitivity after the 8-week training intervention. The p-value and fold change in (A) were calculated using limma-analysis, the p- and r-value in (B) were calculated using a Pearson r correlation. Residuals of the correlation analyses were tested for normally distribution (p-value $>$ 0.05) using the Shapiro-Wilk normality test. N = 25 (LRE = 11, RES = 14). AU: arbitrary units, FC: fold change.

To conclude, AKR1C3 is a promising candidate with a training-induced differential regulation in RES and LRE. Although we did not observe altered insulin signaling or mitochondrial respiration, further studies are needed to clarify the causes and potential consequences of this relation. Even though PERM1 and PPME1 were not differentially regulated on transcript or epigenetic level in RES and LRE, the difference in protein abundance is a strong argument for a potential functional significance.

4.3 Changes in serum proteins after acute exercise and the 8-week training and the relation to metabolic parameters

From the transcriptomics and epigenomics datasets we found IL34 as a potential interesting secreted cytokine, its role or function, however, in regulating peripheral insulin sensitivity remains to be discovered. Nevertheless, it hinted towards the potential relevance of secreted cytokines. Therefore we wanted to investigate the response of other secreted factors to acute and prolonged exercise. The following results were already published in Goj et al. [163]. Exercise-regulated cytokines can support exercise adaptations and contribute to the beneficial effects on insulin sensitivity and body fat regulation. To investigate the regulation of cytokines in response to acute exercise and training in the NRE2 study, serum samples from 22 out of 25 participants were analyzed using a proximity extension assay (PEA) (section 3.15 for detailed information), which provided relative concentrations of cytokines. From three participants, serum samples at T1 – T4 were not collected. The anthropometry and clinical data from the 22 participants are shown in Table S3. The assay comprised, in total, a set of 92 cytokines. We included in our analysis all cytokines which contained at least 80 % measured values above the limit of detection in at least one of the four time points. This resulted in 69 cytokines included in the analysis, of which 61 showed a significant increase

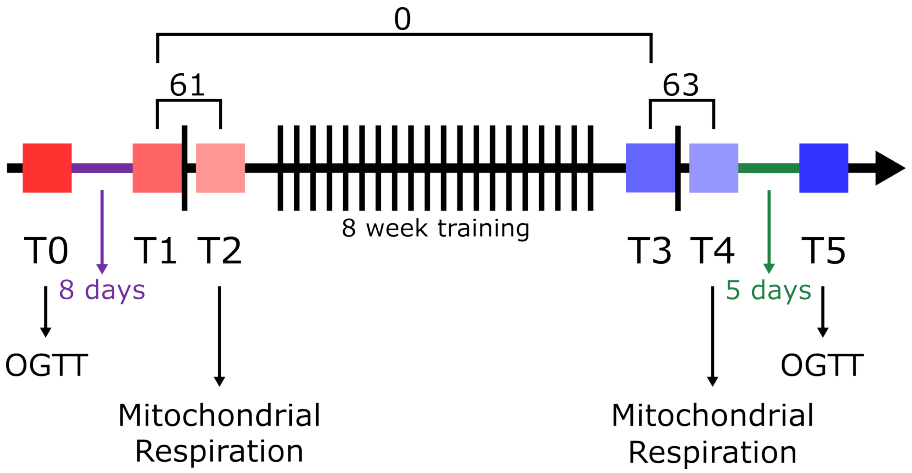

Figure 38: Differential cytokine regulation between the time points. A schematic representation of the differential cytokine regulation of the training intervention study. The numbers represent the significantly up- or downregulated (adjusted p-value < 0.05) transcripts at indicated time point comparison. The p-values were adjusted using the Benjamini-Hochberg method to correct for multiple testing. N = 22, or 21 for T1. OGTT: oral glucose tolerance test.

(adjusted p-value < 0.05) comparing T2T1 (Figure 38). By applying a fold change greater than 1.2 (corresponding to a minimum 20 % up- or downregulation), 40 cytokines still show an increase after the first bout of exercise (Figure 39A). Additionally, 10 cytokines exhibited at least a 1.6-fold increase with an adjusted p-value < 0.0001. The highest increases were observed for OSM (2.31-fold, oncostatin M), TGFA (2.07-fold, transforming growth factor α), CXCL5 (1.99-fold, C-X-C motif chemokine ligand 5), TNFSF14 (1.93-fold, tumor necrosis factor superfamily member 14) and CXCL1 (1.89-fold C-X-C motif chemokine ligand 1) (Figure 39A). Interestingly, although IL6 (interleukin 6) is known as an exercise-induced cytokine in plasma [164–166], it only exhibited a 1.29-fold increase (adjusted p-value < 0.0001) after acute exercise. The pro-inflammatory cytokine TNF (tumor necrosis factor) exhibited a similar high increase as IL6 with a 1.26-fold increase (adjusted p-value < 0.0001).

Comparing the time points T4 and T3 after the 8-week training intervention, 63 cytokines were significantly increased (adjusted p-value < 0.05) (Figure 38), and 37 cytokines displayed an increase of at least 1.2-fold. The cytokines with the highest increase were similar to those observed before

the intervention. OSM exhibited a 2.36-fold increase, TGFA had a 2.17-fold increase, TNFSF14 had a 2.15-fold increase, CXCL5 showed a 1.98-fold increase, and CXCL1 1.94-fold, all with an adjusted p-value $<$ 0.0001 (Figure 39B). To assess whether there were differences in the cytokine response to acute exercise before and after the training intervention, individual fold changes were analyzed using a Student's t-test. However, no statistical difference (p-value $>$ 0.05) was found for any of the cytokines. The mean fold changes of T2T1 and T4T3 were plotted in Figure 39C.

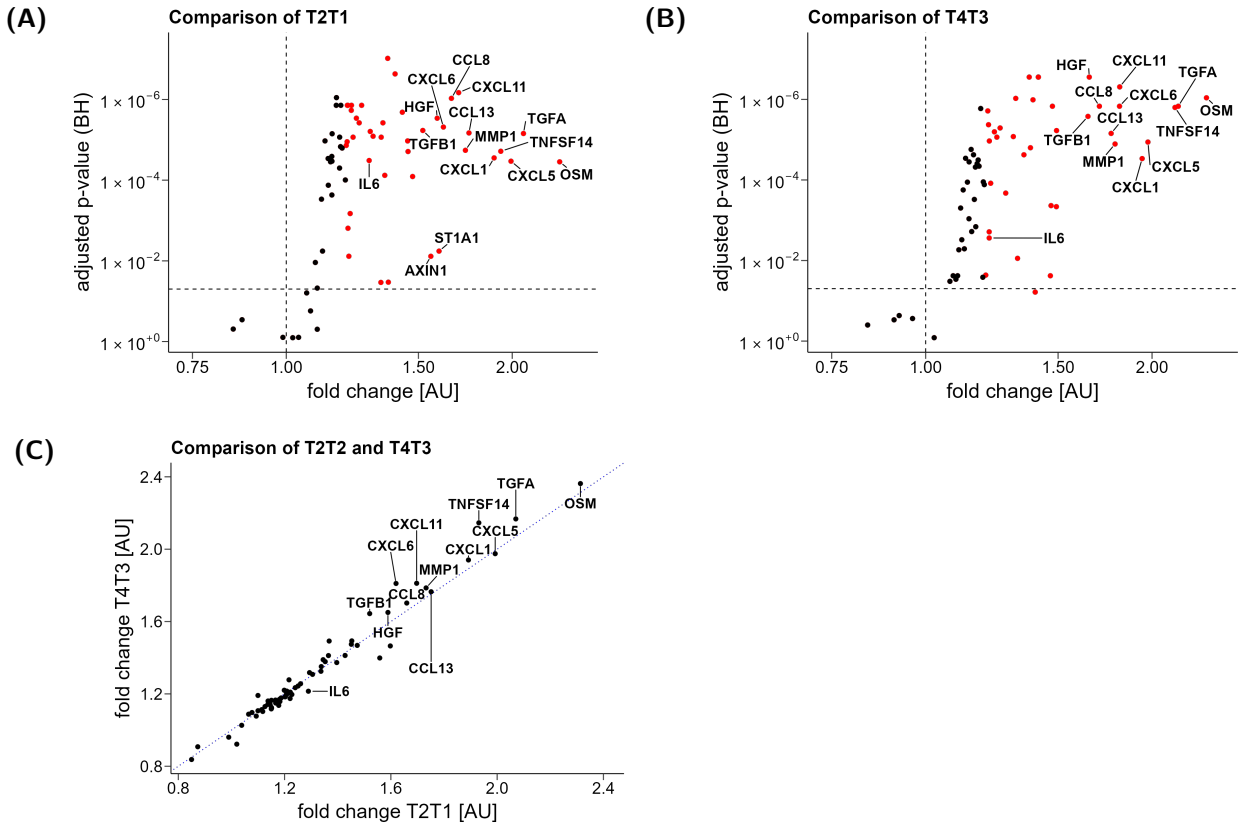

Figure 39: Changes of exercise-induced alterations in circulating cytokines. (A, B) The alterations in the expression of circulating cytokines after 30 min cycling are shown in a volcano plot. The changes are shown for the comparison (A) T2T1 representing untrained individuals and (B) T4T3 representing trained individuals. Cytokines with an increase of at least 1.2 were marked in red. The red color highlights a fold change greater than 1.2. Interleukin 6 (IL6) and all cytokines with an increase of at least 1.5 are annotated. (C) Comparison between the changed abundance of cytokines at T2T1 and T4T3 The dotted line represents equality. The p-values were adjusted for multiple testing using to Benjamini-Hochberg (BH). N = 21 for T2T1, or 22 for T4T3. AU: arbitrary units.

The acute cytokine response is known to be dependent on the number of leukocytes, especially natural killer cells (NK cells), which increase in the blood after exercise [167]. However, this study did not investigate the regulation of leukocytes in response to acute exercise. To compensate for this lack of knowledge, mRNA levels of the most upregulated cytokines (OSM, TNF, TGFA, TNFSF14, CXCL1, and CXCL5) and IL6 were measured in whole blood (Figure 40), collected at T1 – T4. Surprisingly, the well-studied cytokines in response to exercise, IL6 and TNF (Figure 40C, F), exhibited no alterations. Significant increases in response to acute exercise were observed for CXCL1 (Figure 40A) before the training intervention and both before and after the training intervention for OSM and TGFA (Figure 40D, E). Furthermore, the acute response was even stronger after the training intervention for CXCL5 and TNFSF14 (Figure 40B, G). This acute response was solely observed in trained individuals and not in untrained individuals. While this does not prove that leukocytes in the blood lead to an increase in cytokines in the serum, the possibility of an influence cannot be excluded.

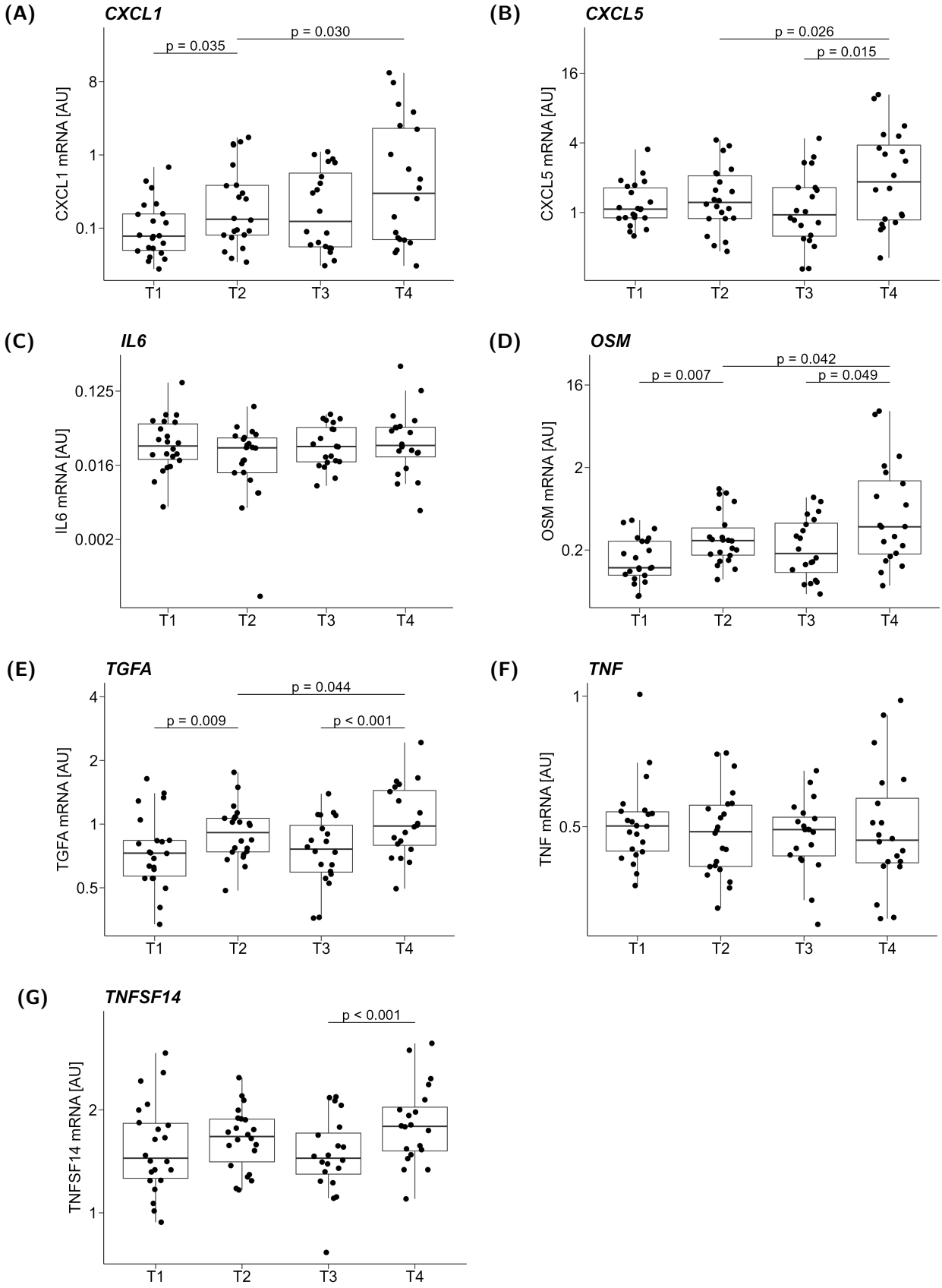

Figure 40: Transcript levels of most upregulated cytokines in leukocytes. The transcript levels of cytokines showing the greatest increase in serum levels were measured in whole blood. The measured transcript levels are shown as boxplots for *CXCL1* (A), *CXCL5* (B), *IL6* (C), *OSM* (D), *TGFA* (E), *TNF* (F), and *TNFSF14* (G). The box represents the interquartile range (IQR, 25th to 75th percentile). The black line represents the median of the data. The whiskers extend the box to the lowest or largest value no further than 1.5 × IQR. Only significant changes are shown. N = 20 – 22. AU: arbitrary units.

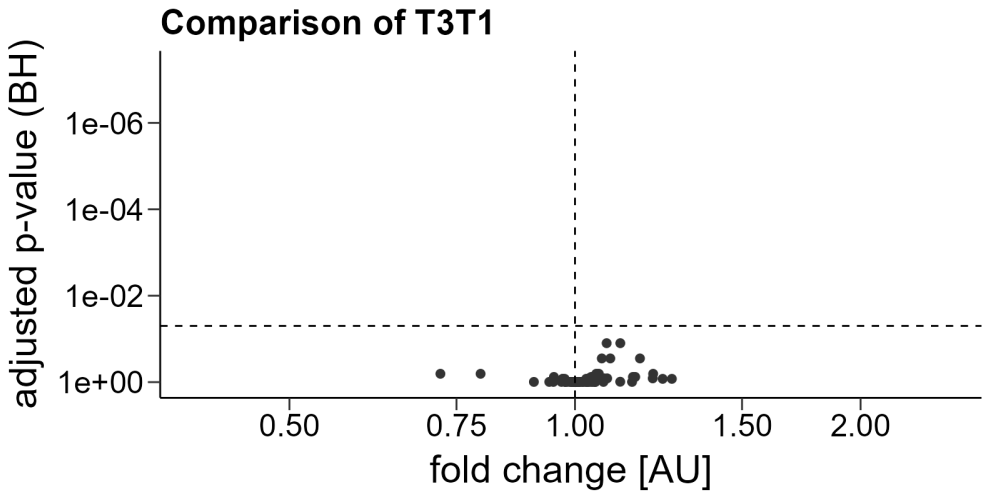

Figure 41: Volcano plot of cytokine change at resting level before versus after training intervention. The resting levels of cytokines after the training intervention (T3) were compared with the resting levels of cytokines before the training intervention (T1) and shown as a volcano plot. Cytokines with no significant change are shown in black. The p-values were adjusted for multiple testing using Benjamini-Hochberg (BH). AU: arbitrary units.

We also investigated whether the training intervention altered cytokine levels in the resting state by comparing fasted blood samples at (T3T1). However, the data revealed that the cytokine levels remained unchanged (Figure 41).

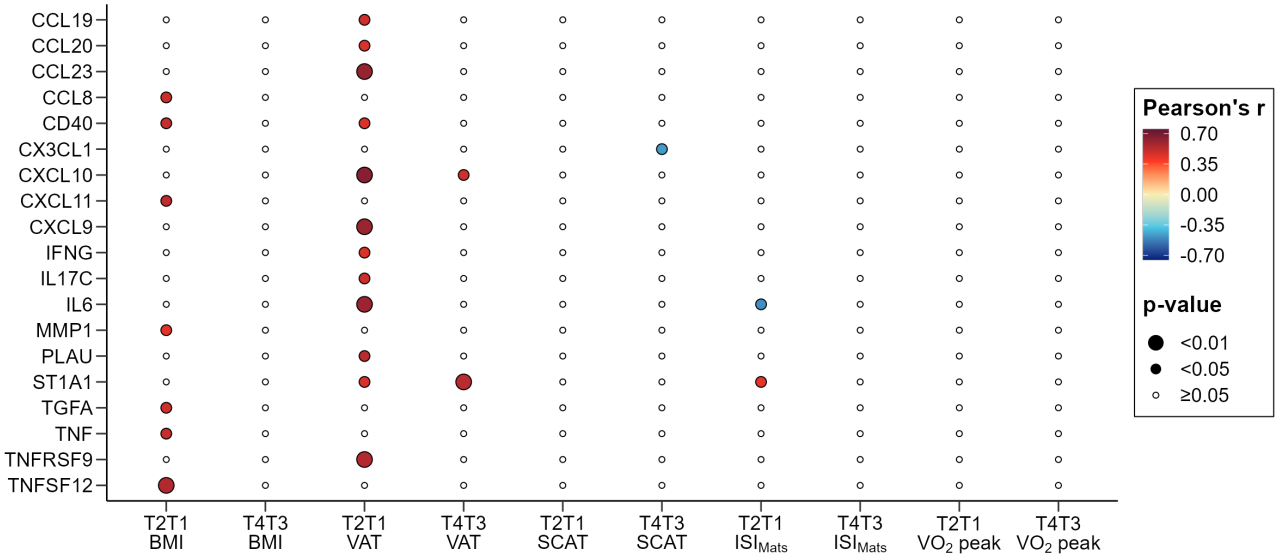

Figure 42: Correlations of individual change in acute cytokine with clinical metabolic parameters after acute exercise. The individual change of cytokines to one bout of acute exercise of untrained (T2T1) or trained (T4T3) participants was correlated to the individual clinical and metabolic parameters before or after the 8-week training intervention, respectively. Only cytokines significantly correlated to at least one clinical parameter are shown. Cytokines were correlated to body mass index (BMI), amount of visceral adipose tissue (VAT) or subcutaneous adipose tissue (SCAT), insulin sensitivity according to DeFronzo and Matsuda (ISI_{Mats}), and peak oxygen consumption (VO_2peak). Red colors indicate a significant positive correlation, while blue colors indicate a significant negative correlation. The circle size represents the significance level. Non-significant correlations are shown as small empty circles.

Subsequently, correlation analyses were performed to explore the potential influence of the metabolic and fitness parameters on the acute cytokine response (Figure 42). The fitness level defined by VO_2peak and IAT did not correlate with the change in any of the measured cytokines. In untrained individuals, correlations with the acute response were not observed with pre-intervention SCAT but, therefore, with VAT and BMI. However, after the training intervention, only the increase in CXCL10 (C-X-C motif chemokine ligand 10) and ST1A1 (sulfotransferase family 1A member 1) were significantly correlated. Additionally, ST1A1 correlated positively with the ISI_{Mats}, while IL6 exhibited a negative correlation in untrained individuals. After the training intervention, these correlations diminished and were not significant.

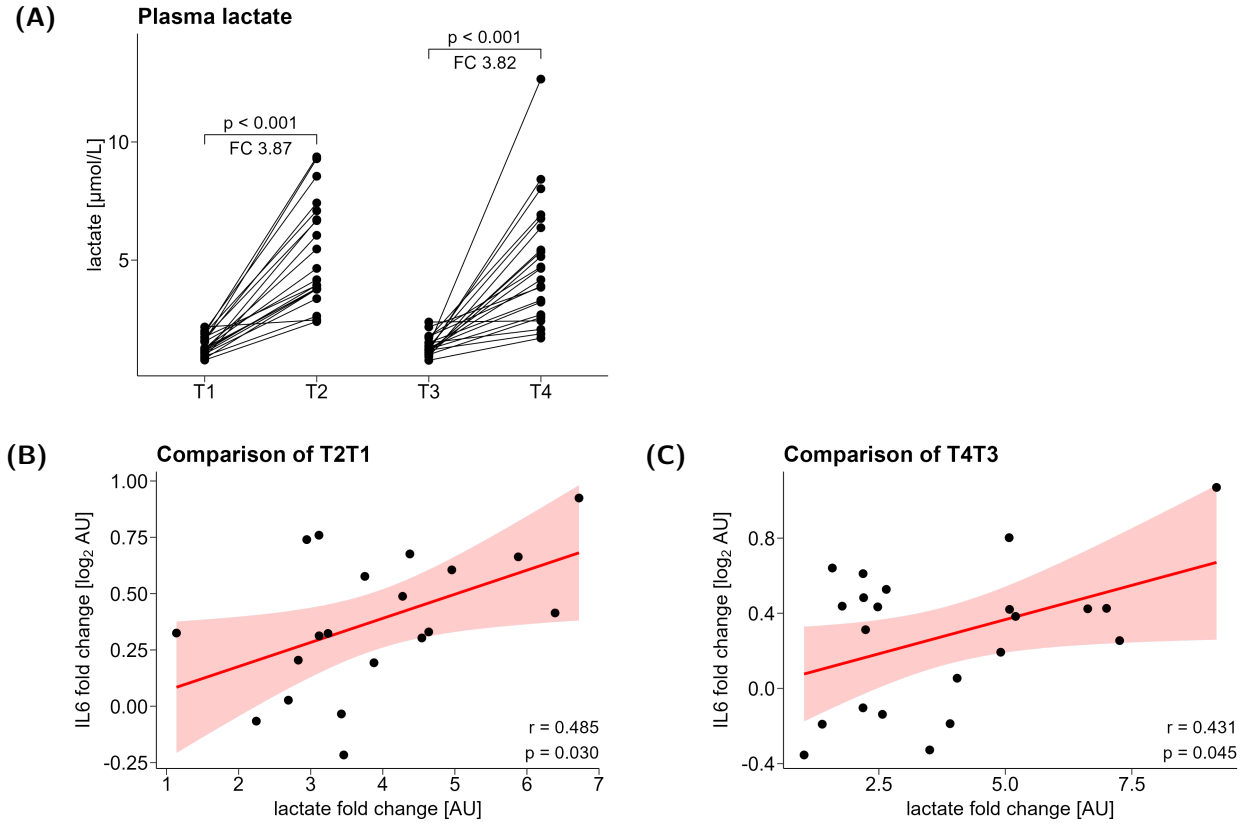

Figure 43: Correlation of plasma lactate levels with IL6 after acute exercise. (A) Plasma lactate concentrations were obtained before and after one bout of acute exercise. The data is shown for untrained and trained participants before and after the 8-week training intervention. (B, C) Correlation of the response of plasma lactate increase and change in interleukin 6 (IL6) in untrained participants (B) and trained participants (C), respectively. The red area shaded around the regression line represents the 95 % confidence level. N=21 for T2T1 or 22 for T4T3. AU: arbitrary units.

Lastly, we examined whether lactate production influenced the acute cytokine response, as lactate is a well-known marker for metabolic energy production, and its production and release are influenced by exercise intensity. Lactate plasma levels were assessed and showed an increase in all subjects before (T2T1) and after the training intervention (T4T3) in response to acute exercise. The increase was similar in both exercise bouts, with 3.87-fold and 3.82-fold, respectively, with a p-value < 0.001 calculated using a paired Student's t-test (Figure 43A). Subsequently, the acute response of all cytokines was correlated to the corresponding increase in lactate. Notably, out of all cytokines, only IL6 exhibited a significant positive correlation with the increase in lactate both before and after the training intervention (p-value $= 0.03$, Pearson's r $= 0.48$ for T2T1; p-value $= 0.045$, Pearson's r $= 0.57$ for T4T3) (Figure 43B, C). Additionally, MCP1 (monocyte chemoattractant protein-1, p-value $= 0.036$, Pearson's r $= 0.47$) and CST5 (cystatin D, p-value $= 0.0085$, Pearson's r $= 0.57$) exhibited a significant positive correlation with increased lactate secretion at T2T1 (data not shown).

Therefore, it might be of potential interest to investigate the question why this positive correlation is only seen in untrained individuals and not in trained anymore. Studying their function in response to acute exercise might give us more insight.

To summarize briefly, we analyzed the human skeletal muscle transcriptome and epigenome for exercise-induced changes that could explain the differences seen in the ISI_{Mats} between the RES and LRE groups. These analyses resulted in the investigation of IL34 and AKR1C3 together with AKR1C1 and AKR1C2. Although the experimental approaches could not explain the observed differences between the response groups, these candidates still hold potential for further studies. Additionally, we studied the human skeletal muscle proteome alone and in combination with the transcriptome and epigenome. This analysis lead to the discovery of PPME1 and PERM1 as potential novel candidates, however, they still need to be validated by functional analyses. Lastly, due to the prior discovery of IL34 in our early analysis, we investigated other cytokines in the serum after acute and prolonged exercise, which resulted in the discovery of multiple yet unexplored cytokines in the context of exercise such as OSM, TGFA or TNFSF14.

5 Discussion

The beneficial effects of exercise for multiple diseases have been validated in several studies. It is known that the individual exercise response is dependent on various parameters. Not every individual can perform exercise at the same duration and intensity. However, even if these parameters are adjusted to achieve a comparable individual physical and metabolic challenge, participants respond differently to a structured and controlled training intervention. Subjects showing the desired response, such as improvement in insulin sensitivity, are classified as responders (RES), whereas the others are called low-responders (LRE). Although this knowledge has existed for years, the molecular mechanisms behind it are not well understood. Our goal was, therefore, to determine the molecular differences in the human skeletal muscle of RES and LRE in insulin sensitivity to discover genes and proteins that can induce the differential response in subjects during exercise. We used multi-omics analyses and evaluated the datasets separately as well as combined. Furthermore, we took the acute changes after the first and last training sessions into account. This makes it a new approach in understanding the effectiveness of physical activity therapy in the prevention of T2DM.

5.1 Molecular changes on transcriptional and epigenetic level

5.1.1 Transcriptomics data

We first evaluated the changes on the transcriptional level in skeletal muscle over all participants. The most changes were seen after an acute bout of exercise, and only a few regulated transcripts were found comparing the resting state before and after the intervention (T5T0). Moreover, the fold change of regulated transcript was much more pronounced after acute exercise compared to the long-term regulation. It is known that the expression of transcripts in response to muscle contraction occurs rapidly, and most transcripts return to baseline values within 24 h after the exercise bout [32]. During long-term training intervention, each acute transcriptional regulation contributes to a cumulative effect on protein abundance [31, 32, 168], which will also be discussed in section 5.2. Many studies evaluated the acute and long-term response of skeletal muscle transcripts to exercise. In 2020, Pillon et al. [169] published a paper in which 66 published data sets were combined and analyzed. The results are available as "Meta-analysis of Skeletal Muscle Response to Exercise", `https://metamex.eu/`. They found *NR4A3* as the most upregulated transcript after acute exercise and strongly decreased by inactivity. This matches perfectly with our data since *NR4A3* showed the strongest increase of all transcripts after acute exercise by 222-fold. It was shown by Pillon et al. that silencing *NR4A3* expression diminishes the effect on glucose uptake after electric pulse stimulation of primary human myotubes significantly. Furthermore, reduced expression of *NR4A3* resulted in altered expression of exercise- and inactivity-responsive genes [169], suggesting that *NR4A3* is an important regulator for glucose uptake following contraction and exercise-related gene, although the mechanism is not known.

Following acute exercise at T2T0, under our top 50 we found, additionally to *NR4A3*, a significant increase in *EGR1* and a significant decrease in *MSTN*, both of which belong to the top regulated transcripts after acute exercise in MetaMEx. By comparing the top 50 regulated transcripts after acute exercise in our study, 49 transcripts showed the same direction of expression post-exercise in the MetaMEx analysis, of which 36 were additionally significantly regulated. Notably, we found a significant increase of *NMRK2* and *CA14*, which were among the most downregulated transcripts following inactivity listed in MetaMEx. Thus, the acute transcriptional regulation in response to exercise over all participants is well in line with published data. When we compared our results of the training intervention (T5T0) with the published data from MetaMEx analyzing long-term aerobic training studies, the overlap was very poor. Out of the top 50 transcripts at T5T0, solely *MYH9* and *SLC7A8* also showed a significant regulation in the same direction in the MetaMEx

database. Twenty-three transcripts in our analysis showed a non-significant regulation in the same direction as described in MetaMEx. The poor overlap can be explained by the time point of the muscle biopsy of our study. Most studies in MetaMEx collected the muscle biopsies within 24 h – 72 h after the last exercise session, whereas the biopsies in our study were collected 5 days after the last exercise session. This shows that the transcriptional adaptation after long-term exercise is mostly diminished after 5 days without exercise, and it suggests a robust regulation of *MYH9* and *SLC7A8* transcripts that might also be important for muscle adaptation to long-term training. None of the published studies in MetaMEx evaluated the acute response of exercise before and after the training intervention as we did. In our study, 13 transcripts (*BHLHE40*, *HK2*, *HSPA1A*, *HSPA1B*, *IP6K3*, *MKNK2*, *NR4A1*, *NR4A3*, *PKDCC*, *SLC25A25*, *SLC25A33*, *TRIM63*, *TUBB4B*) showed a reduced expression comparing T4T2. Notably, all these transcripts were upregulated in response to acute exercise at T2T0 and according to the MetaMEx analysis. One of these transcripts is *NR4A3*, which suggests that in the trained skeletal muscle, the fold increase in NR4A3 is diminished and that the activation of *NR4A3* gene transcription is mediated by mechanisms particularly activated in the untrained muscle.

Subsequently, we analyzed by gene enrichment analysis all significantly regulated transcripts to get insight into the most important pathways in muscle adaptation. After performing gene enrichment analysis for the acute exercise (T2T0), multiple terms associated with mitochondria and mitochondrial pathways were found. This reflects the high energy demand of the skeletal muscle during aerobic exercise and the induction of transcriptional regulation as a first step toward adaptation of energy metabolism by increasing the number of mitochondria and their content. A general induction of transcription was reflected by pathways associated with activated transcription. Worth mentioning is that no inflammatory pathway is among the top five terms in all categories of pathways, although exercise is known as a stress factor to induce inflammation [170]. By comparing the effect of prolonged training on the acute response (T4T2), we still observed multiple mitochondrial pathways, however, a shift to mitochondrial function, such as the TCA cycle and OXPHOS, is seen instead of mitochondrial biogenesis. This might suggest that the skeletal muscle adapts to chronic endurance training first by increasing the abundance of mitochondrial proteins in general and afterwards by improving the energy metabolism for increased ATP production. Furthermore, several pathways were related to the ECM, suggesting exercise-induced remodeling of tissue architecture and function. Since many ECM-related pathways were also enriched in the gene enrichment analysis of the training response T5T0, this appears to be a stable long-term effect on transcription rather than an acute regulation. This long-term remodeling effect on the ECM may be associated with tissue adaptations and improved mechanical properties of the skeletal muscle. ECM is known to be essential for physiological processes during muscle growth, regeneration, and force production [171, 172]. It has been shown that the ECM plays an important role in muscle adaption but also insulin resistance [173]. The gene enrichment analysis of the training response (T5T0) also revealed multiple pathways associated with platelets, suggesting the activation of repair mechanisms in skeletal muscle resulting from the highly intensive exercise. Platelets are known to secrete content from their alpha granules in response to injury, which contain polypeptides such as protease inhibitors, von Willebrand factor, growth factors, and fibrinogen [174]. It was shown in a comparative study that the injection of platelets-rich plasma after acute muscle injury resulted in a faster healing process underlying the function of platelets for muscle regeneration [175]. Although there is a large discussion about the importance of platelets, especially due to high discrepancies between human and animal studies, platelets might have great potential in muscle regeneration after acute injury [176–179].

Since we aimed to determine new molecular regulators involved in improving insulin sensitivity, we compared the transcriptional response in the RES and LRE groups. The insulin sensitivity was estimated by calculating the Matsuda index based on glucose and insulin values during an OGTT,

which is widely used in the literature [23]. Across all subjects, we did not find a significant difference between insulin sensitivity before and after the 8-week training intervention. However, as already reported, some participants improved their insulin sensitivity (fold change > 1.15), whereas others did not or showed reduced insulin sensitivity. By applying this fold change, our participants were split into 14 (56 %) RES and 11 (44 %) LRE.

The groups exhibited substantial disparities across all time point comparisons, with a range of 900 to 1500 significantly differentially regulated transcripts. These findings indicate that differences in exercise response are already present at an early stage. When we looked closer at the transcripts with the highest fold change between both groups, a transcript with a higher fold change in the RES group was *HSPA1A* after both acute exercise (T2T0) and after the training intervention (T5T0). The increase in HSPA1A after training was also positively correlated to the increase in insulin sensitivity. Heat shock proteins, also called chaperones, are known to protect various cell types from damage by stress-induced misfolded proteins and protein aggregations by inducing protein degradation [180]. Overexpression of HSPA1A in skeletal muscle increased mitochondrial volume, fatty acid oxidation, and endurance capacity in mice [181], thereby increasing insulin sensitivity [182]. The higher increase in the RES group after acute exercise (T2T0) suggests that the group is protected better against misfolded proteins, whereas the downregulation in the LRE group after the training intervention (T5T0) might predict an impaired insulin sensitivity by less protection to cellular stress. On the other hand, the RES group showed lower expression of *CHRNA1*, a subunit of the nicotinic cholinergic receptor with high abundance in skeletal muscle tissue, after acute exercise (T2T0). Ligand binding to the receptor leads to sodium influx, followed by calcium release and, therefore, muscle contraction [183]. However, a recent study showed that overexpression of *CHRNA1* leads to decreased muscle innervation, decreased muscle mass, and decreased muscle action potential [184], suggesting impaired muscle contractility in the LRE group compared to the RES group. Furthermore, after training intervention, *CHRNA1* was upregulated in the LRE but not in RES, which was confirmed by the negative correlation of the fold change in *CHRNA1* with the fold change in insulin sensitivity. *CHRNA1* was shown to be upregulated by inactivity [169], suggesting that skeletal muscle from the LRE transitions to a state that resembles inactivity after the intervention. Worth mentioning is also the high upregulation of all three members of the AKR1C family in the LRE after acute exercise and the upregulation of *AKR1C3* in the LRE comparing T5T0. This protein family will be discussed later in section 5.1.4.

Furthermore, when comparing the training response (T5T0), *IL32*, which is known to be involved in the regulation of insulin sensitivity [185], showed a greater fold change in the LRE group, whereas it was unchanged in the RES group. *IL32* showed a significant negative correlation with the change in ISI_{Mats}, supporting the hypothesis of its involvement in regulating insulin sensitivity. It was shown that silencing *IL32* in human myotubes results in increased AKT phosphorylation, leading to the hypothesis that upregulation leads to impaired insulin sensitivity. This hypothesis was also tested in mice that overexpressed *IL32* in skeletal muscle, which resulted in decreased insulin action *in vivo*. The differential regulation of *IL32* we observed between RES and LRE suggests that the *IL32* protein might play a role in the response in insulin sensitivity after training. When we compared both acute time points (T4T2), *CSRP3* showed an increased fold change in the RES and a decreased fold change in the LRE group. However, *CSRP3* did not show a significant correlation with the change in ISI_{Mats}. The study by Jensen et al. detected an upregulation of *CSRP3* in skeletal muscle after acute exercise and showed its association with muscle cell proliferation and differentiation. This could suggest an improved activation and differentiation of satellite cells in the RES group supporting muscle repair in response to prolonged acute exercise [186]. This hypothesis is further supported by the increased expression of *MATN2* in the RES group and slightly decreased expression in the LRE group at T4T2. This is due to the fact that the LRE showed an acute response after

the first exercise bout but no response after the last exercise bout, whereas the RES showed a reversed pattern in which an upregulation was only seen after the last exercise bout (data not shown). Furthermore, the LRE highly expressed *MATN2* comparing T5T0, whereas no change was seen in the RES. Therefore, *MATN2* exhibited a significant negative correlation with the ISI_{Mats}. It is known that *MATN2* is involved in ECM remodeling [187, 188], which is essential for muscle repair and development [189]. This suggests an impaired muscle adaptation of the LRE group, resulting in potentially greater muscle damage after prolonged exercise, and, therefore, a high upregulation of *MATN2*. However, as seen in the CRP measurements in the clinical data, we did not observe clinically increased inflammation.

The LRE group showed a slightly upregulated *SLC2A3*, also known as GLUT3, whereas a downregulation was seen in the RES group comparing T4T2. GLUT3 is responsible for basal glucose uptake, and although it is considered the main glucose transporter in the brain [190], there is evidence of its expression in skeletal muscle as well [191, 192]. No significant correlation with the change in ISI_{Mats} was seen comparing T5T0. Nevertheless, this increase could be due to impaired glucose uptake in the LRE group, leading to a compensatory mechanism resulting from the high energy demand after acute training. This, however, still needs to be validated in future experiments.

To detect pathways significantly regulated by training in RES and LRE, gene enrichment analyses were performed using the significantly correlated changes in transcripts with the change in insulin sensitivity. Mainly global terms related to transcription and translation are strongly enriched, which does not allow to draw specific conclusions about which particular signaling pathways are important in regulating insulin sensitivity. However, in previous studies, we found a higher induction of ECM transcripts in LRE in insulin sensitivity, which is potentially regulated by chronic activation of TGF1β in the muscles of LRE and involves miRNA-143 [144, 146]. In the current analysis, the term ECM was not enriched when comparing the exercise-regulated transcriptional pattern of RES and LRE, which is due to the fact that no threshold of fold change was applied. If the selection of transcripts were restricted to transcripts displaying at least a 20 % difference, the ECM emerged as the most dominant term in the enrichment analysis (data not shown).

To conclude, the analyses indicate that the transcriptional regulation highly differs between both response groups. We highlighted some genes that might be involved in the discrimination between RES and LRE, which have not yet been studied for their function in human skeletal muscle. As a next step, we combined the differential regulation of the transcriptome with differences in the regulation in the epigenome to provide an additional validation of potential candidates.

5.1.2 Merged transcriptomics and epigenomics data

In the second approach, we analyzed the epigenomics data in combination with the transcriptomics data. Three participants were excluded from the epigenomics data since the "sex" parameter showed a significant influence, although CpG sites on the gonosomal chromosomes were not considered. Sex differences on the epigenetic level are known and have been extensively studied [193–195]. Furthermore, age-related epigenetic changes are known [156]. To exclude age-specific effects, we excluded 2 participants due to their higher age than the other participants. Additionally, we used only participants with a complete dataset, resulting in 18 out of 25 participants. Although this reduced the sample size and limited our analysis, it was necessary to maintain data quality. After analyzing the epigenomics data alone, we observed the most changes by comparing the acute time points (T4T2) and the resting time points after the training intervention (T5T0), indicating that multiple exercise sessions are necessary for stable regulation. This is supported by other studies reporting several changes after prolonged training interventions [196–198]. Furthermore, these studies have

shown that epigenetic changes can emerge rapidly within 30 min after an acute exercise bout, whereas more changes are seen around 3 h – 6 h after exercise. This explains the relatively low amount of significant difference after the acute bout of exercise (T2T0) in our study since the muscle biopsy was collected 1 h after the exercise session. When we analyzed the differentially regulated methylation sites between the RES and LRE groups comparing the response at T2T0, T5T0, and T4T2, we consistently observed a similar pattern in the amount of significant changes for all comparisons, as seen in the transcriptomics dataset. This supports the hypothesis that differences between the groups are already evident at an early stage, even at the epigenetic level.

For the combined analysis with the transcriptome data, as mentioned in section 4.1.2, we elongated the position of the transcripts on the chromosomes by 2,000 bp. This approach ensures coverage of full gene length coverage and additional short-distance regulatory elements [199, 200]. We additionally considered the direction of methylation and transcriptional expression (Figure 14). Multiple studies reported that hypermethylation in the promoter leads to decreased transcriptional expression by preventing the binding of transcription factors [201, 202]. Conversely, hypomethylation in the promoter allows transcriptional induction by binding relevant transcription factors. Methylation in the gene body and its function is less well understood. It has been reported that highly expressed genes exhibited hypermethylation in the gene body [203, 204], suggesting a positive correlation between gene expression and methylation, while low-expressed genes often exhibited decreased gene body methylation. One potential mechanism leading to increased methylation in highly expressed genes might involve the open chromatin structure of these genes, making them accessible to transcriptional proteins and DNA methylation proteins, thereby resulting in hypermethylation [205]. This is supported by the study of Samaranayake et al., which demonstrates the interaction of the DNA methyltransferase 1 (DNMT1) with the RNA polymerase II (RNA Pol II), resulting in hypermethylation without affecting the transcription [206]. Therefore, methylation in the promotor directly influences the transcription, whereas methylation on the gene body can be a consequence of occurring transcription.

Interestingly, of all significantly regulated transcripts across all subjects, we found 47 %, 58 %, or 74 % of these transcripts containing at least one CpG site at the time point comparisons T2T0, T4T2, or T5T0, respectively. This suggests that the epigenetic modifications lead to a stably altered transcriptional expression. Furthermore, we observed substantial differences in the amount of differentially methylated CpG sites, whereas most CpG sites inside regulated genes were found for T5T0 and T4T0, the comparison of T2T0 showed the least regulated CpG sites, further supporting the hypothesis that epigenetic changes take longer to emerge. Furthermore, when we compared the RES and LRE in the combined dataset, we found similar amounts of significantly regulated transcripts and CpG sites at the different time points. Of all significantly regulated transcripts between the response groups, 65 % – 67 % of these transcripts show at least one regulated CpG site.

The main drawback in the analysis of the combined dataset was the exclusion of 7 participants, which decreased the statistical power of our analysis. To overcome this limitation, we took the differentially regulated transcripts in the NRE1 study into account and merged transcriptomics datasets from NRE1 and NRE2. Only 7 transcripts correlated with the change in insulin sensitivity over all 41 participants and exhibited significant differential regulation on both transcriptional and epigenetic levels at T5T0 in NRE2 were considered. The change of the 7 transcripts showed a negative correlation with the change in insulin sensitivity (data not shown). Among these genes, we found Prolyl-3-hydroxylase (*P3H2*), which was highly increased in the LRE and slightly decreased in the RES and was correlated negatively with the change in insulin sensitivity (data not shown), similar to collagens and ECM-related transcripts [144, 146]. *P3H2* plays a critical role in collagen chain assembly, which has been shown by the interaction with COL4A1 [207], one of the top 50

regulated transcripts at T4T2 and T5T0 in our study, emphasizing the importance of ECM in insulin sensitivity. Proteolipid protein 1 (*PLP1*) is a major protein in the formation of myelin in the central nervous system [208, 209], which makes it not accessible for studies in skeletal muscle cell cultures. Sperm antigen with calponin homology and coiled-coil domains 1 (*SPECC1*) is mainly expressed in the testis, brain tissue, and bone marrow [210]. Furthermore, its expression in the skeletal muscle was rather low (data not shown), thus we did not consider it as a potential candidate for further analyses. Spi-1 Proto-Oncogene (*SPI1*), also known as PU-1, is a key regulator in controlling the hematopoietic cell fate [211, 212]. SPI1 might play a role in immune cell recruitment in the muscle, and a mutation in the gene was shown to reduce the number of intramuscular macrophages [213]. Furthermore, we identified tumor necrosis factor superfamily member 14 (*TNFSF14*) in our analysis, which was also covered as a secreted and soluble protein in our analysis of serum samples. Our data show a slightly increased expression of *TNFSF14* in the LRE and a strongly decreased expression in the RES group in skeletal muscle cells after the training intervention (T5T0). *TNFSF14* is widely expressed in immune cells [214]. In a study from Waldemer-Streyer and Jen, it was reported that silencing *TNFSF14* reduced the myoblast fusion of mouse skeletal muscle cells C2C12, whereas treatment with soluble TNFSF14 protein increased the fusion index [215]. Of note, TNFSF14 protein was increased in serum after the acute exercise bout before and after the training intervention. In addition, we measured *TNFSF14* transcript levels in whole blood after acute exercise. However, the increase of TNFSF14 serum protein was not correlated to the change in insulin sensitivity or any other clinical parameter. Thus, we did not consider it further as a promising candidate to explain the different outcomes in metabolic control in RES and LRE, but we cannot exclude local differences in TNFSF14 protein abundance in skeletal muscle.

Instead, we focused on investigating IL34 and *AKR1C3* in cell culture experiments of skeletal muscle cells, along with its two highly related proteins, *AKR1C1* and *AKR1C2*. IL34 has the advantage of being a soluble interleukin that can be directly utilized for cell treatment. The AKR1C1–3 were chosen since all three were under the top 5 most significantly regulated transcripts between the RES and LRE after acute exercise (T2T0), and AKR1C3 was still under the top 5 after the training intervention (T5T0). Furthermore, the combined analysis of transcriptomics and epigenomics strengthened the different regulation of AKR1C3 in RES and LRE. Importantly, of all 7 transcripts, only AKR1C3 was also detected in the proteome analysis of skeletal muscle biopsies. The change in AKR1C3 protein abundance in RES and LRE after the 8-week training intervention convincingly reflects its regulation on transcriptional and epigenetic levels (Figure 23H, Figure 37A) and provides a strong basis for functional studies in skeletal muscle cells.

5.1.3 IL34

IL34, belonging to the family of cytokines [216], plays a crucial role in various physiological processes. Its functional receptor, CSF1R, was discovered in 2008 and has since been associated with macrophage depletion and an osteopetrotic phenotype in mice [217]. Both CSF1 and IL34 exhibit overlapping functions mediated by the receptor, triggering the activation of the PI3K-AKT, ERK, and AMPK pathways [157–159]. Syndecan 1 (SDC1) has been found to modulate IL34-CSF1R signaling by influencing receptor recruitment and IL34 bioavailability [218]. In the context of metabolic disorders, IL34 has been studied in relation to T2DM and GDM. Circulating IL34 levels were found to be elevated in T2DM and GDM patients, showing correlations with insulin resistance and glucose concentrations [219–221]. Additionally, IL34 has been suggested as a potential inflammatory biomarker for diabetic complications [222]. However, limited research has been conducted on the interaction between IL34 and skeletal muscle cells. One study showed that IL34 is involved in myogenesis through the phosphorylation of STAT3, which determines cell fate and differentiation [222]. Furthermore, the knockout of *IL34* impaired muscle regeneration by altering the differentiation of

satellite cells, affecting the expression of *IGFBP5* and disturbing AKT activity [223]. In our study, *IL34* was differently regulated by training in the responder groups. In both studies, NRE1 and NRE2, the RES group showed a lower fold change of *IL34* compared to the LRE group, and a similar pattern was observed for its receptor *CSF1R*. In cell culture experiments, we observed an upregulation of the *IL34* transcript during the differentiation of human myoblasts into hMTs and an increase of secreted IL34 protein in the supernatant, suggesting potential importance during differentiation. This could be elucidated in future experiments by knockdown or knockout experiments. When treating hMTs with recombinant IL34, no enhanced phosphorylation of AKT, ERK, or CSF1R was observed, although an activation of these pathways was seen in treated THP-1 cells. This may be attributed to the high expression of *CSF1* and low expression of *CSF1R* in hMTs, potentially saturating the receptor and leading to no further downstream signaling induction. This would also suggest that skeletal muscle cells do not react directly to IL34 *in vivo* but release IL34, which activates other cell types in skeletal muscle. Immune cells such as macrophages and monocytes are known to interact with skeletal muscle cells, especially after acute muscle injury resulting from exercise, supporting muscle repair [224]. These cells react to IL34 [225, 226] and might, therefore, secret other cytokines that interact with the skeletal muscle cells or myofibers *in vivo*. Therefore, co-cultivation experiments with immune and skeletal muscle cells might give more insight. Since the increased expression of *IL34* and its receptor *CSF1R* was seen in the LRE but not RES after the training intervention (T5T0), one could speculate that the inflammatory response is dysregulated in the LRE group. This might lead to low-grade inflammation and potentially explain the impaired response in insulin sensitivity in the LRE group [227]. Overall, IL34 emerges as an essential factor in various physiological processes, including metabolic disorders, inflammation, and myogenesis. However, more research is needed to elucidate the precise mechanisms and significance of IL34 signaling in skeletal muscle cells.

5.1.4 AKR1C3

The second selected candidate for further functional analyses was AKR1C3, along with its family members AKR1C1 and AKR1C2. AKRs are enzymes involved in detoxifying and transforming aldehydes and ketones, originating from endogenous metabolic processes or environmental sources like nutrition, drugs, and toxins [228]. The AKR1C subgroup catalyzes oxidation and reduction reactions on steroids and prostaglandins [229]. AKR1C3 was previously known as prostaglandin F synthase, converting prostaglandin H_2 into prostaglandin F2α and prostaglandin D_2 into 9α,11β-prostaglandin F2α [162]. AKR1C3 also possesses 17β-hydroxysteroid dehydrogenase activity, converting androstanedione and testosterone, as well as estradiol and estrone [160, 161]. Recent studies revealed that AKR1C3 plays a role in fat mass reduction by inhibiting adipogenesis and lipogenesis and promoting lipolysis through androgen receptor activation in adipose tissue [230]. AKR1C3 expression is insulin-stimulated through the PI3K/AKT/mTOR signaling pathway and may regulate androgen receptor activity through stabilization. Thereby, AKR1C3 has been involved in the polycystic ovary syndrome characterized by insulin resistance and hyperandrogenism [231, 232]. Although AKR1C1–3 are expressed in skeletal muscle according to the human protein atlas, their specific functions in skeletal muscle are yet to be explored. To study their impact on insulin signaling, we induced an overexpression in the mouse muscle cell line C2C12 after differentiation. Although an increased protein abundance could be detected, neither of the three AKRs changed the insulin-dependent phosphorylation of AKT, suggesting that the AKR1C proteins do not directly influence insulin sensitivity. We also tested the hypothesis that mitochondrial respiration could be influenced. However, neither AKR1C family member influenced any key parameter measured by Seahorse, and no significant difference was observed. These data argue against a direct and strong influence of AKR1C1-3 on insulin signal transduction and mitochondrial respiration, even though the high variation of the

data might hide minor effects. The conversion of steroids and prostaglandins by the AKR1C family can also influence the metabolic adaptation to exercise, which can be difficult to constitute in cell culture systems but can at least be tested by adding testosterone or prostaglandins. Testosterone and dihydrotestosterone increase rapidly after an acute exercise bout [233], leading to increased muscle mass and adaptation to chronic exercise [234, 235]. The skeletal muscle can convert the highly active dihydrotestosterone into the weak 3α-androstanediol [236, 237], a conversion that AKR1C family members are also capable to do [161]. An increase of the AKR1Cs might suggest a faster conversion of the active androgen to the more inactive form and therefore decreased muscle adaptation in the LRE. Overall, more research is needed to better understand the essential roles of the AKR1C family in the skeletal muscle in response to exercise. It should also be considered that the different regulation of AKR1C1–3 in RES and LRE can reflect the different metabolic adaptations to exercise, i.e., a training-induced change in systemic or local insulin and glucose concentrations, with different consequences for the insulin-regulated expression of the transcripts and proteins.

5.2 Molecular changes on protein level

In the next step, we used the proteomics dataset of the skeletal muscle biopsies to identify potential mediators of the different responses in insulin sensitivity in the two response groups. Our analysis showed that very few or no significant changes over all subjects occur after an acute exercise bout, whereas most changes with 316 regulated proteins (adjusted p-value < 0.05) were seen after the training intervention (T5T0). It is reported that changes in protein abundance occur within hours to days after acute exercise [31]. Therefore, one cannot expect significant changes in the protein abundance one hour after the acute exercise bout. Studies showed a cumulative effect of prolonged chronic exercise, leading to higher protein abundance and ultimately to functional improvements and performance [238–240]. Well in line, the vast majority of proteins showed a significantly higher abundance after the training intervention (309 vs. 7 proteins). Additionally, we observed that most protein changes seen at T5T0 were already visible at T4T0, showing that five days without structured physical activity ("detraining") does not lead to a reduction in the training-induced protein levels. This suggests a stable expression pattern during the resting period. Detraining effects have been extensively studied, however, mostly on cardiorespiratory parameters, showing a 4 % – 25 % decrease not earlier than 2 weeks after the last training session [241–243]. Limited research has been conducted on the effects of short-term detraining on specific protein content, such as GLUT4, which showed a 17 % decrease six days after training [244]. The prolonged upregulation of proteins after training is in sharp contrast to the regulation of the corresponding transcripts, which showed no longer an upregulation after 5 days without training. These different kinetics must be considered when comparing the regulation of a certain gene on the transcriptional and protein level. Gene-enrichment analysis revealed that the most enriched terms belong to mitochondrial pathways. Most significantly regulated proteins in the mitochondrial pathways were associated with energy metabolism, including OXPHOS, electron carriers, as well as carbohydrate and lipid metabolism. Increased abundance of mitochondrial proteins and mitochondrial structures is a key feature of the metabolic adaptation to prolonged endurance training and is the causal link to increased mitochondrial respiration in isolated myofibers, as also reported in our study [145, 245–247]. In this regard, the non-mitochondrial proteins that showed a positive correlation with increased mitochondrial respiration in our particular dataset raised our attention as potential novel regulators of mitochondrial respiration. The nine proteins BRAWNIN, CD93, CYB5R1, GATD3B, GOT1, GPT, PERM1, PSMD4, and SCCPDH showed a positive correlation with the increase in mitochondrial respiration and were non-mitochondrial according to MitoCarta 3.0. However, a closer look revealed that some of them were already associated with mitochondrial function or were, in the meantime, localized to mitochondria since the MitoCarta database was last updated in 2020 and thus did not

reflect the most current information. This is true in the case of the protein BRAWNIN, which has recently been found to have a significant role in the assembly and function of respiratory complexes III and IV [248–250]. As a result, it was renamed to UQCC6 to reflect its mitochondrial function. Other proteins, such as GATD3B, also known as ES1 [251], and CYB5R1 are predicted to have a mitochondrial function according to GeneCards. GOT1 and GPT1 are indeed non-mitochondrial proteins, but GOT1 serves as a key enzyme in the malate-aspartate shuttle, which plays a crucial role in mitochondrial metabolism [252, 253]. GPT1 is also in close relation to mitochondrial metabolism since it converts alanine to pyruvate (and vice versa), which can be transported into the mitochondria. Both transaminases have mitochondrial counterparts, namely GOT2 and GPT2 [254–256]. CD93, a cell surface glycoprotein, was significantly increased after the training intervention in our study (data not shown) and was shown to interact with IGFBP7 (insulin-like growth factor binding protein) [257], however, a mitochondrial function is not known. Furthermore, it is known for its involvement in controlling inflammation, which is stimulated by exogenous DNA [258]. PSMD4 is a subunit of the 19S proteasome complex [259] and therefore ubiquitously expressed. It is essential for the full assembly of the complex [260] and is thought to be the only existing subunit that is not degraded when it is unassembled, however, it is not known whether its upregulation alters the number of fully assembled proteasomes [261]. SCCPDH was found in multiple compartments of the cell such as the nucleus [262], lipid droplets in human skeletal muscle that are associated with mitochondria [263], but also in the mitochondria itself where it is involved in the TCA cycle [264]. Lastly, we analyzed the significantly regulated proteins with their correlation with the change in insulin sensitivity. Only 2 out of the 316 proteins showed a significant positive correlation with the change in insulin sensitivity, which both were non-mitochondrial proteins. These two proteins of interest were PERM1 and PPME1.

5.2.1 PPME1

Protein phosphatase methylesterase 1 (PPME1), also known as PME1, has been shown in different cellular systems to play important roles in the regulation of AKT and ERK signaling through the regulation of PP2A [265, 266]. Furthermore, the study from Lipina and Hundal showed that PPME1 regulates GLUT4 translocation through the PP2A-AKT-pathway in the rat skeletal muscle cell line L6 [267]. RES in insulin sensitivity showed a higher fold change in PPME1 than the LRE group. This supports the hypothesis that PPME1 plays a role in regulating insulin sensitivity by potentially influencing GLUT4 translocation and insulin-induced AKT phosphorylation. Furthermore, the hypothesis is underlined by the positive correlation observed in the basal expression levels before and after the training intervention. Subjects with good insulin sensitivity displayed a higher abundance of PPME1, reinforcing the idea that PPME1 may be linked to improved insulin sensitivity. Therefore, future cell culture experiments in hMTs could give more insight into whether a knockdown impairs insulin-induced AKT phosphorylation and glucose uptake.

5.2.2 PERM1

PPARGC1 and ESRR induced regulator 1 (PERM1) regulates the expression of PGC1α, the master regulator of mitochondrial biogenesis [32, 268–270]. PERM1, therefore, contributes to muscle mitochondrial biogenesis and oxidative capacity, regulation of energy metabolism by altering glucose and lipid metabolism, and energy transfer [271, 272]. Furthermore, PERM1 is reported to interact and activate CaMKII in response to acute exercise bouts in skeletal muscle, and silencing *PERM1* impairs muscle contraction [273]. Interestingly, one of the transcripts that showed the greatest negative correlation with *PERM1* in the MetaMEx database was *CHRNA1*, which was already discussed in section 5.1.1. In our data analyses, PERM1 significantly correlated with an increase in mitochondrial respiration and insulin sensitivity. This could be due to the regulation of PGC1α and, subsequently, the regulation of GLUT4, however, direct evidence for this interaction is still missing.

Therefore, it is of high interest to perform knockdown, knockout, and overexpression experiments in hMTs to see whether the glucose uptake, insulin signaling, and mitochondrial respiration are altered. It was shown that silencing *PERM1* in mice cardiac cardiomyocytes resulted in reduced mitochondrial respiration determined by Seahorse measurement [274], however, studies in human skeletal muscle cells still need to be performed. Furthermore, our results characterize PERM1 clearly as a training-induced transcript and protein, at least in part due to the differential regulation of 4 methylated CpG sites.

5.3 Molecular changes in serum proteins

In the last section of this thesis, we wanted to determine whether the response of serum cytokines to the 8-week training is different in RES and LRE, which could give a hint to a different adaptation of circulating but also tissue-resident immune cells. Using the transcriptomics and epigenomics datasets we already detected IL34 as a potential cytokine influencing the insulin sensitivity. Therefore, we investigated a panel of 92 other cytokines in the serum for a broader look on inflammatory processes after acute and prolonged exercise. Modulation of inflammatory processes but also alterations in the number of immune cells can influence insulin sensitivity. However, in the serum samples collected in the fasting state before the acute exercise bout at the beginning (T1) and the end of the training period (T3), no differences in cytokine levels were observed. This appears surprising since exercise is known for its anti-inflammatory effect [275], which is not represented by these results. Our participants are overweight to obese but otherwise healthy. This is also evident by the resting IL6 levels, which did not suggest subclinical inflammatory processes [276]. The absence of a pro-inflammatory phenotype in our participants might be the cause of why a reduction in the resting cytokine levels cannot be observed. In contrast, most of the cytokines were highly upregulated by acute exercise, which is well in line with several studies in healthy individuals [277]. The regulation was very stable when comparing the upregulation induced by the first and the last exercise bout of the 8-week training periods. This could be explained by the training intensity, chosen to be 80 % VO_2peak, and the corresponding heart rate at that intensity was used for monitoring. Thus, using this approach, the exercise performance measured in [W] increased over time and was significantly higher at the last bout of exercise compared to the first. Therefore, the absolute intensity increases, whereas the relative individual intensity remains similar, suggesting a linear relation of the cytokines with the relative intensity. Previous studies reported a decreased acute exercise-induced regulation of plasma cytokines before and after a 6-week training intervention when the absolute intensity was considered [278]. These findings are in line with a study that reported a reduced IL6 release after a 6-week high-intensity interval training when the same absolute intensity was used [279], however, when the intensity was adjusted based on the increased maximal power performance, the IL6 increase was comparable to the previous levels [280]. Similarly, in healthy sedentary and endurance-trained subjects, IL6 and IL8 increased to a comparable extent after exercise when the individual 75 % VO_2peak was used, however, the trained participants had, on average, a 50 % higher VO_2peak [281]. Therefore, distinguishing between the individual relative and absolute intensity is essential when comparing the exercise-induced cytokine response.

The most upregulated cytokines were OSM (oncostatin M), TGFA (transforming growth factor alpha), and TNFSF14 (TNF superfamily member 14), which are yet not well described as exercise-regulated cytokines. OSM was shown to be increased in serum by 60 min of cycling or swimming in humans [282], together with an increased transcriptional expression in mice skeletal muscle [283]. It is mainly expressed in immune cells such as monocytes, macrophages, or mast cells [284–286], but it was also detected to be secreted by human skeletal muscle cells [287], which suggests it to be a myokine. However, our study did not observe a significantly increased OSM transcription after

acute exercise in skeletal muscle (data not shown). TNFSF14 was already discussed in section 5.1.2 due to its significant correlation on transcriptional level with the change in insulin sensitivity and significantly altered CpG sites between the response groups after the training intervention (T5T0). TGFA was highly increased on protein level in serum and transcriptional level measured in whole blood at both acute time point comparisons (T2T1 and T4T3). This indicates that the increased protein level might involve circulating immune cells [288]. TGFA is a mitogenic protein [289], however, its function in skeletal muscle is not known. One study reported an insulin-like effect in adipocytes to increase the GLUT4 translocation and, subsequently, glucose uptake, suggesting a similar mechanism in skeletal muscle cells due to similar receptor expression levels [290]. While this would suggest TGFA as a candidate to influence the adaptation of glucose metabolism to exercise and thus insulin sensitivity, the acute increase in TGFA was not correlated to the change in insulin sensitivity (data not shown). Of note, no correlation was observed between any of the acutely increased cytokines and the change in insulin sensitivity. Thus, the differences in the metabolic outcome in our study cannot be explained by differences in the acute response of systemic cytokine levels. Furthermore, one of the most extensively studied cytokines in exercising humans, the IL6 [291–294], was only moderately increased in our study. Additionally, no increase in transcriptional level was seen in whole blood, suggesting that the increase is not mediated by immune cells but by muscle cells. However, the transcription of *IL6* at the acute time point comparison (T2T0) was not increased in skeletal muscle. This supports the hypothesis that a rapid increase can be mediated by the release from vesicles storing IL6 protein [295]. This release is enhanced by lactate via a protease-mediated mechanism, which is supported by the correlation of the increase in IL6 with plasma lactate level after acute exercise, also observed in our study [296, 297].

We also tested whether clinical parameters of obesity, insulin sensitivity, and fitness were associated with the acute exercise-induced regulation of cytokines. We observed several positive correlations with the BMI and VAT, but not SCAT before the training intervention (T2T1), but not after the training intervention (T4T3). This suggests that VAT plays an important role in the regulation of cytokines in response to exercise. The VAT is reported to be higher innervated and to contain a higher amount of immune cells, such as NK cells, T-cells, or macrophages, than the SCAT, which leads to a greater release of cytokines [298–300]. A potential mechanism could be that exercise leads to the activation of resident immune cells in the VAT, resulting in an increase in the systemic cytokines concentrations. After the training intervention, the number, composition, and activation status of these cells might be changed, but we have no experimental validation for this hypothesis. Of note, VAT was decreased after the training intervention, which indicates that training had an impact on this fat compartment.

To summarize, these results show the great potential of using whole cytokine panels or performing an untargeted approach when analyzing cytokine responses to exercise interventions or acute bouts of exercise. We reported multiple cytokines with great potential interest in exercise intervention, such as OSM, TGFA, or TNFSF14, due to their robust increase that is yet to be explored. Further studies and experiments are needed to give insight into the potential mechanisms of these cytokines in muscle adaptation to acute or prolonged exercise.

6 Conclusion and outlook

In conclusion, this study aimed to give insight on molecular factors explaining the different regulation of insulin sensitivity observed in individuals following prolonged endurance training. Using multi-omics analyses of human skeletal muscle biopsies consisting of transcriptomics, epigenomics, and proteomics, and additionally serum cytokine analyses, several key findings have emerged. Notably, the discovery of IL34 and AKR1C3, as potential contributors to the differential responses observed between the responder (RES) and low-responder (LRE) groups, holds potential for advancing our understanding of the molecular basis of training-induced changes. The proteomic analyses unveiled PERM1 and PPME1 as candidates with high interest for functional investigations, which could yield more insights into their influence on critical cellular processes related to insulin sensitivity and mitochondrial function. However, important to mention is that although, the muscle is an important organ contributing to peripheral insulin sensitivity, exercise-induced molecular adaptations in other tissues must also be considered. This needs to be addressed in future studies. We did not detect training-induced changes in systemic cytokine concentrations, but modulation of the immune response to a certain stimulus could not be excluded and can also take part in the long-term effect on insulin sensitivity.

The obtained datasets provide a knowledge base for deeper explorations into the intricate network of factors influencing insulin sensitivity responses to endurance training. The multifaceted nature of the human body suggests that no single protein may hold the key to understanding these complex variations. Instead, it is likely the interplay of numerous factors that shapes individual responses. By using the comprehensive datasets generated in this study, further investigations could result in additional candidates not yet explored, such as proteins linked to the improvement in mitochondrial respiration and exercise performance. Ultimately, this enhanced understanding has the potential to optimize the design of personalized training sessions, facilitating the transformation of insulin-resistant individuals into insulin-sensitive ones. By deciphering the contributing molecular mechanisms, this research contributes to the broader goal of improving strategies for diabetes prevention and management through tailored exercise interventions.

7 Supplementary Material

Table S1: Anthropometric data of all participants from the NRE2 study. The numbers are shown as mean ± SD. Numbers in brackets show the range from minimum to maximum. The p-values were calculated using a paired Student's t-test or Wilcoxon signed rank test for non-normal distributed parameters.

Parameter	Pre-8-week	Post-8-week	p-value
Sex	16 females, 9 males		-
Age [years]	29.8 ± 8.20 (19 – 59)	29.9 ± 8.15 (19 – 59)	-
Height [cm]	170 ± 9.70 (157 – 193)		-
Body mass [kg]	91.6 ± 15.9 (69.9 – 132)	90.7 ± 16.2 (67.2 – 130)	**0.030**
BMI [kg/m^2]	31.5 ± 4.17 (27.5 – 45.5)	31.1 ± 4.32 (26.3 – 45.2)	**0.030**
Waist-to-hip ratio	0.89 ± 0.06 (0.76 – 1.03)	0.88 ± 0.06 (0.74 – 0.98)	>0.1
Total AT tissue volume [L]	39.9 ± 11.1 (25.3 – 74.2)	39.0 ± 10.9 (22.8 – 73.9)	**0.002**
Subcutaneous AT [L]	15.1 ± 4.17 (8.42 – 32.2)	14.6 ± 5.59 (7.20 – 33.1)	**0.008**
Visceral AT [L]	3.42 ± 1.58 (0.81 – 7.26)	3.27 ± 1.50 (0.94 – 6.68)	**0.022**
IAT_{ergo}/BM [W/kg]	1.11 ± 0.21 (0.77 – 1.55)	1.33 ± 0.25 (0.89 – 1.87)	**<0.001**
VO_2peak_{ergo}/BM [mL/(kg × min)]	25.1 ± 4.01 (18.3 – 32.3)	27.0 ± 4.55 (16.0 – 34.9)	**0.007**
Glucose fasting [mmol/L]	5.11 ± 0.39 (4.61 – 6.00)	5.02 ± 0.37 (4.33 – 5.61)	>0.1
Glucose $OGTT_{120\ min}$ [mmol/L]	5.68 ± 1.22 (3.44 – 8.00)	5.52 ± 1.53 (3.50 – 11.6)	0.075
Insulin fasting [pmol/L]	105 ± 42.6 (38.0 – 188)	100 ± 36.6 (50.0 – 170)	>0.1
Insulin $OGTT_{120\ min}$ [pmol/L]	545 ± 410 (65.0 – 1,766)	457 ± 340 (61.0 – 1,345)	**0.032**
ISI_{Mats} [AU]	8.71 ± 5.04 (3.12 – 27.0)	9.22 ± 4.46 (4.47 – 21.4)	>0.1
HbA_{1C} [mmol/mol Hb]	34.3 ± 2.59 (28.0 – 39.0)	33.6 ± 2.53 (26.0 – 37.0)	0.092
HbA_{1C} [%]	5.29 ± 0.23 (4.71 – 5.72)	5.22 ± 0.23 (4.53 – 5.54)	0.092
Leukocytes [1/µL]	6,959 ± 1,434 (4,740 – 10,200)	6,480 ± 1,360 (4,220 – 9,220)	0.071
CRP [mg/dL]	0.48 ± 0.67 (0.01 – 3.02)	0.36 ± 0.38 (0.01 – 1.30)	>0.1

Table S2: Anthropometric data of all participants from the NRE1 study. The numbers are shown as mean ± SD. Numbers in brackets show the range from minimum to maximum. The p-values were calculated using a paired Student's t-test or Wilcoxon signed rank test for non-normal distributed parameters.

Parameter	Pre-8-week	Post-8-week	p-value
Sex	12 females, 7 males		-
Age [years]	46.4 ± 10.5 (24.0 – 63.0)	46.5 ± 10.5 (24.0 – 63.0)	-
Height [cm]	171 ± 9.69 (148 – 184)		-
Body mass [kg]	95.4 ± 13.5 (71.1 – 132)	94.8 ± 13.6 (71.1 – 134)	0.091
BMI [kg/m^2]	32.7 ± 4.59 (23.6 – 42.0)	32.5 ± 4.64 (23.6 – 41.8)	0.074
Waist-to-hip ratio	0.90 ± 0.07 (0.75 – 1.02)	0.91 ± 0.08 (0.73 – 1.05)	>0.1
Total AT tissue volume [L]	42.9 ± 11.3 (24.4 – 58.9)	42.0 ± 11.5 (21.4 – 60.0)	0.075
Subcutaneous AT [L]	15.2 ± 4.61 (7.42 – 22.1)	15.1 ± 4.99 (6.18 – 22.7)	>0.1
Visceral AT [L]	5.01 ± 3.02 (1.20 – 13.7)	4.85 ± 3.00 (1.21 – 14.0)	>0.1
IAT_{ergo}/BM [W/kg]	1.12 ± 0.30 (0.58 – 1.61)	1.29 ± 0.35 (0.82 – 1.92)	**<0.001**
VO_2peak_{ergo}/BM [mL/(kg × min)]	23.1 ± 5.26 (16.7 – 33.8)	24.6 ± 5.31 (14.5 – 35.8)	0.081
Glucose fasting [mmol/L]	5.60 ± 0.47 (4.61 – 6.61)	5.71 ± 0.54 (4.78 – 6.89)	>0.1
Glucose $OGTT_{120\ min}$ [mmol/L]	6.49 ± 1.06 (4.92 – 9.06)	6.39 ± 1.08 (4.61 – 8.39)	>0.1
Insulin fasting [pmol/L]	82.8 ± 41.2 (27.0 – 197)	74.6 ± 38.6 (19.0 – 174)	>0.1
Insulin $OGTT_{120\ min}$ [pmol/L]	568 ± 691 (58.0 – 3,259)	468 ± 489 (63.0 – 2,238)	>0.1
ISI_{Mats} [AU]	11.6 ± 8.93 (1.88 – 31.8)	12.8 ± 10.7 (2.64 – 50.5)	>0.1
HbA_{1C} [mmol/mol Hb]	36.8 ± 4.20 (29.0 – 43.0)	36.4 ± 3.67 (28.0 – 42.0)	>0.1
HbA_{1C} [%]	5.52 ± 0.38 (4.80 – 6.08)	5.48 ± 0.34 (4.71 – 5.99)	>0.1
Leukocytes [1/µL]	6,297 ± 1,729 (3,960 – 10,940)	6,127 ± 1,630 (4,000 – 9,930)	>0.1
CRP [mg/dL]	0.22 ± 0.24 (0.01 – 0.77)	0.42 ± 0.75 (0.03 – 3.25)	>0.1

Table S3: Anthropometric data of participants for OLink analysis from the NRE2 study. The numbers are shown as mean ± SD. Numbers in brackets show the range from minimum to maximum. The p-values were calculated using a paired Student's t-test or Wilcoxon signed rank test for non-normal distributed parameters.

Parameter	Pre-8-week	Post-8-week	p-value
Sex	14 females, 8 males		-
Age [years]	30.0 ± 8.20 (19 – 59)	30.1 ± 8.15 (19 – 59)	-
Height [cm]	171 ± 9.47 (157 – 193)		-
Body mass [kg]	92.6 ± 16.1 (69.9 – 132)	91.4 ± 16.6 (67.2 – 130)	**0.008**
BMI [kg/m^2]	31.7 ± 4.38 (27.5 – 45.5)	31.3 ± 4.58 (26.3 – 45.2)	**0.006**
Waist-to-hip ratio	0.89 ± 0.06 (0.76 – 1.03)	0.89 ± 0.06 (0.74 – 0.98)	>0.1
Total AT tissue volume [L]	40.4 ± 11.5 (25.3 – 74.2)	39.4 ± 11.6 (22.8 – 73.9)	**0.004**
Subcutaneous AT [L]	15.3 ± 5.73 (8.42 – 32.2)	14.7 ± 5.93 (7.20 – 33.1)	**0.006**
Visceral AT [L]	3.53 ± 1.61 (0.81 – 7.26)	3.38 ± 1.54 (0.94 – 6.68)	**0.012**
IAT_{ergo}/BM [W/kg]	1.11 ± 0.22 (0.77 – 1.55)	1.32 ± 0.26 (0.89 – 1.87)	**<0.001**
VO_2peak_{ergo}/BM [mL/(kg × min)]	25.2 ± 4.15 (18.3 – 32.3)	26.5 ± 4.55 (16.0 – 34.9)	**0.042**
Glucose fasting [mmol/L]	5.09 ± 0.39 (4.61 – 6.00)	5.02 ± 0.39 (4.33 – 5.61)	>0.1
Glucose $OGTT_{120\ min}$ [mmol/L]	5.70 ± 1.17 (3.44 – 8.00)	5.52 ± 1.58 (3.50 – 11.6)	0.089
Insulin fasting [pmol/L]	110 ± 40.0 (38.0 – 188)	103 ± 36.9 (50.0 – 170)	>0.1
Insulin $OGTT_{120\ min}$ [pmol/L]	546 ± 400 (65.0 – 1,766)	472 ± 341 (61.0 – 1,345)	0.095
ISI_{Mats} [AU]	8.35 ± 4.90 (3.12 – 27.0)	8.86 ± 4.20 (4.47 – 21.4)	>0.1
HbA_{1c} [mmol/mol Hb]	34.2 ± 2.41 (28.0 – 39.0)	33.5 ± 2.64 (26.0 – 37.0)	**0.050**
HbA_{1c} [%]	5.28 ± 0.22 (4.71 – 5.72)	5.22 ± 0.24 (4.53 – 5.54)	**0.050**
Leukocytes [1/µL]	6,890 ± 1,513 (4,740 – 10,200)	6,485 ± 1,437 (4,220 – 9,220)	>0.1
CRP [mg/dL]	0.36 ± 0.45 (0.01 – 1.84)	0.35 ± 0.40 (0.01 – 1.30)	>0.1

Declaration

I hereby declare that I have independently written the thesis submitted for doctoral studies entitled "Differences in epigenetic, transcriptional and protein adaptations to exercise in skeletal muscle of responders and low-responders in insulin sensitivity", that I have used only the sources and aids indicated and that I have marked passages taken over verbatim or in citations as such. I declare that the guidelines for ensuring good scientific practice at the University of Tübingen (resolution of the Senate of 25.5.2000) have been observed. I affirm in lieu of oath that this information is true and that I have not concealed anything. I am aware that making a false affirmation in lieu of an oath is punishable by imprisonment of up to three years or a fine.

At the moment I am not accepted or registered at another university as doctoral student. There were no former interrupted or terminated PhD procedures or corresponding examinations, which I have taken. This work has not been submitted for any other degree or professional qualification except as specified. I did not take part in any commercially arranged opportunities to take up the current PhD procedure. I especially did not contact any organizations which engage in the active search for supervisors for the PhD thesis and receive money for this service. I also do clearly exclude that I used such organizations, which adopt the applicant's obligations and take care of the academic records partially or entirely. Furthermore, I confirm to be aware of the legal consequences of using a commercial thesis writing agency (exclusion from acceptance as a doctoral student and exclusion from admission to the doctoral qualification process, an end to the doctoral qualification process and annulment of the degree). I have no penal convictions, disciplinary measures and pending criminal- and disciplinary proceedings to declare.

Part of this work has been published:
Goj, T., Hoene, M., Fritsche, L., Schneeweiss, P., Machann, J., Petrera, A., Hauck, S. M., Fritsche, A., Birkenfeld, A. L., Peter, A., Heni, M., Niess, A. M., Moller, A., and Weigert, C. "The Acute Cytokine Response to 30-Minute Exercise Bouts Before and After 8-Week Endurance Training in Individuals With Obesity". In: *The Journal of Clinical Endocrinology & Metabolism* vol. 108.4 (2022), pp. 865–875. DOI: 10.1210/clinem/dgac623

Thomas Goj
Tübingen, 05.10.2023

Acknowledgment

I want to express my deepest gratitude to my supervisor, Prof. Dr. Cora Weigert, for her invaluable guidance, mentorship, and unwavering support throughout the entire journey of my doctoral thesis. Her expertise, insightful feedback, and endless encouragement significantly contributed to the successful completion of this research project.

I am deeply thankful to my second supervisor, Prof. Dr. Hubert Preißl, for his critical insights and constructive feedback that enriched the depth and scope of my thesis. His contributions were instrumental in shaping my research and enhancing its overall quality.

I extend my sincere appreciation to each member of my research group — Dr. Simon Dreher, Dr. Miriam Hoene, Jennifer Maurer, Nadine Sanabria Valdés, and Paul Grubba. Your collaborative efforts, assistance in the laboratory procedures, and careful proofreading greatly improved the accuracy and quality of this work. Your dedication have been motivation throughout this academic journey. Especially thanks to Jennifer Maurer and Nadine Sanabria Valdés for all the small chats during our lunch break while enjoying a hot coffee.

I want to thank all my collaboration partners for their help and support in generating the data and proofreading my thesis.

I am especially grateful to Ani for supporting and uplifting me during difficult times, providing motivation and bringing peace after long working days.

Lastly, I am profoundly grateful to my friends and family for their unwavering support, love, and encouragement. Your belief in me, constant encouragement, and understanding of the demands of this endeavor have always motivated me. Thank you for being the pillars of strength in my life.

Thank you all for being an integral part of this journey.

References

[1] Hiller-Sturmhöfel, S. and Bartke, A. "The endocrine system: an overview". In: *Alcohol Health and Research World* vol. 22.3 (1998). PMID: 15706790, pp. 153–164.

[2] Qaid, M. M. and Abdelrahman, M. M. "Role of insulin and other related hormones in energy metabolism: A review". In: *Cogent Food Agriculture* vol. 2.1 (2016). DOI: 10.1080/23311932.2016.1267691.

[3] Rahman, M. S., Hossain, K. S., Das, S., et al. "Role of Insulin in Health and Disease: An Update". In: *International Journal of Molecular Sciences* vol. 22.12 (2021), p. 6403. DOI: 10.3390/ijms22126403.

[4] Karamanou, M. "Milestones in the history of diabetes mellitus: The main contributors". In: *World Journal of Diabetes* vol. 7.1 (2016), p. 1. DOI: 10.4239/wjd.v7.i1.1.

[5] Lakhtakia, R. "The History of Diabetes Mellitus". In: *Sultan Qaboos University Medical Journal* vol. 13.3 (2013), pp. 368–370. DOI: 10.12816/0003257.

[6] Zimmet, P., Alberti, K. G. M. M., and Shaw, J. "Global and societal implications of the diabetes epidemic". In: *Nature* vol. 414.6865 (2001), pp. 782–787. DOI: 10.1038/414782a.

[7] World Health Organization. *Global Report on Diabetes*. Genève, Switzerland: World Health Organization, 2016. ISBN: 978-92-4-156525-7.

[8] Magliano, D. and Boyko, E. J. *IDF Diabetes Atlas*. 10th ed. Brussels,Belgium: International Diabetes Federation, 2021. ISBN: 978-2-930229-98-0.

[9] Bommer, C., Heesemann, E., Sagalova, V., et al. "The global economic burden of diabetes in adults aged 20–79 years: a cost-of-illness study". In: *The Lancet Diabetes & Endocrinology* vol. 5.6 (2017), pp. 423–430. DOI: 10.1016/s2213-8587(17)30097-9.

[10] Romieu, I., Dossus, L., et al. "Energy balance and obesity: what are the main drivers?" In: *Cancer Causes Control* vol. 28.3 (2017), pp. 247–258. DOI: 10.1007/s10552-017-0869-z.

[11] Shaw, J., Sicree, R., and Zimmet, P. "Global estimates of the prevalence of diabetes for 2010 and 2030". In: *Diabetes Research and Clinical Practice* vol. 87.1 (2010), pp. 4–14. DOI: 10.1016/j.diabres.2009.10.007.

[12] Kahn, S. E., Hull, R. L., and Utzschneider, K. M. "Mechanisms linking obesity to insulin resistance and type 2 diabetes". In: *Nature* vol. 444.7121 (2006), pp. 840–846. DOI: 10.1038/nature05482.

[13] Aras, M., Tchang, B. G., and Pape, J. "Obesity and Diabetes". In: *Nursing Clinics of North America* vol. 56.4 (2021), pp. 527–541. DOI: 10.1016/j.cnur.2021.07.008.

[14] Toplak, H., Leitner, D. R., Harreiter, J., et al. ""Diabesity" – Adipositas und Typ-2-Diabetes (Update 2019)". In: *Wiener klinische Wochenschrift* vol. 131.1 (2019), pp. 71–76. DOI: 10.1007/s00508-018-1418-9.

[15] Karow, T. and Lang-Roth, R. *Allgemeine und spezielle Pharmakologie und Toxikologie: vorlesungsorientierte Darstellung und klinischer Leitfaden für Studium und Praxis : 2023/24*. 31st ed. Köln, Deutschland, 2022. ISBN: 978-3-9821223-3-5.

[16] Flier, J. S., Underhill, L. H., and Eisenbarth, G. S. "Type I Diabetes Mellitus". In: *New England Journal of Medicine* vol. 314.21 (1986), pp. 1360–1368. DOI: 10.1056/nejm198605223142106.

[17] Pozzilli, P., Mario, U., and Andreani, D. "Cell-mediated immunity and immune complexes in the pathogenesis of type 1 (insulin-dependent) diabetes". In: *Acta Diabetologica Latina* vol. 19.4 (1982), pp. 295–300. DOI: 10.1007/bf02629252.

[18] The Diabetes Control and Complications Trial Research Group. "The Effect of Intensive Treatment of Diabetes on the Development and Progression of Long-Term Complications in Insulin-Dependent Diabetes Mellitus". In: *New England Journal of Medicine* vol. 329.14 (1993), pp. 977–986. DOI: 10.1056/nejm199309303291401.

[19] Bennettjenson, A. "PANCREATIC ISLET-CELL DAMAGE IN CHILDREN WITH FATAL VIRAL INFECTIONS". In: *The Lancet Diabetes & Endocrinology* vol. 316.8190 (1980), pp. 354–358. DOI: 10.1016/s0140-6736(80)90349-9.

[20] Raile, K., Boss, K., Braune, K., et al. "Versorgung von Kindern und Jugendlichen mit Typ-1-Diabetes: Lösungen für technische und psychosoziale Herausforderungen". In: *Bundesgesundheitsblatt - Gesundheitsforschung - Gesundheitsschutz* vol. 63.7 (2020), pp. 856–863. DOI: 10.1007/s00103-020-03162-3.

[21] Gao, F., Luo, H., Jones, K., et al. "Gestational Diabetes and Health Behaviors Among Women: National Health and Nutrition Examination Survey, 2007–2014". In: *Preventing Chronic Disease* vol. 15 (2018). DOI: 10.5888/pcd15.180094.

[22] Amanat, S., Ghahri, S., Dianatinasab, A., et al. "Exercise and Type 2 Diabetes". In: *Physical Exercise for Human Health*. Vol. 1228. Springer Singapore, 2020, pp. 91–105. ISBN: 978-981-15-1791-4. DOI: 10.1007/978-981-15-1792-1_6.

[23] ElSayed, N. A., Aleppo, G., Aroda, V. R., et al. "2. Classification and Diagnosis of Diabetes: Standards of Care in Diabetes—2023". In: *Diabetes Care* vol. 46.1 (2022), pp. 19–40. DOI: 10.2337/dc23-s002.

[24] Ortiz-Martínez, M., González-González, M., Martagón, A. J., et al. "Recent Developments in Biomarkers for Diagnosis and Screening of Type 2 Diabetes Mellitus". In: *Current Diabetes Reports* vol. 22.3 (2022), pp. 95–115. DOI: 10.1007/s11892-022-01453-4.

[25] Melmed, S. and Polonsky, K. S. *Williams textbook of endocrinology*. 12th ed. Philadelphia, USA: Saunders Elsevier, 2011. ISBN: 978-1-4377032-4-5.

[26] Einarson, T. R., Acs, A., Ludwig, C., et al. "Prevalence of cardiovascular disease in type 2 diabetes: a systematic literature review of scientific evidence from across the world in 2007–2017". In: *Cardiovascular Diabetology* vol. 17.1 (2018). DOI: 10.1186/s12933-018-0728-6.

[27] Gheith, O., Farouk, N., Nampoory, N., et al. "Diabetic kidney disease: world wide difference of prevalence and risk factors". In: *Journal of Nephropharmacology* vol. 5.1 (2016). PMID: 28197499, pp. 49–56.

[28] Ferrannini, E., Simonson, D. C., Katz, L. D., et al. "The disposal of an oral glucose load in patients with non-insulin-dependent diabetes". In: *Metabolism* vol. 37.1 (1988), pp. 79–85. DOI: 10.1016/0026-0495(88)90033-9.

[29] DeFronzo, R. A. and Tripathy, D. "Skeletal Muscle Insulin Resistance Is the Primary Defect in Type 2 Diabetes". In: *Diabetes Care* vol. 32.2 (2009), pp. 157–163. DOI: 10.2337/dc09-s302.

[30] Frontera, W. R. and Ochala, J. "Skeletal Muscle: A Brief Review of Structure and Function". In: *Calcified Tissue International* vol. 96.3 (2014), pp. 183–195. DOI: 10.1007/s00223-014-9915-y.

[31] Egan, B. and Sharples, A. P. "Molecular responses to acute exercise and their relevance for adaptations in skeletal muscle to exercise training". In: *Physiological Reviews* vol. 103.3 (2023), pp. 2057–2170. DOI: 10.1152/physrev.00054.2021.

[32] Egan, B. and Zierath, J. R. "Exercise Metabolism and the Molecular Regulation of Skeletal Muscle Adaptation". In: *Cell Metabolism* vol. 17.2 (2013), pp. 162–184. DOI: 10.1016/j.cmet.2012.12.012.

[33] Richter, E. A. and Hargreaves, M. "Exercise, GLUT4, and Skeletal Muscle Glucose Uptake". In: *Physiological Reviews* vol. 93.3 (2013), pp. 993–1017. DOI: 10.1152/physrev.00038.2012.

[34] Plomgaard, P. and Weigert, C. "Do diabetes and obesity affect the metabolic response to exercise?" In: *Current Opinion in Clinical Nutrition and Metabolic Care* vol. 20.4 (2017), pp. 294–299. DOI: 10.1097/MCO.0000000000000379.

[35] Weigert, C., Lehmann, R., Hartwig, S., et al. "The secretome of the working human skeletal muscle-A promising opportunity to combat the metabolic disaster?" In: *PROTEOMICS - Clinical Applications* vol. 8.1-2 (2014), pp. 5–18. DOI: 10.1002/prca.201300094.

[36] Maurer, J., Hoene, M., and Weigert, C. "Signals from the Circle: Tricarboxylic Acid Cycle Intermediates as Myometabokines". In: *Metabolites* vol. 11.8 (2021), p. 474. DOI: 10.3390/metabo11080474.

[37] Kullmann, S., Goj, T., Veit, R., et al. "Exercise restores brain insulin sensitivity in sedentary adults who are overweight and obese". In: *JCI Insight* vol. 7.18 (2022). DOI: 10.1172/jci.insight.161498.

[38] Pedersen, B. K. and Febbraio, M. A. "Muscle as an Endocrine Organ: Focus on Muscle-Derived Interleukin-6". In: *Physiological Reviews* vol. 88.4 (2008), pp. 1379–1406. DOI: 10.1152/physrev.90100.2007.

[39] Hoffmann, C. and Weigert, C. "Skeletal Muscle as an Endocrine Organ: The Role of Myokines in Exercise Adaptations". In: *Cold Spring Harbor Perspectives in Medicine* vol. 7.11 (2017), p. 029793. DOI: 10.1101/cshperspect.a029793.

[40] Kramer, A. "An Overview of the Beneficial Effects of Exercise on Health and Performance". In: *Physical Exercise for Human Health*. Vol. 1228. Springer Singapore, 2020, pp. 3–22. ISBN: 978-981-15-1791-4. DOI: 10.1007/978-981-15-1792-1_1.

[41] He, N. and Ye, H. "Exercise and Hyperlipidemia". In: *Physical Exercise for Human Health*. Vol. 1228. Springer Singapore, 2020, pp. 79–90. ISBN: 978-981-15-1791-4. DOI: 10.1007/978-981-15-1792-1_5.

[42] Alpsoy, Ş. "Exercise and Hypertension". In: *Physical Exercise for Human Health*. Vol. 1228. Springer Singapore, 2020, pp. 153–167. ISBN: 978-981-15-1791-4. DOI: 10.1007/978-981-15-1792-1_10.

[43] Akyuz, A. "Exercise and Coronary Heart Disease". In: *Physical Exercise for Human Health*. Vol. 1228. Springer Singapore, 2020, pp. 169–179. ISBN: 978-981-15-1791-4. DOI: 10.1007/978-981-15-1792-1_11.

[44] García-Cabo, C. and López-Cancio, E. "Exercise and Stroke". In: *Physical Exercise for Human Health*. Vol. 1228. Springer Singapore, 2020, pp. 195–203. ISBN: 978-981-15-1791-4. DOI: 10.1007/978-981-15-1792-1_13.

[45] Li, G., Li, J., and Gao, F. "Exercise and Cardiovascular Protection". In: *Physical Exercise for Human Health*. Vol. 1228. Springer Singapore, 2020, pp. 205–216. ISBN: 978-981-15-1791-4. DOI: 10.1007/978-981-15-1792-1_14.

[46] Gur, D. O. "Exercise and Peripheral Arteriosclerosis". In: *Physical Exercise for Human Health*. Vol. 1228. Springer Singapore, 2020, pp. 181–193. ISBN: 978-981-15-1791-4. DOI: 10.1007/978-981-15-1792-1_12.

[47] Burgis, E. *Intensivkurs: Allgemeine und Spezielle Pharmakologie*. 3rd ed. Intensivkurs. München, Deutschland: Urban & Fischer in Elsevier, 2004. ISBN: 978-3-437-42612-4.

[48] ElSayed, N. A., Aleppo, G., Aroda, V. R., et al. "3. Prevention or Delay of Type 2 Diabetes and Associated Comorbidities: Standards of Care in Diabetes—2023". In: *Diabetes Care* vol. 46.1 (2022), pp. 41–48. DOI: 10.2337/dc23-s003.

[49] Knowler, W. C., Barrett-Connor, E., Fowler, S. E., et al. "Reduction in the Incidence of Type 2 Diabetes with Lifestyle Intervention or Metformin". In: *New England Journal of Medicine* vol. 346.6 (2002), pp. 393–403. DOI: 10.1056/nejmoa012512.

[50] Group, D. P. P. O. S. R., Orchard, T. J., Temprosa, M., et al. "Long-term effects of the Diabetes Prevention Program interventions on cardiovascular risk factors: a report from the DPP Outcomes Study". In: *Diabetic Medicine* vol. 30.1 (2012), pp. 46–55. DOI: 10.1111/j.1464-5491.2012.03750.x.

[51] Group, D. P. P. R. "Long-term effects of lifestyle intervention or metformin on diabetes development and microvascular complications over 15-year follow-up: the Diabetes Prevention Program Outcomes Study". In: *The Lancet Diabetes & Endocrinology* vol. 3.11 (2015), pp. 866–875. DOI: 10.1016/s2213-8587(15)00291-0.

[52] Lindström, J., Louheranta, A., Mannelin, M., et al. "The Finnish Diabetes Prevention Study (DPS)". In: *Diabetes Care* vol. 26.12 (2003), pp. 3230–3236. DOI: 10.2337/diacare.26.12.3230.

[53] Gong, Q., Zhang, P., Wang, J., et al. "Morbidity and mortality after lifestyle intervention for people with impaired glucose tolerance: 30-year results of the Da Qing Diabetes Prevention Outcome Study". In: *The Lancet Diabetes & Endocrinology* vol. 7.6 (2019), pp. 452–461. DOI: 10.1016/s2213-8587(19)30093-2.

[54] Haddad, E., Wells, G. A., Sigal, R. J., et al. "Meta-analysis of the effect of structured exercise training on cardiorespiratory fitness in Type 2 diabetes mellitus". In: *Diabetologia* vol. 46.8 (2003), pp. 1071–1081. DOI: 10.1007/s00125-003-1160-2.

[55] Boulé, N. G., Haddad, E., Kenny, G. P., et al. "Effects of Exercise on Glycemic Control and Body Mass in Type 2 Diabetes Mellitus". In: *JAMA* vol. 286.10 (2001), p. 1218. DOI: 10.1001/jama.286.10.1218.

[56] Kelley, G. and Kelley, K. "Effects of aerobic exercise on lipids and lipoproteins in adults with type 2 diabetes: A meta-analysis of randomized-controlled trials". In: *Public Health* vol. 121.9 (2007), pp. 643–655. DOI: 10.1016/j.puhe.2007.02.014.

[57] Steinhaus, A. H. "CHRONIC EFFECTS OF EXERCISE". In: *Physiological Reviews* vol. 13.1 (1933), pp. 103–147. DOI: 10.1152/physrev.1933.13.1.103.

[58] Åstrand, P. O. "Human Physical Fitness With Special Reference to Sex and Age". In: *Physiological Reviews* vol. 36.3 (1956), pp. 307–335. DOI: 10.1152/physrev.1956.36.3.307.

[59] Lavin, K. M., Coen, P. M., Baptista, L. C., et al. "State of Knowledge on Molecular Adaptations to Exercise in Humans: Historical Perspectives and Future Directions". In: *Comprehensive Physiology* vol. 12.2 (2022), pp. 3193–3279. DOI: 10.1002/cphy.c200033.

[60] Hawley, J. A., Hargreaves, M., Joyner, M. J., et al. "Integrative Biology of Exercise". In: *Cell* vol. 159.4 (2014), pp. 738–749. DOI: 10.1016/j.cell.2014.10.029.

[61] Bortoluzzi, S., Scannapieco, P., Cestaro, A., et al. "Computational reconstruction of the human skeletal muscle secretome". In: *Proteins: Structure, Function, and Bioinformatics* vol. 62.3 (2005), pp. 776–792. DOI: 10.1002/prot.20803.

[62] Keller, P., Vollaard, N. B. J., Gustafsson, T., et al. "A transcriptional map of the impact of endurance exercise training on skeletal muscle phenotype". In: *Journal of Applied Physiology* vol. 110.1 (2011), pp. 46–59. DOI: 10.1152/japplphysiol.00634.2010.

[63] McGee, S. L. and Hargreaves, M. "Exercise adaptations: molecular mechanisms and potential targets for therapeutic benefit". In: *Nature Reviews Endocrinology* vol. 16.9 (2020), pp. 495–505. DOI: 10.1038/s41574-020-0377-1.

[64] Wilkinson, S. B., Phillips, S. M., Atherton, P. J., et al. "Differential effects of resistance and endurance exercise in the fed state on signalling molecule phosphorylation and protein synthesis in human muscle". In: *The Journal of Physiology* vol. 586.15 (2008), pp. 3701–3717. DOI: 10.1113/jphysiol.2008.153916.

[65] Konopka, A. R. and Harber, M. P. "Skeletal Muscle Hypertrophy After Aerobic Exercise Training". In: *Exercise and Sport Sciences Reviews* vol. 42.2 (2014), pp. 53–61. DOI: 10.1249/jes.0000000000000007.

[66] Terjung, R. L. and Hood, D. A. "Biochemical Adaptations in Skeletal Muscle Induced by Exercise Training". In: *ACS Symposium Series*. Vol. 294. American Chemical Society, 1986, pp. 8–26. ISBN: 978-0-84120-949-7. DOI: 10.1021/bk-1986-0294.ch002.

[67] Holloszy, J. O. "Biochemical adaptations in muscle. Effects of exercise on mitochondrial oxygen uptake and respiratory enzyme activity in skeletal muscle". In: *Journal of Biological Chemistry* vol. 242.9 (1967). PMID: 4290225, pp. 2278–2282.

[68] Robinson, D. M., Ogilvie, R. W., Tullson, P. C., et al. "Increased peak oxygen consumption of trained muscle requires increased electron flux capacity". In: *Journal of Applied Physiology* vol. 77.4 (1994), pp. 1941–1952. DOI: 10.1152/jappl.1994.77.4.1941.

[69] Mackie, B. G. and Terjung, R. L. "Influence of training on blood flow to different skeletal muscle fiber types". In: *Journal of Applied Physiology* vol. 55.4 (1983), pp. 1072–1078. DOI: 10.1152/jappl.1983.55.4.1072.

[70] Sexton, W. L. and Laughlin, M. H. "Influence of endurance exercise training on distribution of vascular adaptations in rat skeletal muscle". In: *American Journal of Physiology-Heart and Circulatory Physiology* vol. 266.2 (1994), pp. 483–490. DOI: 10.1152/ajpheart.1994.266.2.h483.

[71] Codella, R., Terruzzi, I., and Luzi, L. "Why should people with type 1 diabetes exercise regularly?" In: *Acta Diabetologica* vol. 54.7 (2017), pp. 615–630. DOI: 10.1007/s00592-017-0978-x.

[72] Colberg, S. R., Sigal, R. J., Yardley, J. E., et al. "Physical Activity/Exercise and Diabetes: A Position Statement of the American Diabetes Association". In: *Diabetes Care* vol. 39.11 (2016), pp. 2065–2079. DOI: 10.2337/dc16-1728.

[73] Dubé, J. J., Allison, K. F., Rousson, V., et al. "Exercise Dose and Insulin Sensitivity". In: *Medicine & Science in Sports & Exercise* vol. 44.5 (2012), pp. 793–799. DOI: 10.1249/mss.0b013e31823f679f.

[74] Fedewa, M. V., Gist, N. H., Evans, E. M., et al. "Exercise and Insulin Resistance in Youth: A Meta-Analysis". In: *Pediatrics* vol. 133.1 (2014), pp. 163–174. DOI: 10.1542/peds.2013-2718.

[75] Janež, A., Guja, C., Mitrakou, A., et al. "Insulin Therapy in Adults with Type 1 Diabetes Mellitus: a Narrative Review". In: *Diabetes Therapy* vol. 11.2 (2020), pp. 387–409. DOI: 10.1007/s13300-019-00743-7.

[76] Sigal, R. J., Alberga, A. S., Goldfield, G. S., et al. "Effects of Aerobic Training, Resistance Training, or Both on Percentage Body Fat and Cardiometabolic Risk Markers in Obese Adolescents". In: *JAMA Pediatrics* vol. 168.11 (2014), p. 1006. DOI: 10.1001/jamapediatrics.2014.1392.

[77] Perseghin, G., Price, T. B., Petersen, K. F., et al. "Increased Glucose Transport–Phosphorylation and Muscle Glycogen Synthesis after Exercise Training in Insulin-Resistant Subjects". In: *New England Journal of Medicine* vol. 335.18 (1996), pp. 1357–1362. DOI: 10.1056/nejm199610313351804.

[78] Burgomaster, K. A., Cermak, N. M., Phillips, S. M., et al. "Divergent response of metabolite transport proteins in human skeletal muscle after sprint interval training and detraining". In: *American Journal of Physiology-Regulatory, Integrative and Comparative Physiology* vol. 292.5 (2007), pp. 1970–1976. DOI: 10.1152/ajpregu.00503.2006.

[79] Stuart, C. A., Lee, M. L., South, M. A., et al. "Muscle hypertrophy in prediabetic men after 16 wk of resistance training". In: *Journal of Applied Physiology* vol. 123.4 (2017), pp. 894–901. DOI: 10.1152/japplphysiol.00023.2017.

[80] Hanson, P. I., Meyer, T., Stryer, L., et al. "Dual role of calmodulin in autophosphorylation of multifunctional cam kinase may underlie decoding of calcium signals". In: *Neuron* vol. 12.5 (1994), pp. 943–956. DOI: 10.1016/0896-6273(94)90306-9.

[81] Rose, A. J. and Hargreaves, M. "Exercise Increases Ca^{2+}–Calmodulin-Dependent Protein Kinase II Activity in Human Skeletal Muscle". In: *The Journal of Physiology* vol. 553.1 (2003), pp. 303–309. DOI: 10.1113/jphysiol.2003.054171.

[82] Ojuka, E. O., Goyaram, V., and Smith, J. A. H. "The role of CaMKII in regulating GLUT4 expression in skeletal muscle". In: *American Journal of Physiology-Endocrinology and Metabolism* vol. 303.3 (2012), pp. 322–331. DOI: 10.1152/ajpendo.00091.2012.

[83] Hopkins, T., Dyck, J., and Lopaschuk, G. "AMP-activated protein kinase regulation of fatty acid oxidation in the ischaemic heart". In: *Biochemical Society Transactions* vol. 31.1 (2003), pp. 207–212. DOI: 10.1042/bst0310207.

[84] Chen, Q., Xie, B., Zhu, S., et al. "A Tbc1d1 Ser231Ala-knockin mutation partially impairs AICAR- but not exercise-induced muscle glucose uptake in mice". In: *Diabetologia* vol. 60.2 (2016), pp. 336–345. DOI: 10.1007/s00125-016-4151-9.

[85] Steinberg, G. R. and Hardie, D. G. "New insights into activation and function of the AMPK". In: *Nature Reviews Molecular Cell Biology* vol. 24.4 (2022), pp. 255–272. DOI: 10.1038/s41580-022-00547-x.

[86] Suwa, M., Nakano, H., and Kumagai, S. "Effects of chronic AICAR treatment on fiber composition, enzyme activity, UCP3, and PGC-1 in rat muscles". In: *Journal of Applied Physiology* vol. 95.3 (2003), pp. 960–968. DOI: 10.1152/japplphysiol.00349.2003.

[87] Scarpulla, R. C. "Metabolic control of mitochondrial biogenesis through the PGC-1 family regulatory network". In: *Biochimica et Biophysica Acta (BBA) - Molecular Cell Research* vol. 1813.7 (2011), pp. 1269–1278. DOI: 10.1016/j.bbamcr.2010.09.019.

[88] Cantó, C., Gerhart-Hines, Z., Feige, J. N., et al. "AMPK regulates energy expenditure by modulating NAD+ metabolism and SIRT1 activity". In: *Nature* vol. 458.7241 (2009), pp. 1056–1060. DOI: 10.1038/nature07813.

[89] Goodman, C. A. "The Role of mTORC1 in Regulating Protein Synthesis and Skeletal Muscle Mass in Response to Various Mechanical Stimuli". In: *Reviews of Physiology, Biochemistry and Pharmacology*. Vol. 166. Springer International Publishing, 2013, pp. 43–95. ISBN: 978-3-319-04905-2. DOI: 10.1007/112_2013_17.

[90] Srikanthan, P. and Karlamangla, A. S. "Relative Muscle Mass Is Inversely Associated with Insulin Resistance and Prediabetes. Findings from The Third National Health and Nutrition Examination Survey". In: *The Journal of Clinical Endocrinology & Metabolism* vol. 96.9 (2011), pp. 2898–2903. DOI: 10.1210/jc.2011-0435.

[91] Haines, M. S., Dichtel, L. E., Santoso, K., et al. "Association between muscle mass and insulin sensitivity independent of detrimental adipose depots in young adults with overweight/obesity". In: *International Journal of Obesity* vol. 44.9 (2020), pp. 1851–1858. DOI: 10.1038/s41366-020-0590-y.

[92] Schiaffino, S., Dyar, K. A., Ciciliot, S., et al. "Mechanisms regulating skeletal muscle growth and atrophy". In: *FEBS Journal* vol. 280.17 (2013), pp. 4294–4314. DOI: 10.1111/febs.12253.

[93] Yoshida, T. and Delafontaine, P. "Mechanisms of IGF-1-Mediated Regulation of Skeletal Muscle Hypertrophy and Atrophy". In: *Cells* vol. 9.9 (2020), p. 1970. DOI: 10.3390/cells9091970.

[94] Bonifacio, A., Sanvee, G. M., Brecht, K., et al. "IGF-1 prevents simvastatin-induced myotoxicity in C2C12 myotubes". In: *Archives of Toxicology* vol. 91.5 (2016), pp. 2223–2234. DOI: 10.1007/s00204-016-1871-z.

[95] Carnero, A., Blanco-Aparicio, C., Renner, O., et al. "The PTEN/PI3K/AKT Signalling Pathway in Cancer, Therapeutic Implications". In: *Current Cancer Drug Targets* vol. 8.3 (2008), pp. 187–198. DOI: 10.2174/156800908784293659.

[96] Chen, Z., Li, L., Wu, W., et al. "Exercise protects proliferative muscle satellite cells against exhaustion via the Igfbp7-Akt-mTOR axis". In: *Theranostics* vol. 10.14 (2020), pp. 6448–6466. DOI: 10.7150/thno.43577.

[97] Bodine, S. C., Stitt, T. N., Gonzalez, M., et al. "Akt/mTOR pathway is a crucial regulator of skeletal muscle hypertrophy and can prevent muscle atrophy in vivo". In: *Nature Cell Biology* vol. 3.11 (2001), pp. 1014–1019. DOI: 10.1038/ncb1101-1014.

[98] Pallafacchina, G., Calabria, E., Serrano, A. L., et al. "A protein kinase B-dependent and rapamycin-sensitive pathway controls skeletal muscle growth but not fiber type specification". In: *Proceedings of the National Academy of Sciences* vol. 99.14 (2002), pp. 9213–9218. DOI: 10.1073/pnas.142166599.

[99] Eguez, L., Lee, A., Chavez, J. A., et al. "Full intracellular retention of GLUT4 requires AS160 Rab GTPase activating protein". In: *Cell Metabolism* vol. 2.4 (2005), pp. 263–272. DOI: 10.1016/j.cmet.2005.09.005.

[100] Sano, H., Kane, S., Sano, E., et al. "Insulin-stimulated Phosphorylation of a Rab GTPase-activating Protein Regulates GLUT4 Translocation". In: *Journal of Biological Chemistry* vol. 278.17 (2003), pp. 14599–14602. DOI: 10.1074/jbc.c300063200.

[101] Manning, B. D. and Cantley, L. C. "AKT/PKB Signaling: Navigating Downstream". In: *Cell* vol. 129.7 (2007), pp. 1261–1274. DOI: 10.1016/j.cell.2007.06.009.

[102] Shende, P., Plaisance, I., Morandi, C., et al. "Cardiac Raptor Ablation Impairs Adaptive Hypertrophy, Alters Metabolic Gene Expression, and Causes Heart Failure in Mice". In: *Circulation* vol. 123.10 (2011), pp. 1073–1082. DOI: 10.1161/circulationaha.110.977066.

[103] Romanino, K., Mazelin, L., Albert, V., et al. "Myopathy caused by mammalian target of rapamycin complex 1 (mTORC1) inactivation is not reversed by restoring mitochondrial function". In: *Proceedings of the National Academy of Sciences* vol. 108.51 (2011), pp. 20808–20813. DOI: 10.1073/pnas.1111448109.

[104] Cunningham, J. T., Rodgers, J. T., Arlow, D. H., et al. "mTOR controls mitochondrial oxidative function through a YY1–PGC-1α transcriptional complex". In: *Nature* vol. 450.7170 (2007), pp. 736–740. DOI: 10.1038/nature06322.

[105] Laplante, M. and Sabatini, D. M. "Regulation of mTORC1 and its impact on gene expression at a glance". In: *Journal of Cell Science* (2013). DOI: 10.1242/jcs.125773.

[106] Sharples, A. P., Polydorou, I., Hughes, D. C., et al. "Skeletal muscle cells possess a 'memory' of acute early life TNF-α exposure: role of epigenetic adaptation". In: *Biogerontology* vol. 17.3 (2015), pp. 603–617. DOI: 10.1007/s10522-015-9604-x.

[107] Camera, D. M., Smiles, W. J., and Hawley, J. A. "Exercise-induced skeletal muscle signaling pathways and human athletic performance". In: *Free Radical Biology and Medicine* vol. 98 (2016), pp. 131–143. DOI: 10.1016/j.freeradbiomed.2016.02.007.

[108] Bouchard, C, Leon, A. S., Rao, D. C., et al. "The HERITAGE family study. Aims, design, and measurement protocol". In: *Medicine & Science in Sports & Exercise* vol. 27.5 (1995). PMID: 7674877, pp. 721–729.

[109] Borel, A.-L., Nazare, J.-A., Smith, J., et al. "Improvement in insulin sensitivity following a 1-year lifestyle intervention program in viscerally obese men: contribution of abdominal adiposity". In: *Metabolism* vol. 61.2 (2012), pp. 262–272. DOI: 10.1016/j.metabol.2011.06.024.

[110] Boulé, N. G., Weisnagel, S. J., Lakka, T. A., et al. "Effects of Exercise Training on Glucose Homeostasis". In: *Diabetes Care* vol. 28.1 (2005), pp. 108–114. DOI: 10.2337/diacare.28.1.108.

[111] Hagberg, J. M., Jenkins, N. T., and Spangenburg, E. "Exercise training, genetics and type 2 diabetes-related phenotypes". In: *Acta Physiologica* vol. 205.4 (2012), pp. 456–471. DOI: 10.1111/j.1748-1716.2012.02455.x.

[112] Kraus, W. E., Torgan, C. E., Duscha, B. D., et al. "Studies of a targeted risk reduction intervention through defined exercise (STRRIDE)". In: *Medicine & Science in Sports & Exercise* vol. 33.10 (2001), pp. 1774–1784. DOI: 10.1097/00005768-200110000-00025.

[113] Osler, M. E., Fritz, T., Caidahl, K., et al. "Changes in Gene Expression in Responders and Nonresponders to a Low-Intensity Walking Intervention". In: *Diabetes Care* vol. 38.6 (2015), pp. 1154–1160. DOI: 10.2337/dc14-2606.

[114] MORSS, G. M., JORDAN, A. N., SKINNER, J. S., et al. "Dose-Response to Exercise in Women Aged 45–75 yr (DREW): Design and Rationale". In: *Medicine & Science in Sports & Exercise* vol. 36.2 (2004), pp. 336–344. DOI: 10.1249/01.mss.0000113738.06267.e5.

[115] Church, T. S., Earnest, C. P., Skinner, J. S., et al. "Effects of Different Doses of Physical Activity on Cardiorespiratory Fitness Among Sedentary, Overweight or Obese Postmenopausal Women With Elevated Blood Pressure". In: *JAMA* vol. 297.19 (2007), p. 2081. DOI: 10.1001/jama.297.19.2081.

[116] Stephens, N. A., Xie, H., Johannsen, N. M., et al. "A transcriptional signature of "exercise resistance" in skeletal muscle of individuals with type 2 diabetes mellitus". In: *Metabolism* vol. 64.9 (2015), pp. 999–1004. DOI: 10.1016/j.metabol.2015.06.008.

[117] Thompson, A. M., Mikus, C. R., Rodarte, R. Q., et al. "Inflammation and exercise (INFLAME): Study rationale, design, and methods". In: *Contemporary Clinical Trials* vol. 29.3 (2008), pp. 418–427. DOI: 10.1016/j.cct.2007.09.009.

[118] Yates, T., Davies, M. J., Edwardson, C., et al. "Adverse Responses and Physical Activity". In: *Medicine & Science in Sports & Exercise* vol. 46.8 (2014), pp. 1617–1623. DOI: 10.1249/mss.0000000000000260.

[119] Stephens, N. A. and Sparks, L. M. "Resistance to the Beneficial Effects of Exercise in Type 2 Diabetes: Are Some Individuals Programmed to Fail?" In: *The Journal of Clinical Endocrinology & Metabolism* vol. 100.1 (2015), pp. 43–52. DOI: 10.1210/jc.2014-2545.

[120] Sparks, L. M., Johannsen, N. M., Church, T. S., et al. "Nine Months of Combined Training Improves Ex Vivo Skeletal Muscle Metabolism in Individuals With Type 2 Diabetes". In: *The Journal of Clinical Endocrinology & Metabolism* vol. 98.4 (2013), pp. 1694–1702. DOI: 10.1210/jc.2012-3874.

[121] Böhm, A., Weigert, C., Staiger, H., et al. "Exercise and diabetes: relevance and causes for response variability". In: *Endocrine* vol. 51.3 (2015), pp. 390–401. DOI: 10.1007/s12020-015-0792-6.

[122] Ross, R., Goodpaster, B. H., Koch, L. G., et al. "Precision exercise medicine: understanding exercise response variability". In: *British Journal of Sports Medicine* vol. 53.18 (2019), pp. 1141–1153. DOI: 10.1136/bjsports-2018-100328.

[123] Kahlmeier, S., Wijnhoven, T. M. A., Alpiger, P., et al. "National physical activity recommendations: systematic overview and analysis of the situation in European countries". In: *BMC Public Health* vol. 15.1 (2015). DOI: 10.1186/s12889-015-1412-3.

[124] World Health Organization. *WHO guidelines on physical activity and sedentary behaviour*. Genève, Switzerland: World Health Organization, 2020. ISBN: 978-92-4-001512-8.

[125] Savikj, M. and Zierath, J. R. "Train like an athlete: applying exercise interventions to manage type 2 diabetes". In: *Diabetologia* vol. 63.8 (2020), pp. 1491–1499. DOI: 10.1007/s00125-020-05166-9.

[126] Sigal, R. J., Kenny, G. P., Boulé, N. G., et al. "Effects of Aerobic Training, Resistance Training, or Both on Glycemic Control in Type 2 Diabetes". In: *Annals of Internal Medicine* vol. 147.6 (2007), p. 357. DOI: 10.7326/0003-4819-147-6-200709180-00005.

[127] Winding, K. M., Munch, G. W., Iepsen, U. W., et al. "The effect on glycaemic control of low-volume high-intensity interval training versus endurance training in individuals with type 2 diabetes". In: *Diabetes, Obesity and Metabolism* vol. 20.5 (2018), pp. 1131–1139. DOI: 10.1111/dom.13198.

[128] Brook, M. S., Wilkinson, D. J., Mitchell, W. K., et al. "Synchronous deficits in cumulative muscle protein synthesis and ribosomal biogenesis underlie age-related anabolic resistance to exercise in humans". In: *The Journal of Physiology* vol. 594.24 (2016), pp. 7399–7417. DOI: 10.1113/jp272857.

[129] Welle, S., Totterman, S., and Thornton, C. "Effect of Age on Muscle Hypertrophy Induced by Resistance Training". In: *The Journals of Gerontology Series A: Biological Sciences and Medical Sciences* vol. 51A.6 (1996), pp. 270–275. DOI: 10.1093/gerona/51a.6.m270.

[130] Kosek, D. J., Kim, J. su, Petrella, J. K., et al. "Efficacy of 3 days/wk resistance training on myofiber hypertrophy and myogenic mechanisms in young vs. older adults". In: *Journal of Applied Physiology* vol. 101.2 (2006), pp. 531–544. DOI: 10.1152/japplphysiol.01474.2005.

[131] Wahren, J., Felig, P., Ahlborg, G., et al. "Glucose metabolism during leg exercise in man". In: *Journal of Clinical Investigation* vol. 50.12 (1971), pp. 2715–2725. DOI: 10.1172/jci106772.

[132] Robinson, M. M., Dasari, S., Konopka, A. R., et al. "Enhanced Protein Translation Underlies Improved Metabolic and Physical Adaptations to Different Exercise Training Modes in Young and Old Humans". In: *Cell Metabolism* vol. 25.3 (2017), pp. 581–592. DOI: 10.1016/j.cmet.2017.02.009.

[133] Broskey, N. T., Boss, A., Fares, E.-J., et al. "Exercise efficiency relates with mitochondrial content and function in older adults". In: *Physiological Reports* vol. 3.6 (2015), p. 12418. DOI: 10.14814/phy2.12418.

[134] Peters, S. J., Samjoo, I. A., Devries, M. C., et al. "Perilipin family (PLIN) proteins in human skeletal muscle: the effect of sex, obesity, and endurance training". In: *Applied Physiology, Nutrition, and Metabolism* vol. 37.4 (2012), pp. 724–735. DOI: 10.1139/h2012-059.

[135] Skelly, L. E., Gillen, J. B., MacInnis, M. J., et al. "Effect of sex on the acute skeletal muscle response to sprint interval exercise". In: *Experimental Physiology* vol. 102.3 (2017), pp. 354–365. DOI: 10.1113/ep086118.

[136] Churchward-Venne, T. A., Tieland, M., Verdijk, L. B., et al. "There Are No Nonresponders to Resistance-Type Exercise Training in Older Men and Women". In: *Journal of the American Medical Directors Association* vol. 16.5 (2015), pp. 400–411. DOI: 10.1016/j.jamda.2015.01.071.

[137] Pesta, D., Jelenik, T., Zaharia, O.-P., et al. "NDUFB6 Polymorphism Is Associated With Physical Activity-Mediated Metabolic Changes in Type 2 Diabetes". In: *Frontiers in Endocrinology* vol. 12 (2021). DOI: 10.3389/fendo.2021.693683.

[138] Stephens, N. A., Brouwers, B., Eroshkin, A. M., et al. "Exercise Response Variations in Skeletal Muscle PCr Recovery Rate and Insulin Sensitivity Relate to Muscle Epigenomic Profiles in Individuals With Type 2 Diabetes". In: *Diabetes Care* vol. 41.10 (2018), pp. 2245–2254. DOI: 10.2337/dc18-0296.

[139] Liu, Y., Wang, Y., Ni, Y., et al. "Gut Microbiome Fermentation Determines the Efficacy of Exercise for Diabetes Prevention". In: *Cell Metabolism* vol. 31.1 (2020), 77–91.e5. DOI: 10.1016/j.cmet.2019.11.001.

[140] Solomon, T. P., Malin, S. K., Karstoft, K., et al. "Association Between Cardiorespiratory Fitness and the Determinants of Glycemic Control Across the Entire Glucose Tolerance Continuum". In: *Diabetes Care* vol. 38.5 (2015), pp. 921–929. DOI: 10.2337/dc14-2813.

[141] Rosenthal, M., Haskell, W. L., Solomon, R., et al. "Demonstration of a Relationship Between Level of Physical Training and Insulin-stimulated Glucose Utilization in Normal Humans". In: *Diabetes* vol. 32.5 (1983), pp. 408–411. DOI: 10.2337/diab.32.5.408.

[142] Totsikas, C., Röhm, J., Kantartzis, K., et al. "Cardiorespiratory fitness determines the reduction in blood pressure and insulin resistance during lifestyle intervention". In: *Journal of Hypertension* vol. 29.6 (2011), pp. 1220–1227. DOI: 10.1097/hjh.0b013e3283469910.

[143] Balducci, S., Zanuso, S., Cardelli, P., et al. "Changes in Physical Fitness Predict Improvements in Modifiable Cardiovascular Risk Factors Independently of Body Weight Loss in Subjects With Type 2 Diabetes Participating in the Italian Diabetes and Exercise Study (IDES)". In: *Diabetes Care* vol. 35.6 (2012), pp. 1347–1354. DOI: 10.2337/dc11-1859.

[144] Böhm, A., Hoffmann, C., Irmler, M., et al. "TGF-β Contributes to Impaired Exercise Response by Suppression of Mitochondrial Key Regulators in Skeletal Muscle". In: *Diabetes* vol. 65.10 (2016), pp. 2849–2861. DOI: 10.2337/db15-1723.

[145] Hoffmann, C., Schneeweiss, P., Randrianarisoa, E., et al. "Response of Mitochondrial Respiration in Adipose Tissue and Muscle to 8 Weeks of Endurance Exercise in Obese Subjects". In: *The Journal of Clinical Endocrinology & Metabolism* vol. 105.11 (2020), pp. 4023–4037. DOI: 10.1210/clinem/dgaa571.

[146] Dreher, S. I., Höckele, S., Huypens, P., et al. "TGF-β Induction of miR-143/145 Is Associated to Exercise Response by Influencing Differentiation and Insulin Signaling Molecules in Human Skeletal Muscle". In: *Cells* vol. 10.12 (2021), p. 3443. DOI: 10.3390/cells10123443.

[147] Seoane, J. "Escaping from the TGF anti-proliferative control". In: *Carcinogenesis* vol. 27.11 (2006), pp. 2148–2156. DOI: 10.1093/carcin/bgl068.

[148] Jang, C.-W., Chen, C.-H., Chen, C.-C., et al. "TGF-β induces apoptosis through Smad-mediated expression of DAP-kinase". In: *Nature Cell Biology* vol. 4.1 (2001), pp. 51–58. DOI: 10.1038/ncb731.

[149] Schuster, N. and Krieglstein, K. "Mechanisms of TGF-β-mediated apoptosis". In: *Cell and Tissue Research* vol. 307.1 (2002), pp. 1–14. DOI: 10.1007/s00441-001-0479-6.

[150] Shull, M. M., Ormsby, I., Kier, A. B., et al. "Targeted disruption of the mouse transforming growth factor-β1 gene results in multifocal inflammatory disease". In: *Nature* vol. 359.6397 (1992), pp. 693–699. DOI: 10.1038/359693a0.

[151] Tatler, A. L. and Jenkins, G. "TGF-β Activation and Lung Fibrosis". In: *Proceedings of the American Thoracic Society* vol. 9.3 (2012), pp. 130–136. DOI: 10.1513/pats.201201-003aw.

[152] Leask, A. and Abraham, D. J. "TGF-β signaling and the fibrotic response". In: *The FASEB Journal* vol. 18.7 (2004), pp. 816–827. DOI: 10.1096/fj.03-1273rev.

[153] Aschner, Y. and Downey, G. P. "Transforming Growth Factor-β: Master Regulator of the Respiratory System in Health and Disease". In: *American Journal of Respiratory Cell and Molecular Biology* vol. 54.5 (2016), pp. 647–655. DOI: 10.1165/rcmb.2015-0391tr.

[154] Matsuda, M. and DeFronzo, R. A. "Insulin sensitivity indices obtained from oral glucose tolerance testing: comparison with the euglycemic insulin clamp." In: *Diabetes Care* vol. 22.9 (1999), pp. 1462–1470. DOI: 10.2337/diacare.22.9.1462.

[155] Kulak, N. A., Pichler, G., Paron, I., et al. "Minimal, encapsulated proteomic-sample processing applied to copy-number estimation in eukaryotic cells". In: *Nature Methods* vol. 11.3 (2014), pp. 319–324. DOI: 10.1038/nmeth.2834.

[156] Xiao, F.-H., Wang, H.-T., and Kong, Q.-P. "Dynamic DNA Methylation During Aging: A "Prophet" of Age-Related Outcomes". In: *Frontiers in Genetics* vol. 10 (2019). DOI: 10.3389/fgene.2019.00107.

[157] Boulakirba, S., Pfeifer, A., Mhaidly, R., et al. "IL-34 and CSF-1 display an equivalent macrophage differentiation ability but a different polarization potential". In: *Scientific Reports* vol. 8.1 (2018). DOI: 10.1038/s41598-017-18433-4.

[158] Wei, S., Nandi, S., Chitu, V., et al. "Functional overlap but differential expression of CSF-1 and IL-34 in their CSF-1 receptor-mediated regulation of myeloid cells". In: *Journal of Leukocyte Biology* vol. 88.3 (2010), pp. 495–505. DOI: 10.1189/jlb.1209822.

[159] Jacquel, A., Benikhlef, N., Paggetti, J., et al. "Colony-stimulating factor-1–induced oscillations in phosphatidylinositol-3 kinase/AKT are required for caspase activation in monocytes undergoing differentiation into macrophages". In: *Blood* vol. 114.17 (2009), pp. 3633–3641. DOI: 10.1182/blood-2009-03-208843.

[160] Deyashiki, Y., Ohshima, K., Nakanishi, M., et al. "Molecular Cloning and Characterization of Mouse Estradiol 17β-Dehydrogenase (A-Specific), a Member of the Aldoketoreductase Family". In: *Journal of Biological Chemistry* vol. 270.18 (1995), pp. 10461–10467. DOI: 10.1074/jbc.270.18.10461.

[161] Barski, O. A., Tipparaju, S. M., and Bhatnagar, A. "The Aldo-Keto Reductase Superfamily and its Role in Drug Metabolism and Detoxification". In: *Drug Metabolism Reviews* vol. 40.4 (2008), pp. 553–624. DOI: 10.1080/03602530802431439.

[162] Suzuki-Yamamoto, T., Nishizawa, M., Fukui, M., et al. "cDNA cloning, expression and characterization of human prostaglandin F synthase". In: *FEBS Letters* vol. 462.3 (1999), pp. 335–340. DOI: 10.1016/s0014-5793(99)01551-3.

[163] Goj, T., Hoene, M., Fritsche, L., et al. "The Acute Cytokine Response to 30-Minute Exercise Bouts Before and After 8-Week Endurance Training in Individuals With Obesity". In: *The Journal of Clinical Endocrinology & Metabolism* vol. 108.4 (2022), pp. 865–875. DOI: 10.1210/clinem/dgac623.

[164] Northoff, H. and Berg, A. "Immunologic Mediators as Parameters of the Reaction to Strenuous Exercise". In: *International Journal of Sports Medicine* vol. 12.1 (1991), pp. 9–15. DOI: 10.1055/s-2007-1024743.

[165] Ostrowski, K., Rohde, T., Asp, S., et al. "Pro- and anti-inflammatory cytokine balance in strenuous exercise in humans". In: *The Journal of Physiology* vol. 515.1 (1999), pp. 287–291. DOI: 10.1111/j.1469-7793.1999.287ad.x.

[166] Pedersen, B. K. and Hoffman-Goetz, L. "Exercise and the Immune System: Regulation, Integration, and Adaptation". In: *Physiological Reviews* vol. 80.3 (2000), pp. 1055–1081. DOI: 10.1152/physrev.2000.80.3.1055.

[167] Nieman, D. C., Henson, D. A., Aaustin, M. D., et al. "Immune Response to a 30-Minute Walk". In: *Medicine & Science in Sports & Exercise* vol. 37.1 (2005), pp. 57–62. DOI: 10.1249/01.mss.0000149808.38194.21.

[168] Seaborne, R. A. and Sharples, A. P. "The Interplay Between Exercise Metabolism, Epigenetics, and Skeletal Muscle Remodeling". In: *Exercise and Sport Sciences Reviews* vol. 48.4 (2020), pp. 188–200. DOI: 10.1249/jes.0000000000000227.

[169] Pillon, N. J., Gabriel, B. M., Dollet, L., et al. "Transcriptomic profiling of skeletal muscle adaptations to exercise and inactivity". In: *Nature Communications* vol. 11.1 (2020). DOI: 10.1038/s41467-019-13869-w.

[170] Silveira, L. S., Moura Mello Antunes, B. de, Minari, A. L. A., et al. "Macrophage Polarization: Implications on Metabolic Diseases and the Role of Exercise". In: *Critical Reviews in Eukaryotic Gene Expression* vol. 26.2 (2016), pp. 115–132. DOI: 10.1615/critreveukaryotgeneexpr.2016015920.

[171] Grounds, M. D., Sorokin, L., and White, J. "Strength at the extracellular matrix-muscle interface". In: *Scandinavian Journal of Medicine & Science in Sports* vol. 15.6 (2005), pp. 381–391. DOI: 10.1111/j.1600-0838.2005.00467.x.

[172] Mavropalias, G., Boppart, M., Usher, K. M., et al. "Exercise builds the scaffold of life: muscle extracellular matrix biomarker responses to physical activity, inactivity, and aging". In: *Biological Reviews* vol. 98.2 (2022), pp. 481–519. DOI: 10.1111/brv.12916.

[173] Williams, A. S., Kang, L., and Wasserman, D. H. "The extracellular matrix and insulin resistance". In: *Trends in Endocrinology & Metabolism* vol. 26.7 (2015), pp. 357–366. DOI: 10.1016/j.tem.2015.05.006.

[174] Fitch-Tewfik, J. L. and Flaumenhaft, R. "Platelet Granule Exocytosis: A Comparison with Chromaffin Cells". In: *Frontiers in Endocrinology* vol. 4 (2013). DOI: 10.3389/fendo.2013.00077.

[175] Bubnov, R. "Ultrasound guided injections of Platelets Rich Plasma for muscle injury in professional athletes. Comparative study". In: *Medical Ultrasonography* vol. 15.2 (2013), pp. 101–105. DOI: 10.11152/mu.2013.2066.152.rb1vy2.

[176] Nguyen, R. T., Borg-Stein, J., and McInnis, K. "Applications of Platelet-Rich Plasma in Musculoskeletal and Sports Medicine: An Evidence-Based Approach". In: *PM&R* vol. 3.3 (2011), pp. 226–250. DOI: 10.1016/j.pmrj.2010.11.007.

[177] Brossi, P. M., Moreira, J. J., Machado, T. S., et al. "Platelet-rich plasma in orthopedic therapy: a comparative systematic review of clinical and experimental data in equine and human musculoskeletal lesions". In: *BMC Veterinary Research* vol. 11.1 (2015). DOI: 10.1186/s12917-015-0403-z.

[178] Lee, K. S., Wilson, J. J., Rabago, D. P., et al. "Musculoskeletal Applications of Platelet-Rich Plasma: Fad or Future?" In: *American Journal of Roentgenology* vol. 196.3 (2011), pp. 628–636. DOI: 10.2214/ajr.10.5975.

[179] Scully, D., Naseem, K. M., and Matsakas, A. "Platelet biology in regenerative medicine of skeletal muscle". In: *Acta Physiologica* vol. 223.3 (2018), p. 13071. DOI: 10.1111/apha.13071.

[180] Kettern, N., Dreiseidler, M., Tawo, R., et al. "Chaperone-assisted degradation: multiple paths to destruction". In: *Biological Chemistry* vol. 391.5 (2010), pp. 481–489. DOI: 10.1515/bc.2010.058.

[181] Henstridge, D. C., Bruce, C. R., Drew, B. G., et al. "Activating HSP72 in Rodent Skeletal Muscle Increases Mitochondrial Number and Oxidative Capacity and Decreases Insulin Resistance". In: *Diabetes* vol. 63.6 (2014), pp. 1881–1894. DOI: 10.2337/db13-0967.

[182] Chung, J., Nguyen, A.-K., Henstridge, D. C., et al. "HSP72 protects against obesity-induced insulin resistance". In: *Proceedings of the National Academy of Sciences* vol. 105.5 (2008), pp. 1739–1744. DOI: 10.1073/pnas.0705799105.

[183] Martyn, J. A. J., Fagerlund, M. J., and Eriksson, L. I. "Basic principles of neuromuscular transmission". In: *Anaesthesia* vol. 64 (2009), pp. 1–9. DOI: 10.1111/j.1365-2044.2008.05865.x.

[184] Liao, Z., Xiao, M., Chen, J., et al. "CHRNA1 induces sarcopenia through neuromuscular synaptic elimination". In: *Experimental Gerontology* vol. 166 (2022), p. 111891. DOI: 10.1016/j.exger.2022.111891.

[185] Davegårdh, C., Broholm, C., Perfilyev, A., et al. "Abnormal epigenetic changes during differentiation of human skeletal muscle stem cells from obese subjects". In: *BMC Medicine* vol. 15.1 (2017). DOI: 10.1186/s12916-017-0792-x.

[186] Jensen, J. H., Conley, L. N., Hedegaard, J., et al. "Gene expression profiling of porcine skeletal muscle in the early recovery phase following acute physical activity". In: *Experimental Physiology* vol. 97.7 (2012), pp. 833–848. DOI: 10.1113/expphysiol.2011.063727.

[187] Deák, F., Piecha, D., Bachrati, C., et al. "Primary Structure and Expression of Matrilin-2, the Closest Relative of Cartilage Matrix Protein within the von Willebrand Factor Type A-like Module Superfamily". In: *Journal of Biological Chemistry* vol. 272.14 (1997), pp. 9268–9274. DOI: 10.1074/jbc.272.14.9268.

[188] Colombatti, A and Bonaldo, P. "The superfamily of proteins with von Willebrand factor type A-like domains: one theme common to components of extracellular matrix, hemostasis, cellular adhesion, and defense mechanisms". In: *Blood* vol. 77.11 (1991), pp. 2305–2315. DOI: 10.1182/blood.v77.11.2305.2305.

[189] Csapo, R., Gumpenberger, M., and Wessner, B. "Skeletal Muscle Extracellular Matrix – What Do We Know About Its Composition, Regulation, and Physiological Roles? A Narrative Review". In: *Frontiers in Physiology* vol. 11 (2020). DOI: 10.3389/fphys.2020.00253.

[190] Bell, G. I., Kayano, T., Buse, J. B., et al. "Molecular Biology of Mammalian Glucose Transporters". In: *Diabetes Care* vol. 13.3 (1990), pp. 198–208. DOI: 10.2337/diacare.13.3.198.

[191] Stuart, C. A., Wen, G., Gustafson, W., et al. "Comparison of GLUT1, GLUT3, and GLUT4 mRNA and the subcellular distribution of their proteins in normal human muscle". In: *Metabolism* vol. 49.12 (2000), pp. 1604–1609. DOI: 10.1053/meta.2000.18559.

[192] Wang, T., Wang, J., Hu, X., et al. "Current understanding of glucose transporter 4 expression and functional mechanisms". In: *World Journal of Biological Chemistry* vol. 11.3 (2020), pp. 76–98. DOI: 10.4331/wjbc.v11.i3.76.

[193] Inoshita, M., Numata, S., Tajima, A., et al. "Sex differences of leukocytes DNA methylation adjusted for estimated cellular proportions". In: *Biology of Sex Differences* vol. 6.1 (2015). DOI: 10.1186/s13293-015-0029-7.

[194] Mandell, K. A. P., Price, A. J., Wilton, R., et al. "Characterizing the dynamic and functional DNA methylation landscape in the developing human cortex". In: *Epigenetics* vol. 16.1 (2020), pp. 1–13. DOI: 10.1080/15592294.2020.1786304.

[195] Singmann, P., Shem-Tov, D., Wahl, S., et al. "Characterization of whole-genome autosomal differences of DNA methylation between men and women". In: *Epigenetics & Chromatin* vol. 8.1 (2015). DOI: 10.1186/s13072-015-0035-3.

[196] Seaborne, R. A., Strauss, J., Cocks, M., et al. "Human Skeletal Muscle Possesses an Epigenetic Memory of Hypertrophy". In: *Scientific Reports* vol. 8.1 (2018). DOI: 10.1038/s41598-018-20287-3.

[197] Turner, D. C., Seaborne, R. A., and Sharples, A. P. "Comparative Transcriptome and Methylome Analysis in Human Skeletal Muscle Anabolism, Hypertrophy and Epigenetic Memory". In: *Scientific Reports* vol. 9.1 (2019). DOI: 10.1038/s41598-019-40787-0.

[198] Maasar, M.-F., Turner, D. C., Gorski, P. P., et al. "The Comparative Methylome and Transcriptome After Change of Direction Compared to Straight Line Running Exercise in Human Skeletal Muscle". In: *Frontiers in Physiology* vol. 12 (2021). DOI: 10.3389/fphys.2021.619447.

[199] Bondarenko, V. A., Liu, Y. V., Jiang, Y. I., et al. "Communication over a large distance: enhancers and insulators". In: *Biochemistry and Cell Biology* vol. 81.3 (2003), pp. 241–251. DOI: 10.1139/o03-051.

[200] Guarente, L. "UASs and enhancers: Common mechanism of transcriptional activation in yeast and mammals". In: *Cell* vol. 52.3 (1988), pp. 303–305. DOI: 10.1016/s0092-8674(88)80020-5.

[201] Kiselev, I. S., Kulakova, O. G., Boyko, A. N., et al. "DNA Methylation As an Epigenetic Mechanism in the Development of Multiple Sclerosis". In: *Acta Naturae* vol. 13.2 (2021), pp. 45–57. DOI: 10.32607/actanaturae.11043.

[202] Choy, M.-K., Movassagh, M., Goh, H.-G., et al. "Genome-wide conserved consensus transcription factor binding motifs are hyper-methylated". In: *BMC Genomics* vol. 11.1 (2010). DOI: 10.1186/1471-2164-11-519.

[203] Suzuki, M. M. and Bird, A. "DNA methylation landscapes: provocative insights from epigenomics". In: *Nature Reviews Genetics* vol. 9.6 (2008), pp. 465–476. DOI: 10.1038/nrg2341.

[204] Ball, M. P., Li, J. B., Gao, Y., et al. "Targeted and genome-scale strategies reveal gene-body methylation signatures in human cells". In: *Nature Biotechnology* vol. 27.4 (2009), pp. 361–368. DOI: 10.1038/nbt.1533.

[205] Zhong, Z., Feng, S., Duttke, S. H., et al. "DNA methylation-linked chromatin accessibility affects genomic architecture in *Arabidopsis*". In: *Proceedings of the National Academy of Sciences* vol. 118.5 (2021). DOI: 10.1073/pnas.2023347118.

[206] Samaranayake, M., Estève, P.-O., Chin, H. G., et al. "Transcription Coupled DNA Methylation Mediated by RNA Pol II and DNMT1". In: *Epigenetic Diagnosis & Therapy* vol. 1.2 (2016), pp. 132–140. DOI: 10.2174/2214083201666140912003819.

[207] Tiainen, P., Pasanen, A., Sormunen, R., et al. "Characterization of Recombinant Human Prolyl 3-Hydroxylase Isoenzyme 2, an Enzyme Modifying the Basement Membrane Collagen IV". In: *Journal of Biological Chemistry* vol. 283.28 (2008), pp. 19432–19439. DOI: 10.1074/jbc.m802973200.

[208] Greer, J. M. and Lees, M. B. "Myelin proteolipid protein—the first 50 years". In: *The International Journal of Biochemistry & Cell Biology* vol. 34.3 (2002), pp. 211–215. DOI: 10.1016/s1357-2725(01)00136-4.

[209] Pham-Dinh, D., Birling, M.-C., Roussel, G., et al. "Proteolipid DM-20 predominates over PLP in peripheral nervous system". In: *NeuroReport* vol. 2.2 (1991), pp. 89–92. DOI: 10.1097/00001756-199102000-00006.

[210] Nemec, P. S., Kapatos, A., Holmes, J. C., et al. "Cancer-testis antigens in canine histiocytic sarcoma and other malignancies". In: *Veterinary and Comparative Oncology* vol. 17.3 (2019), pp. 317–328. DOI: 10.1111/vco.12475.

[211] DeKoter, R. P., Kamath, M. B., and Houston, I. B. "Analysis of concentration-dependent functions of PU.1 in hematopoiesis using mouse models". In: *Blood Cells, Molecules, and Diseases* vol. 39.3 (2007), pp. 316–320. DOI: 10.1016/j.bcmd.2007.06.004.

[212] Pham, T.-H., Minderjahn, J., Schmidl, C., et al. "Mechanisms of in vivo binding site selection of the hematopoietic master transcription factor PU.1". In: *Nucleic Acids Research* vol. 41.13 (2013), pp. 6391–6402. DOI: 10.1093/nar/gkt355.

[213] Wang, Y., Welc, S. S., Wehling-Henricks, M., et al. "Myeloid cell-specific mutation of Spi1 selectively reduces M2-biased macrophage numbers in skeletal muscle, reduces age-related muscle fibrosis and prevents sarcopenia". In: *Aging Cell* vol. 21.10 (2022). DOI: 10.1111/acel.13690.

[214] Kwon, B. S., Tan, K. B., Ni, J., et al. "A Newly Identified Member of the Tumor Necrosis Factor Receptor Superfamily with a Wide Tissue Distribution and Involvement in Lymphocyte Activation". In: *Journal of Biological Chemistry* vol. 272.22 (1997), pp. 14272–14276. DOI: 10.1074/jbc.272.22.14272.

[215] Waldemer-Streyer, R. J. and Chen, J. "Myocyte-derived Tnfsf14 is a survival factor necessary for myoblast differentiation and skeletal muscle regeneration". In: *Cell Death & Disease* vol. 6.12 (2015), pp. 2026–2026. DOI: 10.1038/cddis.2015.375.

[216] Lin, H., Lee, E., Hestir, K., et al. "Discovery of a Cytokine and Its Receptor by Functional Screening of the Extracellular Proteome". In: *Science* vol. 320.5877 (2008), pp. 807–811. DOI: 10.1126/science.1154370.

[217] Dai, X.-M., Ryan, G. R., Hapel, A. J., et al. "Targeted disruption of the mouse colony-stimulating factor 1 receptor gene results in osteopetrosis, mononuclear phagocyte deficiency, increased primitive progenitor cell frequencies, and reproductive defects". In: *Blood* vol. 99.1 (2002), pp. 111–120. DOI: 10.1182/blood.v99.1.111.

[218] Segaliny, A. I., Brion, R., Mortier, E., et al. "Syndecan-1 regulates the biological activities of interleukin-34". In: *Biochimica et Biophysica Acta (BBA) - Molecular Cell Research* vol. 1853.5 (2015), pp. 1010–1021. DOI: 10.1016/j.bbamcr.2015.01.023.

[219] Chang, E.-J., Lee, S. K., Song, Y. S., et al. "IL-34 Is Associated with Obesity, Chronic Inflammation, and Insulin Resistance". In: *The Journal of Clinical Endocrinology & Metabolism* vol. 99.7 (2014), pp. 1263–1271. DOI: 10.1210/jc.2013-4409.

[220] Mostafa, T. M., El-Gharbawy, N. M., and Werida, R. H. "Circulating IRAPe, Irisin, and IL-34 in Relation to Insulin Resistance in Patients With Type 2 Diabetes". In: *Clinical Therapeutics* vol. 43.7 (2021), pp. 230–240. DOI: 10.1016/j.clinthera.2021.05.003.

[221] Piao, C., Wang, X., Peng, S., et al. "IL-34 causes inflammation and beta cell apoptosis and dysfunction in gestational diabetes mellitus". In: *Endocrine Connections* vol. 8.11 (2019), pp. 1503–1512. DOI: 10.1530/EC-19-0436.

[222] Zorena, K., Jachimowicz-Duda, O., and Waz, P. "The cut-off value for interleukin 34 as an additional potential inflammatory biomarker for the prediction of the risk of diabetic complications". In: *Biomarkers* vol. 21.3 (2016), pp. 276–282. DOI: 10.3109/1354750X.2016.1138321.

[223] Su, Y., Cao, Y., Liu, C., et al. "Inactivating IL34 promotes regenerating muscle stem cell expansion and attenuates Duchenne muscular dystrophy in mouse models". In: *Theranostics* vol. 13.8 (2023), pp. 2588–2604. DOI: 10.7150/thno.83817.

[224] Pillon, N. J., Bilan, P. J., Fink, L. N., et al. "Cross-talk between skeletal muscle and immune cells: muscle-derived mediators and metabolic implications". In: *American Journal of Physiology-Endocrinology and Metabolism* vol. 304.5 (2013), pp. 453–465. DOI: 10.1152/ajpendo.00553.2012.

[225] Lin, W., Xu, D., Austin, C. D., et al. "Function of CSF1 and IL34 in Macrophage Homeostasis, Inflammation, and Cancer". In: *Frontiers in Immunology* vol. 10 (2019). DOI: 10.3389/fimmu.2019.02019.

[226] Muñoz-Garcia, J., Cochonneau, D., Télétchéa, S., et al. "The twin cytokines interleukin-34 and CSF-1: masterful conductors of macrophage homeostasis". In: *Theranostics* vol. 11.4 (2021), pp. 1568–1593. DOI: 10.7150/thno.50683.

[227] Li, H., Meng, Y., He, S., et al. "Macrophages, Chronic Inflammation, and Insulin Resistance". In: *Cells* vol. 11.19 (2022), p. 3001. DOI: 10.3390/cells11193001.

[228] Bachur, N. R. "Cytoplasmic Aldo-Keto Reductases: A Class of Drug Metabolizing Enzymes". In: *Science* vol. 193.4253 (1976), pp. 595–597. DOI: 10.1126/science.959821.

[229] Penning, T. M., Burczynski, M. E., Joseph M., J. E. Z., et al. "Human 3α-hydroxysteroid dehydrogenase isoforms (AKR1C1–AKR1C4) of the aldo-keto reductase superfamily: functional plasticity and tissue distribution reveals roles in the inactivation and formation of male and female sex hormones". In: *Biochemical Journal* vol. 351.1 (2000), pp. 67–77. DOI: 10.1042/bj3510067.

[230] Paulukinas, R. D., Mesaros, C. A., and Penning, T. M. "Conversion of Classical and 11-Oxygenated Androgens by Insulin-Induced AKR1C3 in a Model of Human PCOS Adipocytes". In: *Endocrinology* vol. 163.7 (2022). DOI: 10.1210/endocr/bqac068.

[231] Paulukinas, R. D. and Penning, T. M. "Insulin-Induced AKR1C3 Induces Fatty Acid Synthase in a Model of Human PCOS Adipocytes". In: *Endocrinology* vol. 164.5 (2023). DOI: 10.1210/endocr/bqad033.

[232] Navarro, G., Allard, C., Xu, W., et al. "The role of androgens in metabolism, obesity, and diabetes in males and females". In: *Obesity* vol. 23.4 (2015), pp. 713–719. DOI: 10.1002/oby.21033.

[233] Sgrò, P., Minganti, C., Lista, M., et al. "Dihydrotestosterone (DHT) rapidly increase after maximal aerobic exercise in healthy males: the lowering effect of phosphodiesterase's type 5 inhibitors on DHT response to exercise-related stress". In: *Journal of Endocrinological Investigation* vol. 44.6 (2020), pp. 1219–1228. DOI: 10.1007/s40618-020-01409-z.

[234] Herbst, K. L. and Bhasin, S. "Testosterone action on skeletal muscle". In: *Current Opinion in Clinical Nutrition and Metabolic Care* vol. 7.3 (2004), pp. 271–277. DOI: 10.1097/00075197-200405000-00006.

[235] Griggs, R. C., Kingston, W., Jozefowicz, R. F., et al. "Effect of testosterone on muscle mass and muscle protein synthesis". In: *Journal of Applied Physiology* vol. 66.1 (1989), pp. 498–503. DOI: 10.1152/jappl.1989.66.1.498.

[236] Jardí, F., Laurent, M. R., Dubois, V., et al. "Androgen and estrogen actions on male physical activity: a story beyond muscle". In: *Journal of Endocrinology* vol. 238.1 (2018), pp. 31–52. DOI: 10.1530/joe-18-0125.

[237] Swerdloff, R. S., Dudley, R. E., Page, S. T., et al. "Dihydrotestosterone: Biochemistry, Physiology, and Clinical Implications of Elevated Blood Levels". In: *Endocrine Reviews* vol. 38.3 (2017), pp. 220–254. DOI: 10.1210/er.2016-1067.

[238] Perry, C. G. R., Lally, J., Holloway, G. P., et al. "Repeated transient mRNA bursts precede increases in transcriptional and mitochondrial proteins during training in human skeletal muscle". In: *The Journal of Physiology* vol. 588.23 (2010), pp. 4795–4810. DOI: 10.1113/jphysiol.2010.199448.

[239] Egan, B., O'Connor, P. L., Zierath, J. R., et al. "Time Course Analysis Reveals Gene-Specific Transcript and Protein Kinetics of Adaptation to Short-Term Aerobic Exercise Training in Human Skeletal Muscle". In: *PLOS ONE* vol. 8.9 (2013), p. 74098. DOI: 10.1371/journal.pone.0074098.

[240] Hammarström, D., Øfsteng, S. J., Jacobsen, N. B., et al. "Ribosome accumulation during early phase resistance training in humans". In: *Acta Physiologica* vol. 235.1 (2022). DOI: 10.1111/apha.13806.

[241] Martin, W. H., Coyle, E. F., Bloomfield, S. A., et al. "Effects of physical deconditioning after Intense endurance training on left ventricular dimensions and stroke volume". In: *Journal of the American College of Cardiology* vol. 7.5 (1986), pp. 982–989. DOI: 10.1016/s0735-1097(86)80215-7.

[242] Coyle, E. F., Martin, W. H., Sinacore, D. R., et al. "Time course of loss of adaptations after stopping prolonged intense endurance training". In: *Journal of Applied Physiology* vol. 57.6 (1984), pp. 1857–1864. DOI: 10.1152/jappl.1984.57.6.1857.

[243] Moore, R. L., Thacker, E. M., Kelley, G. A., et al. "Effect of training/detraining on submaximal exercise responses in humans". In: *Journal of Applied Physiology* vol. 63.5 (1987), pp. 1719–1724. DOI: 10.1152/jappl.1987.63.5.1719.

[244] Vukovich, M. D., Arciero, P. J., Kohrt, W. M., et al. "Changes in insulin action and GLUT-4 with 6 days of inactivity in endurance runners". In: *Journal of Applied Physiology* vol. 80.1 (1996), pp. 240–244. DOI: 10.1152/jappl.1996.80.1.240.

[245] Lundby, C. and Jacobs, R. A. "Adaptations of skeletal muscle mitochondria to exercise training". In: *Experimental Physiology* vol. 101.1 (2015), pp. 17–22. DOI: 10.1113/ep085319.

[246] Gan, Z., Fu, T., Kelly, D. P., et al. "Skeletal muscle mitochondrial remodeling in exercise and diseases". In: *Cell Research* vol. 28.10 (2018), pp. 969–980. DOI: 10.1038/s41422-018-0078-7.

[247] Cartee, G. D., Hepple, R. T., Bamman, M. M., et al. "Exercise Promotes Healthy Aging of Skeletal Muscle". In: *Cell Metabolism* vol. 23.6 (2016), pp. 1034–1047. DOI: 10.1016/j.cmet.2016.05.007.

[248] Zhang, S., Reljić, B., Liang, C., et al. "Mitochondrial peptide BRAWNIN is essential for vertebrate respiratory complex III assembly". In: *Nature Communications* vol. 11.1 (2020). DOI: 10.1038/s41467-020-14999-2.

[249] Dennerlein, S., Poerschke, S., Oeljeklaus, S., et al. "Defining the interactome of the human mitochondrial ribosome identifies SMIM4 and TMEM223 as respiratory chain assembly factors". In: *eLife* vol. 10 (2021). DOI: 10.7554/elife.68213.

[250] Liang, C., Zhang, S., Robinson, D., et al. "Mitochondrial microproteins link metabolic cues to respiratory chain biogenesis". In: *Cell Reports* vol. 40.7 (2022), p. 111204. DOI: 10.1016/j.celrep.2022.111204.

[251] Utsumi, S., Sakamoto, K., Yamashita, T., et al. "Presence of ES1 homolog in the mitochondrial intermembrane space of porcine retinal cells". In: *Biochemical and Biophysical Research Communications* vol. 524.3 (2020), pp. 542–548. DOI: 10.1016/j.bbrc.2020.01.127.

[252] Monné, M., Miniero, D. V., Bisaccia, F., et al. "The mitochondrial oxoglutarate carrier: from identification to mechanism". In: *Journal of Bioenergetics and Biomembranes* vol. 45.1-2 (2012), pp. 1–13. DOI: 10.1007/s10863-012-9475-7.

[253] Weißhaar, N. "The malate aspartate shuttle in T cell metabolic fitness: Glutamic oxaloacetic transaminase 1 antagonizes T cell exhaustion". In: *Heidelberger Dokumentenserver* (2020). DOI: 10.11588/HEIDOK.00028814.

[254] McCommis, K. S. and Finck, B. N. "The Hepatic Mitochondrial Pyruvate Carrier as a Regulator of Systemic Metabolism and a Therapeutic Target for Treating Metabolic Disease". In: *Biomolecules* vol. 13.2 (2023), p. 261. DOI: 10.3390/biom13020261.

[255] Bowman, C. E., Zhao, L., Hartung, T., et al. "Requirement for the Mitochondrial Pyruvate Carrier in Mammalian Development Revealed by a Hypomorphic Allelic Series". In: *Molecular and Cellular Biology* vol. 36.15 (2016), pp. 2089–2104. DOI: 10.1128/mcb.00166-16.

[256] Yang, R.-Z., Park, S., Reagan, W. J., et al. "Alanine aminotransferase isoenzymes: Molecular cloning and quantitative analysis of tissue expression in rats and serum elevation in liver toxicity". In: *Hepatology* vol. 49.2 (2008), pp. 598–607. DOI: 10.1002/hep.22657.

[257] Sun, Y., Chen, W., Torphy, R. J., et al. "Blockade of the CD93 pathway normalizes tumor vasculature to facilitate drug delivery and immunotherapy". In: *Science Translational Medicine* vol. 13.604 (2021). DOI: 10.1126/scitranslmed.abc8922.

[258] Nativel, B., Ramin-Mangata, S., Mevizou, R., et al. "CD93 is a cell surface lectin receptor involved in the control of the inflammatory response stimulated by exogenous DNA". In: *Immunology* vol. 158.2 (2019), pp. 85–93. DOI: 10.1111/imm.13100.

[259] Ferrell, K., Deveraux, Q., Nocker, S. van, et al. "Molecular cloning and expression of a multiubiquitin chain binding subunit of the human 26S protease". In: *FEBS Letters* vol. 381.1-2 (1996), pp. 143–148. DOI: 10.1016/0014-5793(96)00101-9.

[260] Gu, Z. C. and Enenkel, C. "Proteasome assembly". In: *Cellular and Molecular Life Sciences* vol. 71.24 (2014), pp. 4729–4745. DOI: 10.1007/s00018-014-1699-8.

[261] Haberecht-Müller, S., Krüger, E., and Fielitz, J. "Out of Control: The Role of the Ubiquitin Proteasome System in Skeletal Muscle during Inflammation". In: *Biomolecules* vol. 11.9 (2021), p. 1327. DOI: 10.3390/biom11091327.

[262] Mateo, S. de, Castillo, J., Estanyol, J. M., et al. "Proteomic characterization of the human sperm nucleus". In: *PROTEOMICS* vol. 11.13 (2011), pp. 2714–2726. DOI: 10.1002/pmic.201000799.

[263] Zhang, H., Wang, Y., Li, J., et al. "Proteome of Skeletal Muscle Lipid Droplet Reveals Association with Mitochondria and Apolipoprotein A-I". In: *Journal of Proteome Research* vol. 10.10 (2011), pp. 4757–4768. DOI: 10.1021/pr200553c.

[264] Zhao, X., León, I. R., Bak, S., et al. "Phosphoproteome Analysis of Functional Mitochondria Isolated from Resting Human Muscle Reveals Extensive Phosphorylation of Inner Membrane Protein Complexes and Enzymes". In: *Molecular & Cellular Proteomics* vol. 10.1 (2011), p. 110.000299. DOI: 10.1074/mcp.m110.000299.

[265] Puustinen, P., Junttila, M. R., Vanhatupa, S., et al. "PME-1 Protects Extracellular Signal-Regulated Kinase Pathway Activity from Protein Phosphatase 2A–Mediated Inactivation in Human Malignant Glioma". In: *Cancer Research* vol. 69.7 (2009), pp. 2870–2877. DOI: 10.1158/0008-5472.can-08-2760.

[266] Wandzioch, E., Pusey, M., Werda, A., et al. "PME-1 Modulates Protein Phosphatase 2A Activity to Promote the Malignant Phenotype of Endometrial Cancer Cells". In: *Cancer Research* vol. 74.16 (2014), pp. 4295–4305. DOI: 10.1158/0008-5472.can-13-3130.

[267] Lipina, C. and Hundal, H. S. "Carnosic acid stimulates glucose uptake in skeletal muscle cells via a PME-1/PP2A/PKB signalling axis". In: *Cellular Signalling* vol. 26.11 (2014), pp. 2343–2349. DOI: 10.1016/j.cellsig.2014.07.022.

[268] Wang, H., Wang, X., Ma, L., et al. "PGC-1 alpha regulates mitochondrial biogenesis to ameliorate hypoxia-inhibited cementoblast mineralization". In: *Annals of the New York Academy of Sciences* vol. 1516.1 (2022), pp. 300–311. DOI: 10.1111/nyas.14872.

[269] Li, P. A., Hou, X., and Hao, S. "Mitochondrial biogenesis in neurodegeneration". In: *Journal of Neuroscience Research* vol. 95.10 (2017), pp. 2025–2029. DOI: 10.1002/jnr.24042.

[270] Wende, A. R., Schaeffer, P. J., Parker, G. J., et al. "A Role for the Transcriptional Coactivator PGC-1α in Muscle Refueling". In: *Journal of Biological Chemistry* vol. 282.50 (2007), pp. 36642–36651. DOI: 10.1074/jbc.m707006200.

[271] Oka, S.-I., Sreedevi, K., Shankar, T. S., et al. "PERM1 regulates energy metabolism in the heart via ERRα/PGC-1α axis". In: *Frontiers in Cardiovascular Medicine* vol. 9 (2022). DOI: 10.3389/fcvm.2022.1033457.

[272] Cho, Y., Hazen, B. C., Russell, A. P., et al. "Peroxisome Proliferator-activated Receptor γ Coactivator 1 (PGC-1)- and Estrogen-related Receptor (ERR)-induced Regulator in Muscle 1 (PERM1) Is a Tissue-specific Regulator of Oxidative Capacity in Skeletal Muscle Cells". In: *Journal of Biological Chemistry* vol. 288.35 (2013), pp. 25207–25218. DOI: 10.1074/jbc.m113.489674.

[273] Cho, Y., Tachibana, S., Hazen, B. C., et al. "Perm1 regulates CaMKII activation and shapes skeletal muscle responses to endurance exercise training". In: *Molecular Metabolism* vol. 23 (2019), pp. 88–97. DOI: 10.1016/j.molmet.2019.02.009.

[274] Oka, S.-I., Sabry, A. D., Horiuchi, A. K., et al. "Perm1 regulates cardiac energetics as a downstream target of the histone methyltransferase Smyd1". In: *PLOS ONE* vol. 15.6 (2020), p. 0234913. DOI: 10.1371/journal.pone.0234913.

[275] Petersen, A. M. W. and Pedersen, B. K. "The anti-inflammatory effect of exercise". In: *Journal of Applied Physiology* vol. 98.4 (2005), pp. 1154–1162. DOI: 10.1152/japplphysiol.00164.2004.

[276] Garvin, P., Nilsson, E., Ernerudh, J., et al. "The joint subclinical elevation of CRP and IL-6 is associated with lower health-related quality of life in comparison with no elevation or elevation of only one of the biomarkers". In: *Quality of Life Research* vol. 25.1 (2015), pp. 213–221. DOI: 10.1007/s11136-015-1068-6.

[277] Suzuki, K., Nakaji, S., Yamada, M., et al. "Systemic inflammatory response to exhaustive exercise. Cytokine kinetics." In: *Exercise immunology review* vol. 8 (2002). PMID: 12690937, pp. 6–48.

[278] Fonseca, T. R., Mendes, T. T., Ramos, G. P., et al. "Aerobic Training Modulates the Increase in Plasma Concentrations of Cytokines in response to a Session of Exercise". In: *Journal of Environmental and Public Health* vol. 2021 (2021), pp. 1–13. DOI: 10.1155/2021/1304139.

[279] Croft, L., Bartlett, J. D., MacLaren, D. P., et al. "High-intensity interval training attenuates the exercise-induced increase in plasma IL-6 in response to acute exercise". In: *Applied Physiology, Nutrition, and Metabolism* vol. 34.6 (2009), pp. 1098–1107. DOI: 10.1139/h09-117.

[280] Fischer, C. P., Plomgaard, P., Hansen, A. K., et al. "Endurance training reduces the contraction-induced interleukin-6 mRNA expression in human skeletal muscle". In: *American Journal of Physiology-Endocrinology and Metabolism* vol. 287.6 (2004), pp. 1189–1194. DOI: 10.1152/ajpendo.00206.2004.

[281] Landers-Ramos, R. Q., Jenkins, N. T., Spangenburg, E. E., et al. "Circulating angiogenic and inflammatory cytokine responses to acute aerobic exercise in trained and sedentary young men". In: *European Journal of Applied Physiology* vol. 114.7 (2014), pp. 1377–1384. DOI: 10.1007/s00421-014-2861-6.

[282] Hwang, J. H., McGovern, J., Minett, G. M., et al. "Mobilizing serum factors and immune cells through exercise to counteract age-related changes in cancer risk." In: *Exercise immunology review* vol. 26 (2020). PMID: 32139350, pp. 80–99.

[283] Hojman, P., Dethlefsen, C., Brandt, C., et al. "Exercise-induced muscle-derived cytokines inhibit mammary cancer cell growth". In: *American Journal of Physiology-Endocrinology and Metabolism* vol. 301.3 (2011), pp. 504–510. DOI: 10.1152/ajpendo.00520.2010.

[284] Masjedi, A., Hajizadeh, F., Dargani, F. B., et al. "Oncostatin M: A mysterious cytokine in cancers". In: *International Immunopharmacology* vol. 90 (2021), p. 107158. DOI: 10.1016/j.intimp.2020.107158.

[285] Tseng, P.-Y. and Hoon, M. A. "Oncostatin M can sensitize sensory neurons in inflammatory pruritus". In: *Science Translational Medicine* vol. 13.619 (2021). DOI: 10.1126/scitranslmed.abe3037.

[286] Abe, H., Takeda, N., Isagawa, T., et al. "Macrophage hypoxia signaling regulates cardiac fibrosis via Oncostatin M". In: *Nature Communications* vol. 10.1 (2019). DOI: 10.1038/s41467-019-10859-w.

[287] Raschke, S., Eckardt, K., Holven, K. B., et al. "Identification and Validation of Novel Contraction-Regulated Myokines Released from Primary Human Skeletal Muscle Cells". In: *PLOS ONE* vol. 8.4 (2013), p. 62008. DOI: 10.1371/journal.pone.0062008.

[288] Chung, A. S. and Kao, W. J. "Fibroblasts regulate monocyte response to ECM-derived matrix: The effects on monocyte adhesion and the production of inflammatory, matrix remodeling, and growth factor proteins". In: *Journal of Biomedical Materials Research Part A* vol. 89A.4 (2009), pp. 841–853. DOI: 10.1002/jbm.a.32431.

[289] Ojeda, S. R., Ma, Y. J., and Rage, F. "The transforming growth factor alpha gene family is involved in the neuroendocrine control of mammalian puberty". In: *Molecular Psychiatry* vol. 2.5 (1997), pp. 355–358. DOI: 10.1038/sj.mp.4000307.

[290] Gogg, S. and Smith, U. "Epidermal Growth Factor and Transforming Growth Factor α Mimic the Effects of Insulin in Human Fat Cells and Augment Downstream Signaling in Insulin Resistance". In: *Journal of Biological Chemistry* vol. 277.39 (2002), pp. 36045–36051. DOI: 10.1074/jbc.m200575200.

[291] Steensberg, A., Hall, G., Osada, T., et al. "Production of interleukin-6 in contracting human skeletal muscles can account for the exercise-induced increase in plasma interleukin-6". In: *The Journal of Physiology* vol. 529.1 (2000), pp. 237–242. DOI: 10.1111/j.1469-7793.2000.00237.x.

[292] Kamimura, D., Ishihara, K., and Hirano, T. "IL-6 signal transduction and its physiological roles: the signal orchestration model". In: *Reviews of Physiology, Biochemistry and Pharmacology*. Vol. 149. Springer Berlin Heidelberg, 2003, pp. 1–38. ISBN: 978-3-540-20213-4. DOI: 10.1007/s10254-003-0012-2.

[293] Nielsen, A. R. and Pedersen, B. K. "The biological roles of exercise-induced cytokines: IL-6, IL-8, and IL-15". In: *Applied Physiology, Nutrition, and Metabolism* vol. 32.5 (2007), pp. 833–839. DOI: 10.1139/h07-054.

[294] Febbraio, M. A. and Pedersen, B. K. "Muscle-derived interleukin-6: mechanisms for activation and possible biological roles". In: *The FASEB Journal* vol. 16.11 (2002), pp. 1335–1347. DOI: 10.1096/fj.01-0876rev.

[295] Lauritzen, H. P., Brandauer, J., Schjerling, P., et al. "Contraction and AICAR Stimulate IL-6 Vesicle Depletion From Skeletal Muscle Fibers In Vivo". In: *Diabetes* vol. 62.9 (2013), pp. 3081–3092. DOI: 10.2337/db12-1261.

[296] Hojman, P., Brolin, C., Nørgaard-Christensen, N., et al. "IL-6 release from muscles during exercise is stimulated by lactate-dependent protease activity". In: *American Journal of Physiology-Endocrinology and Metabolism* vol. 316.5 (2019), pp. 940–947. DOI: 10.1152/ajpendo.00414.2018.

[297] Minetto, M. A., Rainoldi, A., Gazzoni, M., et al. "Interleukin-6 response to isokinetic exercise in elite athletes: relationships to adrenocortical function and to mechanical and myoelectric fatigue". In: *European Journal of Applied Physiology* vol. 98.4 (2006), pp. 373–382. DOI: 10.1007/s00421-006-0285-7.

[298] O'Rourke, R. W., Metcalf, M. D., White, A. E., et al. "Depot-specific differences in inflammatory mediators and a role for NK cells and IFN-γ in inflammation in human adipose tissue". In: *International Journal of Obesity* vol. 33.9 (2009), pp. 978–990. DOI: 10.1038/ijo.2009.133.

[299] Ibrahim, M. M. "Subcutaneous and visceral adipose tissue: structural and functional differences". In: *Obesity Reviews* vol. 11.1 (2010), pp. 11–18. DOI: 10.1111/j.1467-789x.2009.00623.x.

[300] Cancello, R., Tordjman, J., Poitou, C., et al. "Increased Infiltration of Macrophages in Omental Adipose Tissue Is Associated With Marked Hepatic Lesions in Morbid Human Obesity". In: *Diabetes* vol. 55.6 (2006), pp. 1554–1561. DOI: 10.2337/db06-0133.

R Packages

Aboyoun, P., Pagès, H., and Lawrence, M. *GenomicRanges: Representation and manipulation of genomic intervals*. 2022. DOI: 10.18129/B9.bioc.GenomicRanges. URL: https://bioconductor.org/packages/GenomicRanges.

Ahlmann-Eltze, C. and Patil, I. *ggsignif: Significance Brackets for ggplot2*. 2021. URL: https://CRAN.R-project.org/package=ggsignif.

Ahlmann-Eltze, C., Hickey, P., and Pagès, H. *MatrixGenerics: S4 Generic Summary Statistic Functions that Operate on Matrix-Like Objects*. 2022. DOI: 10.18129/B9.bioc.MatrixGenerics. URL: https://bioconductor.org/packages/MatrixGenerics.

Allaire, J. J., Horner, J., Xie, Y., et al. *markdown: Render Markdown with the C Library Sundown*. 2019. URL: https://github.com/rstudio/markdown.

Analytics, R. and Weston, S. *iterators: Provides Iterator Construct*. 2022. URL: https://github.com/RevolutionAnalytics/iterators.

Andrews, S. V., Ladd-Acosta, C., Feinberg, A. P., et al. "'Gap hunting' to characterize clustered probe signals in Illumina methylation array data". In: *Epigenetics & Chromatin* vol. 9.1 (2016), p. 56. DOI: 10.1186/s13072-016-0107-z.

Arora, S., Morgan, M., Carlson, M., et al. *GenomeInfoDb: Utilities for manipulating chromosome names, including modifying them to follow a particular naming style*. 2022. DOI: 10.18129/B9.bioc.GenomeInfoDb. URL: https://bioconductor.org/packages/GenomeInfoDb.

Aryee, M. J., Jaffe, A. E., Corrada-Bravo, H., et al. "Minfi: A flexible and comprehensive Bioconductor package for the analysis of Infinium DNA Methylation microarrays". In: *Bioinformatics* vol. 30.10 (2014), pp. 1363–1369. DOI: 10.1093/bioinformatics/btu049.

Auguie, B. *gridExtra: Miscellaneous Functions for "Grid" Graphics*. 2017. URL: https://CRAN.R-project.org/package=gridExtra.

Bache, S. M. and Wickham, H. *magrittr: A Forward-Pipe Operator for R*. 2022. URL: https://CRAN.R-project.org/package=magrittr.

Bachelier, V., ZAWAM, J.-E., and Guillem, F. *manipulateWidget: Add Even More Interactivity to Interactive Charts*. 2021. URL: https://github.com/rte-antares-rpackage/manipulateWidget.

Baggerly, K., Bengtsson, H., Hansen, K. D., et al. *illuminaio: Parsing Illumina Microarray Output Files*. 2022. URL: https://github.com/HenrikBengtsson/illuminaio.

Bates, D., Maechler, M., Bolker, B., et al. *lme4: Linear Mixed-Effects Models using Eigen and S4*. 2022. URL: https://github.com/lme4/lme4/.

Bates, D., Maechler, M., and Jagan, M. *Matrix: Sparse and Dense Matrix Classes and Methods*. 2022. URL: https://CRAN.R-project.org/package=Matrix.

Bates, D., Mächler, M., Bolker, B., et al. "Fitting Linear Mixed-Effects Models Using lme4". In: *Journal of Statistical Software* vol. 67.1 (2015), pp. 1–48. DOI: 10.18637/jss.v067.i01.

Bengtsson, H. *matrixStats: Functions that Apply to Rows and Columns of Matrices (and to Vectors)*. 2022. URL: https://github.com/HenrikBengtsson/matrixStats.

Bolstad, B. *preprocessCore: A collection of pre-processing functions*. 2022. URL: https://github.com/bmbolstad/preprocessCore.

Butcher, L. *Illumina450ProbeVariants.db: Annotation Package combining variant data from 1000 Genomes Project for Illumina HumanMethylation450 Bead Chip probes*. 2022. DOI: 10.18129/B9.bioc.Illumina450ProbeVariants.db. URL: https://bioconductor.org/packages/release/data/experiment/html/Illumina450ProbeVariants.db.html.

Butcher, L. M. and Beck, S. "Probe Lasso: A novel method to rope in differentially methylated regions with 450K DNA methylation data". In: *Methods* vol. 72 (2015), pp. 21–28. DOI: 10.1016/j.ymeth.2014.10.036.

Chen, H. *VennDiagram: Generate High-Resolution Venn and Euler Plots*. 2022. URL: https://CRAN.R-project.org/package=VennDiagram.

Chen, J. and Behnam, E. *SmartSVA: Fast and Robust Surrogate Variable Analysis*. 2017. URL: https://CRAN.R-project.org/package=SmartSVA.

Constantin, A.-E. and Patil, I. "ggsignif: R Package for Displaying Significance Brackets for 'ggplot2'". In: *PsyArXiv* (2021). DOI: 10.31234/osf.io/7awm6.

Corporation, M. and Weston, S. *doSNOW: Foreach Parallel Adaptor for the snow Package*. 2022. URL: https://CRAN.R-project.org/package=doSNOW.

Dunn, P. K. and Smyth, G. K. "Randomized quantile residuals". In: *Journal of Computational and Graphical Statistics* vol. 5 (1996), pp. 236–244. DOI: 10.2307/1390802.

Durinck, S. and Huber, W. *biomaRt: Interface to BioMart databases (i.e. Ensembl)*. 2022. DOI: 10.18129/B9.bioc.biomaRt. URL: https://bioconductor.org/packages/release/bioc/html/biomaRt.html.

Durinck, S., Spellman, P. T., Birney, E., et al. "Mapping identifiers for the integration of genomic datasets with the R/Bioconductor package biomaRt". In: *Nature Protocols* vol. 4 (2009), pp. 1184–1191. DOI: 10.1038/nprot.2009.97.

Durinck, S., Moreau, Y., Kasprzyk, A., et al. "BioMart and Bioconductor: a powerful link between biological databases and microarray data analysis". In: *Bioinformatics* vol. 21 (2005), pp. 3439–3440. DOI: 10.1093/bioinformatics/bti525.

Fortin, J.-P. and Hansen, K. D. "Reconstructing A/B compartments as revealed by Hi-C using long-range correlations in epigenetic data". In: *Genome Biology* vol. 16.1 (2015), p. 180. DOI: 10.1186/s13059-015-0741-y.

Fortin, J.-P., Labbe, A., Lemire, M., et al. "Functional normalization of 450k methylation array data improves replication in large cancer studies". In: *Genome Biology* vol. 15.12 (2014), p. 503. DOI: 10.1186/s13059-014-0503-2.

Fortin, J.-P., Triche, T. J., and Hansen, K. D. "Preprocessing, normalization and integration of the Illumina HumanMethylationEPIC array with minfi". In: *Bioinformatics* vol. 33.4 (2017), pp. 558–560. DOI: 10.1093/bioinformatics/btw691.

Gentleman, R., Carey, V., Morgan, M., et al. *Biobase: Base functions for Bioconductor*. 2022. DOI: 10.18129/B9.bioc.Biobase. URL: https://bioconductor.org/packages/Biobase.

Gentleman, R., Carey, V. J., Huber, W., et al. *genefilter: methods for filtering genes from high-throughput experiments*. 2022. DOI: 10.18129/B9.bioc.genefilter. URL: https://bioconductor.org/packages/release/bioc/html/genefilter.html.

Genz, A. and Bretz, F. *Computation of Multivariate Normal and t Probabilities*. 1st ed. Lecture Notes in Statistics. Heidelberg: Springer, 2009. ISBN: 978-3-642-01688-2.

Genz, A., Bretz, F., Miwa, T., et al. *mvtnorm: Multivariate Normal and t Distributions*. 2021. URL: http://mvtnorm.R-forge.R-project.org.

Giner, G. and Smyth, G. K. "statmod: probability calculations for the inverse Gaussian distribution". In: *The R Journal* vol. 8.1 (2016), pp. 339–351. DOI: 10.48550/arXiv.1603.06687.

Grosjean, P. *svDialogs: SciViews - Standard Dialog Boxes for Windows, MacOS and Linuxes*. 2022. URL: https://CRAN.R-project.org/package=svDialogs.

Grosjean, P. *tcltk2: Tcl/Tk Additions*. 2014. URL: http://www.sciviews.org/SciViews-R.

Grosjean, P. *SciViews::R*. UMONS. 2022. URL: https://sciviews.r-universe.dev/.

Grosjean, P. *SciViews-R: A GUI API for R*. UMONS. 2022. URL: http://www.sciviews.org/SciViews-R.

Gu, Z. *ComplexHeatmap: Make Complex Heatmaps*. 2022. DOI: 10.18129/B9.bioc.ComplexHeatmap. URL: https://bioconductor.org/packages/release/bioc/html/ComplexHeatmap.html.

Gu, Z. "Complex Heatmap Visualization". In: *iMeta* (2022). DOI: 10.1002/imt2.43.

Gu, Z., Eils, R., and Schlesner, M. "Complex heatmaps reveal patterns and correlations in multidimensional genomic data". In: *Bioinformatics* (2016). DOI: 10.1093/bioinformatics/btw313.

Hansen, K. D. *IlluminaHumanMethylationEPICmanifest: Manifest for Illumina's EPIC methylation arrays*. 2016. DOI: 10.18129/B9.bioc.IlluminaHumanMethylationEPICmanifest. URL: https://bioconductor.org/packages/release/data/annotation/html/IlluminaHumanMethylationEPICmanifest.html.

Hansen, K. D., Aryee, M., and Irizarry, R. A. *minfi: Analyze Illumina Infinium DNA methylation arrays*. 2022. URL: https://github.com/hansenlab/minfi.

Henry, L. and Wickham, H. *purrr: Functional Programming Tools*. 2020. URL: https://CRAN.R-project.org/package=purrr.

Henry, L. and Wickham, H. *rlang: Functions for Base Types and Core R and Tidyverse Features*. 2022. URL: https://CRAN.R-project.org/package=rlang.

Hothorn, T. *TH.data: TH's Data Archive*. 2022. URL: https://CRAN.R-project.org/package=TH.data.

Hothorn, T., Zeileis, A., Farebrother, R. W., et al. *lmtest: Testing Linear Regression Models*. 2022. URL: https://CRAN.R-project.org/package=lmtest.

Hothorn, T., Bretz, F., and Westfall, P. *multcomp: Simultaneous Inference in General Parametric Models*. 2022. URL: https://CRAN.R-project.org/package=multcomp.

Hothorn, T., Bretz, F., and Westfall, P. "Simultaneous Inference in General Parametric Models". In: *Biometrical journal* vol. 50.3 (2008), pp. 346–363. DOI: 10.1002/bimj.200810425.

Houseman, E. A., Sc.D., Koestler, D. C., et al. *RPMM: Recursively Partitioned Mixture Model*. 2017. URL: https://CRAN.R-project.org/package=RPMM.

Hu, Y. and Smyth, G. K. "ELDA: extreme limiting dilution analysis for comparing depleted and enriched populations in stem cell and other assays". In: *Journal of immunological methods* vol. 347.1 (2009), pp. 70–78. DOI: 10.1016/j.jim.2009.06.008.

Huber, W., Carey, V. J., Gentleman, R., et al. "Orchestrating high-throughput genomic analysis with Bioconductor". In: *Nature Methods* vol. 12.2 (2015), pp. 115–121. DOI: 10.1038/nmeth.3252.

Irizarry, R. A., Aryee, M., Hansen, K. D., et al. *bumphunter: Bump Hunter*. 2022. URL: https://github.com/rafalab/bumphunter.

Jaffe, A. E., Murakami, P., Lee, H., et al. "Bump hunting to identify differentially methylated regions in epigenetic epidemiology studies". In: *International Journal of Epidemiology* vol. 41.1 (2012), pp. 200–209. DOI: 10.1093/ije/dyr238.

Keitt, T. *colorRamps: Builds Color Tables*. 2022. URL: https://CRAN.R-project.org/package=colorRamps.

Kolberg, L. and Raudvere, U. *gprofiler2: Interface to the g:Profiler Toolset*. 2021. URL: https://CRAN.R-project.org/package=gprofiler2.

Lawrence, M., Huber, W., Pagès, H., et al. "Software for Computing and Annotating Genomic Ranges". In: *PLOS Computational Biology* vol. 9.8 (2013), p. 1003118. DOI: 10.1371/journal.pcbi.1003118.

Leek, J. T., Johnson, W. E., Parker, H. S., et al. *sva: Surrogate Variable Analysis*. 2022. DOI: 10.18129/B9.bioc.sva. URL: https://bioconductor.org/packages/release/bioc/html/sva.html.

Loader, C. *locfit: Local Regression, Likelihood and Density Estimation*. 2022. URL: https://CRAN.R-project.org/package=locfit.

Love, M., Anders, S., and Huber, W. *DESeq2: Differential gene expression analysis based on the negative binomial distribution*. 2022. URL: https://github.com/mikelove/DESeq2.

Love, M. I., Huber, W., and Anders, S. "Moderated estimation of fold change and dispersion for RNA-seq data with DESeq2". In: *Genome Biology* vol. 15.12 (2014), p. 550. DOI: 10.1186/s13059-014-0550-8.

Maechler, M., Rousseeuw, P., Struyf, A., et al. *cluster: "Finding Groups in Data": Cluster Analysis Extended Rousseeuw et al.* 2022. URL: https://svn.r-project.org/R-packages/trunk/cluster/.

Maksimovic, J., Gordon, L., and Oshlack, A. "SWAN: Subset quantile Within-Array Normalization for Illumina Infinium HumanMethylation450 BeadChips". In: *Genome Biology* vol. 13.6 (2012), p. 44. DOI: 10.1186/gb-2012-13-6-r44.

Marchini, J. L., Heaton, C., and Ripley, B. D. *fastICA: FastICA Algorithms to Perform ICA and Projection Pursuit*. 2021. URL: https://CRAN.R-project.org/package=fastICA.

Miettinen, J., Nordhausen, K., and Taskinen, S. "Blind Source Separation Based on Joint Diagonalization in R: The Packages JADE and BSSasymp". In: *Journal of Statistical Software* vol. 76.2 (2017), pp. 1–31. DOI: 10.18637/jss.v076.i02.

Morgan, M., Wang, J., Obenchain, V., et al. *BiocParallel: Bioconductor facilities for parallel evaluation*. 2022. URL: https://github.com/Bioconductor/BiocParallel.

Morgan, M., Obenchain, V., Hester, J., et al. *SummarizedExperiment: SummarizedExperiment container*. 2022. DOI: 10.18129/B9.bioc.SummarizedExperiment. URL: https://bioconductor.org/packages/SummarizedExperiment.

Morris, T. J., Butcher, L. M., Teschendorff, A. E., et al. "ChAMP: 450k Chip Analysis Methylation Pipeline". In: *Bioinformatics* vol. 30.3 (2014), pp. 428–430. DOI: 10.1093/bioinformatics/btt684.

Müller, K. and Wickham, H. *tibble: Simple Data Frames*. 2022. URL: https://CRAN.R-project.org/package=tibble.

Nordhausen, K., Cardoso, J.-F., Miettinen, J., et al. *JADE: Blind Source Separation Methods Based on Joint Diagonalization and Some BSS Performance Criteria*. 2020. URL: https://CRAN.R-project.org/package=JADE.

Pagès, H. and Aboyoun, P. *XVector: Foundation of external vector representation and manipulation in Bioconductor*. 2022. DOI: 10.18129/B9.bioc.XVector. URL: https://bioconductor.org/packages/XVector.

Pagès, H., Aboyoun, P., Gentleman, R., et al. *Biostrings: Efficient manipulation of biological strings*. 2022. DOI: 10.18129/B9.bioc.Biostrings. URL: https://bioconductor.org/packages/Biostrings.

Pagès, H., Aboyoun, P., and Lawrence, M. *IRanges: Foundation of integer range manipulation in Bioconductor*. 2022. DOI: 10.18129/B9.bioc.IRanges. URL: https://bioconductor.org/packages/IRanges.

Pagès, H., Lawrence, M., and Aboyoun, P. *S4Vectors: Foundation of vector-like and list-like containers in Bioconductor*. 2022. DOI: 10.18129/B9.bioc.S4Vectors. URL: https://bioconductor.org/packages/S4Vectors.

Peters, T. and Buckley, M. *DMRcate: Methylation array and sequencing spatial analysis methods*. 2022. DOI: 10.18129/B9.bioc.DMRcate. URL: https://bioconductor.org/packages/release/bioc/html/DMRcate.html.

Peters, T. J., Buckley, M. J., Statham, A. L., et al. "De novo identification of differentially methylated regions in the human genome". In: *Epigenetics & Chromatin* vol. 8 (2015), p. 6. DOI: 10.1186/1756-8935-8-6.

Peters, T. J., Buckley, M. J., Chen, Y., et al. "Calling differentially methylated regions from whole genome bisulphite sequencing with DMRcate". In: *Nucleic acids research* vol. 49 (2021). DOI: 10.1093/nar/gkab637.

Phipson, B. and Smyth, G. K. "Permutation p-values should never be zero: calculating exact p-values when permutations are randomly drawn". In: *Statistical Applications in Genetics and Molecular Biology* vol. 9.1 (2010), p. 39. DOI: 10.2202/1544-6115.1585.

Pinheiro, J. C. and Bates, D. M. *Mixed-Effects Models in S and S-PLUS*. 1st ed. New York, USA: Springer, 2000. ISBN: 978-1-4757-8144-1.

Pinheiro, J., Bates, D., and Team, R. C. *nlme: Linear and Nonlinear Mixed Effects Models*. 2022. URL: https://svn.r-project.org/R-packages/trunk/nlme/.

Qiu, Y. and Mei, J. *RSpectra: Solvers for Large-Scale Eigenvalue and SVD Problems*. 2022. URL: https://github.com/yixuan/RSpectra.

Team, R. C. *R: A Language and Environment for Statistical Computing*. R Foundation for Statistical Computing. 2022. URL: https://www.R-project.org/.

Analytics, R. and Weston, S. *foreach: Provides Foreach Looping Construct*. 2022. URL: https://cran.r-project.org/web/packages/foreach/index.html.

Ripley, B. *MASS: Support Functions and Datasets for Venables and Ripley's MASS*. 2022. URL: http://www.stats.ox.ac.uk/pub/MASS4/.

Ritchie, M. E., Phipson, B., Wu, D., et al. "limma powers differential expression analyses for RNA-sequencing and microarray studies". In: *Nucleic Acids Research* vol. 43.7 (2015), p. 47. DOI: 10.1093/nar/gkv007.

Rowe, B. L. Y. *futile.logger: A Logging Utility for R*. 2016. URL: https://CRAN.R-project.org/package=futile.logger.

Schauberger, P. and Walker, A. *openxlsx: Read, Write and Edit xlsx Files*. 2021. URL: https://CRAN.R-project.org/package=openxlsx.

Seshan, V. E. and Olshen, A. *DNAcopy: DNA copy number data analysis*. 2022. DOI: 10.18129/B9.bioc.DNAcopy. URL: https://bioconductor.org/packages/release/bioc/html/DNAcopy.html.

Sievert, C. *Interactive Web-Based Data Visualization with R, plotly, and shiny*. 1st ed. Chapman and Hall/CRC, 2020. ISBN: 978-1-138-33145-7.

Sievert, C., Parmer, C., Hocking, T., et al. *plotly: Create Interactive Web Graphics via plotly.js*. 2021. URL: https://CRAN.R-project.org/package=plotly.

Slowikowski, K. *ggrepel: Automatically Position Non-Overlapping Text Labels with ggplot2*. 2021. URL: https://github.com/slowkow/ggrepel.

Smith, Mike, L., Baggerly, et al. "illuminaio: An open source IDAT parsing tool for Illumina microarrays". In: *F1000Research* vol. 2.264 (2013), p. 264. DOI: 10.12688/f1000research.2-264.v1.

Smyth, G. K. "Optimization and nonlinear equations". In: *Encyclopedia of Biostatistics* (2005), pp. 3088–3095. DOI: 10.1002/0470011815.b2a14027.

Smyth, G. K. "An efficient algorithm for REML in heteroscedastic regression". In: *Journal of Computational and Graphical Statistics* vol. 11.4 (2002), pp. 836–847. DOI: 10.1198/106186002871.

Smyth, G., Hu, Y., Ritchie, M., et al. *limma: Linear Models for Microarray Data*. 2022. URL: http://bioinf.wehi.edu.au/limma.

Smyth, G., Hu, Y., Dunn, P., et al. *statmod: Statistical Modeling*. 2022. URL: https://CRAN.R-project.org/package=statmod.

Storey, J. D., Bass, A. J., Dabney, A., et al. *qvalue: Q-value estimation for false discovery rate control*. 2022. URL: http://github.com/jdstorey/qvalue.

Suderman, M., Hemani, G., and Min, J. *meffil: Efficient algorithms for DNA methylation*. 2023. URL: https://github.com/perishky/meffil.

Team, T. B. D. *BiocGenerics: S4 generic functions used in Bioconductor*. 2022. DOI: 10.18129/B9.bioc.BiocGenerics. URL: https://bioconductor.org/packages/BiocGenerics.

Therneau, T. M. and Grambsch, P. M. *Modeling Survival Data: Extending the Cox Model*. 1st ed. New York, USA: Springer, 2000. ISBN: 978-0-387-98784-2.

Teschendorff, A. E. *isva: Independent Surrogate Variable Analysis*. 2017. URL: https://CRAN.R-project.org/package=isva.

Therneau, T. M. *survival: Survival Analysis*. 2022. URL: https://github.com/therneau/survival.

Tian, Y., Morris, T., Stirling, L., et al. *ChAMPdata: Data Packages for ChAMP package*. 2022. DOI: 10.18129/B9.bioc.ChAMPdata. URL: https://bioconductor.org/packages/release/data/experiment/html/ChAMPdata.html.

Tian, Y., Morris, T. J., Webster, A. P., et al. "ChAMP: updated methylation analysis pipeline for Illumina BeadChips". In: *Bioinformatics* vol. 33.3 (2017), p. 513. DOI: 10.1093/bioinformatics/btx513.

Tierney, L., Rossini, A. J., Li, N., et al. *snow: Simple Network of Workstations*. 2021. URL: https://CRAN.R-project.org/package=snow.

Triche, T. J., Weisenberger, D. J., Van Den Berg, D., et al. "Low-level processing of Illumina Infinium DNA Methylation BeadArrays". In: *Nucleic Acids Research* vol. 41.7 (2013), pp. 90–90. DOI: 10.1093/nar/gkt090.

Turlach, B. A. and Weingessel, A. *quadprog: Functions to Solve Quadratic Programming Problems*. 2019. URL: https://CRAN.R-project.org/package=quadprog.

Urbanek, S. and Horner, J. *Cairo: R Graphics Device using Cairo Graphics Library for Creating High-Quality Bitmap (PNG, JPEG, TIFF), Vector (PDF, SVG, PostScript) and Display (X11 and Win32) Output*. 2022. URL: http://www.rforge.net/Cairo/.

Ushey, K., Allaire, J. J., Wickham, H., et al. *rstudioapi: Safely Access the RStudio API*. 2022. URL: https://CRAN.R-project.org/package=rstudioapi.

Vaidyanathan, R., Xie, Y., Allaire, J. J., et al. *htmlwidgets: HTML Widgets for R*. 2021. URL: https://github.com/ramnathv/htmlwidgets.

Venables, W. N. and Ripley, B. D. *Modern Applied Statistics with S*. 4th ed. New York, USA: Springer, 2002. ISBN: 978-0-387-95457-0.

Wickham, H. *forcats: Tools for Working with Categorical Variables (Factors)*. 2022. URL: https://CRAN.R-project.org/package=forcats.

Wickham, H. *httr: Tools for Working with URLs and HTTP*. 2022. URL: https://CRAN.R-project.org/package=httr.

Wickham, H. *plyr: Tools for Splitting, Applying and Combining Data*. 2022. URL: https://CRAN.R-project.org/package=plyr.

Wickham, H. *reshape2: Flexibly Reshape Data: A Reboot of the Reshape Package*. 2020. URL: https://github.com/hadley/reshape.

Wickham, H. *stringr: Simple, Consistent Wrappers for Common String Operations*. 2022. URL: https://CRAN.R-project.org/package=stringr.

Wickham, H. *tidyverse: Easily Install and Load the Tidyverse*. 2022. URL: https://CRAN.R-project.org/package=tidyverse.

Wickham, H. *ggplot2: Elegant Graphics for Data Analysis*. 2nd ed. Springer, 2016. ISBN: 978-3-319-24277-4.

Wickham, H. "The Split-Apply-Combine Strategy for Data Analysis". In: *Journal of Statistical Software* vol. 40.1 (2011), pp. 1–29. DOI: 10.18637/jss.v040.i01.

Wickham, H. "Reshaping Data with the reshape Package". In: *Journal of Statistical Software* vol. 21.12 (2007), pp. 1–20. DOI: 10.18637/jss.v021.i12.

Wickham, H. and Girlich, M. *tidyr: Tidy Messy Data*. 2022. URL: https://CRAN.R-project.org/package=tidyr.

Wickham, H., François, R., Henry, L., et al. *dplyr: A Grammar of Data Manipulation*. 2022. URL: https://CRAN.R-project.org/package=dplyr.

Wickham, H., Chang, W., Henry, L., et al. *ggplot2: Create Elegant Data Visualisations Using the Grammar of Graphics*. 2022. URL: https://CRAN.R-project.org/package=ggplot2.

Wickham, H., Hester, J., and Bryan, J. *readr: Read Rectangular Text Data*. 2022. URL: https://CRAN.R-project.org/package=readr.

Wickham, H., Averick, M., Bryan, J., et al. "Welcome to the tidyverse". In: *Journal of Open Source Software* vol. 4.43 (2019), p. 1686. DOI: 10.21105/joss.01686.

Wood, S. *mgcv: Mixed GAM Computation Vehicle with Automatic Smoothness Estimation*. 2022. URL: https://CRAN.R-project.org/package=mgcv.

Wood, S. N. "Fast stable restricted maximum likelihood and marginal likelihood estimation of semi-parametric generalized linear models". In: *Journal of the Royal Statistical Society Series B: Statistical Methodology* vol. 73.1 (2010), pp. 3–36. DOI: 10.1111/j.1467-9868.2010.00749.x.

Wood, S. N. "Stable and efficient multiple smoothing parameter estimation for generalized additive models". In: *Journal of the American Statistical Association* vol. 99.467 (2004), pp. 673–686. DOI: 10.1198/016214504000000980.

Wood, S. N. *Generalized Additive Models: An Introduction with R*. 2nd ed. Chapman and Hall/CRC, 2017. ISBN: 978-1-3153702-7-9.

Wood, S. N. "Thin-plate regression splines". In: *Statistical Methodology* vol. 65.1 (2003), pp. 95–114. DOI: 10.1111/1467-9868.00374.

Wood, S. N., Pya, N., and Säfken, B. "Smoothing parameter and model selection for general smooth models". In: *Journal of the American Statistical Association* vol. 111.516 (2016), pp. 1548–1563. DOI: 10.1080/01621459.2016.1180986.

Xie, Y. *knitr: A General-Purpose Package for Dynamic Report Generation in R*. 2022. URL: https://yihui.org/knitr/.

Xie, Y. *Dynamic Documents with R and knitr*. 2nd ed. Boca Raton, Florida: Chapman and Hall/CRC, 2015. ISBN: 978-1-4987-1696-2.

Xie, Y. *knitr: A Comprehensive Tool for Reproducible Research in R*. 1st ed. Chapman and Hall/CRC, 2014. ISBN: 978-1-466-56159-5.

Xie, Y., Cheng, J., and Tan, X. *DT: A Wrapper of the JavaScript Library DataTables*. 2022. URL: https://github.com/rstudio/DT.

Yuan, T. *ChAMP: Chip Analysis Methylation Pipeline for Illumina HumanMethylation450 and EPIC*. 2022. DOI: 10.18129/B9.bioc.ChAMP. URL: https://www.bioconductor.org/packages/release/bioc/html/ChAMP.html.

Zeileis, A. "Econometric Computing with HC and HAC Covariance Matrix Estimators". In: *Journal of Statistical Software* vol. 11.10 (2004), pp. 1–17. DOI: 10.18637/jss.v011.i10.

Zeileis, A. "Object-Oriented Computation of Sandwich Estimators". In: *Journal of Statistical Software* vol. 16.9 (2006), pp. 1–16. DOI: 10.18637/jss.v016.i09.

Zeileis, A. and Grothendieck, G. "zoo: S3 Infrastructure for Regular and Irregular Time Series". In: *Journal of Statistical Software* vol. 14.6 (2005), pp. 1–27. DOI: 10.18637/jss.v014.i06.

Zeileis, A. and Hothorn, T. "Diagnostic Checking in Regression Relationships". In: *R News* vol. 2.3 (2002), pp. 7–10. URL: https://CRAN.R-project.org/doc/Rnews/.

Zeileis, A. and Lumley, T. *sandwich: Robust Covariance Matrix Estimators*. 2022. URL: https://sandwich.R-Forge.R-project.org/.

Zeileis, A., Grothendieck, G., and Ryan, J. A. *zoo: S3 Infrastructure for Regular and Irregular Time Series (Z's Ordered Observations)*. 2022. URL: https://zoo.R-Forge.R-project.org/.

Zeileis, A., Köll, S., and Graham, N. "Various Versatile Variances: An Object-Oriented Implementation of Clustered Covariances in R". In: *Journal of Statistical Software* vol. 95.1 (2020), pp. 1–36. DOI: 10.18637/jss.v095.i01.

Zheng, X., Gogarten, S., Gailly, J.-l., et al. *gdsfmt: R Interface to CoreArray Genomic Data Structure (GDS) Files*. 2023. URL: https://github.com/zhengxwen/gdsfmt.

Zheng, X., Levine, D., Shen, J., et al. "A High-performance Computing Toolset for Relatedness and Principal Component Analysis of SNP Data". In: *Bioinformatics* vol. 28.24 (2012), pp. 3326–3328. DOI: 10.1093/bioinformatics/bts606.

Zheng, X., Gogarten, S., Lawrence, M., et al. "SeqArray – A storage-efficient high-performance data format for WGS variant calls". In: *Bioinformatics* vol. 33.15 (2017), pp. 2251–2257. DOI: 10.1093/bioinformatics/btx145.